Towards the usage of *Phaeodactylum tricornutum* as biofactory for omega-3 fatty acids

Dissertation
zur Erlangung des Doktorgrades
der Naturwissenschaften

Vorgelegt beim Fachbereich 15- Biowissenschaften
der Johann Wolfgang Goethe-Universität
in Frankfurt am Main

von Liv Celin Krämer
geboren in Waldbröl

Frankfurt am Main (2022)
(D30)

Vom Fachbereich Biowissenschaften der

Johann Wolfgang Goethe-Universität als Dissertation angenommen.

Dekan:	Prof. Dr. Sven Klimpel
Gutachter:	Prof. Dr. Claudia Büchel
	Prof. Dr. Eckhard Boles

Datum der Disputation:

“As you have sown so shall you reap.”

Marcus Tullius Cicero

Abstract

The increasing demand of the high value ω-3 fatty acids due to its beneficial role for human health, explains the huge need for alternative production ways of ω-3 fatty acids. The oleaginous alga *Phaeodactylum tricornutum* is a prominent candidate and has been investigated as biofactory for ω-3 fatty acids, e.g. the synthesis of eicosapentaenoic acid (EPA). In general, the growth and the lipid content of diatoms can be enhanced by genetic engineering or are influenced by environmental factors, e.g. nutrients, light or temperature.

In this study, the potential of *P. tricornutum* as biofactory was improved by heterologously expressing the hexose uptake protein 1 (HUP1) from the Chlorophyte *Chlorella kessleri*.

An *in situ* localization study revealed that only the full length HUP1 protein fused to eGFP was correctly targeted to the plasma membrane, whereas the N-terminal sequence of the protein is only sufficient to enter the ER. Protein and gene expression data displayed that the gene-promoter combination was relevant for the expression level of HUP1, while only cells expressing the protein under the light-inducible fcpA promoter showed a significant expression. In these mutants an efficient glucose uptake was detectable under mixotrophic growth condition, low light intensities and low glucose concentrations leading to an increased cell dry weight.

In a second approach, the growth and lipid content of wildtype cells were analyzed in a small 1l photobioreactor. Here, a commercial F/2 medium and a common culture medium, ASP and modified versions were compared. There was neither a significant impact on the growth and lipid content in *P. tricornutum* cells due to the supplemention of trace elements nor due to elevated salt concentrations in the media. In a modified version of ASP medium, with adapted nitrate and phosphate concentration a constantly high biomass productivity was achieved, yielding the highest value of 82 mg l^{-1} d^{-1} during the first three days. This was achieved even though light intensity was reduced by 40%. The differences in biomass productivity as well as the lipid content and the lipid composition underlined the importance of the choice of culture medium and the harvest time for enhanced growth and EPA yields in *P. tricornutum*.

Table of Contents

Abbreviations

aa	Amino acids
ACCase	Acetyl-coa carboxylase
ACP	Acyl carrier protein
ALA	α-linolenic acid
CCM	CO_2 concentrating mechanism
CDW	Cell dry weight
CER	Chloroplast/endoplasmic reticulum compartment
CERM	Chloroplast/endoplasmic reticulum compartment membrane
DAG	Diacylglycerol
DHA	Docosahexaenoic acid
DIC	Dissolved inorganic carbon
DPA	Docosapentaenoic acid
DW	Dry weight
eGFP	Enhanced green fluorescent protein
ELO	Fatty acid elongases
EPA	Eicosapentaenoic acid
ESAW	Enriched seawater
F	Flask
FAD	Fatty acid desaturases
FAS	Fatty acid synthase
fcpA	Fucoxanthin-chlorophyll binding protein A
G3P	Glycerol 3 phosphate
GLNA	Glutamine synthetase
GLUT	Human glucose transporters
HB PBR	Hanging bag photobioreactor
HF PBR	Horizontal fence photobioreactor
HUP1	Hexose uptake protein
IMPs	Integral membrane proteins
IS	Internal standard
LC	Long chain
LPC	Lysophosphatidylcholine
Lyso-PA	Lysophosphatidic acid
MAG	1-palmitoyl glycerol
MFS	Major facilitator superfamily

MUFA	Monounsaturated fatty acid
N	Nitrogen
NPQ	Non-photochemical quenching
NR	Nitrate reductase
P	Phosphorus
PA	Phosphatidic acid
PALM	Photoactivated localization microscopy
PBR	Photobioreactor
PC	Phosphatidylcholine
PE	Phosphatidylethanolamine
PET	Polyethylene terephthalate
PG	Phosphatidylglycerol
PI	Phosphatidylinositol
PUFA	Polyunsaturated fatty acid
RFU	Relative fluorescence signal
RP	Raceway pond
RT	Room temperature
SFA	Saturated fatty acid
SRP	Signal recognition particle
SR-SIM	Structured illumination microscopy
STP	Sugar transport protein
TAG	Triacylglycerol
TCA	Tricarboxylic acid
TLC	Thin layer chromatography
TM	Transmembrane helices
VLC	Very long chain
ω-3	Omega-3
C14:0	Myristic acid
C16:3	Hexadecatrienoic acid

1. General introduction

Based on the three-domain hypothesis, cellular life is divided into the groups eubacteria, archaebacteria and eucaryotes. The birth of photosynthetic eucaryotes was initiated by a first endosymbiotic event where a cyanobacteria-like cell was engulfed by a heterotrophic eukaryote, more than 1500 million years ago (Cavalier-Smith 1982; Yoon et al. 2004). As a consequence, the super-group Archaeplastida, including the phylum of Viridiplantae (Chlorophyta and land plants), Glaucophyta and Rhodophyta (red algae) had evolved (Adl et al. 2012; Falkowski and Knoll 2007). During the evolution process the phagocyted cyanobacteria developed to the now known photosynthetic organelles, the plastids. The so-called primary plastids possess two envelope membranes, whereas the so-called secondary plastids are surrounded by three or four membranes. According to the chromalveolate hypothesis by Cavalier (1999), these complex plastids are the result of a second endosymbiotic event, where a red algae was engulfed by a nonphotosynthetic eucaryote. In contrast, other studies claim that there is evidence for multiple endosymbiosis events for the origin of red algal derived plastids (Archibald and Keeling 2002; Green 2011). A recent study showed that the hypothesis of several endosymbiosis events is chronologically possible using molecular clock analysis combined with phylogenomics (Strassert et al. 2021). However, many open questions remain regarding the question of the evolutionary background, which need to be solved with more sequenced genomes available.

However, based on the chromalveolate hypothesis the second endosymbiotic event gave rise to the phylum of the Chromalveolate algae, consisting of Cryptophyta, Haptophyta, Apicomplexa, Perkinsidae, Dinophyta and Heterokontophyta (Gould et al. 2008). Within this thesis, the group of algae is collectively named Chromalveolates.

As a result of endosymbiotic events, gene transfer between different organelles occurred, e.g from the engulfed plastid to the nucleus of the host cell. Hence, nucleus encoded proteins are synthesized in the cytosol and retargeted to the place of action. Here, targeting sequences are necessary and recognized by specific receptors or function as a “localization address”, e.g. an N-terminal transit peptid for targeting proteins to primary plastids (for review, see: Bolte et al. 2009).

1.1. *Phaeodactylum tricornutum* and its application

In the phylum of Chromalveolates, one major group of the Heterokonts are diatoms. This group is responsible for a significantly high contribution to the global primary production (Falkowski et al. 1998). Two diatoms are intensively studied, *Thalassiosira pseudonana* and *Phaeodactylum tricornutum* and they are of great value because of their high lipid content, especially in omega-3 fatty acids (ω-3 fatty acids) (Draaisma et al. 2013) and their major light

harvesting pigment fucoxanthin (Bauer et al. 2019). There is a huge need for sustainable alternative products, especially for ω-3 and ω-6 fatty acids, due to increasing demand concomitant with the importance of these fatty acids for beneficial health (Ward and Singh 2005; and references herein). For example, the intake of two ω-3 fatty acids, namely eicosapentaenoic acid (EPA, C20:5 ω-3) and docosahexaenoic acid (DHA, C22:6 ω-3) have a positive effect on human health (Weylandt et al. 2015), even being discussed as therapeutic strategies for symptoms of the recent COVID-19 disease (Oliver et al. 2020; and reference therein). In detail, scientists have proven that the intake of 250 mg EPA and DHA per day showed prevention against cardiovascular diseases (Kris-Etherton et al. 2009). Microalgae are the primary source of ω-3 fatty acids, but so far mainly animal based products are used in industrial products (Fig. 1). Microalgae are a sustainable alternative, as they can utilize, for example, non-arable land and naturally produce these high-value products. A list of of commercially available products of EPA and DHA from microalgae is given in the review of Martins et al. (2013).

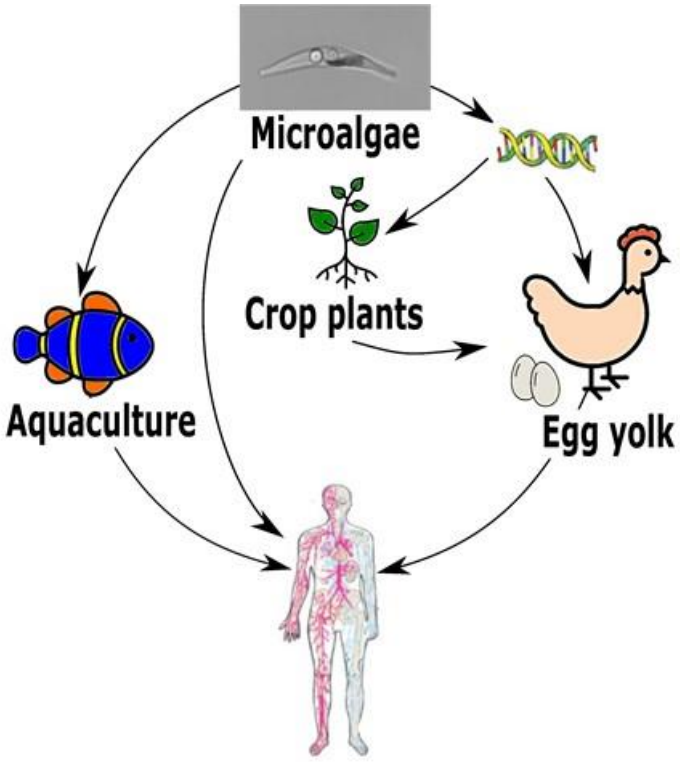

Fig. 1 The natural source of ω-3 fatty acids and its cycle to enter human nutrition. Microalgae, in this case the oleaginous alga *Phaeodactylum tricornutum*, are the primary source of ω-3 fatty acids and can be used in diverse ways to supplement human nutrition. The image is modified from Kitessa et al. 2014.

Especially the oleaginous diatom *P. tricornutum* serves as model organism for the above mentioned research topics, due to its sequenced genome and the accessibilty of genome editing methods (Bowler et al. 2008).

P. tricornutum has been sampled worldwide, while three different morphotypes, fusiform, oval and tridiate have been described (Fig. S 1). In addition to differences in morphology (Martino

et al. 2011), genomic diversity within the species has also been reported, most likely due to different evolution pressure in their natural habitats (Martino et al. 2007; Rastogi et al. 2020). The sampled *P. tricornutum* strains are available in stock centers around the world, labeling the cells according to their nomenclature (accession number), for example Culture collection of Algae at The University of Texas at Austin, calling the strains UTEX. Martino et al. (2007) introduced specific library names (Pt1-10) for the first time, allowing an assignment and comparison of *P. tricornutum* strains and their corresponding accession numbers (Fig. S 1). Nevertheless, a clear assignment is only possible with the accession number. In line with the previous study, Rastogi and colleagues (2020) presented a more comprehensive study about the genetic, structural and functional diversity within the species. They used the previous library names and divided their chosen ten accessions into four genetic clades (A, B, C, D), each showing specific genetic and functional characteristics. One strain, namely Pt4 (CCMP2559) is clustered alone in clade B due to its outstanding characteristics, as has been proven by several studies (Rastogi et al. 2020, and references therein). The strains of *P. tricornutum* categorized as Pt4 are the genetically most diverse *P. tricornutum* strains, and were found in brackish water in a rock pool in Finland in 1951. In contrast, the most studied strains categorized as Pt1 were collected in coastal water in the UK around 1956 (Martino et al. 2007).

Diatoms are unicellular algae that are eposed to changing light intensities and light qualities. Thus, photosynthetic eukaryots have evolved short-term adaption mechanisms, like one of the most important protection mechanism non-photochemical quenching (NPQ), where not utilizes light energy is dissipated as heat (Goss and Lepetit 2015; Müller et al. 2001). As one example of high adaption to its natural habitat, the strain used in this study, Pt4 (UTEX 646) is believed to have lower NPQ capacity compared to Pt1 (CCMP632) (Kuzminov and Gorbunov 2016). Differences between growth behaviour and lipid metabolism within the species *P. tricornutum* are explained in detail later.

As described earlier, microalgae derived products are being highly discussed as replacement for common industrial animal products, e.g. fish oil (Kitessa et al. 2014). Besides being a renewable alternative to crude oil, they have developed a biosynthesis pathway that produces highly specific products. Especially diatoms that produce many high-value products have become the focus of research (D'Adamo et al. 2019; Hamilton et al. 2015; Wang et al. 2018). A bibliometric analysis of studies addressing microalgae can be found in Rumin et al. (2020), which presents the huge number of scientific publications about the characterization of *Phaeodactylum sp.* at the European level, by 2019 a total of 478 publications were counted.

In particular, the *P. tricornutum* strain Pt4 (UTEX 646) has become an object of interest, after its genome was sequenced in the year 2009 (Fig. 2), resulting in an increased number of publications worldwide. Compared to the bibliometric analysis at the European level for publications concerning the *Phaeodactylum* species (Rumin et al. 2020), approximately one fifth of all publications deal with this particular strain UTEX 646.

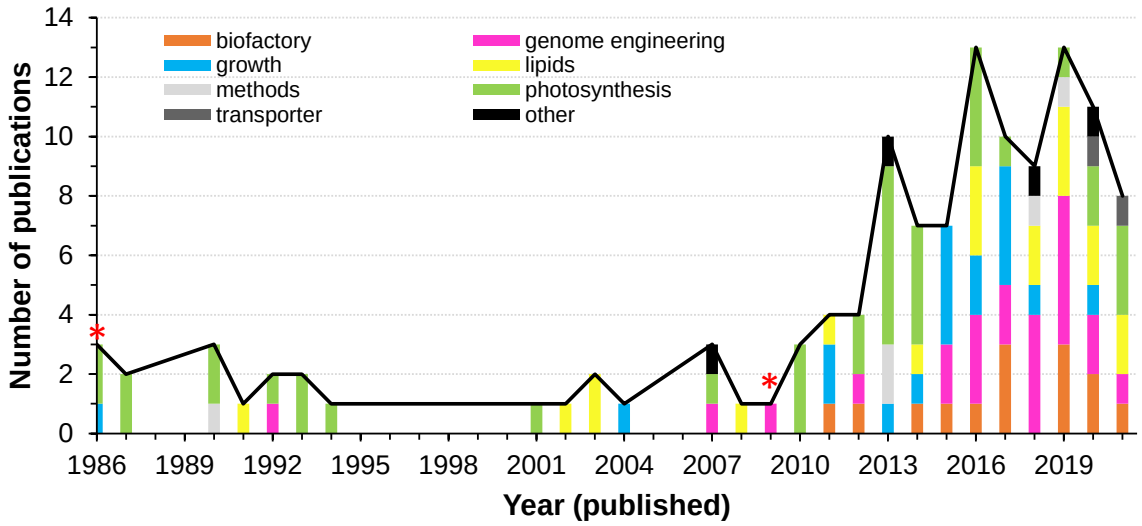

Fig. 2 Overview of publications using the *Phaeodactylum tricornutum* strain UTEX 646. Literature work using google scholar and the search keywords "UTEX 646" and "Pt4". Detailed list of publications and keywords found in supplementary (Tab. S 1). Years with asteriks included an important research study.

The industry applications for microalgae are diverse and some applications have been investigated using UTEX 646 as biofactory e.g. for the synthesis of antibacterial free fatty acids for drug resistant infections (Desbois et al. 2008), as degradation for polyethylene terephthalate (PET) (Moog et al. 2019) or as source for synthetic polyester from algae oil (Roesle et al. 2014). For most applications, the type of cultivation method is essential to achieve optimum biomass production. But also for high lipid algae, the manipulation of the lipid metabolism plays an important role in increasing both the biomass and the lipid yield.

1.2. Lipid metabolism

In this research *P. tricornutum* is to be optimized in both biomass productivity and lipid production; here I focused on the ω-3 fatty acids. The manipulation of the lipid metabolism has many possibilties (Hess et al. 2018), hence a comprehensive understanding of metabolic pathways is necessary to choose the best way. Because of a lack of information about metabolic pathways in *P. tricornutum*, the lipid metabolism will be explained on the basis of the knowledge of vascular plants and green algae. So far, some enzymes involved in the lipid metabolism in *P. tricornutum* have been characterized and an overview of the status quo is listed in Zulu et al., (2018). Additionally, information from genomic prediction in this research

field in *P. tricornutum* will be used to explain the metabolic pathways. The lipid metabolism can be summarized and split into four main steps (Fig. 3).

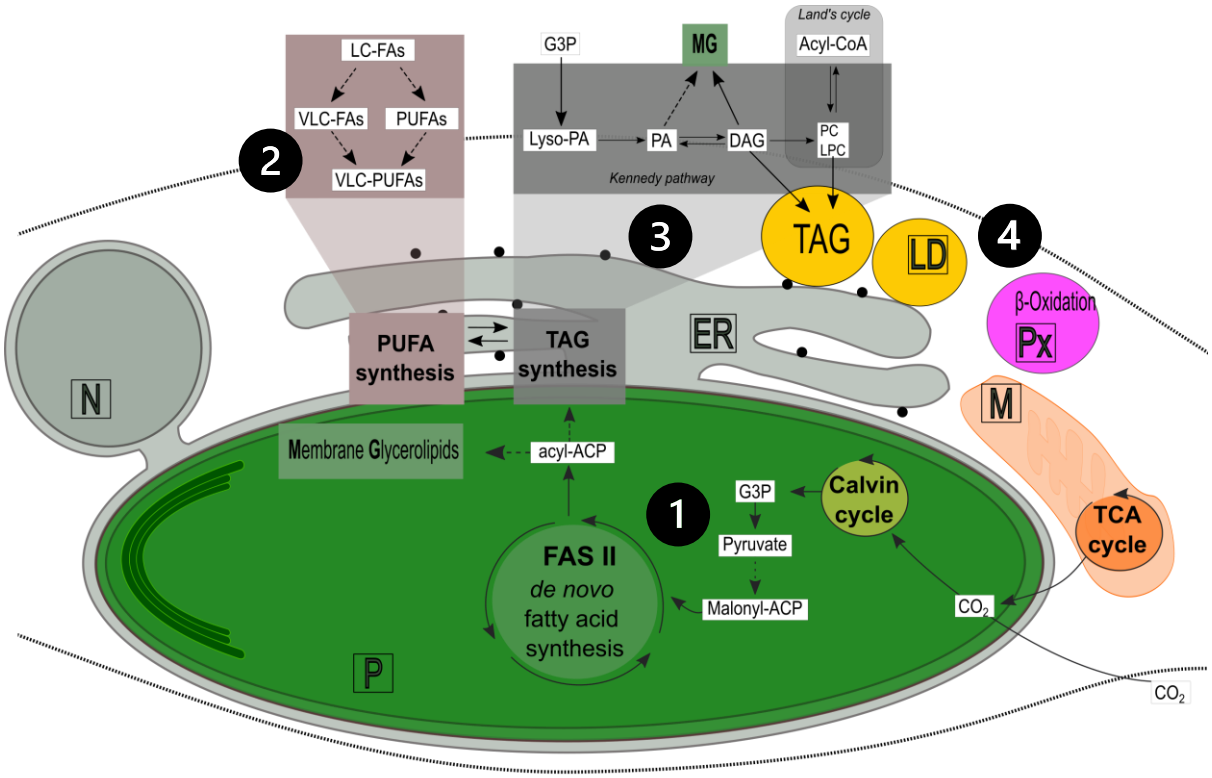

Fig. 3: Simplified overview of lipid metabolism in diatoms. Symbolized are following organelles: ER, endoplasmic reticulum; LD, lipid droplet; M, mitochondria; N, nucleus; P, plastid; Px, peroxisome. The numbers indicate the 4 steps of lipid metabolism that are described in the text: (1) *De novo* synthesis of fatty acids in the plastid; (2) PUFAs synthesis at the ER; (3) Glycerolipid synthesis in the plastid or the ER; (4) Glycerolipid breakdown and β-oxidation. Abbreviation used in this figure: ACP, acyl carrier protein; DAG, diacylglycerol; FAS, fatty acid synthase complex; G3P, glycerol 3 phosphate; Lyso-PA, lysophosphatidic acid; LPC, lysophosphatidylcholine; PA, phosphatidic acid; PC, phosphatidylcholine; PUFA, polyunsaturated fatty acid; TAG, triacylglycerol; TCA, tricarboxylic acid; VLC, very long chain. Dashed lines indicate that steps have been simplified. The figure is modified from Falciatore et al. 2020; Mühlroth et al. 2013; Zulu et al. 2018.

De novo synthesis of fatty acids in the plastid (Fig.3, Step 1)

Similar to vascular plants, in diatoms the fatty acid synthesis takes place in the chloroplast and starts with acetyl-CoA as precursor (Ke et al. 2000; Zulu et al. 2018). The acetyl-CoA biosynthesis in plants is well studied and localized in different organelles (summarized in Harwood 1996) , including a plastidial and a mitochondrial pool (Leonardi et al. 2005). In the first step of de novo fatty acid synthesis the enzyme, acetyl-CoA carboxylase (ACCase), converts acetyl-CoA to malonyl-CoA (Zulu et al. 2018). In the next reactions a multi enzyme complex, called fatty acid synthases (FAS), catalyzes four enzymatic reactions (Li-Beisson et al. 2010). In diatoms and plants it is a FAS II complex that is localized in the plastids (Dolch and Maréchal 2015; Ryall et al. 2003). FASII activity leads to the prolongation of the acyl chain with two carbons per cycle (Cycle=former mentioned four enzymatic reactions) and the

formation ends after seven cycles in the synthesis of C16:0-acyl carrier protein (ACP) (Li-Beisson et al. 2019). Further, C16:0-ACP has three possible pathways: (i) Considered as final step of fatty acid synthesis, it can enter the glycerolipids synthesis pathway, (ii) it can be released as free fatty acid by thioesterase (Zulu et al. 2018), or (iii) it can be further elongated to C18:0-ACP (Li-Beisson et al. 2019).

Polyunsaturated fatty acids (PUFAs) synthesis at the ER (Fig.3, Step 2)

In *P. tricornutum*, these saturated fatty acids (SFAs), C16:0 and C18:0 can be further modified by an enzymatic machinery, including desaturases and elongases (Arao and Yamada 1994; Dolch and Maréchal 2015). The results are monounsaturated fatty acids (MUFAs), long chain-Polyunsaturated fatty acids (LC-PUFAs; 16-18 carbons) and very long chain-PUFAs (VLC-PUFAs; ≥ 20 carbons), including the commercially important ω-3 fatty acids EPA (C20:5ω-3) and DHA (C22:6 ω-3). During the synthesis of VLC-PUFAs, fatty acid desaturases (FAD) and fatty acid elongases (ELO) use the ω-3 and ω-6 pathway to synthesize these fatty acids (Domergue, Zank et al. 2003). In figure 4 below, the combination of these pathways are shown and the proposed pathway for the synsthesis of EPA is highlighted (Sayanova et al. 2017). It is very likely that in *P. tricornutum* the synthesis of EPA is specialized, because only small amounts of the listed intermediates can be detected (Fig. 4; Domergue, Spiekermann et al. 2003).

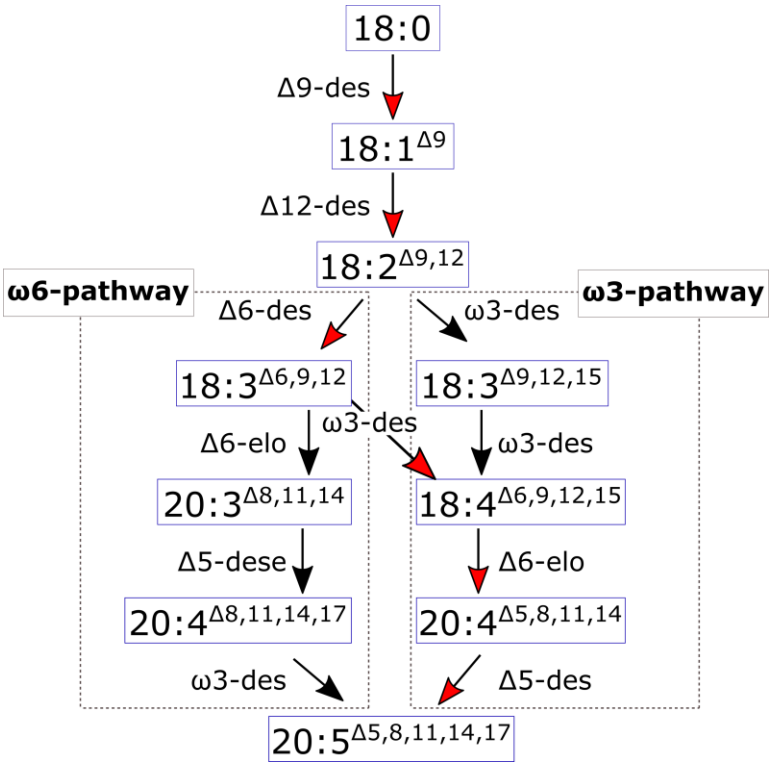

Fig. 4 Synthesis of polyunsaturated fatty acids in *Phaeodactylum tricornutum* simplified based on Domergue (2002). The proposed synthesis for the ω-3 fatty acid EPA (C20:5) is highlighted with red arrows.

Glycerolipid synthesis in the plastid or the ER (Fig.3, Step 3)

The synthesis of Glycerolipids starts with the esterification of free fatty acids to the backbone of glycerol 3-phosphate (G3P) and has been summarized for *A. thaliana* in detail (Li-Beisson et al. 2010). Glycerolipids are the most abundant acyl-lipids and can be divided into polar membrane glycerolipids if one or two fatty acids are esterified to glycerol and storage glycerolipids (also called neutral lipids) if three fatty acids are esterified to the glycerol backbone, forming triacylglycerol (TAG).

Both TAGs and membrane glycerolipids can be synthesized in the plastid (Kennedy-like pathway, formerly called prokaryotic pathway) or the ER (Kennedy pathway, formerly called eukaryotic pathway) (Guéguen et al. 2021), with the former one not being mentioned in detail in this summary. Due to latest investigations, the terms for these pathways have changed, replacing the former terms prokaryotic and eukaryotic pathway, due to misleading information (Sato and Awai 2017).

TAG *de novo* synthesis takes place in an acyl-CoA dependent pathway, the Kennedy pathway (Kennedy 1961) in the ER using acyl-CoA or in the plastid using acyl-ACP. As described previously, it starts with G3P and a transfer from one acyl-CoA at the *sn*-1 position results in lysophosphatidic acid (Lyso-PA). A second esterification at the *sn*-2 position gives rise to phosphatidic acid (PA) that can further be modified to phosphatidylglycerol (PG) or further

dephosphorylated at the sn-3 position to generate diacylglycerol (DAG). DAG is a precursor for the synthesis of most membrane lipids, including phosphatidylcholine (PC), phosphatidylethanolamine (PE), and betaine lipids. The last step of TAG synthesis from *de novo* synthesis ends in the esterification of a third acyl-CoA at the *sn*-3 position. Alternatively, fatty acids from existing membrane lipids can be used, enabling an intense lipid remodeling (Li-Beisson et al. 2010; Li-Beisson et al. 2019; Petroutsos et al. 2014). In organelles called lipid droplets, TAGs are accumulated in *P. tricornutum* in response to stress and are conserved amongst all eukaryotes (Jaussaud et al. 2020; Leyland, Zarka et al. 2020).

Glycerolipid breakdown and β-oxidation (Fig.3, Step 4)

It is very important for every organism to respond to environmental conditions. One known mechanism is the degradation of TAGs and membrane lipids. This lipid breakdown is called lipolysis and needs enzymes called lipases, yielding in free fatty acids and the glycerol backbone. The fatty acids are further catalyzed in the β-oxidation at the peroxisomes, producing acetyl-CoA (Li-Beisson et al. 2019). This effect can be easily achieved by changing the nitrogen content in the medium from low to high, resulting in a degradation and then resynthesis of membrane lipids (Siaut et al. 2011).

1.3. Environmental factors influence growth rate and lipid biosynthesis in *Phaeodactylum tricornutum*

The effects of environmental factors that influence growth and lipid accumulation in microalgae are diverse, although similarities are listed (Guschina and Harwood 2006; Li-Beisson et al. 2019). Some general regulatory mechanisms of microalgae regarding the lipid biosynthesis, including the response to environmental stress, have been recently summarized by Chen and Wang (2021). The next section gives a detailed overview about research in this field for *P. tricornutum* strains.

Salinity and Temperature

Kräbs and Büchel (2011) were able to show eurythermal and very euryhaline characteristics for three different *P. tricornutum* strains (Pt2, SAG 1090-1a;Pt8, NEPCC 640; Pt9, CCMP 633). Furthermore, they defined a growth-salinity range between 5 to 70% and a temperature range from 12 to 24°C, showing almost linear growth rates for these strains (Kräbs and Büchel 2011). Based on genetic and physiological studies on *P. tricornutum* strains (Martino et al. 2007; Martino et al. 2011; Rastogi et al. 2020), as discussed in section 1.1, it can very likely be assumed that the salinity tolerance differs between strains, according to their long-term selective pressure. In a long-term adaption experiment with Pt4 (CCAP 1052/6) and Pt1(CCAP 1052/1) these findings could not be supported (Gillard et al. 2021). In another study with Pt4

(UTEX 646) maximum biomass and lipid content were achieved at a salinity of 20% within the growth medium, while EPA content was highest at lowest salinity (5%) (Wang et al. 2018). In a study with an unknown strain from the culture collection MACC[1], lower salinity of 1.5% showed a decrease in fatty acid content (Qiao et al. 2016), suggesting different effects on lipid metabolism in *P. tricornutum* strains depending on the salinity. Temperature has also an effect on growth and lipid profile. Experiments with Pt7 (CCMP 1327) revealed that membrane lipid profile changes in accordance with the temperature, showing higher EPA levels at low temperatures (Dodson et al. 2014). Further data published by Jiang and Gao (2004) demonstrated higher PUFA content at low temperature and a maximal increase by 85% EPA of total fatty acids when cells are moved from a temperature of 25°C to 10°C (Jiang and Gao 2004). To conclude, *P. tricornutum* cells including Pt4 (UTEX 646), are very likely to change their membrane fluidity at low temperature (10°C), by incorporating higher amounts of EPA into their membranes (Sayanova et al. 2017). The optimum salinity differs among the strains of *P. tricornutum*.

CO_2 and pH-value

With a CO_2 concentrating mechanism (CCM) microalgae are able to prevent CO_2 limitation, avoiding e.g. biomass deficit (Giordano et al. 2005). In diatoms, a biochemical and a biophysical pathway exist (Matsuda et al. 2017), but for *P. tricornutum* the biochemical pathway does not play an essential role (Ewe et al. 2018). By biophysical means they either take up dissolved inorganic carbon (DIC) by a direct uptake through HCO_3^- transporters or CO_2 concentration mechanism is enabled by a passive CO_2 influx faccilitated by carbon anydrases and solubilization from the medium (Hopkinson et al. 2011; Matsuda et al. 2017). In light periods the pH value increases at cell surfaces (Chrachri et al. 2018), hence during growth the pH value in the medium increases accordingly. In general, the pH optimum for diatoms is at 8.1 at surface seawater (Goldman et al. 2017), while the pH range of *P. tricornutum* is between 6 and 9, with an optimum at 7.8 (Bitaubé Pérez et al. 2008). In a recent study the effect of pH and CO_2 concentration in the medium was investigated regarding the growth rate and the lipid content, showing an increase in pH for low and medium CO_2 concentrations (0.0015% and 0.035%, respectively) whereas high concentration (0.15%) lead to low pH values. Furthermore, they proved for the used strain, screened from the East China Sea, that growth rate and lipid content increased significantly with high CO_2 concentrations (Wu et al. 2015). For Pt1 (CCMP 2561) researchers demonstrated, that the increased lipid content is very likely to be related to

[1] Mosonmagyaróvár Algal Culture Collection (MACC)

changes in pH levels. Alkaline stress at pH 9 showed the highest lipid accumulation, but also the addition of $NaHCO_3$ led to higher lipid content (Mus et al. 2013). High CO_2 concentrations in the gas phase (0.64%) promoted the growth rates in *P. tricornutum* strain Pt4 (UTEX 646) at pH values of 7 (Yu Guilan et al. 2017). In summary, higher CO_2 concentrations favor growth in *P. tricornutum*, but the correlation between the lipid accumulation at higher CO_2 concentration and dependence on pH values still need to be investigated in Pt4 (UTEX 646).

Light

Light is an essential source for obligate photoautotroph organisms, using light energy to drive the process of photosynthesis. The effect of light on growth and lipid metabolism is diverse (summarized in Guschina and Harwood 2006), hence the light conditions are subdivided into further categories: *(i)* light intensity, *(ii)* light quality and *(iii)* light period.

(i) Focusing on *P. tricornutum* (UTEX 646), changes in light intensity influenced the growth and lipid content, showing highest lipid abundance and highest growth rate at 300 µmol photons m^{-2} s^{-1} during the exponential growth phase. At higher light intensities (1000 µmol photons m^{-2} s^{-1}) a negative effect, probably due to light stress, was detectable (Heydarizadeh et al. 2019). Other researchers detected a negative effect on growth at lower intensities. With a light intensity range from 30 to 180 µmol photons m^{-2} s^{-1} a decrease in biomass production was already observed at 120 µmol photons m^{-2} s^{-1}. The highest lipid content was measured at 120 and 180 µmol m^{-2} s^{-1}, but associated with a decrease in EPA content (Wang et al. 2018). In CO_2 starved cells a switch in light intensity from high to low light intensities showed similar amounts of lipids and proteins compared to cells moved into medium light (Heydarizadeh et al. 2017). For another *P. tricornutum* strain increased light intensities between 50 and 150 µmol photons m^{-2} s^{-1} showed higher biomass concentrations and a significant increase in DHA per total fatty acids (Qiao et al. 2016). In two further *Phaeodactylum* strains light saturation was measured at 100 µmol photons m^{-2} s^{-1} (Geider et al. 1985; Remmers et al. 2017). To conclude, the optimum varies within the strains of *P. tricornutum.*

(ii) Light quality was investigated for example in the chlorophyte *Chlamydomonas reinhardtii* and showed different lipid accumulation depending on the wavelength, using blue, white-yellow, or red-orange light. For this Chlorophyte the red-orange light resulted in highest biomass accumulation and favored lipid accumulation (Li et al. 2021). In line with this study, in a *P. tricornutum* strain red light also promoted biomass production. Cells grown in red light until the end of the exponential phase and then switched to white light exposure showed an increase in biomass production and lipid content by 2 and 2.3-fold respectively, compared to cells grown solely in white light during the experiment (Sharma et al. 2020). Another study investigated biomass accumulation and fucoxanthin production in relation to light intensity and quality for Pt7 (CCMP 1327). Highest biomass and fucoxanthin production were recorded for a two phase

culture approach, using different red and blue light shifts (Yang and Wei 2020). Shorter wavelength in the blue spectrum led to a higher production of TAGs whereas longer wavelength in the red spectrum increased the synthesis of EPA (Duarte et al. 2021). The amount of research in this field is still rare, and to the best of my knowledge, no research has been conducted in Pt4 (UTEX 646)

(iii) In diatoms growth and lipid metabolism are also influenced by the light period, but the results of studies are controversial. In the diatom *Cyclotella meneghiniana* data suggest that cells grown for a 16h light 8h dark period have their highest lipid accumulation during darkness, together with highest EPA values (Sicko-Good et al. 1988). Controversially, a transcriptional analysis of about 4500 genes of Pt1 showed a different expression pattern during the 16:8h light dark cycle. For example genes involved in fatty acid biosynthesis showed maximum expression levels after the onset of light, whereas at the end of the light period this expression was at its lowest (Chauton et al. 2013). A comparison between a 16:8 h light dark period and continuous light (24 h) showed in Pt4 (UTEX 646) an accumulation of ω-3 fatty acids, especially EPA under the latter condition (Hamilton et al. 2015). In line with previous effects of light intensity and light quality, differences in growth and lipid productivities are observed within the species of *P. tricornutum*. First investigations for Pt4 (UTEX 646) showed a higher content of EPA during light periods (Hamilton et al. 2015).

Phosphate

Phosphorus (P) is a component of e.g. nucleic acids or phospholipids and is indispensable for all living organisms, including microalgae. Therefore, it is not surprising that Pt1 (CCAP 1055/3) cells studied under P deprivation showed a complex adaption to P stress. First P-storage forms are consumed, followed by a degradation of phospholipids. Finally, phospholipids are replaced by nonphosphorous lipids (Alipanah et al. 2018). In accordance with the findings of Alipanah and colleagues, it was found that intracellular membranes, with the exception of chloroplast membranes, were disrupted and disorganized in a Chinese strain (FACHB-863) due to P deprivation (Yang et al. 2014). In the same study, a transcriptome analysis in combination with a biochemical investigation revealed that genes coding for enzymes involved in β-oxidation were downregulated. Furthermore, they were able to show that neutral lipids were increased by 60% after 24h and the number and size of oil bodies were increased (Yang et al. 2014). In conclusion, the response to P deprivation in different *Phaeodactylum* strains revealed variations among them, possibly due to different efficiency in P storage or signaling and metabolic processes (Abida et al. 2015).

For the strain in the focus of this study, Pt4 (UTEX 646), there appears to be a phospholipid recycling mechanism under P deprivation (Huang et al. 2019). In addition, less EPA was found in neutral lipids under P limitations (Huang et al. 2019).

Nitrogen

The effect of Nitrogen (N) deprivation on the lipid accumulation in microalgae is a focus of research (for review see Goncalves et al. 2016; Hu et al. 2008), amongst others also in diatoms (Abida et al. 2015; Hamilton et al. 2014; Huang et al. 2019; Popko et al. 2016; Remmers et al. 2017; Remmers et al. 2018; Rodolfi et al. 2017).

In diatoms compared to chlorophytes the response to N stress condition showed a prominent remodeling of lipid metabolism (Falciatore et al. 2020). Based on transcriptome, proteome and metabolome data obtained during N limitation conditions, Remmers and colleagues (2018) revealed insights into the molecular effect of nitrogen starvation in Pt3 (SAG 1090-b). The data supported results of former studies, showing that lipid remodeling may substantially contribute to TAG distribution but most likely be limited by carbon flux (Remmers et al. 2018). In the same strain, experiments during nitrogen starvation at different light intensities showed that highest values of TAG yield (25% of dry weight) occurred during a light intensity of 60 µmol photons m^{-2} s^{-1}, whereas at light intensities over 100 µmol photons m^{-2} s^{-1} the yield was significantly lower (Remmers et al. 2017). Focusing on Pt4 (UTEX 646), cells stopped growing after 2 days of N depletion, independent of increasing the light intensitiy. The changes in light intensity during N depletion had an effect on the total fatty acid content that increased from 70% to 170%, respectively (Popko et al. 2016). SFA and MUFAs were accumulated under N depletion whereas the proportion of EPA (C20:5, ω-3) (Wang et al. 2018) and DHA (C22:6, ω-3) were both reduced (Popko et al. 2016). In contrast, in Pt1 (CCAP 1055/3) the incorporation of EPA in TAGs increased during N and P starvation (Abida et al. 2015) Pt4 (UTEX 646) cells showed only minor amounts of EPA in TAGs.

In general, during N deprivation TAG content increases immensely, but it could be shown that even within the species *Phaeodactylum*, the TAG accumulation in response to N limitation varies significantly (Abida et al. 2015; Rodolfi et al. 2017). In line with other strains, in Pt4 (UTEX 646) EPA is incorporated into TAGs during N and P starvation only in small amounts (Huang et al. 2019; Popko et al. 2016). Interestingly, the acyl-CoA pool is rich in EPA under normal conditions, as well as under N starvation and high-light intensities (Hamilton et al. 2014; Popko et al. 2016).

1.4. Growth system and trophic mode- what are the possibilities and what is the current state in cultivating *Phaeodactylum tricornutum* for industrial usage?

Most of the former listed studies have been conducted in batch cultures or small photobioreactors (PBRs) with light as main energy source. Those algae are mostly photoautotroph, using light as energy source (photosynthesis) to fix CO_2 (inorganic carbon) to synthesize organic compounds. In contrast, heterotrophic organisms, e.g. diatoms, grow in darkness and replace the fixation of atmospheric CO_2 with organic carbon sources, like glucose or acetate in the media (Lewin 1953). Another trophic mode is mixotrophy which is a combination of photoautotrophy and heterotrophy. Mixotrophic cells use both, atmospheric CO_2, and organic carbon sources to gain energy. The majority of diatoms are photoautotroph, but the metabolic strategies are diverse (Falciatore et al. 2020).

Photoautotroph versus heterotroph

The mechanism behind photoautotrophy is the photosynthesis - a well-known process that is used by plants, algae and some bacteria. In microalgae, in particular diatoms, a lot of research has been conducted during the last 20 years to shed some light on the complex mechanism (for a recent review of diatoms see: Falciatore et al. 2020). Obligate photoautotroph organisms are only able to use light as energy source, instead of organic carbon. In some of these microalgae possible causes for this limitation are suggested, such as for example an inefficient uptake of certain substrates (e.g. glucose) or the incompleteness in carbon metabolism (Chen and Chen 2006; and reference herein).

In industry, common culture systems for photoautotrophic organisms are open ponds or closed PBRs using either natural sunlight or artificial illumination (Apt and Behrens 1999). Each system has some advantages and disadvantages (for a review see Apt and Behrens 1999). Open ponds are most suitable for microalgae with extraordinary requirements and tolerances to extreme environmental conditions, e.g high pH or very high salinity (Apt and Behrens 1999). Outdoor phototrophic growth systems such as closed PBRs or open ponds are influenced by diurnal and seasonal environmental changes, leading among others, to variations in biomass accumulation (Rodolfi et al. 2017). In *P. tricornutum* strain Pt4 products for biomanufacturing have only been synthesized in photoautotrophic culture systems (Tab. 1).

Tab. 1 Towards industrial usage of products derived from *Phaeodactylum tricornutum* UTEX 646. With following abbreviations: RP: Raceway pond; HF PBR: horizontal fence photobioreactor; HB PBR: Hanging bag photobioreactor; F: Flask

Product class	Products for Biomanufacturing	Strain	Cultivation system	Product Yield/Productivity Reported	Ref
Lipids	DHA	(r)	RP (1250 l) HF PBR (550 l)	2.6 µg/mg dry weight (10.3% of total fatty acids) 6.4 µg/mg DW (12.3 % of total fatty acids)	1
	EPA	(r)	RP (1250 l) HF PBR (550 l)	25% of total fatty acids 8.7 % of total fatty acids	
		wt	HB PBR (20 l)	62.55 mg/l	2
Terpenoids	Fucoxanthin	wt	HB PBR (20 l)	8.32 mg/l	
Heterologous compounds and proteins	Human igGαHBSAg antibody against hepatitis B virus	(r)	F (≤1 l)	0.0021% DW (8.7% total soluble protein)	3
	IgG1/kappa Ab CL4mAb antibody against hepatitis B virus	(r)	F (≤1 l)	2.5 mg/L (secreted)	4
	Monoclonal IgG antibodies against the nucleoprotein of Marburg virus	(r)	F (≤1 l)	2 mg/L (secreted)	5
	Polyethylene terephthalate	(r)	F (≤1 l)	n/a	6
		(r)	F (≤1 l)	n/a	7
Other	Polyester-17/19.17/19	wt	F (10 l)	n/a	8

References:1: (Hamilton et al. 2015); 2: (Wang et al. 2018); 3: (Hempel, Lau et al. 2011); 4: (Hempel and Maier 2012); 5: (Hempel et al. 2017); 6: (Moog et al. 2019); 7: (Schnitzler et al. 2021); 8: (Roesle et al. 2014)

Th highest volume of cells was cultivated by Hamilton et al. (2015) using either 1250 l open ponds or 550 l PBRs, both located indoors. They used a recombinant strain of UTEX 646 optimized for the synthesis of DHA. In the open pond higher EPA content was achieved (25% of total fatty acids), but DHA content was lower with 2.6 µg/mg dry weight, compared to PBR experiments (Hamilton et al. 2015). Characteristics of high scale phototrophic systems regarding photosynthetic physiology and biomass partitioning have been investigated by Jallet et al. (2016). They were able to show changes in carbon partitioning in the course of a day/night cycle, such as higher TAG yield at the end of the light period. In addition, the studied strain CCAP 1055/1 showed low NPQ levels (Jallet et al. 2016). In a recent review by Butler et al. (2020) products derived from all *P. tricornutum* strains have been summarized, showing diverse educts. The majority of these educts have been synthesized photoautotrophically, only few used mixotrophic mode as culture system (Tab. S 2).

Interestingly, algae have also been found in environments where no photoautotrophic metabolism is possible, in particular underneath ice layers or buried in sediments (Morales-Sánchez et al. 2015, and reference herein). Algae found in those light-deprived environments can use solely organic sources for their metabolism, hence can be associated to the group of

heterotrophic microalgae (Neilson and Lewin 1974), which can be further be distinguished in obligate and falcultative heterotrophs. Obligate heterotrophs lost their ability to photosynthesize, whereas facultative heterotrophs use photosynthesis and respiration metabolism separately. In general, the list of heterotrophic microalgae is short. Morales-Sánchez and colleagues (2015) showed a list of only 19 studied microalgae under heterotrophic condition, including the diatom *Nitzschia laevis* (Tan and Johns 1996). Several studies have focused on these strain, showing high EPA yields under heterotrophic conditions (Wen and Chen 2000; Wen and Chen 2001). In a recent study, researchers present insights into glucose-induced trophic transition, analyzing *N. leavis* on transcriptomic and metabolic levels, while glucose was added (Mao et al. 2021). In detail, the results suggest that cells cultured with glucose induce upregulation of enzymes associated with e.g., fatty acid elongation, explaining high EPA content (Mao et al. 2021). It is generally known that plasma membrane transporters are needed for the uptake of external carbon sources (e.g. glucose). There is a tremendous amount of current research focusing on glucose transporters in eucaryotes, especially for human glucose transporters (GLUT) (for review see Holman 2020; Mueckler and Thorens 2013). One main reason for this is the relevance of the glucose transporter for diseases like diabetes. Therefore, screening systems for GLUT-targeting drugs have been established (Schmidl et al. 2020). To overcome the limited number of algae that can be used for heterotrophic cultivation, genome editing has been used in some algae (Doebbe et al. 2007; Hamilton et al. 2016; Waissman-Levy et al. 2019). For example, Zaslavskaia and colleagues (2001) were able to show that *P. tricornutum* UTEX 646 can be trophically converted by the expression of a glucose transporter gene (*GLUT1*). In particular, they successfully integrated the human *glut1* transporter gene into genome of *P. tricornutum* and observed heterotrophic growth for these transformants (Zaslavskaia et al. 2001). In 2016 similar results were reached, using the glucose transporter gene from *Physcomitrella patens* (*Ppglut1*), enabling efficient growth in the dark on a glucose concentration of between 1 and 2% (Hamilton et al. 2016). In dark conditions the mutant overexpressed both, the *Ppglut1* and the ∆5-elongase gene from *Ostreococcus tauri* (OtElo5), and showed lower levels of DHA while EPA levels were not reduced compared to light conditions (Hamilton et al. 2016).

Mixotroph

In contrast to facultative heterotrophs, mixotroph organisms can use both light and carbon sources only in the presence of light. During this trophic mode, respiration and photosynthesis are active simultaneously. In general, the research regarding mixotrophic mode in diatoms is rare (Bailleul et al. 2015; Villanova et al. 2017), but a general review article has been published recently (Villanova and Spetea 2021).

Studies on different *P. tricornutum* strains showed various carbonaceous compounds, that can be taken up and metabolized, including acetate, glycerol, fructose and glucose (Liu et al. 2009; Villanova et al. 2017). Recently, scientists used birch and spruce hydrolysates as organic carbon source and observed high biomass productivity in *P. tricornutum* Pt4 (UTEX 646) with 0.254 g $l^{-1}day^{-1}$ (Patel et al. 2019). The most research is done using glycerol as organic carbon source, probably because it enables the most efficient growth compared to other organic carbon sources in many strains of *P. tricornutum* (Cerón García et al. 2000; 2005; 2006; Liu et al. 2009). Cerón Garcí and colleagues optimized the growth and fatty acid content by using glycerol and periodically supplemented urea, achieving 1.52 g $l^{-1}day^{-1}$ biomass and 43.13 mg $l^{-1}day^{-1}$ EPA- the highest EPA productivity for Pt3 (UTEX 640) (Cerón García et al. 2005).
The metabolism behind the carbon and nitrogen assimilation is complex and shows differences between microalgae (for a detailed review see: Perez-Garcia et al. 2011). Hence further research is needed to elucidate it and understand the physiological functions.
Mixotrophic growth conditions for a *P. tricornutum* strain (IOCAS-001) were analyzed by a ^{13}C-labeling experiment using [^{13}C]glycerol, and cells incubated at different growth conditions villanitrogen-limited response and photorespiration is involved in this pathway (Huang et al. 2015). In comparison, another isotope labeling experiment in Pt1 with glycerol and glucose showed different results (Zheng et al. 2013). Most importantly, only the latter Pt1 was able to take up labeled glucose, whereas *P. tricornutum* strain IOCAS-001 showed no uptake. Huang and colleagues suggest that there might be differences in carbon metabolism depending on the ability to utilize glucose (Huang et al. 2015). In conclusion, mixotrophy is reported to stimulated both biomass and lipid production in diatoms. This trophic mode combines the advantages of the highly efficient photosynthesis in light and the utilization of carbon sources to trigger both biomass and lipid production.
In order to further improve growth of *P tricornutum*, genome editing is a promising tool. As a result, the final goal of microalgae as biofactory in industry can be achieved.

1.5. Membrane transporter in *Phaeodactylum tricornutum*

Glucose transporters, or general membrane transporters are integral membrane proteins (IMPS) that are not well studied in diatoms. From the database TransportDB 2.0 a collection of 548 membrane transporters is predicted for *P. tricornutum* CCAP 1055/1 (Elbourne et al. 2017). However, an unknown number is localized at the plasma membrane in *P. tricornutum* strains. For a few years now, some plasma membrane transporters have been partially characterized or proven to be localized at the plasma membrane (Tab. S 3, Dell'Aquila et al. 2020; Liu et al. 2016; Matsui et al. 2018; Morrissey et al. 2015; Nakajima et al. 2013; Oakley 2010; Santin et al. 2021; Villanova et al. 2017). For example, a urea transporter (JGI_Pt_20424), localized at the plasma membrane, was partially characterized by Oakley

(2010). An overexpression mutant of the aforementioned urea transporter gene revealed increased urea uptake in this engineered strain (Oakley 2010). In addition, two aquaporines PtAQP1 and PtAQP2 (Matsui et al. 2018), an HCO_3^- transporter (SLC4-2) (Nakajima et al. 2013) and several phosphate transporters (Dell'Aquila et al. 2020) have been successfully confirmed to be localized at the plasma membrane. So far, no common targeting motif or information about targeting sequences or pathways are known. In contrast, the research in mammalian and plant cells is more advanced and is summarized briefly in the next paragraph. The factors that alter the targeting of IMPs are diverse (Cosson et al. 2013; Shao and Hegde 2011; Spiess et al. 2019) and some of them remain unknown. Hence, targeting prediction and research in this field is complex.

Similar to the secondary chloroplast targeting pathway (Bolte et al. 2009), all IMPs sorted to the ER need a special sequence, mostly N-terminal. Targeting can then be differentiated by either a co-translational pathway by the signal recognition particle (SRP) or SRP-independent. A guideline for the targeting pathways and the corresponding signal sequence is the number of transmembrane domains of the IMP (for review see: Shao and Hegde 2011; Spiess et al. 2019). For example, tail-anchored and very small IMPs (mostly only one transmembrane domain) possess a signal peptide, a cleavable sequence at the N-terminus. They are addressed to the plasma membrane posttranslationally via the SRP-independent pathway (Berndt et al. 2009; Shao and Hegde 2011).

Multi-spanning IMPs, e.g. transporters of the major facilitator superfamily (MFS) (Pao et al. 1998) often use the SRP-dependent pathway, thus requiring co-translational insertion and a signal anchor as targeting sequence. In contrast to signal and transit peptides in secondary chloroplast transport mechanisms across the plastid membranes (Bolte et al. 2009), the signal anchor in IMPs is part of the transmembrane domain. During co-translational insertion in the ER membrane it serves as an anchor, hence is not cleaved (Berndt et al. 2009; Shao and Hegde 2011). After being inserted at the ER membranes as they are synthesized, polytopic IMPs have to be transported to the plasma membrane. In higher plants, conserved N-terminal di-acidic and di-hydrophobic motifs were found to be a recognition motif for coat protein II, the insertion into vesicles and the subsequent transport to the golgi apparatus (Luschnig and Vert 2014; and reference herein). Investigations in *Zea mays* observed that for aquaporines a di-acidic motif is not sufficient to trigger the ER export (Chevalier et al. 2014). Specific mutations in the transmembrane helices 3 (TMs) showed a conserved LxxxA motif. The same motif was also found in PtAQP1 of *P. tricornutum*. There are indications that it is involved in exocytosis, although no di-acidic motif was found (Matsui et al. 2018). In conclusion, it is very likely that, also in diatoms, the targeting signals are more diverse in multi-spanning membrane proteins compared to single-spanning proteins localized at the plasma membrane.

2. Aim of this thesis

P. tricornutum is a natural producer of high-value products, like ω-3 fatty acids, and therefor of biotechnological importance. The aim of this thesis is to improve the potential of the oleaginous alga by molecular and physiological approaches. The overall goal is to increase the lipid content of *P. tricornutum* cells in an economically sensible way by increasing both the production of lipids (here: ω-3 fatty acids) with a concomitant increase of the cell dry weight (dry biomass per culture volume).

The lipid metabolism can be influenced by changing the culture condition of the cells. Therefore, different culture media and its impact on the growth and lipid content of wildtype cells were investigated.

In industrial applications there is a need for stable and robust strains with improved biomass production in culture systems like PBRs.

Therefore, the second goal is to use genetic engineering to improve the growth by inserting a heterologous glucose transporter gene into the genome of *P. tricornutum*.

Chapter I: Improving the growth of *Phaeodactylum tricornutum* using genetic engineering - screening and characterization of mutants expressing a heterologous HUP1 glucose transporter

3. Introduction (Chapter I)

Diatoms like *Phaeodactylum tricornutum* have been used for heterologous protein expression (e.g.: Castell et al. 2021; Fabris et al. 2020; Hempel, Bozarth et al. 2011; Hempel, Lau et al. 2011; Shemesh et al. 2016) due to the accessibility of genetic engineering tools and its natural content of high-value products, like ω-3 fatty acids or fucoxanthin (Falciatore and Bowler 2002). After the genome was sequenced in 2008 (Bowler et al. 2008), the availability of tools, such as the choice of promoter, increased significantly (Erdene-Ochir et al. 2016; Erdene-Ochir et al. 2019; Erdene-Ochir et al. 2021; Kadono et al. 2015; Seo et al. 2015; Watanabe et al. 2018). One can divide the different types of promoters into endogenous versus heterologous promoters and constitutive versus regulatory ones. The native nitrate reductase (NR) promoter has been widely studied and used for heterologous protein expression e.g by overexpression of a human antibody or a *Haematococcus* oil globule protein (Hempel, Lau et al. 2011; Shemesh et al. 2016). However, the disadvantage is the exogenous nitrogen source that is required to enable high expression. An example of an heterologous promoter is the *Chaetoceros lorenzianus* -infecting promoter, CIP1 (Kadono et al. 2015), showing a protein expression depending on the growth stadium (Erdene-Ochir et al. 2016; Kadono et al. 2015). Recently, analysis suggests that, similar to the frequently used promoter of the light harvesting protein fcpA (Zaslavskaia et al. 2000), the CIP1 promoter is also light dependent (Erdene-Ochir et al. 2021). However, native promoters such as the promoter of the glutamine synthetase (GLNA) gene (Erdene-Ochir et al. 2016) and the glyceraldehyde-3-phosphate dehydrogenase (GapC1) gene (Erdene-Ochir et al. 2021) seem to promote a higher constitutive protein expression.

Controversialy results about the promoter activity and the resulting protein expression of engineered lines suggest that the choice of promoter is of relevance and the yield of protein expression also depends on the gene-promoter combination (Pudney et al. 2019).

A high (recombinant) protein expression, simultaneously with the efficient growth of microalgae in industrial application systems, offers a viable and eco-friendly production of substances. Heterotrophic microalgae cultivation has many advantages in growth systems, e.g. no light requirements, hence no self-shading effect with higher cell densities, enabling a significant increase in cell growth as well as protein and lipid productivity (Morales-Sánchez et al. 2015). The required characteristics of strains for heterotrophic cultivation are listed by Chen and Chen

(2006). Briefly summarized, they mentioned the following criteria: (i) capable of cell division and active metabolism without light, (ii) culture media, including carbon sources that are easy to sterilize, (iii) adaptation to fast changing environments, and (iv) unaffected by hydromechanical stress. Few algae are naturally capable of heterotrophic growth and some fit the aforementioned criteria (Apt and Behrens 1999). Species of *Chlorella* belong to the small number of microalgae that can grow on glucose in the dark and have been used for fermentation techniques (Lee 2001; Liu and Hu 2013). Giving one example from Japan and Taiwan, growth in fermenters of *Chlorella* yielded an annual production of around 1100 tons biomass (Liu and Hu 2013 and reference herein).

The hexose /H^+-symporter HUP1 of the Chlorophyte *Chlorella kessleri* belongs to the MFS and is a well-known transporter (Tanner 2000 and references therein). Within the MFS group, the family of sugar porters is comprised of 12 transmembrane helices (Pao et al. 1998) and both the C-terminal and the N-terminal are inside the cytoplasm (Caspari et al. 1994). In order to define the structure and function of this glucose transporter, substrate binding and translocation have been investigated (Caspari et al. 1994; Graßl et al. 2000). For example, the deletion of an exclusiv motif of four amino acids HWFW at the C-terminal leads to a decreased function of the protein (Graßl et al. 2000). Furthermore, studies revealed a glucose induced expression in *C. kessleri* (Komor and Tanner 1971) and a transport capacity of monosaccharide and protons close to 1:1 at a pH of 6.0 - 6.5 (Komor and Tanner 1974). Uniporters like the glucose transporter from human erythrocytes GLUT1 are known to need enhanced external glucose concentrations (Mueckler et al. 1997), whereas hexose /H^+-symporters such as HUP1 from *C. kessleri* transport glucose using a proton gradient. Hence, it was not glucose concentrations, but pH that influenced the activity of the transporter (Komor and Tanner 1974).

In this study I investigate the heterologous expression of HUP1 in *P. tricornutum* to improve biomass accumulation under low glucose concentrations. I tested different promoters to find the best gene promoter combination and analyzed their functionality in *P. tricornutum* in selected transformants. With the results of this study, I want to improve the potential of this oleaginous alga as a biofactory for homologous and heterologous protein expression.

4. Material & Methods (Chapter I)

4.1. Culture and growth conditions

4.1.1. Chlorella kessleri

In the literature, synonyms are used for the chlorophyte *Chlorella kessleri*, namely *Parachlorella kessleri* and *Chlorella vulgaris* (Algaebase: ID=59343), the most common species name *C. kessleri* will be used in this study. From the culture collection of algae at Goettingen university *C. kessleri* (SAG 27.87) was ordered and once used for the amplification of the *hup1* gene. It was cultivated in 300 ml culture tubes at 28°C in Basal medium with peptone (SAG, medium recipe, vers. 03.2007). Under constant air bubbling cells were grown for 14 days under a light intensity of 100 µmol photons $m^{-2} \cdot s^{-1}$ with a 16-hour light/8-hour dark cycle. Unless stated otherwise, this natural circadian rhythm was used for further growth experiments.

4.1.2. Phaeodactylum tricornutum

Different strains of the model organism *P. tricornutum* were categorized in library names Pt1-10, based on genetic and phenotypic characterization (Martino et al. 2007). Wildtype and mutant strains of UTEX 646 (Pt4), from the culture collection of algae at university of Austin, were grown in 100 ml flasks in modified ASP medium (Provasoli et al. 1957). Due to the supplementation of organic carbon sources, bacterial contamination during growth is very likely. Thus, to guarantee axenic culture conditions, the medium was further supplemented with an antibiotic cocktail (kanamycin [100 µg/ml], streptomycin [100 µg/ml] and penicillin [100 µg/ml]). Under the aforementioned natural circadian rhythm (4.1.1), cultivation took place at 18°C under a controlled CO_2 value of 480 ppm and light intensities of approximately 30 µmol photons $m^{-2} \cdot s^{-1}$ white light. Instead of bubbling, cells were shaken at 100 to 150 rpm. The growth was monitored using a plate reader (Tecan, 10M Spark) by measuring the optical density at 750 nm (OD_{750} nm). Furthermore, as a control two already characterized mutants of *P. tricornutum* were cultivated, namely T-eGFP and Glut1-17. T-eGFP was provided by Dr. S. Jäger (University Frankfurt). This mutant expresses cytosolic GFP under the control of the fcpA promoter. The mutant Glut1-17 (hereinafter referred to as Glut1) was provided by Prof. P. Kroth (University Konstanz). This mutant expresses a human glucose transporter as characterized by Zaslavskaia and colleagues (Zaslavskaia et al. 2001).

4.2. Generating Hup1 transformants of *Phaeodactylum tricornutum*

4.2.1. Amplification of the glucose induced *hup1* gene and cloning into chosen expression vectors

As mentioned earlier, hexose/ H^+-symporter can be induced by glucose, thus 500 mM glucose was added at the late exponential phase and cells of *C. kessleri* were cultivated for 72 h in the dark. With the help of molecular methods, the gene was isolated as follows: To avoid alteration in splicing I worked with cDNA, thus RNA was isolated using the ROTI®Quick-Kit (2014, Roth). Following the instructions, 50 ml of cell material was harvested (5000 x g, 10 min, 4°C) and washed with 1 ml of ddH_2O (10000 x g, 5 min, 4°C) to clean the cell material from salts. Afterwards, cDNA was synthesized according to the manufacturer's protocol using the RevertAid First Strand cDNA Synthesis Kit and Oligo $(dT)_{18}$ primers (Thermo Scientific).
For *in situ* localization study an N-terminal sequence of the *hup1* gene (aa 1-48), and for further growth experiments the full-length *hup1* gene (NCBI, accession no.: X55349.1; Komor and Tanner 1971), were amplified using the Phusion™ High-Fidelity DNA Polymerase (Thermo Scientific) and the gene-specific primers (Tab. 2).

Tab. 2 List of primer used in this study for creating expression vectors.

Name	Sequence (5'-3')	Purpose
Ck_a02p_pPHAN	TACCCGGGGATCCTCTAGATCACCCAGCAGTACAACA	-Cloning of pPHAN-HUP, pPHAT-eGFP-SP and pPHAT-eGFP-HUP -Amplification of N-terminal sequence of *hup1* gene (aa 1-48) and full-length *hup1* gene
Ck_e02m_pPHAN	CCTGCAGGTCGACTCTAGATAAGAGCGCCACTGCCCA	-Cloning of pPHAN-HUP -Amplification of full-length *hup1* gene
HF GFP-pPHAN fw	TCGACCTGCAGGCATGCAAGCTTCTCTCGAGATGGTGAGCAA	-Cloning of pPHAN-eGFP -Amplification of eGFP
HF GFP-pPHAN rv	TTAAAGTAAATTGAAGCTATTTACTTGTACAGCTCGTCCATG	-Cloning of pPHAN-eGFP - Amplification of eGFP
CkHUPSP_GFP_e01m_pPHAT	GCCCTTGCTCACCACGTCGAACTTCATCGCCTTTGACAGCT	-Cloning of pPHAT-eGFP-HUP -Amplification of full-length *hup1* gene
CkHUP_GFP_e01m_pPHAT	GCCCTTGCTCACCACGTCGACAGTCACACCGTTGTCATAGC	-Cloning of pPHAT-eGFP-SP -Amplification of N-terminal sequence of *hup1* gene (aa 1-48)
HF SP+Hup+GFP fw	TCGACCTGCAGGCATGCAGCACATAGCACTCCCTTACATC	-Cloning of pPHAN-eGFP-HUP and pPHAN-eGFP-SP -Amplification of N-terminal sequence of *hup1* gene (aa 1-48) and full-length *hup1* gene
HF SP+Hup+GFP rv	CATCTCGAGAGAAGCTGCCTTCATCGCCTTTGACAGCT	-Cloning of pPHAN-eGFP-HUP -Amplification of full-length *hup1* gene
HF SP+GFP rv	CACTCCCTCGAGAGAAGCTGCAGTCACACCGTTGTCATAGC	-Cloning of pPHAN-eGFP-SP -Amplification of N-terminal sequence of *hup1* gene (aa 1-48)

To analyze the impact of different promoters on the heterologous expression of the *hup1* gene, two expression vectors were tested. The pPha-T1 vector (GenBank-accession no.: AF219942, Zaslavskaia et al. 2000) already carrying the enhanced green fluorescent protein (eGFP)

sequence (pPhat-eGFP) and the vector pPha-NR (GenBank-accession no.: JN180663.1; Stork et al. 2012), with exchanged resistance cassette (here, nourseothricin) were used in this study (both vectors were kindly provided by S. Jäger, Uni Frankfurt). For generating a fusion protein with eGFP, the vector pPha-NR was first restricted with HindIII in order to also insert the sequence of eGFP. The sequence of eGFP was amplified from the vector pGREEN35s2x-eGFP using the Phusion™ High-Fidelity DNA Polymerase (Thermo Scientific) and gene-specific primers (Tab. 2). After insertion in the restricted vector using the Hot Fusion method (Fu et al. 2014) and *E. coli* XL1 Blue, the vector pPHAN-eGFP was generated.

The amplified gene sequences of the *hup1* gene were cloned in three different expression vectors with either an fcpA or an NR promoter. The pPha-NR vector and two vectors carrying the *eGFP* gene, namely pPhat-eGFP and pPHAN-eGFP, were chosen as expression vectors. Before initiating the Hot Fusion, the pPha-NR vector was restricted using *Xba*I. The enzyme was heat inactivated before the full-length gene amplificate was inserted. For the fusion protein, the vectors pPhat-eGFP and pPHAN-eGFP were restricted with *Sal*I and *Hind*III respectively and both the *hup1* full-length gene or the N-terminal sequence was inserted by Hot Fusion after heat inactivation of the restriction enzymes. Plasmids were isolated from *E. coli* by ROTI®Prep Plasmid minI-XL (Roth) for transformation of *P. tricornutum* using 10 to 20 ml of an overnight culture at 37°C. The plasmids were verified using test digestion and sequenced by Sanger sequencing (Eurofins Genomics, Ebersberg, Germany). An overview of the generated vectors used in this study is given below (Fig. 5) and a list os all vectors used in this study is listed elsewhere (Tab. S 4).

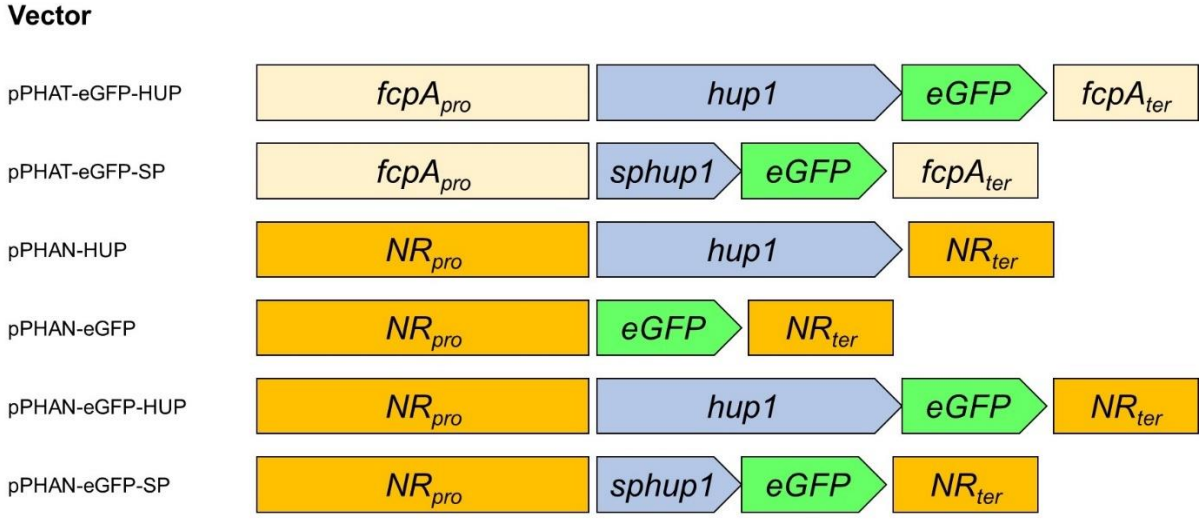

Fig. 5 Vector constructs used for the transformation of *Phaeodactylum tricornutum*. Abbreviations used in this figure: $fcpA_{pro}$ = fcpA promoter; Nr_{pro}= Nitrate reductase promoter; hup1= full length gene of hup1 (ID: X55349.1); sphup1= N-terminal sequence of hup1 gene (1-48 aa); $fcpA_{ter}$= fcpA terminator; NR_{ter}=Nitrate reductase terminator.

4.2.2. Transformation of *Phaeodactylum tricornutum*

P. tricornutum cells in early exponential phase (5-7 days) were transformed using microparticle bombardment or electroporation (NEPA21 Cuvette Electroporation). First, microparticle bombardment as transformation method was carried out according to the protocol of Apt et al. 1996 with some modifications (Angstenberger et al. 2019). The time for the sample preparation and the cost can be reduced and the efficiency improved when using electroporation as the method to transform *P. tricornutum* (Miyahara et al. 2013). Therefore, the protocol of Miyahara et al. 2013 was used and slightly modified. After transformation, cells were recovered for approximately 16 h at 18°C in scattered light. Afterwards, cells were plated on ASP plates (1.3% (w/v) Agar-Agar, Serva) supplemented with zeocin (75-100 µg/ml) or nourseothricin (100 µg/ml), incubated at the same light intensity, same temperature and a 16-hour light/8-hour dark cycle.

4.3. Screening of Engineered Lines

Transformants generated via microparticle bombardment were selected as followed: Engineered lines were first selected on antibiotic plates (see 4.2.2) and antibiotic resistant clones were further sub-cultured 2-3 times in liquid medium under antibiotic pressure by zeocin (100 µg/ml) or nourseothricin (100 µg/ml) to avoid inhomogeneous cultures.
For the high number of colonies achieved with electroporation (>100), cells were screened differently:
For the cells potentially carrying the construct pPHAT-eGFP-HUP a designed high troughput screening was established. First, cells were transferred to a well plate (96 Well or 24 Well cell culture plate, transparent; Sarstedt) and cultivated in ASP medium supplemented with zeocin (100 µg/ml). After 7 and 16 days, cell density and eGFP expression were measured using a plate reader (SPARK 10M, Tecan). The cells were measured with a designed program (Tab. 3) and normalized values were calculated (eGFP fluorescence divided through the cell numbers, measures as OD_{735}). The relative fluorescence signal (RFU) made it possible to better differentiate between clones with a high signal due to high expression or those exhibiting high fluorescence solely of high growth. A threshold was set and chosen transformants were further screened on genomic level.

The integration of the specific genes of interest in the diatom genome were verified after the aforementioned selection. Crude genomic DNA was isolated, using 1-2 ml of cell material. The cell material was washed with 1 ml of ddH_2O (10000 x g, 5 min, RT) and then incubated in 15 µl of 5% Chelex (w/v) (Stratagene) at 95°C for 15 min. After a cooling step on ice, the samples were centrifuged (10000 x g, 5 min, RT) and the supernatant was transferred to clean tubes. 1-2 µl of the supernatant were used for a PCR reaction, to amplify parts of the genes of interest

using the Red Taq DNA Polymerase Master Mix (VWR) according to the manufacturer's instructions and the listed primers (Tab. S 5). Samples were further loaded on agarose gels and the amplicon size was checked.

Tab. 3 Program of measuring growth and fluorescence signal of *Phaeodactylum tricornutum* cells.

Function		**Values**	
Shaking (linear)	Duration	10	s
	Position	Current	
	Amplitude	6	mm
	Frequency	330	rpm
OD_{735} measurment			
	Measurement wavelength	735	nm
	Number of flashes	10	
	Settle time	300	ms
eGFP measurment			
	wavelength	485	nm
Excitation	bandwidth	20	nm
	wavelength	535	nm
Emission	bandwidth	20	nm
	Gain	120	Manual
	Number of flashes	30	
	Integration time	40	µs

4.4. Characterization of transgenic microalgae by molecular approaches

4.4.1. Reverse transcription quantitative PCR (RT-qPCR) analysis

After the successful verification of the *hup1* gene integration, expression levels of chosen engineered lines were analyzed using RT-qPCR, a prominent method to quantify gene expression (Higuchi et al. 1993; Wong and Franz 2013). With the innuPREP Plant RNA Kit (Analytik Jena) and follwoing their manufacturing instructions, total RNA was isolated from wildtype and mutant cells. A volume of 25 ml of exponentially grown cells was harvested (5000 x g, 15 min, 4°C) and incubated with Lysis Solution RL for 10 min at room temperature (RT). After following the protocol, extracted RNA was eluted in 50 µl of H_2O (0.1 % DEPC; Diethyl pyrocarbonate). The RNA was digested with DNase I (Thermo Scientific) to remove residues of genomic DNA and afterwards cDNA was synthesized following the instructions of First Strand cDNA Synthesis standard protocol (NEB #M0253) and the corresponding M-MuLV Reverse Transcriptase (NEB). The DNA binding dye SYBR green, emitting fluorescence when bound to double strand DNA was used (Wittwer et al. 1997). In a reaction volume of 20 µl containing 2x SYBR Green qPCR master mix (Low ROX; Bimake™, USA) chosen genes were amplified and the replication was monitored using the Mx3000P qPCR System (Agilent Technologies). Housekeeping genes, Histone H4 (NCBI, accession no.: XP_002179505.1)

and TATA box binding protein TBP (NCBI, accession no.: XP_002186321.1) were used as controls (Sachse et al. 2013). The primer sequences are listed (Tab. S 5) and the primer efficiency ranged from 99.7 to 109.1%. The $2^{-\Delta\Delta}$Ct-method was used to quantify gene expression (Livak and Schmittgen 2001).

4.4.2. Protein analysis

Depending on the experiment, 1-2 ml cell cultures of different age were harvested and frozen in liquid nitrogen. The cells were mechanically disrupted in 200 µl of 90% of acetone using a homogenizer (Janke&Kunkel (IKA)). The chlorophyll content was determined (Jeffrey and Humphrey 1975) using the supernatant of the disrupted cells after a centrifugation step (10000 x g, 2 min). The pellets were incubated for several hours (up to 4 h) at RT in a calculated volume of ROTI®Load (Roth) yielding a final concentration of 0.5 mg ml^{-1} Chl *a*.

Samples corresponding to 5 µg and or 10 µg Chl *a* were analyzed using SDS-Page according to Laemmli (1970) on a 12% polyacrylamide gel. As protein size reference, the Prestained Protein Molecular Weight Marker (Thermo Scientific) was used.

After the protein samples were separated according to their molecular weight, the gel was placed on a nitrocellulose membrane for western blotting and soaked in transfer buffer [25 mM Tris-HCl (pH 8.3), 0.192 M glycine, 20% (v/v) methanol]. The proteins in the gel were transferred overnight, using a wet tank system (Peqlab) running at 55 mA in transfer puffer. For further protein detection using specific antibodies, the membrane was blocked with 5% milk powder (Carl Roth) in 1x TBS buffer [25 mM Tris, 0.125 M NaCl, pH 7.5] for 1 h at RT. In addition to the detection of eGFP, a loading control was also detected using an antibody against the light-harvesting proteins of *P. tricornutum*, namely α -lhcf1-11 (diluted 1:2000, Juhas and Büchel 2012). To do so, the membrane was cut once, and both parts of the membrane were incubated for 2 h with the corresponding first antibody (stored in TBS buffer, 2% (w/v) milk powder). The eGFP-Fusion proteins were detected using the α-GFP (peroxidase-conjugated, Rockland, no. 600-403-215; diluted 1:5000). After the incubation, the membranes were washed three times with TBST [TBS buffer with 0.1% Tween 20]. The α -lhcf1-11 is not conjugated with a peroxidase and had to be incubated with a secondary antibody (goat anti-rabbit specific peroxidase, Calbiochem catalog no. 401315, diluted 1:10000) for 1h at RT. Residual antibody was removed by three further washing steps in TBST. After incubation in an enhanced chemiluminescence solution (Alegria-Schaffer et al. 2009), the fluorescence signals were detected using the ChemoStar ECL & Fluorescence Imager (Intas).

4.5. Investigations of growth on low glucose concentrations

4.5.1. Growth experiments under different light intensities

Next, Hup mutants were grown at different light intensities, using very low light of 10 µmol photons $m^{-2} \cdot s^{-1}$, a light intensity of 60 µmol photons $m^{-2} \cdot s^{-1}$ and high light of 120 µmol·photons $m^{-2} \cdot s^{-1}$. Batch cultures of 30 ml volume shaken in 100 ml flasks were inoculated with cells in the late exponential phase. Cells were concentrated and a calculated volume of cells was added, leading to a final cell density between 2 to 4 x 10^6 cells ml^{-1} (counted using a Neubauer chamber), correlating to an OD_{750} of 0.1.

Wildtype cells and the published strain Glut1 (Zaslavskaia et al. 2001) served as positive controls. For every experiment, two biological replicates were cultured with or without the addition of 5 mM glucose. The growth was monitored in technical triplicates using 200 µl of cell suspension in 96 well plates (96 Well cell culture plate, transparent; Sarstedt) and a microplate reader (SPARK 10M, Tecan).

4.5.2. Biomass calculation

Cell dry weight (CDW) was determined at the end of the growth experiment in order to compare total biomass between mutant and wildtype cells. A defined volume of cells (8 or 10 ml) was harvested at high speed (~10000 x g) of each biological duplicate (see 4.5.1) in technical duplicates. After two washing steps with 1 ml of ddH_2O (10000 x g, 10 min), residual cells were transferred to weighted reaction tubes. The pellets were shock-frozen (liquid nitrogen) and freeze-dried in a lyophilizer (ALPHA 1-4 LSC, Christ) at 400 mbar for 24 h. At the end, net weights were determined.

4.5.3. HPLC analysis of glucose concentration in the medium

A cheap and easy method to investigate glucose uptake, is the measurement of glucose concentration at the beginning and the end of the growth experiment using the method HPLC. After centrifugation of the cell culture (up to 1 ml) at high speed (~10000 x g), 450 µl supernatant was mixed with 50 µl of 5-sulfosalicylic acid [50% w/v]. The samples were centrifuged (10000 x g, 5 min), and the supernatant transferred to HPLC vials. According to Hitschler and Boles (2020), the analysis was carried out and chromatograms were visualized using the graphic software Prism 5 (GraphPad, USA).

4.6. Pulse chase experiment

4.6.1. Radioactive labeled glucose uptake

With radiolabeled glucose ($^{14}C(U)$, Biotrend) the uptake of glucose can be measured in a so-called pulse-chase experiment. In the first part of the experiment, the glucose uptake of cells

was determined by counting the amount of radiolabeled glucose inside the cells after a certain incubation time. The wildtype and the published Glut1 were used as controls for this experiment as before (4.5.1). First, precultures of mutants and the wildtype were inoculated at an OD_{750} of 0.1 with a total volume of 300 ml. The main experiment was conducted according to Boles and Oreb (2018) with the following changes. In the exponential phase after seven days, cells from preculture were harvested (3000 x g, 15 min, 4°C), washed twice (2500 x g, 15 min, 4°C) with precooled ASP/2 [50% (v/v) ASP] and resuspended in ASP/2. Cells were counted and after a last centrifugation step, resuspended to a final concentration of 10^9 cells ml^{-1}. Aliquots of 110 µl were kept at RT until they were used. ^{14}C- glucose fed cells were incubated for different durations (10, 15, 45, 60 min) at a total glucose concentration of 5 mM [~99% cold glucose, ~1% hot glucose]. The experiment was stopped by washing the cells twice with 10 ml of ice-cold quenching solution [50% ASP, 5% (w/v) unlabeled glucose] to inhibit further glucose uptake. The cells were incubated in scintillation solution (ROTISZINT®plus, Roth) and the uptake of glucose was calculated after finishing the liquid scintillation counting (see equatation 1). Abbreviations used in the equitation: cpm= count per minute, cpm_{total}= cpm of uptake mixture. Glucose concentration = 5 mM = 5 nmol/µl.

Equation 1: $Glucose_{intra}[nmol] = ((cpm_{mutant} - cpm_{WT})/cpm_{total}) \times Glucoseconcentration[nmol/\mu l]$

4.6.2. Radioactive labeled glucose uptake under different pH

In the former experiment, glucose uptake was investigated in the culture medium ASP over defined periods. In the second part of this experiment, the influence of pH on the glucose uptake of wildtype and mutants was investigated.

In a pretest, wildtype cells were incubated in three solutions with different pH values in biological triplicates, to ensure that no changes in the pH of the medium were induced by the cells. The former aforementioned culture medium ASP was used as a control in addition to ASP/2 [pH= 7.7], a Sørensen phosphate buffer [pH: 5.7; 50 mM; Sörensen 1968] and a glycine-NaOH buffer [pH: 10.2 ; 50 mM]. After harvesting (3000 x g; 15 min, 4°C) and washing the cells once in the respective buffer, cells numbers were calculated as described previously (4.5.1). 5 ml cell cultures were prepared with a final concentration of 10^9 cells ml^{-1} with either ASP/2, Sørensen phosphate buffer or glycine-NaOH buffer. For a period of 7 h, cells were incubated in these solutions at RT and the pH levels were controlled every hour.

In vivo chlorophyll measurement allows the measurement of, e.g. changes in the fitness of cells when exposed to environmental stress (Murchie and Lawson 2013, and references herein). With a defined program, chlorophyll fluorescence kinetic information was imaged using the FuorCam FL3000 (Photon Systems Instruments, Brno). After dark adaption of the cells (10

min) in 24 well plates, the minimal fluorescence F_0 was measured using a pulsed measuring light of 617 nm and 1.6 µmol photons $m^{-2}{\cdot}s^{-1}$ intensity. The maximal fluorescence F_M was calculated after applying a saturating light pulse (605 nm, 800 ms, 640 µmol photons $m^{-2}{\cdot}s^{-1}$ intensity) and subsequently the variable fluorescence in dark-adapted state, F_V is calculated. Afterwards, using equation 2, the F_V/F_M value can be calculated which gives information about the maximal quantum yield of photosystem II (Genty et al. 1989; summarized in: Maxwell and Johnson 2000).

Equation 2: $(F_M - F_0)/F_M = F_V/F_M$

For the main experiment, investigating the radioactive labeled glucose uptake under different pH values, the aforementioned protocol was used (4.6.1) with the following changes. Cells were washed and counted in order to be split equally between the buffer systems. The centrifuged cells were resuspended in the corresponding buffer and transferred to 2 ml tubes. After a final washing step, cells were counted and concentrated to a final cell number of 10^9 cells per ml. The incubation of ^{14}C- glucose fed cells were prolonged to 30, 60 and 120 min. Finally, the pH value was checked using pH-indicator strips (pH 0-14; Merck) at the end of the experiment.

4.7. Localization study

4.7.1. Confocal and superresolution structured illumination microscopy (SR-SIM)

The expression of fusion proteins, here Hup1 or the N-terminal peptide of Hup1 (aa 1-48) attached with eGFP helped to localize the heterologous proteins in the engineered cells. Here, the methods of confocal microscopy and superresolution structured illumination microscopy (SR-SIM) were used.

First exponentially grown cells were harvested and resuspended in a small volume of ASP. To further distinguish compartments, the nucleus was visualized with Hoechst 33342 (5 µM, Sigma-Aldrich). The cells were stained with the aforementioned cell-permeant nuclear counterstain and incubated for 1 h at RT. The stained cells were washed 2-3 times with ASP (2500 x g, 5-10 min). Confocal microscope Zeiss LSM 780 and a Plan-Apochromat 63x/1.40 Oil DIC M27 objective lens were used to capture the cells with the settings for detection of autofluorescence of chlorophyl, GFP and Hoechst listed in Tab. 4. The images were visualized and analyzed using the software ZEN lite (vers. 2.0).

A Zeiss ELYRA PS.1 superresolution microscope capable of performing both SR-SIM and photoactivated localization microscopy (PALM) was utilized in SR-SIM mode to achieve a higher resolution of the images and thereby attribute the GFP signal to cellular features. 3D-

stacks were recorded using a Plan-Apochromat 63x/1.4 Oil DIC M27 objective lens, a grid with SIM grating period of 28.0 µm with the listed settings (Tab. 4). During image recording five rotations were applied. The ELYRA PS.1 runs on a ZEN 2012 SP5 FP3 (black) software version and raw image data was processed in 3D Automatic mode.

Tab. 4 Settings for fluorescence microscopy.

Microscope	Setting	Laser	Excitation [nm]	Detection [nm]
Confocal microscope Zeiss LSM 780	Autofluorescence (Chlorophyll)	Argon laser	488	624-730
	GFP	Argon laser	488	499-544
	Hoechst 33342	Diode laser	405	425-476
Zeiss ELYRA PS.1	GFP	Diode laser	488	495-575
	Bright field	Diode laser	488	750 (long pass)

4.7.2. Bioinformatical study of diverse transporters

Different programs were used to analyze sequences of transporters from diverse organisms. Web-based programs (Tab. 5) were used for *in silico* analysis and prediction of transmembrane helices. To investigate characteristics of plasma membrane proteins in *P. tricornutum*, partially well-characterized plasma membrane proteins and non-characterized proteins. predicted to be localized in this membrane were analyzed with these programs. Elbourne and colleagues (2017) assembled an online database TransportDB 2.0, describing predicted cytoplasmic membrane transport proteins, including transporters from the sequenced strain of *P. tricornutum* CCAP 1055/1. Hence, protein IDs were collected from this database.

Tab. 5 Web-based programs used in this study.

Function	Program	Reference
***In silico* analysis**	HECTAR v1.3	(Gschloessl et al. 2008)
	PrediSi	(Hiller et al. 2004)
	WoLFS PORT	Not specified
Prediction of transmembrane helices	TMHMM v2.0	(Krogh et al. 2001)
Sequence analysis	NGPhylogeny.fr	(Lemoine et al. 2019)
Generating sequence motif	WebLogo	(Crooks et al. 2004)

Additionally, glucose transporters from the phylum of Viridiplantae, Fungi, Chromista and Mammalian cells were analyzed with the aforementioned programs. Here, sequences were collected from UniProt (The UniProt Consortium 2021) or the Joint Genome Institute (JGI). Sequences were further analyzed for distinctive motifs (Tab. 5).

5. Results (Chapter I)

5.1. Bioinformatical analysis of integral membrane proteins

In order to genetically manipulate *P. tricornutum* with a foreign membrane transporter, correct targeting of the heterologous transporter is necessary. In advance of the *in situ* localization study and to gain more insight into plasma membrane transporters targeting in diatoms, an *in silico* analysis of IMPs in *P. tricornutum* was carried out. A selection of 20 transporters was analyzed, including a highly conserved nitrate transporter from the diatom *Cylindrotheca fusiformis* (Hildebrand and Dahlin 2000). Some of the listed IMPs are characterized or predicted to be localized at the plasma membrane (Tab. S 3). Two putative glucose transporters VCT3 (Phatr 30620) and an SLC transporter (Phatr 12520) have also been analyzed (Tab. S 6). The prediction of 11 multi-spanning plasma membrane transporters, proven to be localized at the plasma membrane, showed no clear result. Web-based programs like HECTAR and PREDISI predicted a signal peptide or a signal anchor for these polytopic membrane proteins in about 55% and 27% of the cases respectively. The results of WOLFSPORT support the hypothesis of these IMPs being localized at the plasma membrane and predicted this localization for 100% of the proteins, but for small IMPs targeting to the plasma membrane was only predicted in 2 of 5 proteins.

The same analysis was done for 64 proteins functional or putative sugar transporters in plants, fungi and mammals (Tab. S 6). Based on uniport, about 10% have high annotation scores and the sugar transporters GLUT1, GLUT2, GLUT3, HXT1, HXT2, STP1 and HUP1 were confirmed to be localized at the plasma membrane (Bisson et al. 1993; Takata et al. 1992; Yamada et al. 2017). But in line with previous results, the prediction was not clear. HECTAR and PREDISI found signal sequences in about 58% and 70% of the chosen sugar transporters, respectively (Tab. S 6). For the HUP1 protein of *C. kessleri*, PREDISI predicted a putative cleavage side at position 42 aa. This sequence was prolonged by 6 aa and the N-terminal sequence (1-48 aa) expressed in *P. tricornutum* and investigated in an *in situ* localization study.

5.2. Screening of *Phaeodactylum tricornutum* transformants for integration of the *Chlorella kessleri hup1* gene

P. tricornutum was transformed with different expression vectors, differing mainly in the promoter that controls the expression of the gene of interest. In this study I chose the gene of the glucose transporter HUP1 of *C. kessleri* to improve biomass production, by enabling efficient growth on glucose. The full-length *hup1* gene was fused at the C-terminus to eGFP to show the intracellular localization of the heterologous protein. In order to investigate possible targeting sequences for plasma membrane transporters, the N-terminal sequence of the HUP1 protein was also fused to eGFP. The influence of the gene-promoter combination was tested

and both constructs were placed under the control of the fcpA (Zaslavskaia et al. 2000) or the NR promoter (Stork et al. 2012). Biolistically transformed cells were selected on plates with antibiotic pressure. Colonies that appeared were further selected, transferred to liquid media with the corresponding antibiotic pressure and cultivated for at least three cell cycles. The genomic integration was tested via PCR using isolated crude DNA of transformants (Fig. S 2; Fig. S 3; Fig. S 4) and at least two clones of each construct were further investigated (see 4.3). Electroporation was established in 2013 for the model organism *P. tricornutum,* offering high transformation efficiency (Miyahara et al. 2013). Therefore, the construct pPHAT-eGFP-HUP was used to transform *P. tricornutum* also via electroporation in order to increase the number of transformants. Colonies that appeared on antibiotic plates were transferred in either 24 or 96 well plates and grown for several days. GFP expression and cell growth were monitored and normalized (GFP signal/ OD_{735}, see 4.3). Table 6 gives an overview about mutants created and the nomenclature used.

In a pretest for the hight-throughput screening, wildtype cells and two positive controls T-eGFP and T-HUP*(6) were grown until they reached the exponential growth phase and were then diluted. Both mutans are expressing eGFP while mutant T-eGFP is carrying the pPHAT-eGFP vector and T-HUP*(6) is carrying the pPHAT-eGFP-HUP vector. The samples were measured between OD_{735} from 0.17 to 1.48 (Fig. 6 c). The normalized GFP signal of mutant T-HUP*(6) was stable, whereas the values of T-eGFP were oversaturated at higher cell densities. In contrast, wildtype cells showed low RFS of eGFP at high cell numbers but increased with decreasing cell numbers.

Based on this, only clones with higher cell densities of 0.24 and signals higher then 5000 RFS were considered as a putatively high-expressing mutant. Clone #86 and clone #100 showed a normalized signal that exceeded that of T-HUP*(6). The GFP signal of clone #49 was off the range. After 16 days, the RFS had decreased in almost all samples (Fig. 6).

All transformants from biolistic, and 17 out of 80 transformants from electroporation were tested for the genomic integration of the *hup1* full length gene or its N-terminal sequence, using PCR (Tab. 6).

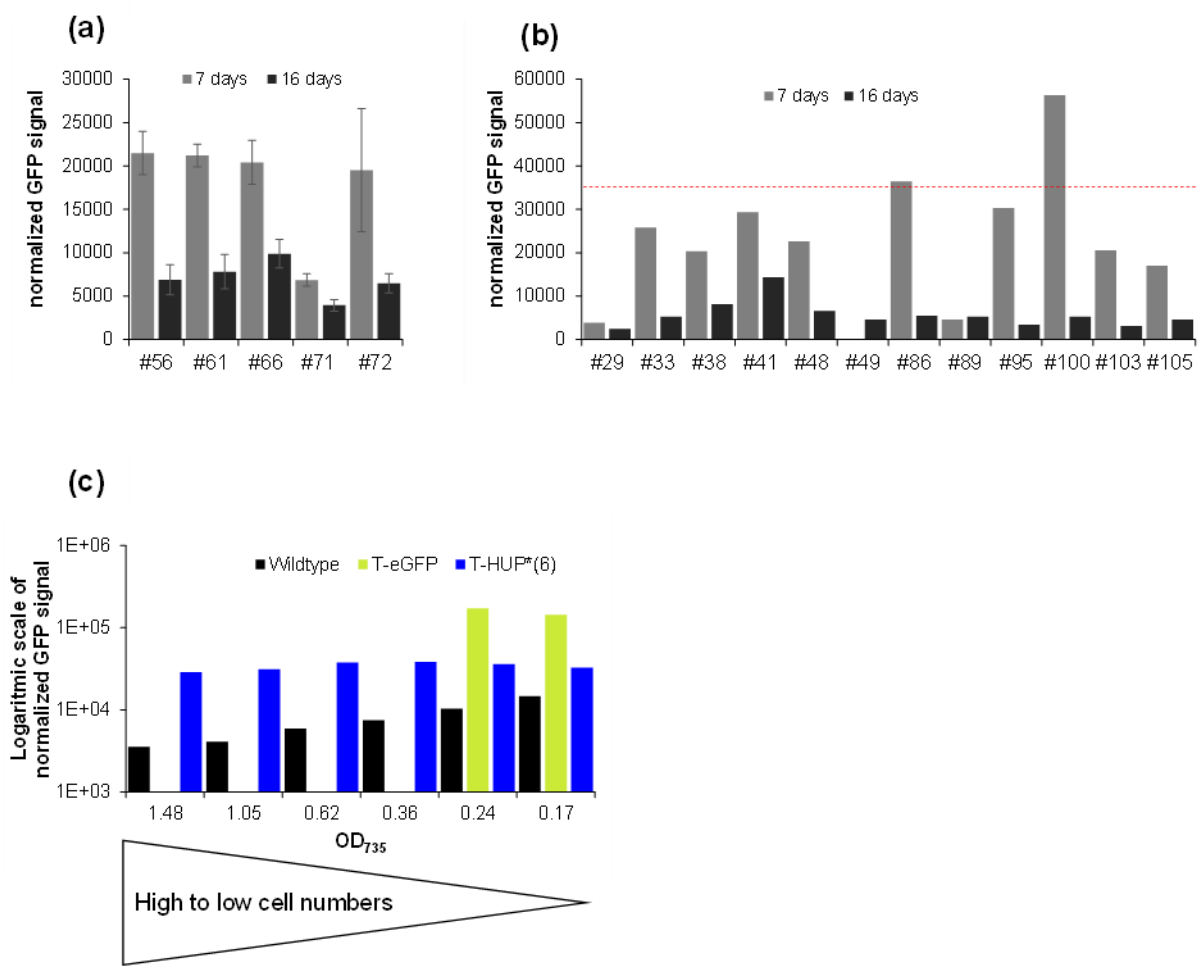

Fig. 6 Normalized GFP fluorescence of *Phaeodactylum tricornutum* mutants selected in a high-troughput screening. The cells of putative T-HUP* transformants were analyzed in either 24 (a) or 96 well plates (b) regarding their normalized GFP signal. Clone #29 was used as negative control. The dashed line (red) was the average of fluorescence signal in T-HUP*(6) from the control experiment (c) and was taken as guide value. Cells grown in 96 well plates were grown in three wells simultaneously (±SD=3). The data of the control experiment (c) was sampled by Marcel Meyer (Uni Frankfurt).

Tab. 6 Overview of constructs and nomenclature for mutants. The setup of the used vectors is displayed in Fig. 5.

Protein length (HUP1)	**Vector**	**Promoter**	**Name of clone**	**Clone number**
1-48 aa	pPHAT-eGFP	fcpA	T-spHUP*	#5; #7
	pPHAN-eGFP	NR	N-spHUP*	#3; #13
Full length (534 aa)	pPHAT-eGFP	fcpA	T-HUP*	#6; #8; #49*
	pPHAN-eGFP	NR	N-HUP*	#3; #8
	pPHAN-nat	NR	N-HUP	#1; #17

*Generated with transformation method of electroporation

5.3. Verification of HUP1 expression on gene and protein level

Next, I tested both common promoters, fcpA and NR, in combination with the full length *hup1* gene and studied the expression on gene and protein levels.

RT-qPCR is a prominent tool to determine mRNA expression levels. As a control, mRNA of wildtype cells was isolated, but cannot be used as a calibrator for the heterologous *hup1* gene expression. The *hup1* gene is a heterologous gene that is not expressed in wildtype cells. Instead, wildtype cells were used as a control for the expression levels of the house keeping genes (TBP and H4, see 4.4.1). In this case, the mean value of mutant T-HUP*(6) served as calibrator and was set to 1 (Fig. 7).

The gene expression of T-HUP*(49) was compared to the expression of the calibrator, and the relative expression of *hup1* was twice as high as in T-HUP*(6). The ASP medium has high nitrate concentration, nevertheless both N-HUP mutants, N-HUP(1) and N-HUP(17), showed very low relative expression levels of the *hup1* gene. Other studies have shown that excess nitrate should ensure high NR promoter activity (Chu et al. 2016).

Due to the low expression level of N-HUP mutants, only T-HUP* mutants were analyzed as to their protein level. Results of the protein level using immunoblots were compared to the gene expression level. The proteins could be detected using the eGFP tag of the fusion protein. Clone T-eGFP was used as a positive control since it expresses eGFP in the cytosol. As expected for its protein size of 26.9 kDA, protein samples of mutant T-eGFP showed a band at 30 kDA (Fig. 7). Wildtype cells served as a negative control and showed no signal for α-GFP. Both T-HUP* mutants showed a signal at around 85 kDa, as expected in case of a molecular weight of the HUP1-eGFP fusion protein of 84.6 kDa. In line with the previous results of RT-qPCR, T-HUP*(49) showed a stronger signal compared to T-HUP*(6). The loading control of the immunoblots, showing the protein level of LHCF proteins, confirmed approximately the same loading for all samples. Therefore, one can conclude that T-HUP*(49) expressed slightly higher levels of the HUP1 protein compared to T-HUP*(6).

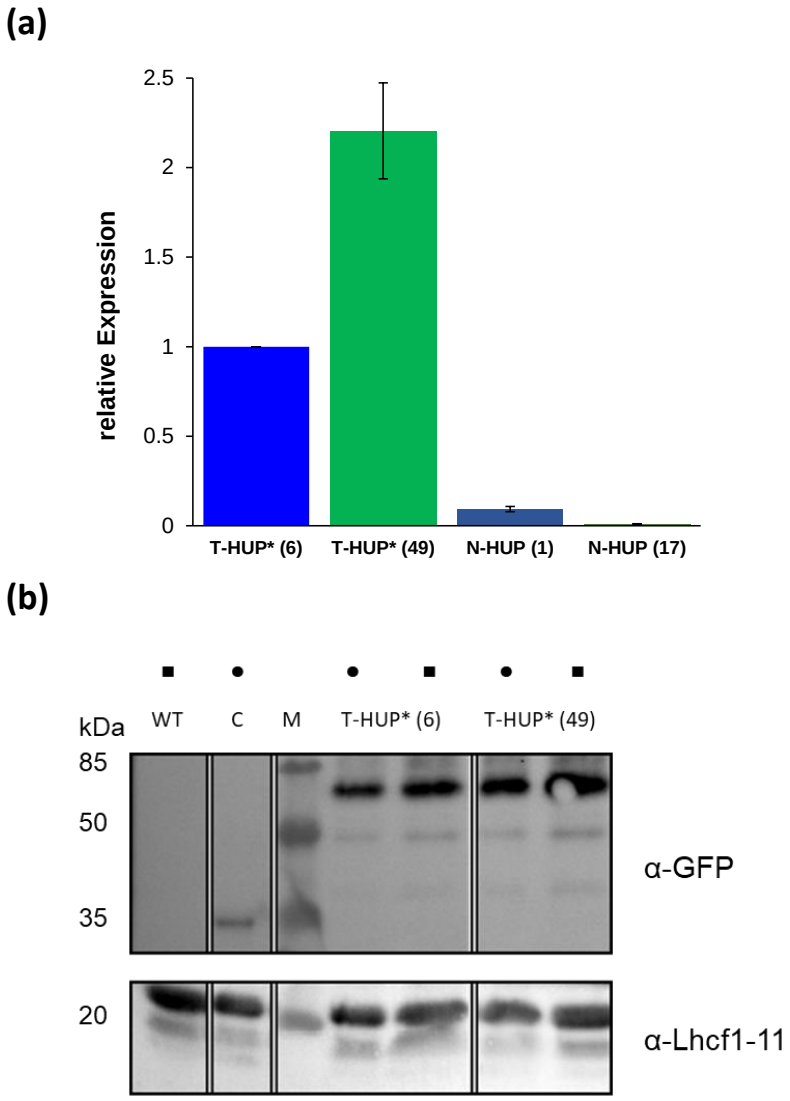

Fig. 7 Comparison of gene and protein expression of Hup mutants. (a) RT-qPCR results of heterologous gene expression of Hup mutants, normalized to the values of two housekeeping genes (H4, TBP) Values are mean ±SD (n=3). (b) Western blot of wild type (WT), a positive control (C) expressing cytoplasmic eGFP and two Hup mutants, T-HUP*(6) and T-HUP*(49). The expected molecular weight of the control is 26.9 kDa and that of the Hup mutants expressing the full-length protein is 84.6 kDa. As loading control, the Lhcf1-11 antibody was used as well as an Coomassie-stained SDS PAGE (see Fig. S 5). 5 µl of the Prestained Protein Molecular Weight Marker (Thermo Scientific) was added as protein size reference. Samples corresponding to 10 µg Chl_a (■) or 5 µg Chl_a (●) were loaded.

5.4. Targeting of eGFP-HUP1 fusion proteins in the heterologous system of *Phaeodactylum tricornutum*

GFP tagged proteins can be used in a versatile manner and, in this experiment made it possible to control the localization of the glucose transporter HUP1-fusion protein in the heterologous organism of *P. tricornutum.* Wildtype cells and the positive control T-eGFP were used as controls again. With a confocal microscope, the localization of proteins was detected using different wavelengths for excitation and detection (Tab. 4, Fig. 8). Chlorophyll autofluorescence was detected in wildtype and all mutant cells. Here, a strong signal visualized the fitness of the cells and the localization of the plastids (Fig. 8). The positive control T-eGFP showed a strong fluorescence signal for eGFP in the cytosol, whereas wildtype cells showed no signal as expected. In T-HUP* mutants an eGFP signal was present at the plasma membrane. Higher resolution was achieved using a Zeiss ELYRA PS.1 superresolution microscope and it confirmed the localization of HUP1 fusion protein at the plasma membrane (Fig. 8,b). With this technique, cytosolic spots of the GFP signal could be found in several cells. These spots are accumulating eGFP tagged proteins, did not overlap with the Hoechst staining that demonstrated the nucleus, and were localized close to the plasma membrane.

Information about the targeting pathway, including N-terminal signal sequences of plasma membrane proteins in diatoms, is still missing. A predicted N-terminal targeting sequence of HUP1 (Fig. 8) had been fused to eGFP to clarify whether this sequence solely targets the fusion protein to the plasma membrane in *P. tricornutum*. Results of confocal microscopy showed for T-spHUP* mutants eGFP signals at the membranes surrounding the chloroplast and nucleus (Fig. 8). Due to evolution, diatoms' nucleus is connected with the plastid by a so-called chloroplast/endoplasmic reticulum compartment (CER) and surrounded by the fourth envelope membrane of the secondary plastids, in short CERM (Flori et al. 2016; Kroth et al. 2008). The results of confocal microscopy show that the fusion proteins containg the N-terminus of the HUP1 and eGFP are targeted to the CERM and are not localized at the plasma membrane.

As expected from the gene expression results for *hup1* under the control of the NR promoter, N-HUP* and N-spHUP* mutants showed only weak eGFP signals (Fig. S 6). Hence, no determination of the localization was possible. In line with previous results, *hup1* gene expression under the control of the NR promoter showed weaker protein signals compared to the expression under the fcpA promoter.

In summary, eGFP signals were visible in sufficient amounts in T-HUP* mutants and the localization was confirmed at the plasma membrane for these mutants. In the following experiments, T-HUP* mutants were characterized in more detail.

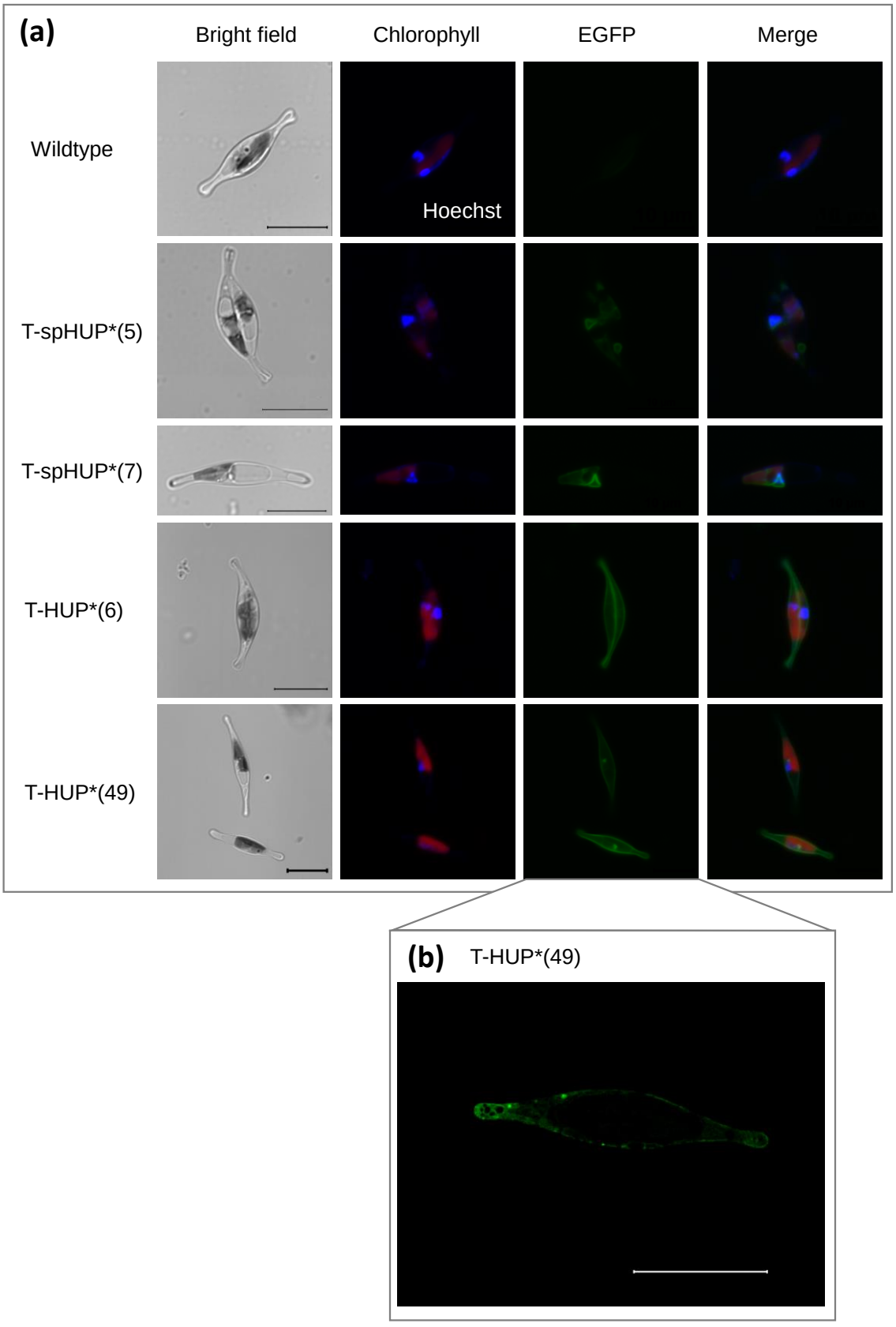

Fig. 8 Subzellular localization of eGFP-tagged glucose transporter in *Phaeodactylum tricornutum*. Mutants expressing full length transporter of hup1 fused to eGFP (a). From left to right: Bright field, Hoechst stained nucleus (blue) and autofluorescence of chlorophyll (red), EGFP signal (green) and merged image. Bars = 10 µm. High resolution image of T-HUP*(49) (b).

5.5. Radioactive labeled glucose assay to measure glucose uptake

The *in situ* localization study showed that the heterologously expressed glucose transporter is correctly targeted at the plasma membrane in *P. tricornutum*. Next, the functionality of the HUP1 transporter in *P. tricornutum* was tested. The HUP1 transporter from *C. kessleri* was investigated using glucose analogues, for example 6-deoxy-d-glucose or 3-O-methyl glucose uptake in *C. kessleri* itself (Komor et al. 1989; Tanner 1969) or in a heterologous system of *Saccharomyces cerevisiae* (Sauer et al. 1990).First, *P. tricornutum* was tested for the toxic glucose antagonist 2-deoxy-glucose, an import test successfully established for screening mutants of *C. reinhardtii* and *H. pluvialis* (Doebbe et al. 2007; Waissman-Levy et al. 2019). The T-HUP* mutants were incubated with different concentrations (2.5, 5 and 10 mM) for over 10 days, but showed no growth inhibition (data not shown). In the chlorophyte *Chlamydomonas reinhardtii* the functionality of the HUP1 protein was shown using a radioactive labeled glucose transport assay (Doebbe et al. 2007). In diatoms this method is not often used (Fischer et al. 1999; Zaslavskaia et al. 2001). In bacteria and yeast, radioactive labeled uptake assays are more common and heterologous systems have been successfully used to express human glucose transporters (Iancu et al. 2013; Schmidl et al. 2020).

In this study I adapted an uptake assay from *S. cerevisiae* and were able to test the functionality of heterologously expressed HUP1 protein in *P. tricornutum* (Boles and Oreb 2018). For time intervals between 10 and 60 min, wildtype cells and T-HUP* mutants were grown in medium supplemented with 5 mM glucose [~99% cold glucose, ~1% hot glucose]. The wildtype showed no efficient growth under the chosen condition and was taken as negative control and used for the calculation of the glucose uptake (Fig. 9Fig. 9). The already characterized mutant Glut1 was taken as positive control (Zaslavskaia et al. 2001). For all cell lines, three independent biological replicates were measured in technical triplicates. For both T-HUP* mutants, cpm values increased over time, due to the accumulation of ^{14}C glucose inside the cells (Fig. 10). At the last time interval measured (60 min), T-HUP*(49) showed a maximum of approximately 3000 nmol glucose inside of 10^8 cells, whereas T-HUP*(6) showed for the same cell number only one third glucose inside the cells. Wildtype and Glut1 samples both showed low cpm values. For Glut1 this value was only half of the value measured for T-HUP*(6).

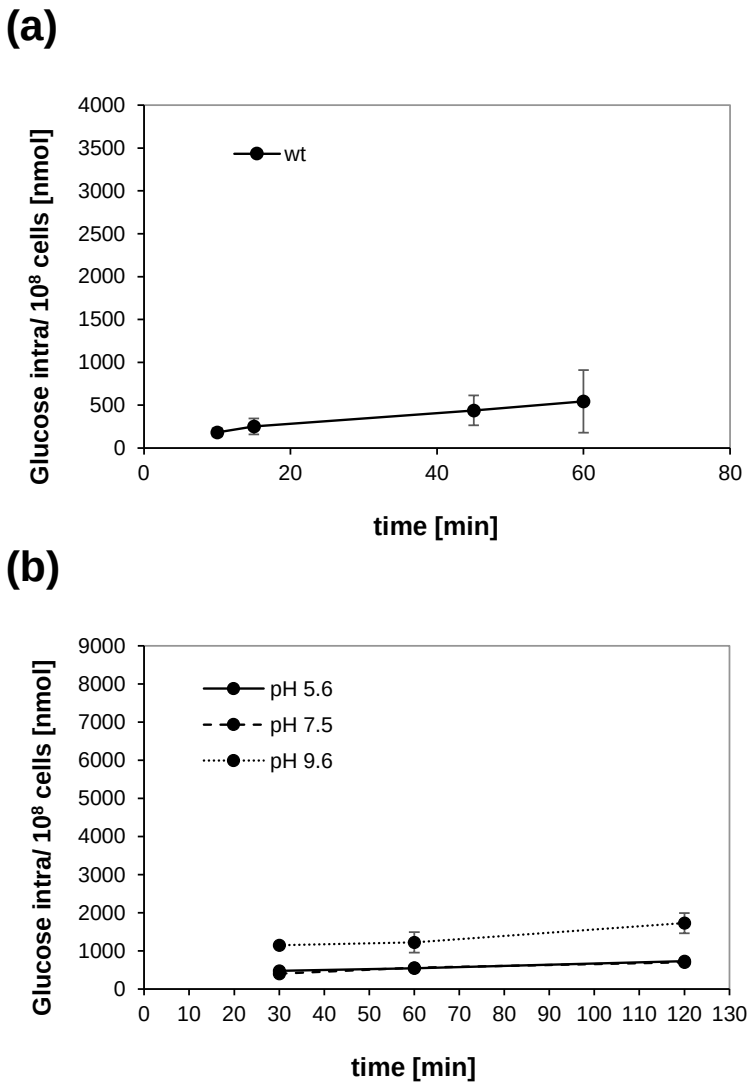

Fig. 9 Radioactive labeled glucose uptake of wildtype cells. ^{14}C radiolabeled glucose uptake was investigated for wildtype (wt) incubated in ASP/2 (a) with 5 mM glucose for different time periods. In a second experiment (b) wildtype was incubated in medium supplemented with 5 mM glucose at different pH values.

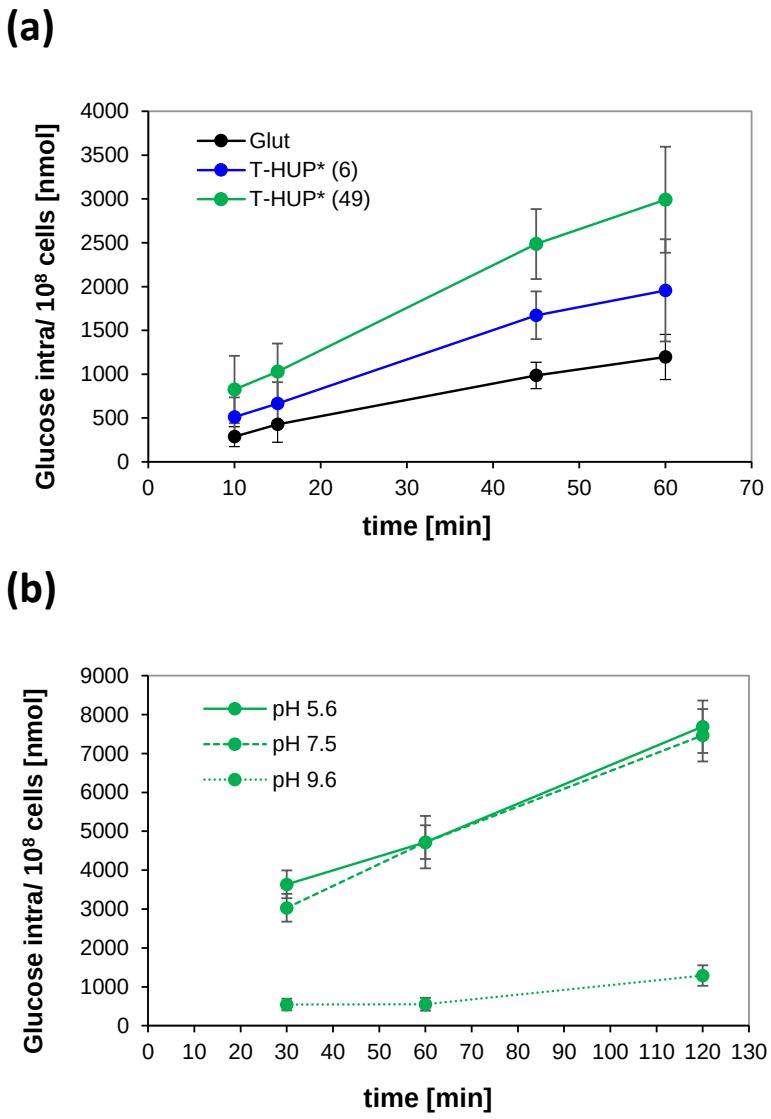

Fig. 10 Radioactive labeled glucose uptake of cells expressing HUP1. ^{14}C radiolabeled glucose uptake was investigated for two T-HUP* mutants and a positive control, Glut1. Cells were incubated in ASP/2 for different time periods (a) in 5 mM glucose. Values are mean ± SD (n=9, three independent biological replicates measured in triplicate each) of the intracellular glucose concentrations. In a second experiment (b) Hup mutant T-HUP*(49) was incubated at different pH values and glucose uptake examined. As control wildtype cells, were also measured. Results are displayed in Fig. 9. Values are mean ± SD (n=6, three independent biological replicates, each measured in duplicates each).

5.6. Functionality of HUP1 transporters in *Phaeodactylum tricornutum* in dependence on pH

In diatoms, during the day when photosynthesis is active, an increase of extracellular pH is detectable (Chrachri et al. 2018), and can reach values of 8.6 or higher in the extracellular medium of *P. tricornutum* cells (Fig. 11). In previous experiments and in line with literature, pH values during growth in the medium of *P. tricornutum* can even exceed pH values of 10 (Fig. 19; Zhang et al. 2016). In diatoms, the internal pH is about 7 to 7.5 (Goldman et al. 2017 and reference herein) with a more acidic pH in the thylakoid lumen (Heldt et al. 1973).

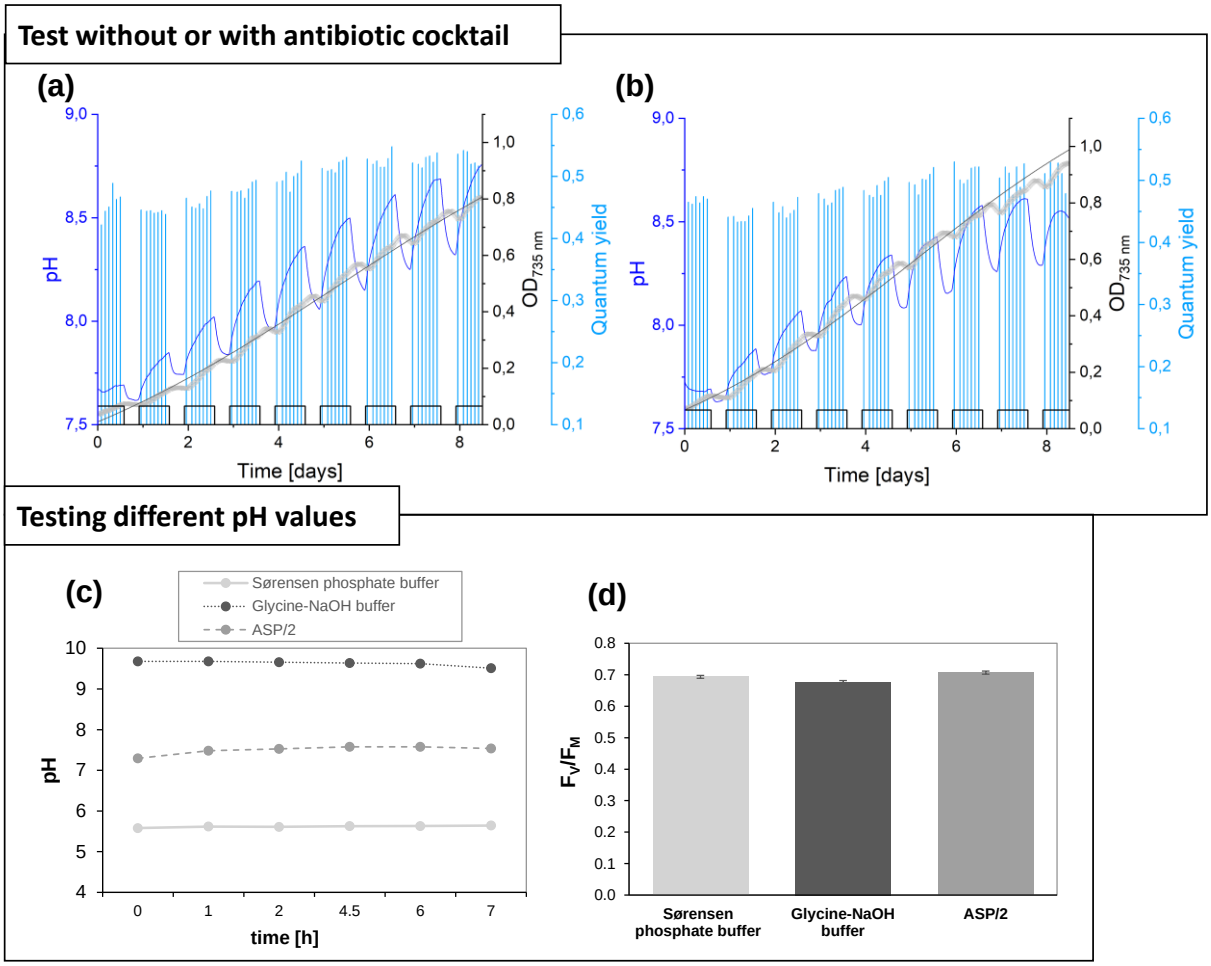

Fig. 11 Pretest to measure influence of antibiotic cocktail and different extracellular pH values on *P. tricornutum* cells. Growth curve of cells cultured in ASP medium without (a) or with (b) the supplemention of an antibiotic cocktail. Cultivation was measured over 8.5 days with a light intensity of 100 µmol·photons m^{-2}·s^{-1} with a 16-hour light/8-hour dark cycle (indicated with white bars) at 18°C. The pH (dark blue) and the optical density, OD_{735} (grey) was monitored constantly, whereas maximum quantum yield of photosystem II (F_V/F_M) was measured only in light periods and is displayed in light blue. Boltzmann regression line is calculated and shown in black with R^2 for the Boltzmannn 99.76 % (a), 99.42 % (b). For more information about the experimental setup see 8.2

In *C. kessleri*, the pH dependence of the hexose/H^+symporter has been shown (Komor and Tanner 1974) and was investigated in the heterologous system of *P. tricornutum*. In a preliminary experiment, the buffer capacity of three different buffer systems was tested to exclude a negative impact on the cells. During a period of 7 h, the extracellular medium of cells

incubated in ASP/2 (pH 7.5), Sørensen phosphate buffer (pH 5.6) and a glycine-NaOH buffer (pH 9.6) showed no significant change in pH values (Fig. 11,c). The measurements of maximum quantum yield of PSII revealed the unchanged fitness of the cells incubated in the three buffer systems ASP/2, Sørensen phosphate buffer and glycine-NaOH buffer (Fig. 11,d). Afterwards, the main experiment was conducted as described in chapter 4.6.1. The impact on the extracellular pH level was measured for wildtype and T-HUP*(49) cells in a maximum time frame of 120 min (Fig. 10). The maximum values of intracellular glucose concentration for 10^8 cells were measured for T-HUP*(49) incubated at pH 5.6 and 7.5 during the whole experiment. After 120 min this value was at the highest glucose uptake in both buffer systems with approximately 7500 nmol glucose per 10^8 cells. In contrast, T-HUP*(49) cells incubated in pH 9.6 showed more than six times less glucose uptake over the same time frame. The values were comparable with cpm values measured for the wildtype under the same pH values (Fig. 9). At pH 5.6 and pH 7.5, values were about two times less for wildtype cells.

5.7. Growth of HUP1 mutants under different light intensities

The results of biochemical and molecular studies identified T-HUP* mutants as high expression mutants of theheterologous HUP1 transporter in *P. tricornutum*. In addition, the correct localization of the HUP1 transporter as well as the radioactive labeled glucose assay confirmed the functionality in the heterologous system. However, an investigation using solid or liquid medium could not detect heterotrophic growth for any mutants (data not shown). Using mixotrophic mode, the HUP1 mutants were investigated as to their growth using different light intensities (10-120 µmol photons·m^{-2}·s^{-1}). The cells were grown with (5 mM) and without glucose in biological duplicates for two weeks. For industrial usage and to inhibit bacterial growth and concomitantly to ensure the exclusive growth of diatom cells, the medium was supplemented with an antibiotic cocktail. In a preliminary experiment, the effect of this antibiotic cocktail was tested for wildtype cells in a small PBR (Fig. 11). It was determined that the antibiotics, kanamycin, streptomycin and penicillin do not affect the growth of *P. tricornutum*. In the first experiment the growth curve and the glucose concentration of the medium were compared. In Fig. 12 the results are exemplarily displayed for cells grown at 120 µmol photons·m^{-2}·s^{-1}.

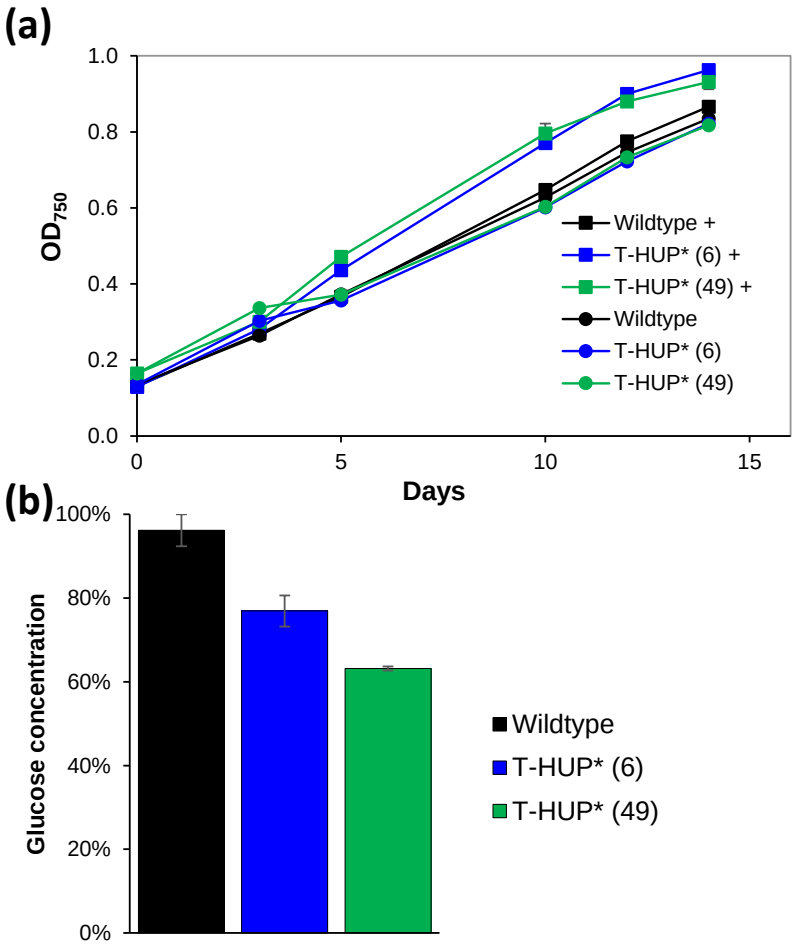

Fig. 12 Growth of wildtype and T-HUP* mutants for 14 days under high light. Cells were grown in biological duplicates under a light field of 120 µmol·m^{-2}·s^{-1} with a 16-hour light/8-hour dark cycle at 18°C and a controlled CO_2 value of 480 ppm, with (+) or without the addition of 5 mM glucose. Growth was measured using a microplate reader monitoring the OD at 750 nm (a). Values are mean ± SD (n=6). Glucose concentration in the medium after 2 weeks of cultivation with 5 mM glucose was investigated using HPLC (b). Values are represented in percent of the original glucose concentration as mean ± SD (n=2).

In addition to the wildtype and T-HUP* mutants, the Glut1 mutant was also cultured under the same condition as a further control (Fig. S 7). The supplemented glucose had no effect on the growth of wildtype cells, meaning that wildtype with and without glucose showed the same growth curves as did T-HUP* mutants without glucose under this light condition. In contrast to this finding, T-HUP* mutants cultured with glucose showed an increased growth after 5 days. The curve increased in a linear manner until day 10 and levelled off slightly by the end of the growth period (14 days). The investigation of the glucose concentration in the medium was an end-point measurement and was analyzed via HPLC (Fig. 12, b). T-HUP*(6) and T-HUP*(49) had consumed 23 ±3.7 and 37 ±4.8%, respectively, of the glucose in the medium. To conclude, both T-HUP* mutants show increased growth when using mixotrophic mode and a low glucose concentration.

In contrast to heterotrophic mode, mixotrophic mode depends on light and organic carbon sources, here glucose. In addition, optimized mixotrophic growth also depends on sufficient heterologous expression of glucose transporters. In the next experiments HUP1 protein abundance was monitored during the whole growth period under different light intensities. At medium light, 60 µmol·photons $m^{-2}·s^{-1}$ protein samples were taken and analyzed after 7, 10 and 14 days (Fig. 13, a, b). At very weak (10 µmol·photons $m^{-2}·s^{-1}$) and at higher light intensities (120 µmol·photons $m^{-2}·s^{-1}$), only end-point measurements of protein levels were compared (Fig. 13, c). Cells were either cultured with the supplementation of glucose [5 mM] or without, enabling the investigation of glucose uptake of mutants. As a loading control, α-Lhcf1-11 was used again to control equal loading of the samples. Thus, under all conditions investigated in these experiments, T-HUP* (49) showed higher protein levels, compared to T-HUP* (6). As expected from monitoring growth at higher light intensities (Fig. 12), protein levels decreased with culture age in both mutants under medium light (Fig. 13, a, b). The comparison of protein abundance in both T-HUP* mutants under different light intensities showed a stronger signal at low light intensity (Fig. 13, c). This is in line with previous studies, showing the highest activity for fcpA promoter under low light (Nymark et al. 2009). No differences in protein abundance can be seen for cultures grown with or without glucose (Fig. 13), implying no glucose sensing in the heterologous system.

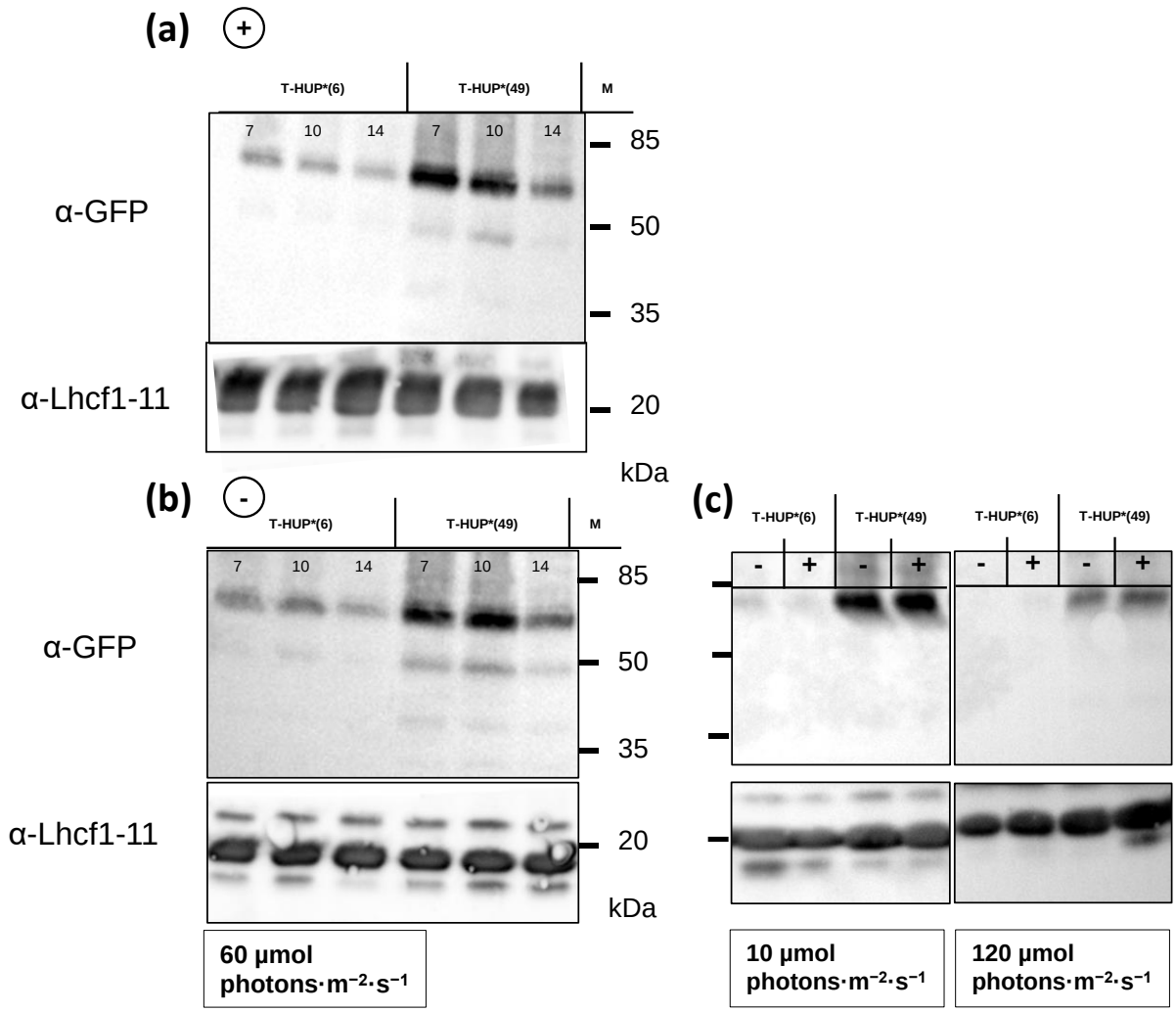

Fig. 13 Comparison of protein expression of Hup mutants. Western blot of two Hup mutants, T-HUP*(6) and T-HUP*(49) sampled after 7, 10 or 14 days at a light intensity of 60 µmol photons·m^{-2}·s^{-1} with (a) or without (b) the supplementation of 5 mM glucose. (c) Cells grown for 14 days with (+) or without (-) 5 mM glucose under low light intensity (10 µmol photons·m^{-2}·s^{-1}) or high light intensity (120 µmol photons·m^{-2}·s^{-1}). The expected molecular weight of the Hup mutants expressing the full-length protein is 84.6 kDa. As loading control, the Lhcf1-11 antibody was used. 5 µl of the Prestained Protein Molecular Weight Marker (Thermo Scientific) was added as protein size reference. Samples corresponding to 10 µg Chl_a were loaded.

Finally, I compared the end-point CDW measurements under chosen light intensities and the effect of light intensity and glucose supplementation on biomass accumulation. First, independent of the strain and the presence or absence of glucose, *P. tricornutum* cells showed increased CDW under high light intensities (Fig. 14, a). In order to better compare the growth experiments at different light intensities, CDW samples were normalized. For every cell line (wildtype, Glut1, T-HUP*(6), T-HUP*(49)) under all light conditions separately, CDW of samples with glucose were normalized to the average of CDW samples without glucose (Fig. 14, b).

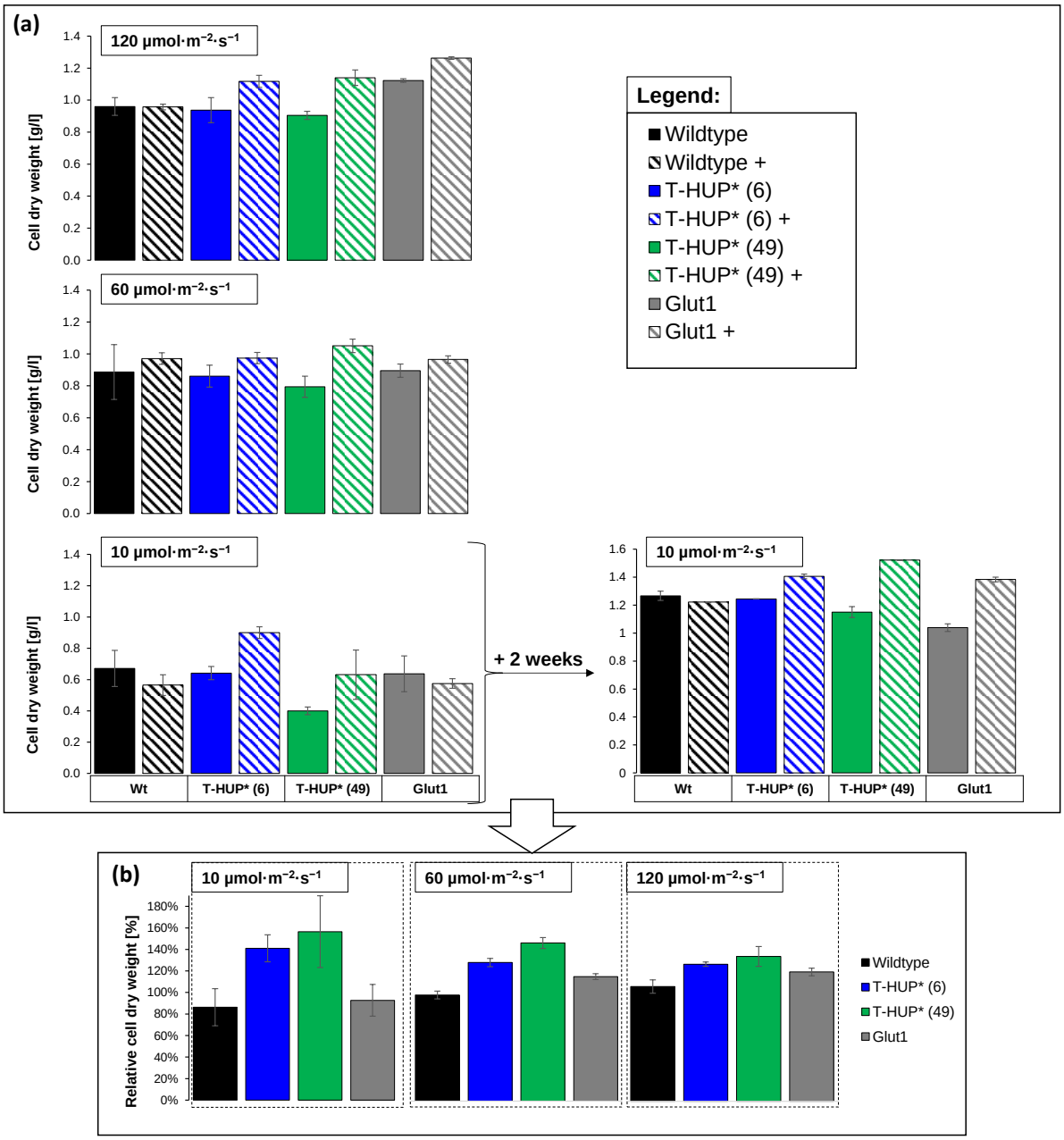

Fig. 14 Overview of CDW after growth with glucose under different light intensities. Wildtype, T-HUP* mutants and as positive control Glut1 cells were grown in biological duplicates under a light intensity of 10, 60 or 120 µmol $m^{-2}·s^{-1}$ with a 16-hour light/8-hour dark cycle at 18°C and a controlled CO_2 value of 480 ppm with (striped bars) or without (blank bars) 5 mM glucose. The final cell dry weight (CDW) was calculated after 2 weeks for al light intensities (a). Values are mean ± SD (n=4) for experiments at 120 and 60 µmol photons $m^{-2}·s^{-1}$ and values are mean ± SD (n=2) for the experiment at 10 µmol photons $m^{-2}·s^{-1}$. After additional 2 weeks CDW was determined for cultures grown at 10 µmol photons $m^{-2}·s^{-1}$. Here, wildtype, T-HUP* mutants and as positive control Glut1 cells were grown in biological triplicates. Values are mean ± SD (n=4). Further, the CDW of cells grown under glucose was normalized to the values of cells grown without (b). Values are mean ± SD (n=4) for experiments at 120 and 60 µmol $m^{-2}·s^{-1}$ and Values are mean ± SD (n=2) for the experiment at 10 µmol $m^{-2}·s^{-1}$. Björn Sabel (Uni Frankfurt) collected the raw CDW data for the growth experiment at 60 µE µmol photons·$m^{-2}·s^{-1}$ and Fabain Haitz (Uni Frankfurt) collected the raw CDW data for the growth experiment at 10 µE µmol photons·m−2·s−1 for 4 weeks.

Relative CDW of wildtype cells did not change with glucose irrespective of the light intensity. In contrast, T-HUP* mutants and the positive control Glut1 showed a positive effect under all

chosen light conditions. For T-HUP* mutants the effect of glucose uptake on relative CDW increased with decreasing light intensity. At high light intensity the relative CDW of both mutants was between 20 and 30% higher when cultured with glucose, and finally reached a maximum of approximately 45% for T-HUP*(49) at low light (Fig. 14, b).

6. Discussion (Chapter I)

The results of the bioinformatical study showed no clear pattern for targeting sequences, neither in plasma membrane transporters nor in analyzed putative glucose transporters. It seemed to be rather variable if e.g. web-based programs predicted a signal peptide or signal anchor (Tab. S 3;Tab. S 6). In general, the family of sugar porters is diverse in sequence and function, whereas the subgroup of MFS are ubiquitous and are best conserved at the N-terminal regions (Pao et al. 1998). The results of my *in situ* localization study of the heterologous HUP1 protein in *P. tricornutum* support the hypothesis that targeting is conserved across different organisms. In line with previous results (Matsui et al. 2018; Nakajima et al. 2013), GFP dots suggest that protein is exported from the ER via vesicles to the Golgi-apparatus and is finally inserted into the plasma membrane. Furthermore, mutants expressing only the N-terminal sequence of the HUP1 protein showed eGFP signals at the CERM. In all probability, correct targeting is not sufficient for just the partial protein of HUP1, because this peptide only reached the ER membranes but was not transferred further to the plasma membrane (Fig. 8). It is highly probable that the sequence of HUP1 possesses a signal anchor that is known to be important for the correct targeting of multi-spanning membrane transporters which is missing in T-spHUP* mutants (Berndt et al. 2009; Shao and Hegde 2011). Further *in situ* localization studies, using either different mutations in the HUP1 sequence or expression of different sequence lengths of HUP1, could help to clarify open questions.

Interestingly, a novel tri-aromatic sorting motif, WxxHxxW was found in a study with sugar transport proteins (STPs) 1 and STP 13 and was identified as an ER export signal (Yamada et al. 2017). Aforementioned putative sugar transporters were screened for this motif (Tab. S 6) and except for five glucose transporters from *H. sapiens* and *P. tricornutum*, this motif or small variations of it can be found in all IMPs (Fig. 15).

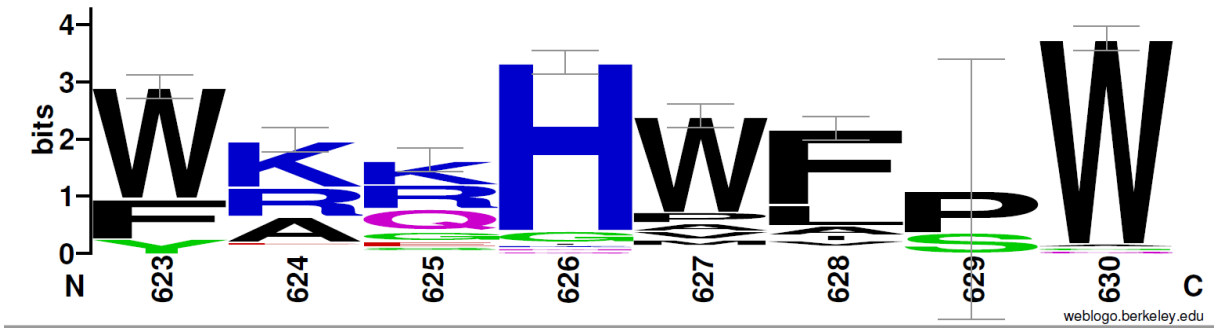

Fig. 15 Motif found in sugar transporters of different species. A novel sorting motif WxxHxxW was found in sugar transporters of different organisms using a MAFT alignment (Katoh and Standley 2013) and was displayed using WebLogo (Crooks et al. 2004). Sequences used for this alignment and the corresponding sequence IDs are listed in Tab. S 6.

In comparison to the sequences of glucose transporters of *A. thaliana*, HUP1 has also the tri-aromatic motif at the C-terminal tail of the protein with a small variation YxxHxxW. Hence, the N-terminal sequence of HUP1 enabled its insertion into the ER, whereas it is highly likely that the tri-aromatic sorting motif at the C-terminal is necessary for the ER export and its proper localization at the plasma membrane. However, this motif was not found in human glucose transporters GLUT1 and GLUT2 nor in two homologous putative glucose transporters that are not yet characterized (Tab. S 6). Nevertheless, Zaslavskaia and colleagues could show a correct targeting at the plasma membrane of *P. tricornutum* for engineered strains expressing the GLUT1 transporter fused to eGFP (Zaslavskaia et al. 2001).

The results of the *in situ* localization study combined with bioinformatical research has provided more insights into plasma membrane protein targeting, but there are still questions that need to be answered. Therefore, diatoms, including *P. tricornutum* need to be screened for more plasma membrane transporters. These transporters then need to be subsequently analyzed bioinformatically, for example with motif-based scans, to identify putative sorting motifs in diatoms. Interestingly, in diatoms, glucose transporters from *S. cerevisiae* are not active, whereas the insertion of human glucose transporters enabled trophic conversion of the *P. tricornutum* cells (Zaslavskaia et al. 2001). Furthermore, previous data has shown that human glucose transporters need to be modified in order to properly function in *S. cerevisiae*, for example a deletion of an external loop in GLUT2 improved the functionality of the transporter (Schmidl et al. 2020; Tripp et al. 2017; Wieczorke et al. 2003). Yeast transporters are well studied and could be a good alternative to chlorophyte glucose transporters, but probably need to be modified to be functional in diatoms too.

Unknown metabolic pathways or, as described earlier, open gaps in targeting pathways hamper the genetical manipulation in microalgae, including diatoms. However, another aspect of limited numbers of microalgae used as an economically viable recombinant expression system is their less efficient growth, especially in industrial systems. Heterotrophic growth is a very promising growth system, for example *C. kessleri* (formerly called *C. vulgaris*) showed highest growth and respiration rates using glucose under heterotrophic growth conditions (Griffiths et al. 1960). Especially glucose is an attractive organic carbon source, having a high standard heat of combustion with 2.8 kJ/mol (Boyle and Morgan 2009) and enabling the production of high-value products (Bumbak et al. 2011; and reference herein). Mixotrophic growth combines advantages of hetero- and phototrophic growth. As explained in the general introduction, there is a genomic and functional diversity within the *P. tricornutum* species (Martino et al. 2007; Rastogi et al. 2020). There also might be differences in the functionality of glucose transporters in *P. tricornutum* strains (Huang et al. 2015; Zheng et al. 2013). For example, research in Pt2 (UTEX 640) showed that cells could uptake glucose, but at least five times more glucose than was used here was necessary to achieve higher biomass

accumulation (Cerón García et al. 2000; Cerón García et al. 2006). In this study I focused on the strain UTEX 646, which showed outstanding characteristics (Rastogi et al. 2020). Recently, for the same strain but grown under overall different culture conditions, researchers could show higher biomass accumulation when cultured with two times more glucose (Patel et al. 2019). Under the chosen conditions in this study, wildtype UTEX 646 showed neither significant glucose uptake (Fig. 9), nor higher biomass accumulation when cultured with glucose (Fig. 14). Further experiments are necessary to analyze the expression of possible homologous glucose transporters (VCT3, Phatr 30620; SLC transporter, Phatr 12520), in *P. tricornutum* strains and subsequently also clarify their localization *in vivo*.

Taken together, previous research and my results presented in this study demonstrates that sugar porters present in *P. tricornutum* are probably not very active *in vivo* at low glucose concentrations. They possibly all belong to the class of uniporters, like Glut1, and hence need a higher glucose concentration to import glucose along a concentration gradient (Mueckler et al. 1997).

Highly efficient heterologous expression depends on many factors, e.g. codon optimization or endogenous enhancers and regulatory elements (Potvin and Zhang 2010). Codon optimization is a tool that has been investigated in *P. tricornutum* (Castell et al. 2021; Fabris et al. 2020; Hempel, Lau et al. 2011). Due to the increasing number of genome sequences available nowadays, the tool itself is gaining more interest, because of its reliability. Thus, I evaluated the necessity of codon-optimization, comparing the codon bias from the host *C. kessleri* to that of *P. tricornutum*. With the web-based program graphical codon usage analyser (Fuhrmann et al. 2004) and the codon table of Kazusa (http://www.kazusa.or.jp/codon/; *Phaeodactylum tricornutum*, 47 CDS's (17851 codons), the codon bias of these two organisms was compared for the sequence of HUP1 (NCBI, accession no. X55349.1). In the sequence of HUP1, two Arginin codons (AGG; pos 196 and 499) were found with a low abundance of approximately 5% in *P. tricornutum*. The rest of the sequence has codons that have an abundance of at least 20% or higher or, in case of a lower abundance of 20%, they only differ in the last base from frequently used codons. Therefore, the *hup1* gene sequence was inserted without codon optimization. In fact, my results underline, that codon optimization is not required for high gene and protein expression (Fig. 7) and this is supported by others (Seo et al. 2015; Shemesh et al. 2016).

Pudney and colleagues demonstrated highest phytase activity in strains engineered with the native fcpA or the viral CIP1 promoter in comparison to strains engineered with the native EF2 promoter, showing less phytase activity (Pudney et al. 2019). In line with this result, the RT-qPCR data together with the *in situ* localization study showed that a gene-promoter combination is relevant for the heterologous expression of the chosen protein, HUP1. Previous

research solely on GFP expression showed that the NR promoter yielded higher expression levels than the fcpA promoter (Chu et al. 2016). In my experiments with an excess of nitrate in the culture medium, the mutants engineered with the native fcpA promoter showed a higher gene and protein expression compared to the native NR promoter.

In conclusion, I showed with respect to high expression mutants T-HUP* that the HUP1 transporter is targeted correctly to the plasma membrane in the heterologous system of *P. tricornutum* and enables the cells to take up glucose at low glucose concentrations.

In contrast, to the integration of human Glut1 (Zaslavskaia et al. 2001) or moos Glut1 (Hamilton et al. 2016), HUP1 from *C. kessleri* did not trophically convert the alga into growing heterotrophically. It is worth mentioning that, based on the study of both, the fcpA promoter is also active in the dark. Therefore, the question still remains: why do mutants not grow heterotrophically (Fig. 16)?

The results of the extended investigation about the protein level in T-HUP* mutants over a growth period or under different light intensities revealed important information. First, the glucose transporter expressed in *P. tricornutum* is not inducible by glucose in the medium, as it was shown in the host, *C. kessleri* (Komor and Tanner 1971). Additionally, data concerning the protein levels under different light intensities showed higher protein levels under low light. Whether the T-HUP* mutants up-regulate the protein expression under low light intensities or if protein abundance indicates the activity of the fcpA promoter under different growth conditions could not be determined. At medium light, cells were sampled over the growth period and protein levels were lower after 14 days, when cells entered the stationary phase. Lower protein expression could be also demonstrated for other *P. tricornutum* strains engineered with the fcpA promoter in older cultures (Erdene-Ochir et al. 2016; Shemesh et al. 2016). It is very likely that, under very weak light intensities, the culture enters the stationary phase later since nutrients start becoming rare after a longer time period (Fig. 14).

In contrast to the sugar sensing that is missing in T-HUP* mutants on the protein level, the data of the radioactive labeled glucose assay under different pH values showed that the pH dependency of the HUP1 transporter is similar in the heterologous system of *P. tricornutum* and in the host *C. kessleri* (Komor and Tanner 1974). During growth at a high cell density of *P. tricornutum* a higher pH value was measured (Fig. 11) and hence the activity of the HUP1 transporter is most likely inhibited. In this experiment, the pH value increased to up to 8.5 at day 7 whereas even higher pH values were measured (Kruijff 2021) as has also been reported in literature (Zhang et al. 2016). Based on these findings, the protein level and the functionality of the glucose transporter decreases over culturing time. Due to the implication of the rising pH values, cells cannot produce enough energy with the limited uptake of glucose under the chosen growth conditions. In conclusion, the choice of media, the culture system (e.g., batch

or fed-batch) and the choice of promoter might be of relevance to further improve HUP1 expression and to achieve even higher CDWs (Fig. 16).

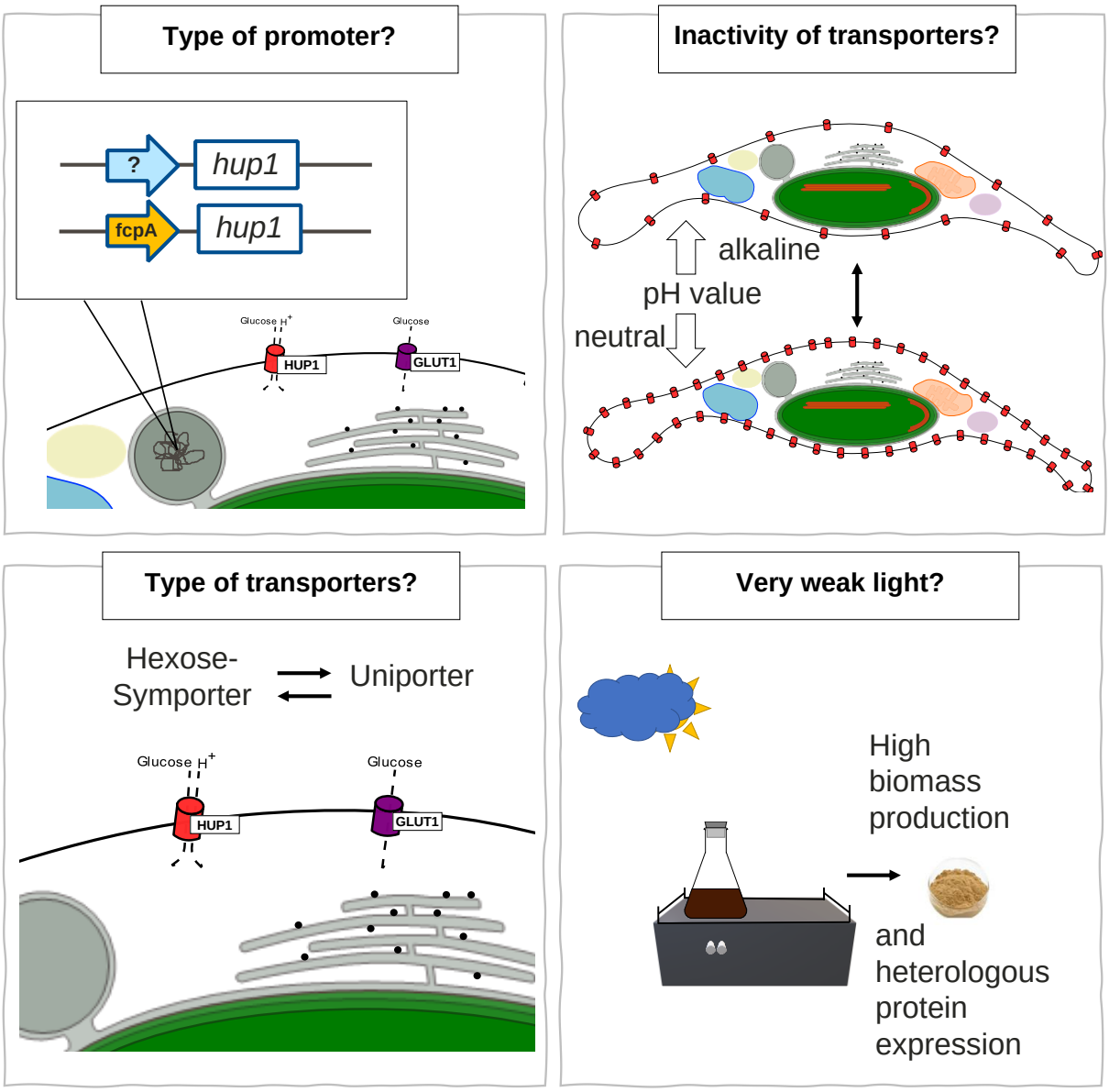

Fig. 16 Schematic overview about possible reasons of the missing heterotrophic growth in engineered strains characterized in this study.

There are controversial results about the effect on the trophic conversion of chlorophytes or diatoms expressing the HUP1 glucose transporter from *C. kessleri* (Doebbe et al. 2007; Fischer et al. 1999; Hallmann and Sumper 1996; Waissman-Levy et al. 2019). Interestingly, engineered strains of *C. fusiformis* could not grow in the dark, even though the glucose uptake at 1 µmol glucose/10^7 cells per hour was much higher than in this study (Fischer et al. 1999). Controversially, Zaslavskaia and colleagues (2001) claimed that cells with an uptake rate of greater than 0.0174 µmol glucose/ 10^8 cells per hour can grow heterotrophically. In this study I measured values of 2.65 µmol glucose/10^8 cells per hour, hence this glucose uptake value

lies between these two studies. Thus, based on the successful heterotrophic growth of the mutants demonstrated by Zaslavskaia, the lack of cell growth in the dark cannot solely be due to the uptake rate of the mutants of this study. The heterologous expression of HUP1 in *H. pluvialis* enabled heterotrophic growth, but mutants showed only minor growth compared to very weak illumination. Hence, authors concluded that light is needed for glucose metabolism (Waissman-Levy et al. 2019). The results of this study support this hypothesis for glucose metabolism in *P. tricornutum*. Here as well, very weak illumination (10 µmol·photons $m^{-2}·s^{-1}$) was sufficient to cause significant differences in growth for T-HUP* mutants when cultured with glucose (Fig. 14). These differences could not be enhanced by increasing the light intensity.

6.1. Conclusion

In this part of the study, *P. tricornutum* mutants that express a heterologous glucose transporter were generated. These genetically engineered strains were characterized regarding the different biochemical and physiological functions of the heterologous protein.
The following aspects can be concluded from the aforementioned results:

1. The HUP1 glucose transporter from the chlorophyte *C.kessleri* was successfully expressed in the diatom *P. tricornutum* without any further editing.
2. Only the full-length fusion protein, HUP1-eGFP is correctly targeted to the plasma membrane, whereas the N-terminal sequence of HUP1 is targeted to the CERM.
3. The highest expression of the *hup1* gene was detected under the control of the fcpA promoter. In contrast, mutants expressing the HUP1 protein under the control of the NR promoter showed little gene and protein expression.
4. The investigated transformants were not trophically converted to enable heterotrophic growth, but low light intensities were sufficient to stimulate growth. Therefore, it is possible that the glucose metabolism is light-dependent in this *P. tricornutum* strain (Pt4, UTEX 646). For T-HUP* mutants, the highest protein expression was measured at low light intensities and low glucose concentrations. These conditions were sufficient to yield 20% higher CDWs compared to the wildtype.
5. The decreasing protein abundance over the culture period and the glucose uptake rate indictae that optimized growth conditions and harvesting time would lead to higher CDW values in these transformants. In detail, the glucose uptake rate at 45 nmol/10^8 cells per minute (Fig. 10) should be 16 times higher compared to what has been measured elsewhere (Fig. 12).

Chapter II: Optimization of the culture medium yielding high lipid profile in wildtype *Phaeodactylum tricornutum* cells

7. Introduction (Chapter II)

Microalgae are an alternative source for many products used in biotechnology and the pharmaceutical industry, including the synthesis of PUFAs (Hamilton et al. 2015; Moog et al. 2019; Roesle et al. 2014). They do not compete with arable land, can grow fast, and have a high and specialized production of lipids. Furthermore, algal biomass can be used in multiple ways, thus waste can be eliminated (Draaisma et al. 2013; Hess et al. 2018). Humans are not able to synthesize some ω-3 PUFAs *de novo*, e.g. EPA (C20:5) or DHA (C22:6) (Apt and Behrens 1999). Humans have a low conversion rate from α-linolenic acid (ALA, C18:3) to EPA, docosapentaenoic acid (DPA, C22:5) and DHA (Weylandt et al. 2015). Because of their high beneficial role in human health, the demand on these ω-3 fatty acids is very high (Kitessa et al. 2014).

Diatoms are the most diverse group of microalgae distributed worldwide. They are one of the main primary producers in the oceans and show remarkable lipid remodeling in response to N limitation (Falciatore et al. 2020). One main model organism of this group, the oleaginous alga *P. tricornutum* has been the focus of researchers in the last decade. Based on data, mainly on most widely studied Pt1, the oleaginous alga is known to have a high content of ω-3 fatty acids, especially EPA (Pérez-López et al. 2014).

Recently, an overview of the genomic diversity of up to ten accessions of *P. tricornutum* revealed a subdivision into four clades based on conserved genetic and functional makeup. One of the ten accessions, Pt4 (here called wildtype; UTEX 646), was clustered in an isolated clade and showed a specific functional specialization, e.g. a high expression of a gene involved in nitrate assimilation (Rastogi et al. 2020). In line with these results for wildtype UTEX 646, a distinct carbon acquisition strategy is proposed due to differences in gene expression e.g. a downregulation of a plasma membrane bicarbonate transporter (Huang et al. 2020). Differences within the species of *P. tricornutum* highlight the relevance for distinguishing between accessions and their characteristics (Kuzminov and Gorbunov 2016; Rastogi et al. 2020). For example, Leyland and colleagues have shown that the number and the size of the lipid droplets is different between Pt1 (CCMP2561) and Pt4 (UTEX 646) (Jaussaud et al. 2020; Leyland, Zarka et al. 2020).

As a single cell organism, *P. tricornutum* has to react to dynamic conditions in order to maintain its metabolic homeostasis. Storage capabilities like lipid droplets are a strategy to react swiftly to environmental changes (Leyland, Boussiba, and Khozin-Goldberg 2020). During N starvation, the lipid remodeling is directed towards TAG synthesis. These TAGs are then

mainly stored in lipid droplets (Jaussaud et al. 2020; Leyland, Zarka et al. 2020; Remmers et al. 2018). In general, the lipid profile of diatoms consisting of SFAs, MUFAs and PUFAs differs between species and is influenced by stress (Cui et al. 2019; Hess et al. 2018; Qiao et al. 2016).

In detail, the lipid composition depends on several abiotic factors, including the light settings (photoperiod, intensity, quality), temperature, salinity, pH-values as well as the nutrient composition, as summarized earlier (1.3). Hence, the medium composition is a huge factor influencing the lipid metabolism.

The usage of small PBRs enables the constant monitoring of growth parameters and reveals the aspects that need to be improved for industrial applications. Some research has been carried out with respect to *P. tricornutum* (Jallet et al. 2016), but rarely using Pt4 (UTEX 646) (Tab. 1).

In this study, I compared a commercial growth medium F/2 with our lab medium ASP, modified from Provasoli et al. (1957). I achieved optimized growth and lipid content by using different concentrations of the nitrogen and phosphate supply.

8. Material and methods (Chapter II)

8.1. Culture and growth conditions

Precultures of the chromalveolate alga *P. tricornutum* (UTEX 646, Pt4) were grown as described in chapter I (4.1.2) with a light intensity of between 60 - 100 µmol photons $m^{-2} \cdot s^{-1}$ white light, depending on the specific growth experiment. In addition to the ASP medium, two media with lower nitrate and phosphate concentrations were used, namely ASP_{LNP} (Low Nitrate and Phosphate concentrations) and ASP_{VLNP} (Very Low Nitrate and Phosphate concentrations) (Tab. 7; Fig. 17; Tab. S 7). The ASP_{VLNP} medium was further modified with additional trace metals and vitamins (based on Berges et al. 2001), further called ASP^{+}_{VLNP} (Tab. S 7).
Furthermore, a commercial medium, F/2 (Cell-Hi F2P, Varicon Aqua, Hallow, Worcestershire, England, United Kingdom) with additional 5g/l NaCl was used. In comparison to ASP it contains identical NaCl concentrations but less Mg, whereas the concentrations of trace elements and vitamins is comparable to ASP^{+}_{VLNP}. In another approach the commercial F/2 was dissolved in seawater (collected from the Helgoland trench, filtered through 0.45 µm and 0.1µm filters and autoclaved, Alfred-Wegener-Institute, Bremerhaven, Bremen, Germany) and the medium called $F/2_{SW}$ (Seawater). The composition of the seawater was assumed to be similar to that reported recently with a salinity of approximately 36 g kg^{-1} (Millero et al. 2008). Therefore, the total salt concentration in this medium is seven times higher salt concentrations were used in the $F/2_{SW}$ medium compared to F/2, two times higher compared to ASP^{+}_{VLNP} and about three times higher compared to ASP_{VLNP} and ASP_{LNP} (Tab. S 7).
In this study a total of six different media were used with differences in nitrate and phosphate concentrations (Tab. 7; Fig. 17), while some also differed in the composition of the micro-nutrients. A detailed overview of the different medium composition is listed in the supplemental information (Tab. 7).

Tab. 7 Overview of growth medium regarding the marco nutrients phosphate and nitrate concentrations used in this study.

			Literature	
Medium	**NO_3^-** [mg/l]	**PO_4^{3-}** [mg/l]	**NO_3^-** and **PO_4^{3-}** concentration	**Medium composition**
ASP	729.5	55.07	(Mann and Myers 1968)	(Provasoli et al. 1957)
ASP_{VLNP}	54.74	3.41	(Guillard 1975)	
ASP^+_{VLNP}				
ASP_{LNP}	109.44	6.84	(Guillard and Rhyter 1962)	
F/2	144	11		(Guillard 1975)
$F/2_{SW}$				

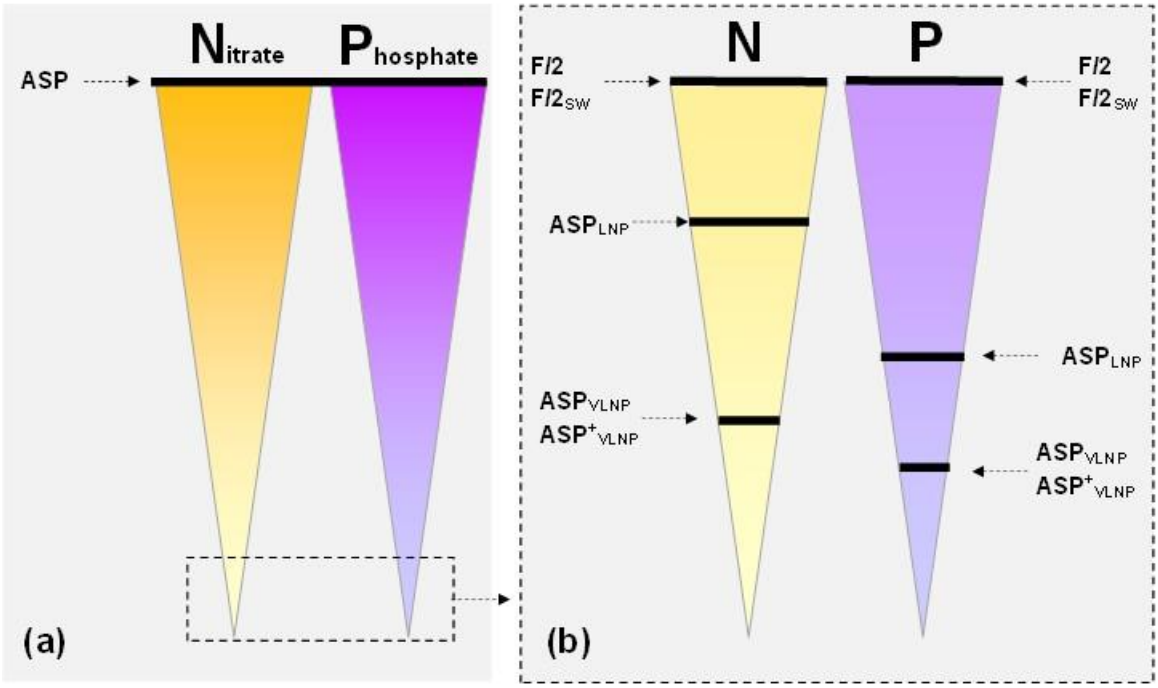

Fig. 17 Nitrate and phosphate concentration of media used in this study graphically symbolized. . The triangles show nitrate (yellow) and phosphate (purple) concentrations used in this study. In figures (a) and (b) the nitrate and phosphate concentrations for the six different media used in this study are displayed (see Tab. 7).

8.2. Operation of a photobioreactor and conditions of growth experiments

For every PBR experiment, precultures grew in the same medium as used in the main experiment. A conventional PBR FMT-150 (Photon Systems Instruments, Drasov, Czech Republic) with a 1-L glass vessel and LED illumination on one side (Fig. 18) was used as culturing system. Light intensity was set to 60 or 100 µmol photons $m^{-2} \cdot s^{-1}$ white and red light,

depending on the growth experiment. Besides an antibiotic cocktail, the sterile growth condition was further guaranteed by first filtering the air (0.2 µm diameter filter) through a humidifier before it entered the U-Loop system of the PBR for some experiments. The filtered air was pumped using an air pump for aquaculture (ProSilent; 400 l h^{-1}, JBL). Additionally, the gas influx system mixed the cells. The pH electrode (InPro 325Xi ISM, Mettler Toledo, Columbus, Ohio, USA) was sterilized with 1 M sodium hydroxide solution and the temperature [18°C] and pH-level were further monitored.

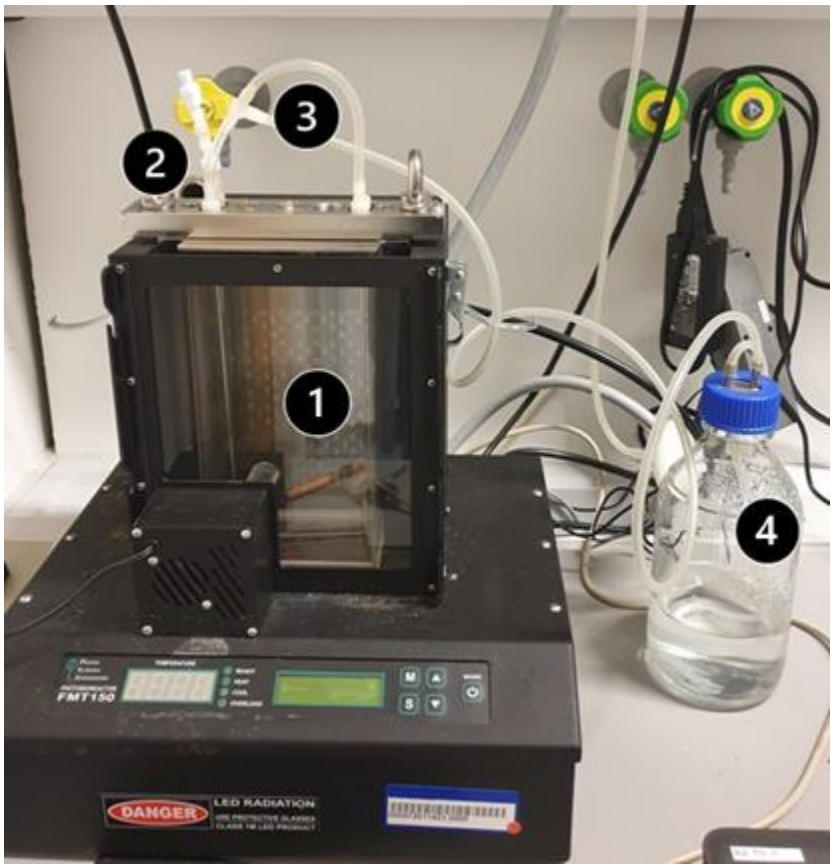

Fig. 18 Photobioreactor FMT150. Numbers indicating following devices: (1) glass vessel; (2) pH electrode; (3) U-loop system; (4) humidifier.

The PBR was filled to a maximum of 1 l volume and the cell concentration was adjusted to 1 to 2 x 10^6 cells/ml. Samples were taken with a syringe during the culture period of 9 or 11 days. Sampling points were chosen before the 8 h dark period, thus the dark period was implemented during the day to do the sampling at daytime. Samplling shortly before dark is known to yield samples with maximal neutral lipid content (Jallet et al. 2016).

The constantly monitored data, e.g. pH-value, temperature, OD_{735} and quantum yield, were partly further processed. To exclude outliers of OD measurements, fast fourier transforms (fft) filters were used to smooth the curve with 10 points using OriginPro (version: 2021b). In addition, the Boltzmann regression of the OD_{735} was calculated in OriginPro for each experiment and is displayed in each graph.

8.3. Rapid lipid analysis using lipid dyes

8.3.1. Fluorescence microscopy

The fluorescent dye BODIPY 505/515 binds specifically to lipid droplets and can be visualized in living cells (Rumin et al. 2015). These organelles have a neutral lipid that is mainly composed of TAGS (Leyland, Boussiba, and Khozin-Goldberg 2020; Yoneda et al. 2016). 200 µl of cell suspension was mixed with 1 µl BODIPY 505/515 [1 µg/µl; in DMSO] (Invitrogen, Carlsbad, California, USA) and incubated at RT for several minutes. In contrast to BODIPY, Nile red is highly sensitive to the polarity of the surrounding environment and stains polar and neutral lipids. Thus, it can be used for visualization of both lipid classes (Rumin et al. 2015). For Nile red staining, 160 µl of cells were mixed with 40 µl Nile red [2µg/ml; dissolved in DMSO]. The samples were analyzed using the fluorescence microscope Zeiss Axiophot with an external USB 3.0 color industrial camera (DFK 33UX174, The Imaging Source Europe GmbH). The chlorophyll was excited from 590 to 720 nm and the chlorophyll autofluorescence was detected at 675 nm. BODIPY 505/515 was excited at 425 to 445 nm and its fluorescence detected at 460 to 500 nm. Nile red was excited between 530 and 570 nm and detected with a long pass filter (starting 590 nm). The images were processed with the program IC Capture (Version 2.4; The Imaging Source Europe GmbH).

8.3.2. Microplate reader

In contrast to BODIPY, Nile red can be used for microplate reader experiments under the same treatment as described earlier (8.3.1) and analyzed with a spectrometer, among others due to its low background fluorescence (Rumin et al. 2015). Using a microplate reader (Spark 10M; Tecan) and the dye Nile red, a different method was used to rapidly screen the lipid content during cell growth. In technical triplicates, the fluorescence signal for Nile red of the cells was measured with an excitation wavelength of 488 nm (bandwidth 20 nm) and an emission wavelength of 590 nm (bandwidth 20 nm). The number of flashes was set to 30 and the integration time was set to 40 µs. As a control, 160 µl of cells were mixed with 40 µl DMSO. The relative fluorescence signal was calculated as the difference in the absorbance of the stained cells and the control cells.

For better comparison, total neutral lipid productivity and neutral lipid production /mg biomass (DW) were calculated as described below:

Equation 3: Calculation of fluorescence signal of stained cells using the cell dye Nile red.

$$(\boldsymbol{a})\ relative\ fluorescence\ signal\ = stained\ cells\ E_{590}[nm] - control\ cells\ E_{590}[nm]$$

$$(\boldsymbol{b})\ total\ neutral\ lipid\ productivity\ = DW_{day(x)}[mg] \times relative\ fluorescence\ signal$$

$$(\boldsymbol{c})\ \frac{neutral\ lipid\ production}{DW\ [mg]}\ = DW_{day(x)}\left[\frac{mg}{ml}\right] \times 0.160\ [ml] \times relative\ fluorescence\ signal$$

8.4. Biochemical lipid analysis

8.4.1. Lipid extraction with little cell material

First, a defined amount of culture volume was harvested (3000 x g, 15 min, 4°C), transferred to weighted 2 ml tubes and washed twice with 1 ml ddH_2O (3000 x g, 15 min, 4°C). The harvested cells were frozen with liquid nitrogen and freeze-dried in a lyophilizer at 400 mbar for 24 h. Afterwards, the lyophilized cells were weighted and the DW was calculated. These values were also used for the calculation of normalized Nile red signals (8.3.2).

If the cell material was intended to be used for GC-MS analysis, internal standards were added for a better exclusion of outliers in the lipid extraction. Either 10 µg of internal standard 1 (IS1) Decanoic Acid-d19 (IS1a; Cayman Chemical; in chloroform) or 20 µg of a C19:0 PC, namely 1,2-dinonadecanoyl-sn-glycero-3-phosphocholine (IS1b; Avanti polar lipids inc.; in chloroform), was added before extracting the broken cells.

The lipid extraction was performed according to Bligh and Dyer (1959) with minor changes. Cell disruption was performed with glass beads (Ø 0.1/0.3mm, 1:1 (w/w)) and by adding 500 µl chloroform-methanol mixture [4:5 (v/v)]. Afterwards, the tubes were shaken at 50 Hz for 3 min (TissueLyser LT, Qiagen). The lysate was transferred to 15 ml reaction tubes. The 2 ml tubes were rinsed with the chloroform-methanol mixture until a final volume of 2 ml was reached. In addition, the shaking of the tubes was repeated to improve extraction yield if necessary.

Before the phase separation, further cell disruption was achieved by strongly shaking the tubes (5 s, max Hz) and by 3 min incubation in an ultrasonic bath (Merck). With the addition of 1.25 ml Tris-NaCl solution [50 mM Tris, 1 M NaCl; pH 7] the organic solvent was separated from the aqueous phase by a repetition of the latter two steps. After centrifugation (1200 x g, 5 min, RT) the organic phase was transferred in a weighted 2 ml reaction tube. Lastly, 500 µl chloroform was added to the cell extract to improve the lipid yield, followed again by strong shaking of the tubes (5 s, max g), by 3 min incubation in an ultrasonic bath and phase seperation. These reextraction steps were repeated twice.

For the determination of the total lipid content, the solvent was evaporated under a saturated nitrogen atmosphere and samples weighted. The values obtained represent the extracted hydrophobic components, i.e. lipids without the exclusion of remaining cell pigments.

8.4.2. Comparing lipid composition using GC-MS analysis

In a first step, 1.5 ml of sulfuric acid [5% (v/v) in methanol] was added to the dried lipids and the samples were then mixed for 5 s. Secondly, they were incubated for 3 h at 70°C in a heating block. During this reactiom, the fatty acids are being methylated to the corresponding fatty acid methyl esters (FAMEs). To avoid boiling, the samples were mixed. Samples cooled to RT were further mixed several times after adding 200 µl of ddH_2O and 200 µl of Hexane [4°C, cooled] and then inverted for 15 min. The samples were centrifuged (1200 x g, 5 min) and the 200 µl hexane phase was collected and transferred to a new reaction tube. The hexane phase was washed by adding 250 µl of ddH_2O, the samples were mixed by vortexing (5 min) and centrifuged (1200 x g, 5 min). To promote the collection of the hexane phase, samples were frozen at -20°C. With a Pasteur pipette the hexane phase was filled in GC-vials and kept at -20°C until further usage.

Before commencing the GC-MS analysis, a second internal standard (IS2), namely myristic acid methylester-d27, was used. To calibrate the device, a calibration series was prepared using the IS2 and varied volumes of FAME standards (Supelco 37 Component FAME Mix, Sigma).

To prepare the GC samples with transesterificated algae lipids, 5 µl of the hexane phase, 25 µl of IS2 [10 µg/ml; in hexane] and 470 µl hexane were mixed-well. The prepared samples and the calibration series were measured using the GC-MS method as follows:

The gas chromatograph (Agilent 7890A; Aligent Technologies) was coupled to a quadrupole mass selective detector (Agilent 5975C; Aligent Technologies). A sample volume of 1 µL was loaded onto a 30 m HP-5MS UI capillary column (⌀ 0.25 mm; 0.12 µm film thickness). The inlet was operated in splitless mode at 200°C and after 5 min the purge valve was switched on at 50 ml min^{-1}. Helium was used as a carrier gas at a constant flow rate of 1.5 ml min^{-1} through the column. The GC temperature program started at 50 °C (hold time 1 min), followed by an increase to 180 °C at a rate of 7 °C min^{-1}, then to 230 °C at a rate of 2 °C $min^{-1}$and finally to 280 °C at a rate of 10 °C min^{-1} (hold time 3 min). The total runtime was 54.07 min. A solvent delay of 10 min was applied. The transfer line was kept at 280 °C. The ionization energy was 70 eV and the temperature of the ion source and quadrupole was set to 230 °C and 150 °C, respectively. In full scan mode, m/z 40-400 was recorded. In SIM mode, four characteristic fragment ions for each FAME were monitored during the respective retention time slot. Agilent

ChemStation and Enhanced Data Analysis were used for instrument control and data analysis. The GC analysis was carried out by Peng Li from university of Tübingen.

8.4.3. Comparison of lipid classes using thin layer chromatography (TLC)

If not used for the GC-MS analysis, the dried lipid extracts were solved in hexane:isopropanol (3:1) solution, adjusted to a concentration of 10 mg ml^{-1} and loaded on silica plates for a thin layer chromatography (TLC). As a control, different standards were spotted on the plates as well. For neutral lipid separation tripalmitate (TAG), 1,3-palmitoyl glycerol (DAG) and 1-palmitoyl glycerol (MAG) were used as references and for polar lipids phosphatidylinositol (PI), phosphatidylcholine (PC) and phosphatidylglycerol (PG) were used. The samples, together with the standards, were analyzed by TLC on Silica Gel 60 plates (Merck) using two different solvents. One solvent is used for the separation of neutral lipids [NL: hexane–diethylether–acetic acid (70:30:1) (v/v)] and one for polar lipids [PL: chloroform–methane–ammonia solution (65:25:5) (v/v)]. The separated lipids were stained using primulin [50 mg/ml in 80% acetone] and the plates were documented under UV light at 365 nm.

9. Results (Chapter II)

9.1. Testing effect of different media on the growth of wildtype cells

PBRs as culture systems enable the continuous monitoring of cells during growth experiments. For this reason, cells in exponential growth were harvested and transferred to 1L PBRs for further experiments. To estimate the fitness of the cells, the quantum yield and the pH- and OD-values were measured during the experiments.

In a first experiment I compared two different main media, commercial Cell-Hi F2P (varicon aqua; here called F/2) and ASP medium. The latter, ASP, is our common culture medium for *P. tricornutum* cells with excess N and P concentrations (Tab. S 7 and Fig. S 8). To investigate different N and P concentrations, I further used ASP media with reduced concentrations of nitrate and phosphate according to Guillard (1975) or Guillard and Rhyter (1962). ASP_{LNP} had a reduction in phosphate and nitrate by approximately 86% (w/v) (Guillard and Rhyter 1962) and in ASP_{VLNP} nitrate and phosphate were reduced by approximately 93% (w/v) (Guillard 1975) compared to our common ASP media. In addition to these main media, I used two slightly adapted media versions, ASP_{VLNP} with additional trace elements resembling the F/2 trace elements composition, named ASP^{+}_{VLNP} and F/2 with even more trace elements and a higher salinity by using seawater instead of water, namely $F/2_{SW}$. These to adapted media ASP^{+}_{VLNP} and $F/2_{SW}$ have higher total salt concentrations with 1.75% and 3.54% respectively.

The two growth experiments with F/2 and $F/2_{SW}$ showed a sigmoidal growth as generally known for microbes (Sorokin 1969), whereas the two experiments with lower nitrate and phosphate concentrations in the medium showed a flatter curve (Fig. 19). Consequently, the maximum OD_{735} values are about half as high in these cell cultures with low nitrate and phosphate concentrations. Here, the OD_{735} value is around 0.35. The growth curve of cells grown in higher nitrate and phosphate concentrations show twice as high values, with the OD_{735} at around 0.7.

In general, in all four experiments the pH-values increased during the day when cells use photosynthesis to grow, and decreased again during the night period. In line with the OD values, the curve of the pH level is comparable in cells grown in the same nitrate and phosphate concentrations. In all cultures, the initial pH value is 7.5 ±0.3. In F/2 and $F/2_{SW}$ the pH values increased on days 4 to 10 or more. After this peak, the maximum pH value at the end of light periods decreased. In contrast to the commercial F/2, cells grown in ASP_{VLNP} and ASP^{+}_{VLNP} with low nitrogen and phosphate concentration showed almost no peaks in the pH level. In these media the maximal pH values measured between days 3 and 4 were around 8.

The effective photosystem II quantum yield was high during the exponential phase of the cells and decreased when cells entered the stationary phase. In detail, during log- and exponential phase values of the quantum yield were about 0.5 in all experiments. After day 4, values decreased and finally reached about 0.2.

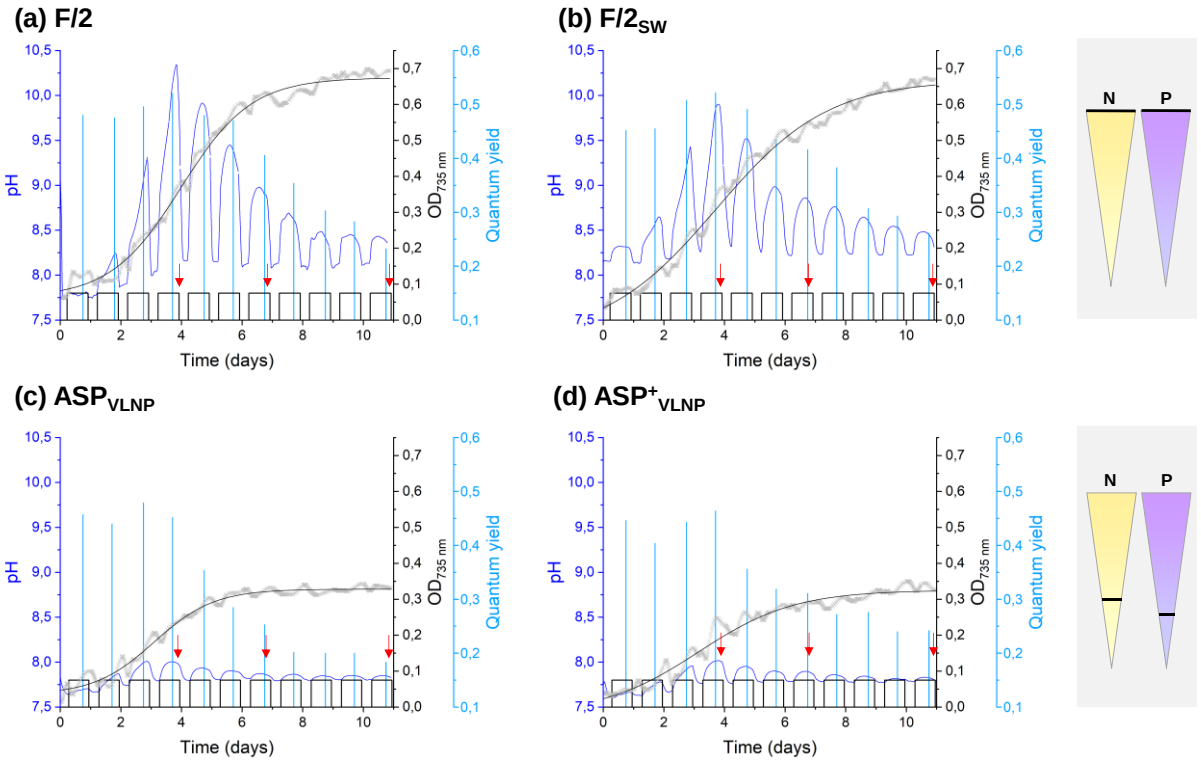

Fig. 19 Growth curve of cells cultured in different media. The medium (a) F/2 and (b) $F/2_{SW}$ have higher nitrate and phosphate concentration than (c) ASP_{VLNP} and (d) ASP^{+}_{VLNP}. Right legend symbolizes these differences in concentration of the growth media (see Fig. 17, Tab. 7). Cultivation was measured over 11 days with a light intensity of 100 µmol·photons $m^{-2}·s^{-1}$ with a 16-hour light/8-hour dark cycle (indicated with white bars) at 18°C. The pH value (dark blue) and the optical density, OD_{735} (grey), was monitored constantly, whereas the maximum quantum yield of photosystem II (F_V/F_M) was measured only in the light period and is displayed in light blue. The Boltzmann regression line is calculated and shown in black with R^2 for the Boltzmannn 99.1% (a), 99.12% (b), 98.44% (c) and 97.14% (d). Red arrows referr to sampling points for further measurements. Data was sampled by Kruijff (2021).

At three time points, after 4, 7 and 11 days samples were taken and analyzed. The analysis of CDW presents a similar trend as seen for the OD values. The highest values are obtained with commercial F/2 with 0.51 g l^{-1} and 0.45 g l^{-1} for cells grown in $F/2_{SW}$ media. With less than half of the nitrate and phosphate concentrations in the media (Fig. 19 c and d), the maximum CDW is also less than half as much, with a value of approximately 0.20 and 0.19 g l^{-1} (Fig. 20). In line with these results, the biomass production per day, the so called biomass productivity [mg l^{-1} d^{-1}], decreases for cells grown in these media after day 4. This trend can also be seen for the cells cultured in $F/2_{SW}$, whereas the biomass productivity for cells grown in solely F/2 increases until day 7 with a maximum of 60 mg l^{-1} d^{-1} (Fig. 20, b).

(a)

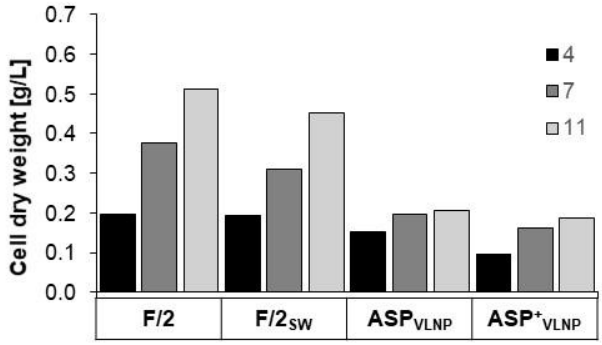

(b)

	Day 1-4	Day 5-7	Day 8-11
Biomass productivity [mg l^{-1} d^{-1}]			
F/2	49.3	53.9	46.5
$F/2_{SW}$	48.6	44.1	41.0
ASP_{VLNP}	37.9	28.2	18.7
ASP^{+}_{VLNP}	24.3	23.3	17.1
Lipid content [%]*			
F/2	47.8	54.5	38.5
$F/2_{SW}$	69.1	45.4	33.5
ASP_{VLNP}	49.1	39.1	38.9
ASP^{+}_{VLNP}	38.2	40.4	40.9
Lipid yield [g/l]*			
F/2	0.094	0.206	0.197
$F/2_{SW}$	0.134	0.140	0.151
ASP_{VLNP}	0.074	0.077	0.080
ASP^{+}_{VLNP}	0.037	0.066	0.077

Fig. 20. Overview of cell dry weight, biomass productivity and lipid content during the culture period in different media. The photobioreactor FMT150 was used, and cells were grown with a light intensity of 100 µmol·photons $m^{-2}·s^{-1}$ in different media (see Fig. 19). In table (b), biomass productivity [mg l^{-1} d^{-1}] is calculated for three time-intervals and values for lipid content [% of dry weight] refer to the day of sampling. Raw data was sampled by Kruijff (2021).

9.2. Comparison of different growth media regarding its lipid profile

Lipid dyes enable rapid lipid analysis in living cells using fluorescence devices, such as a fluorescence microscope or a spectrometer.

During the growth experiments at each sampling point (4, 7, 11 days), the cells were stained with BODIPY to monitor the lipid droplets in the cells of *P. tricornutum*. For exemplary purposes, one or two cells were chosen and images were recorded with different settings (see 8.3). As a control, bright field and autofluorescence channels were also used and are displayed (Fig. S 9). In most cases, between one and two lipid droplets evolved, increasing in size until the sampling point on day 7.

In addition, cell material was analyzed regarding its lipid composition, thus lipid extracts were separated using thin layer chromatography (TLC) or GC-MS analysis. For all GC-Ms analyses shown in this chapter, extracted samples were sent to Peng Li (Uni Tübingen), transesterificated there and raw data obtained.

In TLC analysis, primuline stained plates showed white and black spots, corresponding to lipids and pigments, respectively. I compared the different growth media over the culture period again (Fig. S 10). In addition, I spotted standards on the TLC plates as references for each run. No differences in lipid composition were detectable when cells were grown in the main media (F/2, ASP_{VLNP}) or in the edited versions ($F/2_{SW}$, ASP_{VLNP}^{+}). The analysis of neutral lipids in all growth experiments have in common that samples taken on day 4 and day 7 have a

bright signal at the height for TAGs. In contrast, a signal between DAG and TAG decreased at the end of the culture period (Fig. S 10 a+c).

Some differences in the lipid composition for neutral and polar lipids were detectable for cells grown in less nitrate and phosphate. Here, the results of cells cultured in ASP_{VLNP} and ASP^{+}_{VLNP} showed less fluorescence signals although equal quantities were spotted. The low fluorescence signal made an evaluation of the different lipids difficult (Fig. S 10 a+c).

The polar lipid composition is more diverse than that of neutral lipids when it comes to separation by TLC. Due to a limited number of standards that were used for this experiment, only a general trend for cells grown in F/2 and $F/2_{SW}$ can be seen. In contrast to the neutral lipid composition, polar lipids decreased over the culture period (Fig. S 10 b). In the two media with lower nitrate and phosphate concentrations, ASP_{VLNP} and ASP_{VLNP}^{+}, less signals for polar lipids were detected.

For GC-MS, a technical duplicate of the TLC analysis was used. For this method, the extracted lipids are transesterified, hence split in fatty acid methyl esters. With a pie chart, the percentage of each fatty acid class, namely SFA, MUFA and PUFA, of the total fatty acid content is displayed (Fig. 21, Fig. 22). With this analysis, a significant difference in the distribution of fatty acid classes over the culture period was shown in cells grown with higher nitrate and phosphate concentrations (Fig. 21). Cells grown in F/2 showed a shift between day 4 (mid-exponential growth phase) and day 7 (beginning of the stationary phase, see Fig. 19) regarding their fatty acid classes. 25% of the total fatty acid content changed from PUFA to MUFA, yielding a final distribution of 25% PUFA, 57% MUFA and 18% SFA at day seven. For cells grown in $F/2_{SW}$ a similar trend was visible, albeit that the shift is only by 18% as opposed to 25% (Fig. 21).

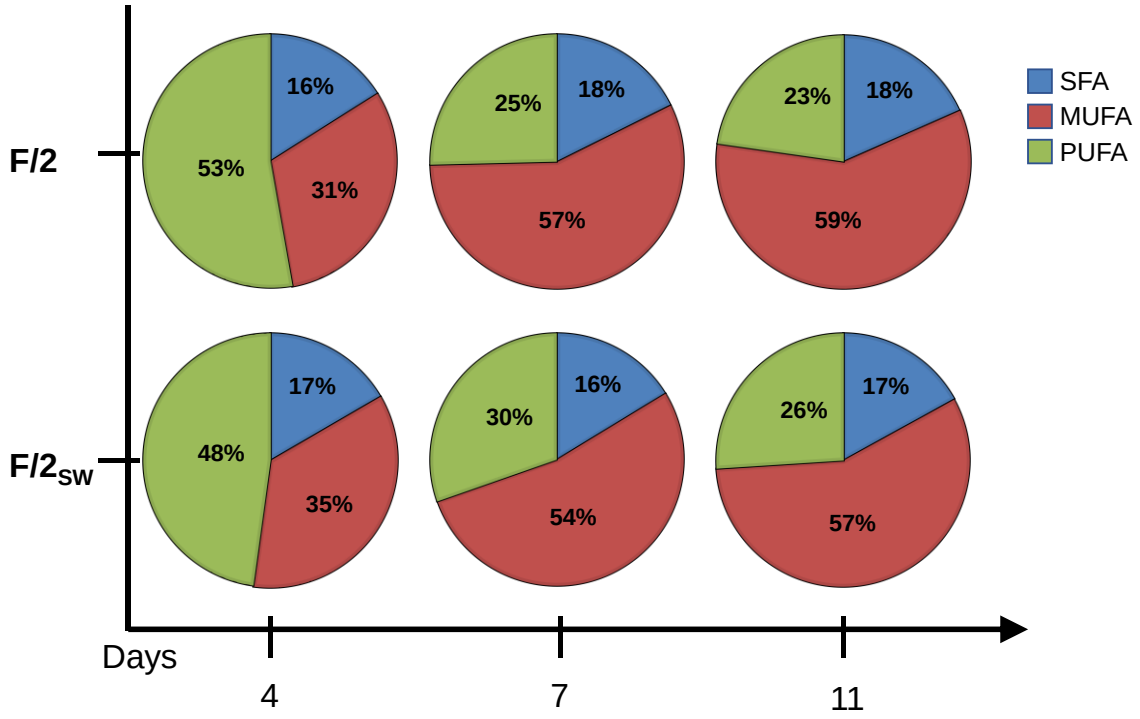

Fig. 21. Pie chart of fatty acid classes over the culture period grown in F/2 and F/2$_{sw}$. On this chart the different fatty acid classes, namely saturated fatty acids (SFA, blue), monounsaturated fatty acids (MUFA, red) and polyunsaturated fatty acids (PUFA, green) are displayed as the percentage of total fatty acids. X-axis: growth time (sampling point); y-axis: medium. Raw data of fatty acid analysis were aquired by Peng Li (Uni Tübingen).

In contrast, cells that grew with approximately half the amount of nitrate and phosphate showed no significant changes in the partitioning of the lipid classes, including PUFAs (Fig. 22). In contrast to the cultures with higher N and P, over 50% of the lipid qwew MUFAs already at day 4. From day 4 to day 11 only a minor additional shift from PUFAs to MUFAs of 6% to 7% was measured in both media.

In line with the former results, all growth experiments showed only slight changes in the lipid composition between day 7 (early stationary growth phase) and day 11 (late stationary growth phase) (Fig. S 11).

No major differences were detected for the relative content of single fatty acids, thus the three most dominant fatty acids (>10% of fatty acid content) were the same, namely palmitic acid (C16:0), palmitoleic acid (PA, C16:1) and EPA (C20:5). In cells grown in F/2 and F/2$_{sw}$, the abundance of EPA and PA was inversed over the growth period, explaining the shift of the fatty acid classes described before. In both media around 40% of all fatty acids were present as EPA on day 4, whereas PA had an abundance of 30%. From day 7 to day 11 the relative content of EPA decreased to 20% or less, whereas the abundance of PA increases to 50% or higher (Fig. S 11 a+b). In contrast, cells grown in medium with lower nitrate and phosphate concentrations showed a high PA abundance with around 50% over the entire culture period. The abundance of EPA is constantly low at 15 to 20% (Fig. S 11 c+d).

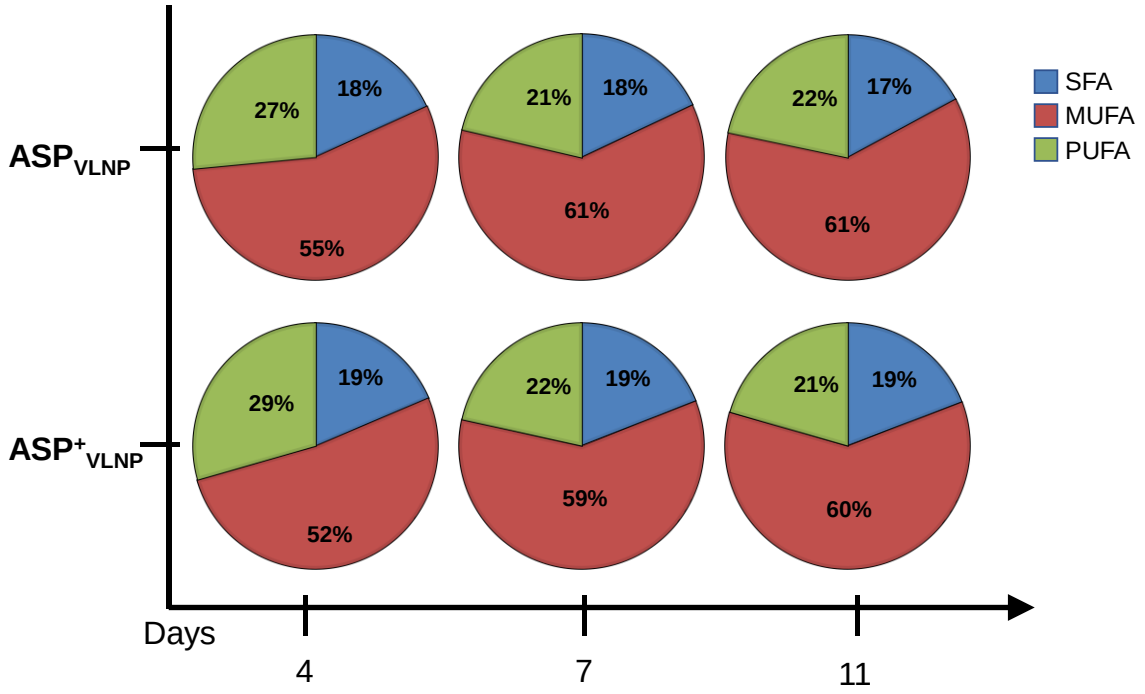

Fig. 22. Pie chart of fatty acid classes during the culture period grown in ASP_{VLNP} and ASP^{+}_{VLNP}. On this chart the different fatty acid classes, namely saturated fatty acids (SFA, blue), monounsaturated fatty acids (MUFA, red) and polyunsaturated fatty acids (PUFA, green) are displayed as a percentage of total fatty acids. X-axis: growth time (sampling point); y-axis: medium. Raw data of fatty acid analysis were aquired by Peng Li (Uni Tübingen).

9.3. Adapted nitrate and phosphate concentration yielding higher biomass productivties

In the following experiment, I grew *P. tricornutum* in a medium with approximately 25% less nitrate and 40% less phosphate compared to the F/2 medium, and about double the amount compared to ASP_{VLNP}, namely ASP_{LNP}. Here the N and P concentrations were adapted to Guillard and Rhyter (1962), showing high cell growth during short culture period for diverse organisms (e.g. Krishnan et al. 2021). Again, the PBR FMT150 1l was used to monitor OD, pH values and the fitness of the cells. As a control a second biological replicate was cultivated (Fig. S 12 a) and technical triplicates from both experiments were analyzed. Additionally, the medium was supplemented with an antibiotic cocktail. To ensure no impact on the fitness of the cells, a growth experiment under the same conditions was conducted without the supplementation of an antibiotic cocktail (Fig. S 12 b).

In the former experiments no significant changes were observed between day 7 and day 11. Therefore, due to the adapted nitrate and phosphate concentrations in this medium, a shorter growth period of 9 days was chosen for the experiment. Furthermore, samples were taken at 4 time points, instead of three. In addition, I decreased the light intensity to 60 µmol photons $m^{-2} \cdot s^{-1}$, thus a light reduction by 40%. The growth curve is comparable to the cells grown in F/2 media but already yields final OD values of 0.75 after 9 days (Fig. 23).

The pH values were balanced between 8 and 8.5 but also showed maxima pH values at the end of the light period. The same was true for the effective quantum yield, which was between 0.45 and 0.5 until day 7.

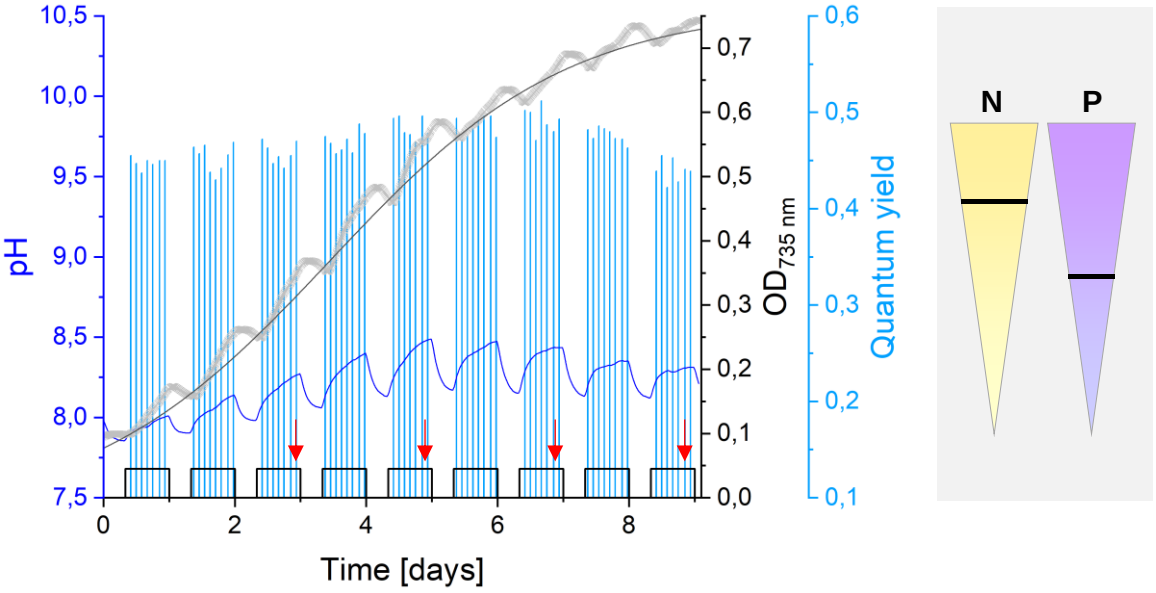

Fig. 23. Growth curve of cells with adapted nitrate and phosphate concentration. The wildtype cells grew in 1l photobioreactor FMT150. The medium ASP_{LNP} was supplemented with an antibiotic cocktail to ensure axenic growth. The growth was measured over 9 days with a light intensity of 60 µmol·photons $m^{-2}·s^{-1}$ with a 16-hour light/8-hour dark cycle (indicated with white bars) at 18°C. The pH (dark blue) and the optical density, OD_{735} (grey) were monitored constantly, whereas the maximum quantum yield of photosystem II (F_V/F_M) was measured only in the light periods and is displayed in light blue. Red arrows referr to the sampling points for further measurements. The Boltzmann regression line is calculated and shown in black with R^2 for the Boltzmannn fit with 99.52 %. As a control another biological replicate was run (Fig. S 12).

At the end of the culture period, the final CDW reached 0.62 g l^{-1}, thus it was approximately 20% higher than the CDW of cells grown for 11 days in the F/2 medium of the pre-experiment with a higher light intensity (Fig. 19 ; Fig. 20; Fig. 24). In line with these results, the biomass productivity was also increased to a maximum of 82 mg l^{-1} d^{-1}, double the value compared to the pre-experiments (Fig. 24). During the entire culture period, the calculated lipid content was about 30% of DW.

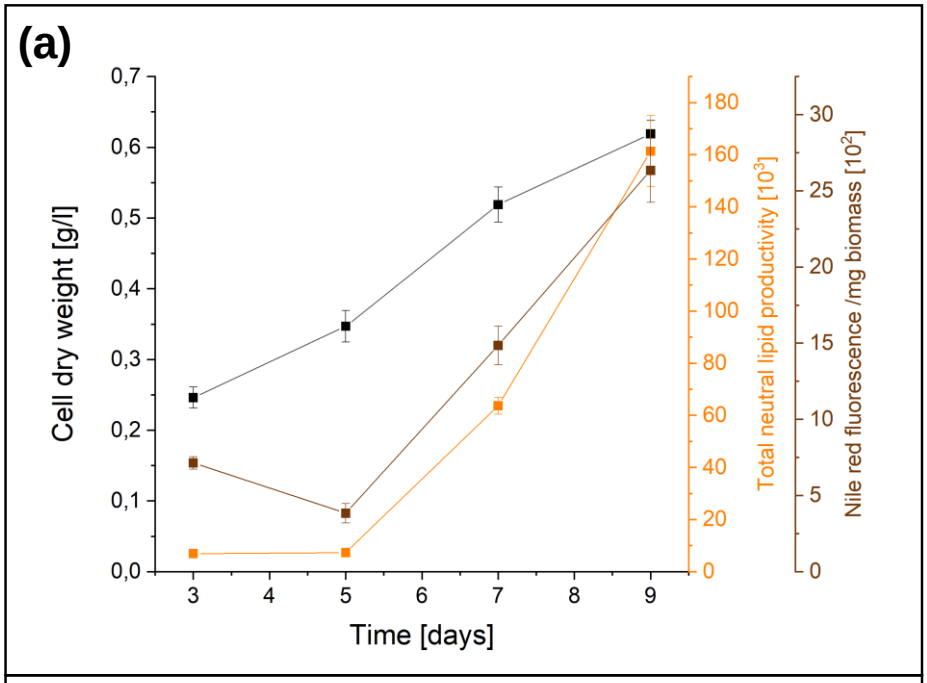

(b)

	Day 1-3	Day 4-5	Day 6-7	Day 8-9
Biomass productivity [mg l^{-1} d^{-1}]				
ASP_{LNP}	82.0±5	69.4±4	74.1±4	68.8. ±2
Lipid content [%]*				
ASP_{LNP}	33.7±5	34.23±4	29.46±3	26.65±5

Fig. 24. Overview of parameters during photobioreactor experiments over the culture period. Wildytpe cells grew in 1L photobioreactor FMT150 (see Fig. 23) in ASP_{LNP} medium and the cells were sampled after 3, 5, 7 and 9 days. Total neutral lipid productivity (orange) monitored over the culture period and neutral lipid prodution per mg biomass (brown) are displayed. For a better comparison, the scale is displayed in 10^3 and 10^2 cells, respectively. The absorbance of Nile red stained cells was measured at 590 nm using a plate reader. The values are the mean of two biological replicates and three technical replicates (n=6).

At all sampling points the cells were stained with Nile red and BODIPY to visualize lipid droplets using a fluorescence microscope. Cells grown in ASP_{LNP} showed enlarged lipid droplets from day 3 to day 9. In the case of the Nile red stained cells, the fluorescence images showed a decreased signal for the Nile red fluorescence signals located at the plastids. The images of the chlorophyll autofluorescence signal suggest a high fitness of the cells during the entire culture period, which was also supported by the F_V/F_M values that only started to decline at day 8.

In addition to the fluorescence microscopy analysis, Nile red stained cells were also investigated using a plate reader, enabling the quantification of the fluorescence signals (Fig. 24). From day 5 to day 9, the total neutral lipid productivity per 10^3 cells and the Nile red fluorescence signal per mg DW for 10^2 cells increased. The relative Nile red signal per DW showed a negative trend in the first days (until day 5).

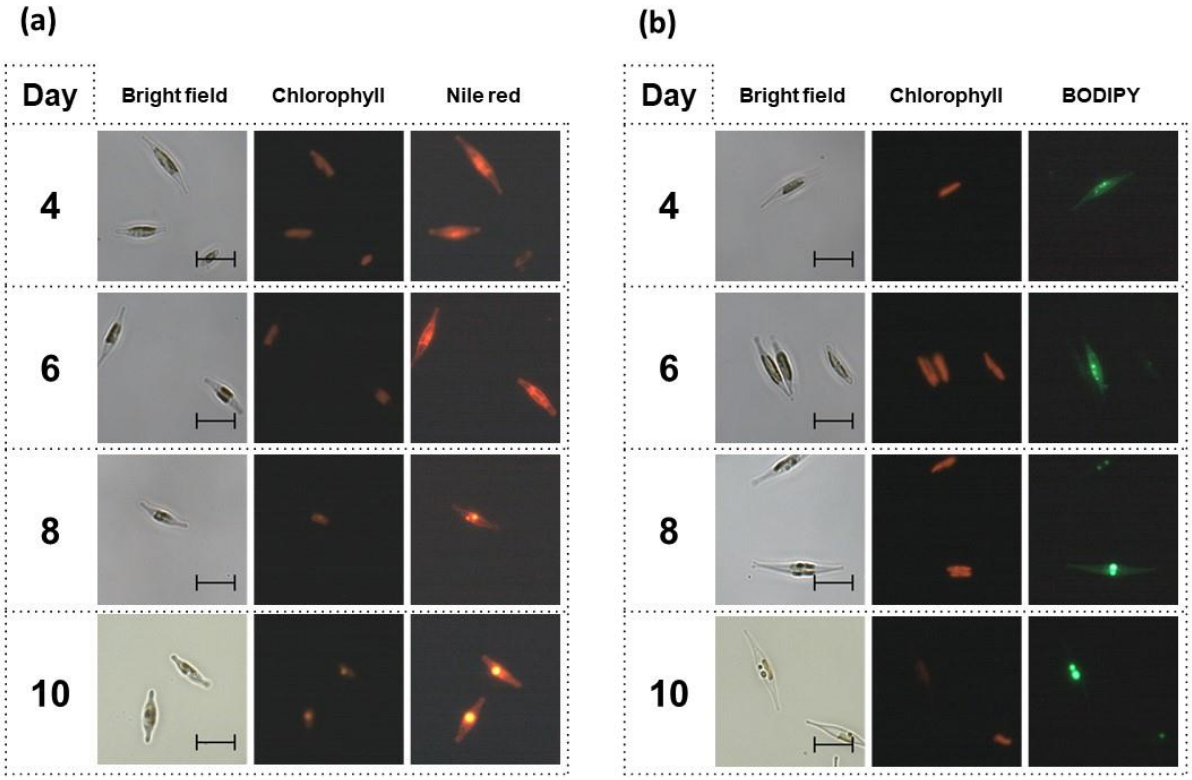

Fig. 25 Visualizing lipids of stained cells grown for 9 days in a photobioreactor. Cells were stained with (a) Nile red or (b) BODIPY 505/515. The wildtype cells grew in 1L photobioreactor FMT150 (see Fig. 23) and cells were sampled after 3, 5, 7 and 9 days. BODIPY 505/515 was excited at 425 - 445 nm and the fluorescence detected at 460 - 500 nm. Nile red was excited at 530 - 570 nm and detected with a long pass filter (starting at 590 nm). The chlorophyll autofluorescence was excited at 570 - 645 nm and detected at 675 nm. Images were captured using Capture 1.5. Scale bars corresponding to 10 µm. For the second biological replicate, the same results were observed (data not shown).

9.4. The lipid profile of cells grown in adapted nitrate and phosphate concentrations

Former experiments proved that changes in nitrogen and phosphate concentration improved the biomass productivity in *P. tricornutum* cells. Next, the lipid profile was analyzed using GC-MS analysis. Due to high variations in the recovery efficiency of the IS1a (C12:0; lauric acid-d19), I tested a new internal standard IS1b (PC19:0). The results of the fatty acid content per DW demonstrated that PA, Hexadecatrienoic acid (C16:3, ω-3) and EPA were the three most prominent fatty acids (Fig. 26). The highest EPA content is seen after 5 days with 22.1 µg mg^{-1} per DW and this content does not change by the end of the culture period. The same trend was seen for the total PUFA content.

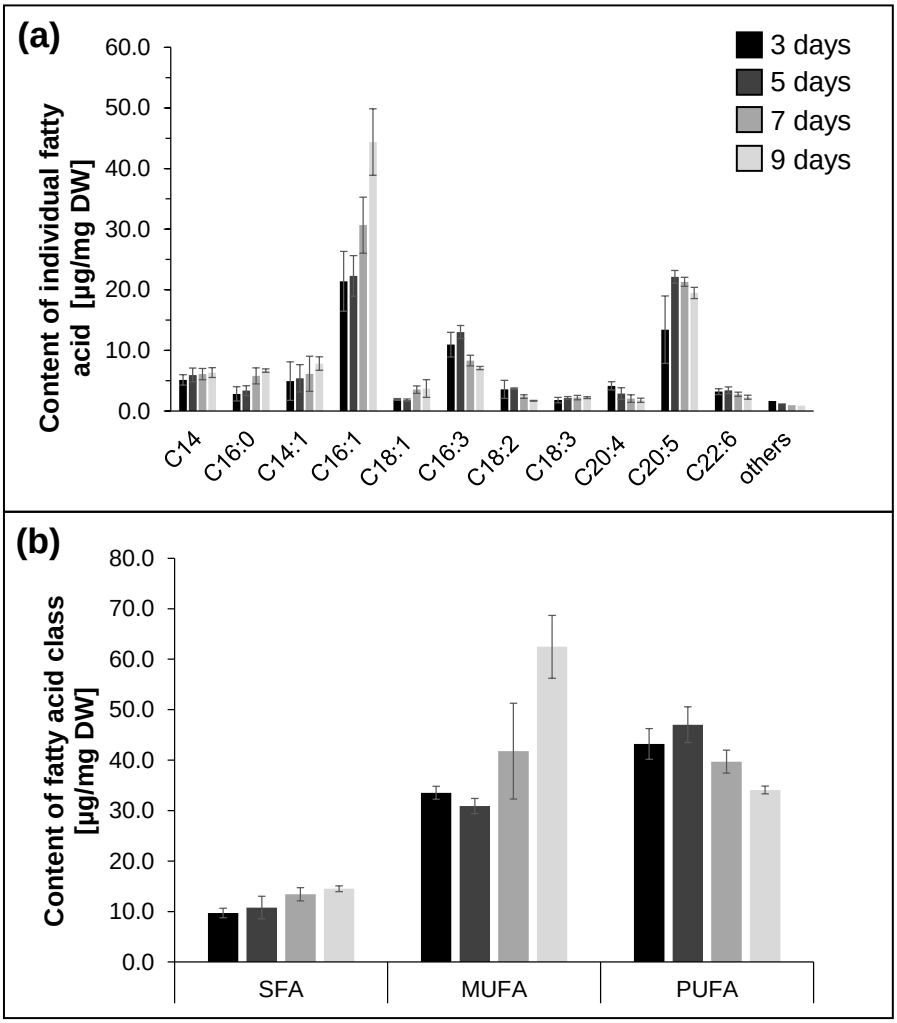

Fig. 26 Fatty acid content per dry weight [µg/mg] analyzed from cells grown in ASP_{LNP} media. *P. tricornutum* was cultured in 1l FMT150 over a period of 9 days and samples were taken after 4, 5, 7 and 9 days (the colour of the bars becomes lightenr, from black to light grey). The fatty acid content per DW [µg/mg] is shown for selected fatty acids with an abundance higher than 2% (a) and the fatty acid content of the lipid classes SFA, MUFA and PUFA is given (b). The lipid extracts of cells were analyzed using GC-MS. Abbreviations used in this figure: SFA: saturated fatty acids; MUFA: monounsaturated fatty acids; PUFA: polyunsaturated fatty acids; TFA: total fatty acids. Values are mean ± SD (n=6, two independent biological replicates measured in technical triplicates). Raw data of fatty acid analysis were aquired by Peng Li (Uni Tübingen).

The MUFA PA showed a high increase from day 7 to day 9 and the same trend was seen for the total MUFA content. For the total SFA content, a slight increase over the growth period was visible. The relative total fatty acid content of the DW revealed that during the first five days no significant change in the lipid profile occurred, except for the ω-3 fatty acid EPA, which increased until day 5. Between day 5 and the end of the culture period the abundance of C16:3 and EPA decreased whereas the MUFA PA increased significantly.

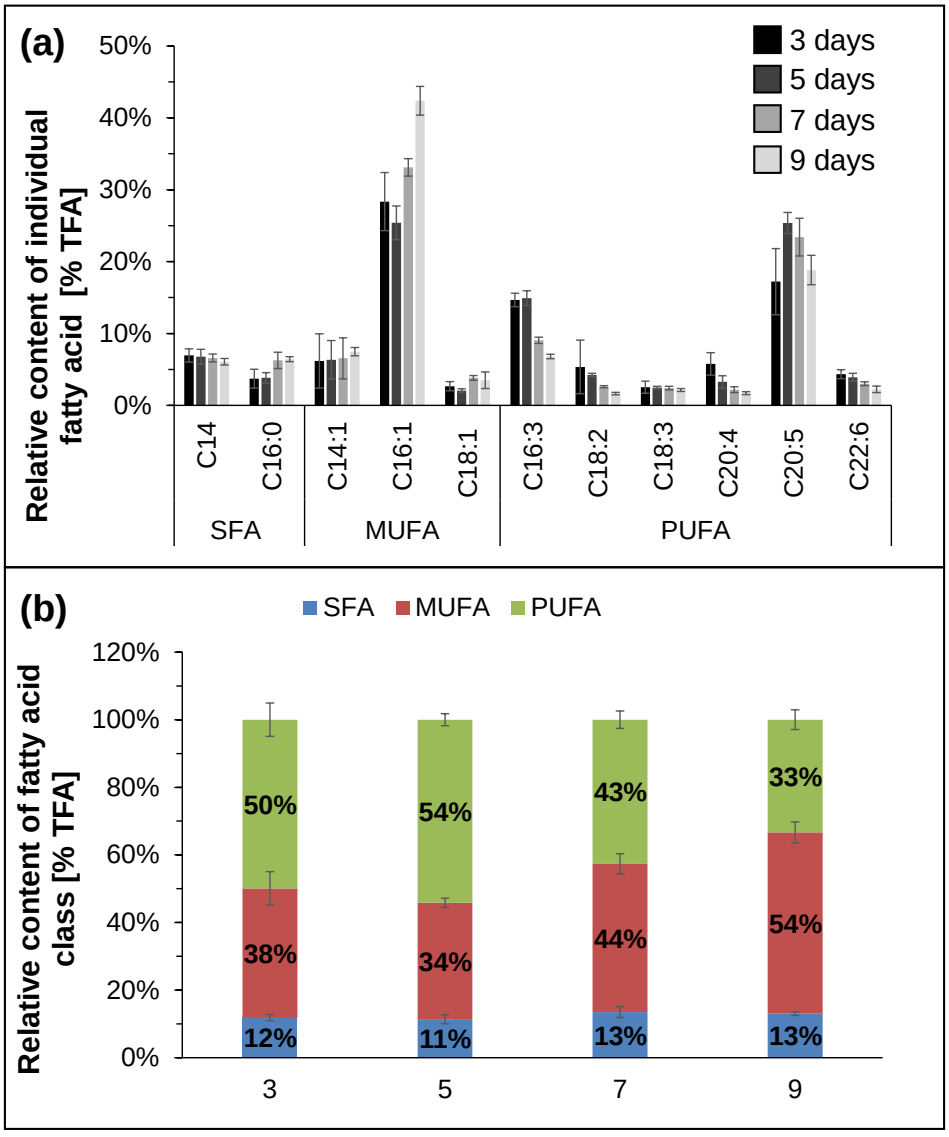

Fig. 27 Relative fatty acid content per biomass [% of TFA] analyzed from cells grown in ASP$_{LNP}$ media. *P. tricornutum* was cultured in 1l FMT150 over a period of 9 days and samples were taken after 4, 5, 7 and 9 days (the colour of the bars becomes lighter, from black to light grey). The fatty acid content per cell dry weight [%] is shown for selected fatty acids with an abundance higher then 2% (a) and an overview of the fatty acid content of the groups of SFA, MUFA and PUFA (b) (n=3). Lipid extracts of cells were analyzed using GC-MS. Abbreviations used in this figure: SFA: saturated fatty acids; MUFA: monounsaturated fatty acids; PUFA: polyunsaturated fatty acids; TFA: total fatty acids. Values are mean ± SD (n=6, two independent biological replicates measured in technical triplicates). Raw data of fatty acid analysis were aquired by Peng Li (Uni Tübingen).

The overview of the relative total content of the different fatty acid classes (Fig. 27) represents the main differences in the aforementioned lipid composition over the culture period. In the first half of the experiment, the cells have a high amount of PUFAs at 50 to 54% and the values for total MUFA and SFA content are low at approximately 35 and 10%, respectively. In the second half, the proportion changes and, on day 9, 54% MUFAs are present in the cells, whereas the PUFA content has decreased to 33%.

9.5. Comparison of the lipid extraction with different cell biomass and the following GC-MS analysis using different internal standards

Organic solvents for the extraction of microalgae lipids have been described to offer moderate extraction efficiencies for algal biofuel (Ranjith Kumar et al. 2015). A modified Bligh and Dyer method, where the basic principle is based on the Folch method (Folch et al. 1957), was used here to extract lipids of lyophilized cells. To exclude changes during the extraction, internal standards were used at different steps of the protocol for the GC-MS analysis. High variations in the recovery of the IS1a (C12:0; lauric acid-d19) between approximately 40% and 120% showed the necessity to start a control experiment (Tab. S 8). The aim was to exclude differences induced by variations in cell dry weight that were used for the lipid extraction. In the first experiment, when different media were tested (Fig. 19), I had a variation in DW from 3.4 mg to 17.9 mg (Tab. S 8).

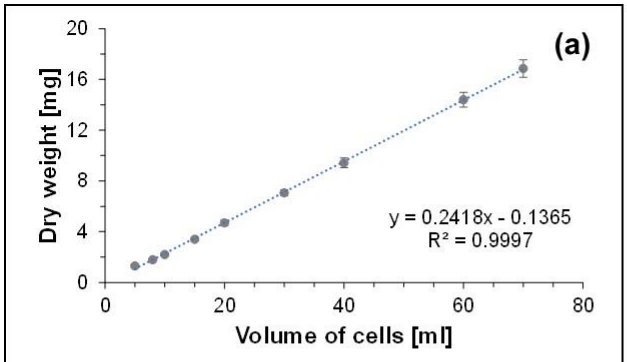

(b)

	Biomass [mg]	Lipid content [%]*
IS1a		
3	3.4±0.08	47.2±10.4
7	7.1±0.24	29.3±4.9
10	9.4±0.39	37.2±3.1
15	14.4±0.57	35.3±3.9
IS1b		
7	6.9±0.24	38.3±4.4
17	16.9±0.68	25.9±1.7

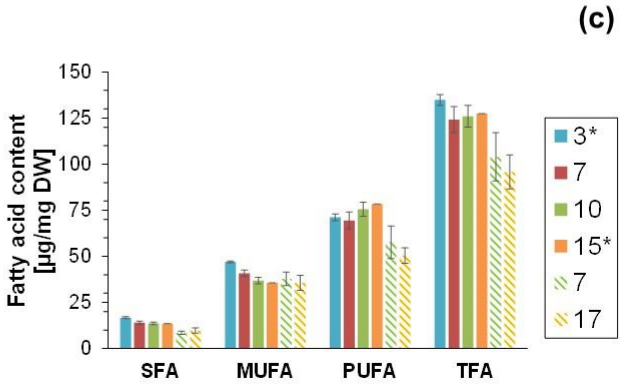

Fig. 28 Control experiment of lipid extraction with different amounts of dry biomass (DW) used in the experiment. The DW [mg] and the volume of cells [ml] is displayed (a). Culture volume used for extraction were lyophilized and the samples were named according to the specific DW values. The lipid content [%] relative to the DW of the samples is also displayed (b). In the GC-MS analysis, either IS1a (solid bars) or IS1b (striped bars) was used as internal standard. The fatty acid content in µg per mg DW is shown for the three fatty acid classes SFA, MUFA, PUFA and the total fatty acid content calculated after the GC-MS analysis. Abbreviations used in this figure: SFA: saturated fatty acids; MUFA: monounsaturated fatty acids; PUFA: polyunsaturated fatty acids; TFA: total fatty acid. Values are mean ± SD (n=3, three independent biological replicates, except samples marked with an asterix with n=2 or n=1 for sample 3* and 15* respectively**).** Raw data of fatty acid analysis were aquired by Peng Li (Uni Tübingen).

In this control experiment, different volume of wildtype cells, cultured in ASP medium, were harvested in the exponential phase (~7 days). For lipid extraction I used either IS1a (indicated as solid bars in the graphs) or in a second experiment IS1b (indicated as striped bars in the graphs). The DW and the volume of cells used correlated linearly with a higher derivation for small DWs lower than 2 mg. The lipid content was strongly influenced by the DW, i.e. the amount of cells used for the lipid extraction. Here, the highest lipid contents were detected for lower DWs used for the lipid extraction, along with higher errors (Fig. 28, b). According to the GC-MS analysis a similar trend was present for the total fatty acid content, displayed in µg fatty acid per mg of DW (Fig. 28, c). Although the two different standars gave deviating results, the trends were the same.

The following paragraphs focus first on the data obtained using standard IS1a (solid bars in Fig. 29 and Fig. 30). For the GC-MS analysis I focused on fatty acids with an abundance of 2.5% or higher. Furthermore, outliers with a recovery of lower than 10% were not included in the analysis, thus for 3 and 15 mg samples less then 3 biological replicates were used (Tab. S 9).

The diagrams below (Fig. 29) display the relative fatty acid content [%]. For the first experiment (solid bars), PA (C16:1), C16:3 and EPA were the three most prominent fatty acids in all samples. However, the estimated abundance for these fatty acids depended on the DW used for extraction. Whereas PA values decreased with increasing DW, the abundance of C16:3 and EPA showed the opposite pattern. The relative total MUFA and PUFA content [%] behaved accordingly.

Next, I tested the influence of using different fatty acids as calibrators (Fig. 30). I chose myristic acid (C14:0) and C16:3 to analyze the extraction efficiency regarding different fatty acid classes. The normalization of the fatty acid content with the SFA C14:0 presented almost similar results to results without calibrator described before (Fig. 29). The same holds for using another fatty acid C16:3, to normalize the values of the GC-MS analysis.

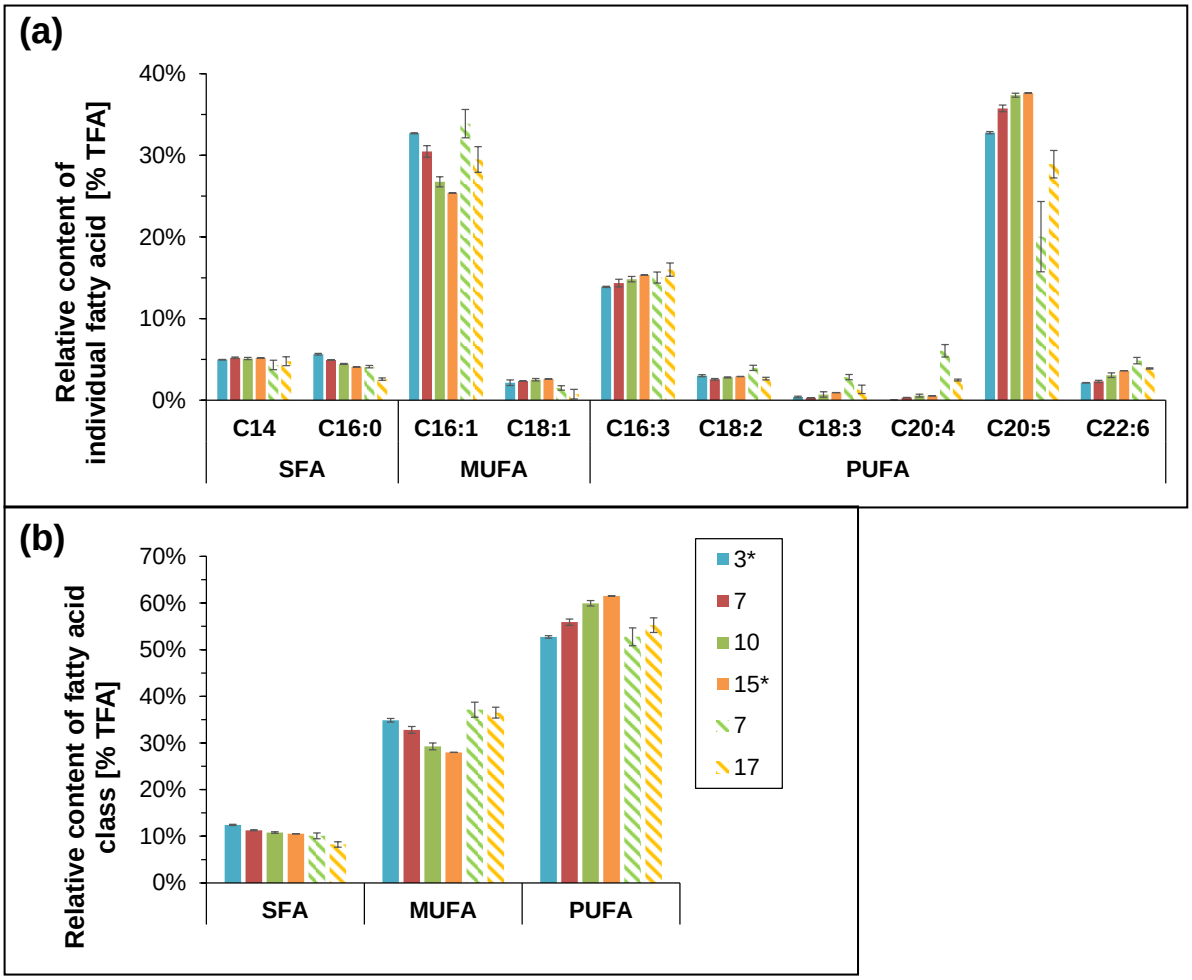

Fig. 29 Relative fatty acid content of wildtype samples varying with the cell dry weight used for lipid extraction. Selected fatty acids are shown with an abundance of >2.5% (a) and the different fatty acid classes are presented in percentage of the total fatty acid content (b). Nomenclature as in Fig. **28**. Abbreviations used in this figure: SFA: saturated fatty acids; MUFA: monounsaturated fatty acids; PUFA: polyunsaturated fatty acids; TFA: total fatty acids. Values are mean ± SD (n=3, three independent biological replicates, except samples marked with an asterix). Raw data of fatty acid analysis were aquired by Peng Li (Uni Tübingen).

In addition to the internal standard IS1a, another standard IS1b, nonadecanoic acid (PC19:0), which is a glycerophospholipid with C19:0 esterificated to the glycerol backbone,was tested that represents the fatty acid class of PUFAs. The experiment using IS1b were done with two different DW for the lipid extraction (Fig. 28). When comparing the data from experiments with IS1a and IS1b one has to take into account, that the cells from the experiment with IS1b had been stored at -80°C for more than six months before analysis. The lipid content of samples using IS1b, calculated directly after the lipid extraction, showed a similar trend to the samples extracted with IS1a (Fig. 28). In contrast, after the GC-MS analysis the samples with IS1b (Fig. 28, striped bars) showed a lower total fatty acid content per DW [µg/mg], due to a lower calculated amount of PUFAs and SFAs.

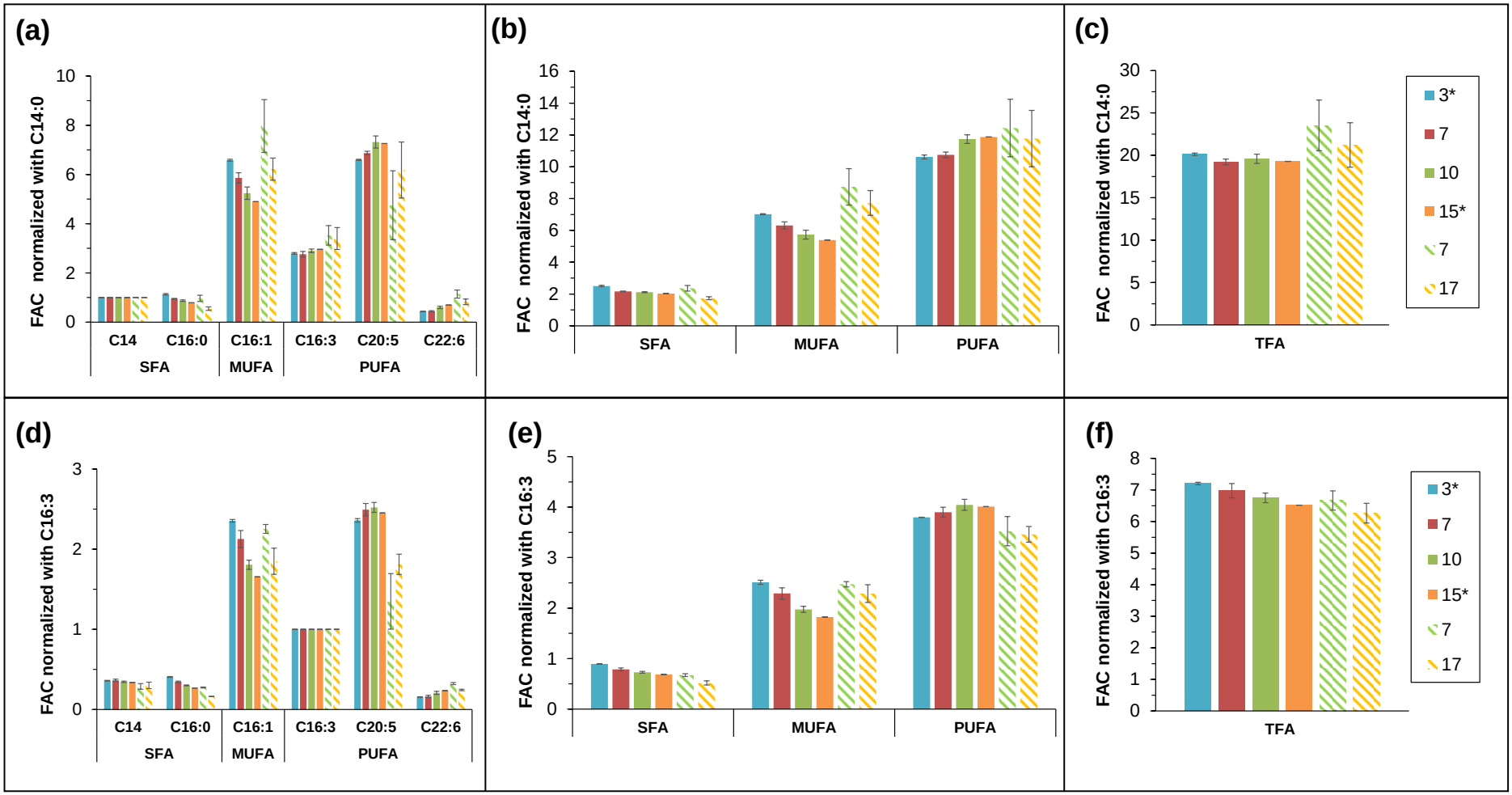

Fig. 30 Normalized fatty acid content of wildtype samples varying in cell dry weight used for the lipid extraction. The GC-MS data was normalized using two calibrators, either C14:0 (a, b, c) or C16:3 (d, e, f). Selected fatty acids are shown (a, d) and the normalized fatty acid classes (b, e) and the fotal fatty acid content (c,f) are presented. The nomenclature is explained elsewhere (Fig. 27). Abbreviations used in this figure: SFA: saturated fatty acids; MUFA: monounsaturated fatty acids; PUFA: polyunsaturated fatty acids; TFA: total fatty acids. Values are mean ± SD (n=3, three independent biological replicates, except samples marked with an asterix). Raw data of fatty acid analysis were aquired by Peng Li (Uni Tübingen).

The comparison of the relative fatty acid content reveals striking differences between the two lipid extractions. Independent of the DW used for lipid extraction, higher percentages of PA (C16:1) and much lower percentages of EPA were detected (Fig. 29), thus the total MUFA content has increased, whereas the PUFA content has decreased. The differences in the fatty acid abundance due to the increasing DW used for the lipid extraction were similar with both internal standards (IS1a and IS1b). The normalized fatty acid content with C14:0 and C16:3 also showed the same trend with both internal standards. The relative total fatty acid content normalized with IS1b was higher with C14:0 as a calibrator and lower with C16:3 as a calibrator (Fig. 30).

10. Discussion (Chapter II)

With the preliminary experiments, different media were tested and possible alternatives for the industrial usage were evaluated. Here, I compared our lab medium ASP (modified from Provasoli et al. 1957) with a commercially available Cell-Hi F2P (varicon aqua; here called F/2).

Seawater is a cheap alternative when the production facility is close to the shore, but high salinity is not always wanted, for example due to to the need of an anti-corrosive coating for growth systems like PBRs (Bumbak et al. 2011). Thus, low salt culture media have their benefits in case cells are able to grow in low salinities. The results of the four different media showed no positive effect on the growth or the lipid content in *P. tricornutum* with higher salinity levels in the media. Wildtype cells showed a lower biomass productivity when cultured in $F/2_{SW}$ compared to the F/2 media, while the relative fatty acid content was almost unchanged (Fig. 20). The same was shown for the different fatty acid classes over the culture period (Fig. 21). The reference of salinity in seawater is said to be 3.54%, thus at least 2 times higher than all the other media tested in this study. The strain used in this study (Pt4, UTEX 646) was solely sampled in brackish water, instead of coastal water (Martino et al. 2007). Other researchers observed an enhanced growth rate and the highest lipid content for this strain when cultured in medium with 2% salinity, but the EPA ratio was almost unchanged in cells grown with different salinity levels (Wang et al. 2018). It is questionable if this effect is due to differences in the overall culture condition or the variations in the adaption of the precultures. In fact, the culture condition differs in terms of light intensity, the overall culture medium and the CO_2 aeritation to my settings (Wang et al. 2018).

In the preliminary experiment, on day 4, the results of cells cultivated in the commercial F/2 and a total salt concentration of 0.54% showed the highest biomass productivity with 53 mg $l^{-1}d^{-1}$ (Fig. 20). Interestingly, cells grown in both F/2 media had their highest pH values and the relatively highest EPA concentrations per DW [%] at the same culture age (Fig. 19, Fig. S 11). As presented in the study of Wang and colleagues, the CO_2 aeritation is often set as a constant influx, thus the influence of the pH levels on the growth or lipid metabolism of cells are often not investigated (Wang et al. 2018).

In contrast, in the PBR experiments of this study the pH value was constantly monitored, and no CO_2 supplementation occurred. The data of cells grown in $F/2_{SW}$ medium displayed high pH values induced by the exponential cell growth concomitant with highest EPA values and highest lipid content (Fig. 20, Fig. S 11). A similiar increase in extracellular pH level during the exponential growth of cells has been seen before and is postulated to be a consequence of alterations of the intracellular pH level (Zhang et al. 2016). For Pt1 (CCMP2561), high pH levels

were strongly related to a high neutral lipid content (Mus et al. 2013). In contrast to my experiments the neutral lipid content increased on day 7 until the end of the culture period, supported by the TLC analysis, the BODIPY staining and the GC-MS measurements (Fig. 21, Fig. S 9, Fig. S 10). More research on the correlation of extracellular pH levels, CO_2 concentrations and lipid metabolism is needed to explain these data properly.

The medium composition of the F/2 is comparable to that of ASP^{+}_{VLNP} (Fig. S 8, Tab. S 7). From the original brochure of their product, the nutrient composition is listed and, with the exception of TRIS, EDTA and Chlorine (Cl), the same micro- and macro-elements are included compared with the composition of the ASP^{+}_{VLNP} medium.

In the ASP_{VLNP} culture medium, the nitrate and phosphate contentrations were very low at 54.7 mg l^{-1} and 3.4 mg l^{-1}, respectively, based on Guillard (1975). Cells cultivated in these media showed a decreased growth (Fig. 19). The growth parameters as well as the analysis of the lipid and fatty acid composition suggest that the cells do not run through the common growth stages of sigmoidal growth (Sorokin 1969). Additionally, this is supported by the decreasing effective photosystem II quantum yield after day 4. Thus, cells appeat to “slide” in the stationary phase. The TLC analysis and the BODIPY staining of the cells displayed an accumulation of TAGs from day 4 to day 11, with small increases at the end of the culture period (Fig. S 9, Fig. S 10). In line with this, analyzed lipid extracts of these cells showed only small changes in the portioning of the fatty acid classes, with the class of MUFAs having the highest percentage of of total fatty acid content (Fig. 22). The total lipid content was comparable to cells grown with higher nitrogen and phosphate concentrations.

In conclusion, it is very likely that, due to the low nitrate and phosphate concentrations used in these media (namely ASP_{VLNP} and ASP^{+}_{VLNP}), an increased amount of TAGs and their incorporated fatty acids (mainly MUFAs) are synthesized. This is also supported by the literature on this and other strains of *P. tricornutum* (Popko et al. 2016; Wang et al. 2018),whereas in this study SFA abundance was almost unaffected (Fig. 21, Fig. 22).

One can assume that P starvation was induced in wildtype cells grown in ASP_{VLNP} medium, probably at the end of the growth experiment. In literature, P limitation with 10 times less phosphate affected the metabolism of the cells from the same strain of *P. trircornutum* after 2 days (Huang et al. 2019). It is important to mention that the authors already grew their precultures with lower N and P concentrations in order to minimize the intracellular amounts of N and P storages.

In this case it is hard to distinguish if N or P limitation induced the reduction in photosynthetic activity or the remodeling of lipid classes. Both favor the partitioning of carbohydrates to neutral lipids. P limitation specific reactions, like the elimination of phospholipids under this starvation (Huang et al. 2019), were not monitored in my study.

Furthermore, I tested the effect of the addition of some trace elements on the growth and lipid content for cells grown in ASP^{+}_{VLNP} medium. The investigated trace element addition was adapted from the enriched seawater (ESAW) medium (Berges et al. 2001) and comparable to the composition of the commercial F/2 medium used in this study. Here, no positive effects were detectable due to the addition of vitamins, fluorine, or selenium or higher amounts of selected trace element, like molybdenum when cells grow in ASP^{+}_{VLNP}. In other studies, CDW values for cells grown in Mann&Meyers medium with higher amounts of trace elements were higher compared to CDW at the end of the culture period of cells grown in F/2 medium with less amounts of trace elements (Song et al. 2020). In contrast, both analyzed strains of *P. tricornutum* showed higher CDW values in F/2 medium (based on Guillard (1975)) during the exponential growth phase (Song et al. 2020).
Foussing on the lipid content, in another study researcher showed highest EPA levels in wildtype cells for a F/2 medium, whereas an ESAW medium (modified after Harrison et al. 1980, with higher amounts of trace elements) showed 1/4 less amount of EPA (Hamilton et al. 2015). It is questionable wether the small impacts on the relative amount of EPA are due to the supplementation of trace elements in the medium, but, if so, this was not detectable in my data, probably due to missing replicates.
Furthermore, the effect of higher salt concentrations on the growth of *P. tricornutum* cells were tested. After the growth period of 11 days, total salt concentration between 1.75% and 3.54% did neither promote the growth nor the lipid content (Fig. 20). Interestingly, cells grown for 4 days in $F/2_{SW}$ with highest salt concentrations showed a maxima lipid content of approximately 70% of DW. This effect was not seen for cells grown in ASP^{+}_{VLNP}. Therefore, it might be interesting to repeat growth experiments in $F/2_{SW}$ to compare my data with previous studies (Wang et al. 2018).

In addition, I modified the ASP medium with N and P concentrations based on Guillard and Rhyter (1962). *P. tricornutum* cells cultured in high N and P concentrations show a flattened curve at the beginning of the culture period (Fig. 12; Song et al. 2020). With a moderate N and P concentration I observed a sigmoidal growth curve that increased growth for cells cultivated in the F/2, $F/2_{SW}$ and ASP_{LNP} media. The final CDWs of the latter experiment were 20% higher and the biomass productivity was constantly higher compared to the results of the F/2 medium, although the light was reduced by 40% in the experiment with ASP_{LNP}. These cells cultivated for 9 days (2 days less compared to the preliminary experiment) showed a high fitness of the cells over the entire culture period (Fig. 23). It is questionable why cells showed higher biomass productivities with lower nitrate and phosphate concentrations in the ASP_{LNP} medium, compared to F/2. One possible reason is the higher fitness of the cells, probably due to the

lower, less stressful light intensities during the the culture period. Another reason for the enhanced growth could be explained by the elevated salt concentrations. This is in line with the literature, showing higher biomass productivities with increasing salt concentrations. In ASP_{LNP} the total salt concentration is approximately twice as high compared to F/2.

Despite this, the results of the lipid staining reveal an increase of lipid droplets and higher neutral lipid productivities after day 5. This indicates that the cells enter the stationary growth phase due to nutrient stress. In line with this, the analysis of the fatty acid content via GC-MS presents a shift in the fatty acid classes from PUFAs to MUFAs (Fig. 27). The lipid content per DW is at 30% ±4% during the culture period, thus lower compared to preliminary experiments, while total fatty acid content showed a slight increase with the culture age. Based on the GC-MS analysis, the highest EPA content in these cells is on day 5 with about 30% of total fatty acid content.

Due to high variations in the recovery of the IS1a I did control experiments. I tested both IS1a and another internal standard IS1b with wildtype cells grown in Erlenmeyer flasks with ASP medium. In addition, I used different DWs for the lipid extraction to exclude variations induced by this step. As expected, the DW correlated linearily with the sample volume. The lipid content, determined including the pigments, varies within this experiment. The higher error for the lipid content of small DWs indcates that errors might be induced by small weights, measured using a precision balance (Fig. 28).

Furthermore, the striking differences between the analysis using IS1a and the one using IS1b are lower total fatty acid amounts and the decrease of PUFAs in case of IS1b. In the analysis that shows the relative content of individual fatty acids per DW, a clear increase in PA (C16:1) and a decrease in EPA was detected, when using IS1b. Generally, the usage of internal standards should eliminate differences in the extraction efficiency, thus the variance of the data points should be decreased. Furthermore, the usage of standards with the same molecular properities compared to the fatty acid of high interest can help to improve its accrurate quantification. For example the internal standard IS1b (PC C19:0) has properities that are more similar to EPA compared to the SFA internal standard IS1a (C14:0). The relative content of EPA in the experiments with IS1b show a medium derivation (Fig. 26 and Fig. 29), but higher compared to experiments with IS1a (Fig. 29).

Thus, it is questionable if whether the lyophilized cells were affected by the storage time at -80°C, or whether the change in fatty acid classes is due to the two different hydrophobicity of the standards. In order to answer this question a control experiment is necessary, using cells with different storage times and extracting their lipids with each standard. Furthermore, different extraction method should be tested, that can lead to differences in the efficiency (Ranjith Kumar et al. 2015). Especially PUFAs are likel to be oxidized by several factors, like heat or oxygen forming oxidative products and the oxidation can be measured by quantifying

enzymes that are involved in this process (Ismail et al. 2016). Eventhough special handling was done, it cannot be excluded that oxidation of the oil extract took place.

Additionally, I evaluated the data by normalizing the fatty acid contents using a fatty acid with a higher abundance. I chose the SFA C14:0 and the PUFA C16:3. Together with the relative data of the content of individual fatty acids per DW in percentage one can conclude: (i) MUFAs and PUFAs have a constrating extraction behavior in dependence on the DW used in the lipid extraction, the MUFA content decreased and the PUFA content increased with higher DW; (ii) the same pattern is calculated in all normalized data. Thus, the lipid extraction and the GC-MS method work. One cannot exclude that at low DW MUFAs and at high DW PUFAs are preferentially extracted.

For the interpretation of my experiments, this could indicate an insufficient concentration of PUFAs, especially EPA, detected by the GC-MS analysis. Thus, the experiments should be repeated, after the control experiments have been clarified. Afterwards, the growth experiments could be compared if all parameter, especially the DW, are constant. Still, the differences of the internal standards hampers comparison between data in literature.

The control of the pH values over the culture period has revealed a new hypothesis that also needs to be validated. As is generally known variations in the pH values were shown to also depend on the stirring of the culture medium (Bitaubé Pérez et al. 2008). For the PBR FMT150 used in this study the stirring was controlled by a common air pump for aquaculture and was not controlled by the system of the PBR. Therefore, it cannot be excluded that changes in the intensity of the stirring occurred in the different experiments. In this study I observed different pH patterns that were not always associated with cell growth but more likely with the nutrients in the medium. At maximal pH values of approximately 10, the highest EPA content was measured. These results are very interesting, as flocculation is a prominent tool for harvesting methods for *P. tricornutum* (Butler et al. 2020, and reference herein).

Up scaling experiments in UTEX 646 for the accumulation of high biomass concomitant with a high productivity of EPA is rare (Tab. 1). This work gives a first insight into the effect of different culture media, lab media versus commercial media and underlines the culture time as a key parameter for optimal product yields.

10.1. Conclusion

In this second part of the study, I investigated the effects of different culture media on the growth and the lipid content of *P. tricornutum* cells in a 1l PBR. A simple medium that is already used in industrial applications, commercial F/2 media (Cell-Hi F2P), was compared to our lab medium ASP. Based on the findings of this study, the following aspects can be concluded:

1. Wildtype cells grown in F/2 medium showed highest EPA content after 7 days. Cells that grew in 6 times higher salt concentrations ($F/2_{SW}$) and cells grown in F/2 had an EPA content per DW of approximately 60 µg/mg. These maxima values were concomitant with a high pH value in the extracellular medium. The higher salt concentrations in the medium had no effect on *P. tricornutum* cells.
2. Cells cultured in very low N and P concentrations entered the stationary growth phase after 4 culture days. They showed higher total lipid content, but the relative EPA concentrations were lower in ASP_{VLNP} compared to cells cultured in F/2 media, 40% to 20%, respectively.
3. The supplementation of trace elements had no significant effect on cells grown in media with low nitrate and phosphate concentrations.
4. Another culture medium, ASP_{LNP}, with adapted nitrate and phosphate concentrations promoted the cell growth even though lower light intensities (60 µmol photons $m^{-2} \cdot s^{-1}$ compared to 100 µmol photons $m^{-2} \cdot s^{-1}$ in the other experiments) were used. Highest biomass productivities were measured for these cells with 82 mg l^{-1} d^{-1}, 2 times higher compared to cells grown in F/2.
5. The results obtained from this study support the hypothesis that the culture period is of great relevance for the enhancement of the ω-3 fatty acid content in *P. tricornutum*.
6. Lipid extraction and GC-MS are sensitive methods that require control experimemts and internal standards for reliable results. The control experiments displayed the necessity to eliminate errors that are very likely induced by different DW used for lipid extraction. This could be avoided by either increasing the number of samples or by reducing the variations in DW used for the lipid extraction.
7. The results of the control experiment revealed that the full potential of the ASP_{LNP} medium for high lipid, especially ω-3 fatty acid accumulating algae is not yet achieved.

11. Summary and Outlook

The diatom *Phaeodactylum tricornutum* is a prominent choice as an alternative biofactory for many products used in the industry (Tab. 1). As an oleganious alga it is a good candidate to produce ω-3 fatty acids. Fish oil and egg yolk are currently the main sources, but their production is limited or has reached its maximum. The increasing demand of ω-3 fatty acids for human health products is increasing, thus microalgae offer an environmentally protected, sustainable alternative that does not compete with arable land.

The aim of this study was to optimize the potential of the *P. tricornutum* strain Pt4 UTEX 646 as a biofactory in industrial applications.

In the first part of this study (Chapter I) I genetically edited this strain to improve its growth. I successfully heterologously expressed the well-known glucose transporter HUP1 of the chlorophyte *Chlorella kessleri* that enabled the *P. tricornutum* mutants to efficiently take up glucose in mixotrophic culture conditions. In line with other studies, my results support the fact that no further editing of the *hup1* gene sequence was necessary and that the gene-promoter combination is of relevance for heterologous protein expression in *P. tricornutum*. For example, N-HUP mutants expressing the HUP1 protein under the control of the NR promoter showed neither sufficient protein nor gene expression. In my study, highest protein expression was displayed for HUP1 proteins under the control of the promoter of the light harvesting gene *fcpA*.

An *in situ* localization study confirmed the correct targeting of the eGFP-HUP1 fusion protein in the engineered strains T-HUP*. Here, only the full length HUP1 proteins were guided to the plasma membrane whereas a predicted N-terminal targeting sequence of the HUP1 protein was only targeted to the membrane of the chloroplast/endoplasmic reticulum compartment (CERM), proving that the N-terminus is sufficient for entering the ER. The targeting pathway of integral membrane proteins (IMPs) located at the plasma membrane is not understood in diatoms and needs further investigation. My results underline the previous hypothesis that plasma membrane transporters are guided to the ER and then transported via exocytosis to the plasma membrane. For this a second sequence motif is needed. The data on the comprehensive *in silico* study of characterized plasma membrane transporters in *P. tricornutum* and glucose transporter of different organisms indicated that these programs are probably not specialized for investigating targeting sequences of IMPs. Nevertheless, a C-terminal motif was present, with minor exceptions, in all glucose transporters and site mutagenesis analysis in this motif should clarify its function as an export signal for vesicle transport to the plasma membrane. I was also able to show that very low light intensities and a low glucose concentration were sufficient to enhance the biomass productivity and yielded 20% higher cell dry weights (CDWs) in T-HUP* mutants. However, the function of homologous

glucose transporters in *P. tricornutum* is still debated. My results confirm that no function of these transporters can be detected under the chosen condition. Here, an overexpression or a knockout mutant is important to reveal their function and activity.

In the second part of this study (Chapter II) I investigated the impact of culture media on growth and lipid content in *P. tricornutum* cells in order to improve these values. By using a photobioreactor (PBR) I permanently monitored the pH values, the effective photosystem II quantum yields and the growth by measuring the OD_{735} values of the cells. After short time periods, cell samples were taken to also analyze the lipid profile of the cells. I compared a commercial F/2 media (Cell-Hi F2P) with our lab medium ASP and modified versions thereof. Cells grown in a modified ASP medium with very low nitrate and phosphate concentrations (ASP_{VLNP}) showed low biomass productivities but an enhanced lipid content over the entire culture period. In this study, neither the addition of trace elements to ASP_{VLNP} medium nor enhanced salt concentrations in the commercial F/2 medium ($F/2_{SW}$) had a significant impact on growth parameters or lipid productivity. However, the latter medium F/2 is of relevance for further investigations. Wildtype cells grown in this medium showed a high biomass productivity and lipid content. Until day 7 of the culture period, biomass productivity and lipid content increased and reached a maximum biomass productivity of 60 mg l^{-1} d^{-1} concomitant with the highest relative EPA concentration per DW. It is worth mentioning that these enhancements were measured at time points with high pH values in the extracellular medium. More experiments are needed to clarify the connection between both observations.

F/2 has an intermediate phosphate and nitrate content. In line with this, cells grown in adapted ASP medium, ASP_{LNP} medium showed constantly higher biomass productivities and, in the first three days, twice as high biomass productivities with 82 mg l^{-1} d^{-1}, the highest value of this study. Even though the light intensity was reduced by 40% and the growth period shortened by 2 days, the adaption in the culture medium promoted the cell growth. In conclusion, the GC-MS method including the lipid extraction need further control experiments. However, the experiments conducted with different internal standards suggest that the ω-3 fatty acid content of cells grown in ASP_{LNP} medium is very likely underestimated.

The results of both parts of this study underline that *P. tricornutum* is a good candidate for heterologous protein expression and as a producer of ω-3 fatty acids, especially EPA. Specifically, the strain Pt4 UTEX 646 is robust and easy to handle and has a high potential for industrial applications. In the future, T-HUP* mutants should be tested in the adapted ASP_{LNP} medium using low glucose concentrations and testing different light intensities. The results of the characterization of these mutants support the hypothesis that very weak light intensities are needed for the glucose metabolism in *P. tricornutum*. Nevertheless, more glucose transporter candidates should be tested to verify these findings. For example, another

alternative could be a modified yeast transporter, based on findings relating to the improved activity of human glucose transporters in yeast systems.

Genetic engineering is a prominent tool that is also used to edit the lipid metabolism in *P. tricornutum*. First results that were not included in this thesis revealed the difficulties of changing this precise metabolism in such a way that stable transformants are created.

In line with the literature, this study has confirmed that the optimization of the culture condition is a major tool that can enhance the lipid content and the biomass productivity in wildtype cells. Both studies underline the importance of the chosen growth period to achieve enhanced protein levels and shed light on the potential of *P. tricornutum* as biofactory for industrial applications.

12. Zusammenfassung

Forschungen zeigen, dass die Einnahme von ω-3 Fettsäuren, besonders Eicosapentaensäure (Englisch: eicosapentanoic acid, abgekürzt EPA) und Docosahexaensäure (Englisch: docosahexaenoic acid, abgekürzt DHA) einen positiven Effekt auf die Gesundheit des Menschen haben (Kris-Etherton et al. 2009; Oliver et al. 2020; Weylandt et al. 2015). Da einige dieser mehrfach ungesättigten Fettsäuren (Englisch: poly unsaturrated fatty acid, abgekürzt PUFA) nicht von dem Menschen synthetisiert werden können (Apt and Behrens 1999), steigt der Bedarf an diesen wertvollen Substanzen stetig und eine Resourcen schonende Alternative wird dringend gebraucht. Mikroalgen stellen diese primäre, umweltfreundliche Quelle für die Synthese von ω-3 Fettsäuren. Die bislang bevorzugte Produktion mittels tierbasierter Quellen wie beispielsweise Fischöl oder Eigelb, okkupiert bebaubares Land und hat ihr Maximum erreicht (Fig. 1; Kitessa et al. 2014).

Zu den als Biofabriken geeigneten ölhaltigen Algen gehören auch die Diatomeen. Sie zählen zur Gruppe der Heterokontophyten die durch eine sekundäre Endosymbiose enstanden sind (Gould et al. 2008) und bilden innerhalb dieser eine große Untergruppe, die für einen signifikanten Anteil der globalen Primärproduktion verantwortlich ist (Falkowski et al. 1998). Trotz des steigenden Interesses an Diatomeen aufgrund der Synthese von wertvollen Substanzen wie beispielsweise EPA, DHA oder auch Fucoxanthin, sind einige Bereiche noch wenig erforscht.

In einem Modelorganismus dieser Familie, *Phaeodactylum tricornutum* Pt4 UTEX 646 stieg in dem letzten Jahrzehnt der Anteil an Studien im Bereich Lipid Metabolismus enorm an (Fig. 2). Es konnte gezeigt werden, dass die Lipidproduktion vielseitig e.g. durch umweltbedingte Stressfaktoren manipulierbar ist (Hess et al. 2018). Die Stressantwort variiert in Diatomeen und auch innerhalb der Spezies *P. tricornutum* zum Teil stark. Neben Salzkonzentrationen, der Temperatur und dem Licht, hat vor allem der Mangel an Phosphor (P) oder Stickstoff (N) einen großen Einfluss auf den Lipidmetabolismus (Huang et al. 2019). Durch P und N Mangel induzierter Stress führt zur Anreicherung von neutralen Speicherlipiden (TAGs) und einem generellen Anstieg des Lipidgehalts.

Die Verwendung von *P. tricornutum* als Biofabrik für industrielle Produkte steht am Anfang und hat immer noch Einschränkungen (Tab. 1). Ineffizientes Wachstum in industriellen Applikationen und unzureichende Synthese von Produkten sind oft die ausschlaggebenden Ursachen für diese Limitation.

P. tricornutum ist eine photoautotrophe Alge, die Licht als Hauptenergiequelle (Photosynthese) nutzt um CO_2 (anorganischen Kohlenstoff) zu fixieren, und daraus organische Stoffe zu synthetisieren. Heterotrophes Wachstum steht im direkten Gegensatz dazu, da Heterotrophie

ein Wachstum ohne Licht und mit der Aufnahme von organischen Substanzen beinhaltet. Diese Trophie ermöglicht eine Kultivierung in geschlossenen Gefäßen, wie beispielsweise Fermentatoren die für eine Produktion von GMP Produkten wünschenswert ist.
Mixotrophie verbindet die Vorteile von beiden trophischen Systemen, da mixotrophe Algen sowohl Energie über die Photosynthese als auch über die Aufnahme von organischen Substanzen bei Licht erhalten können (Villanova and Spetea 2021). Eine oft genutzte Kultivierungsmethode für mixotrophe Algen sind verschiedene Formen des Photobioreaktors (PBRs). Als organische Kohlenstoffquelle wird besonders Glukose favorisiert und ermöglicht die Produktion von wertvollen Substanzen.
In *P. tricornutum* Spezies ist eine genetische und funktionale Diversität vorzufinden, wobei für den hier untersuchten Stamm Pt4 UTEX 646 auffallende Charakteristika aufgezeichnet wurden (Rastogi et al. 2020).
In dieser Arbeit sollte das Potential der ölhaltigen Alge *P. tricornutum* Pt4 UTEX 646 als Biofabrik mithilfe molekular biologischer und physiologischer Ansätze verbessert werden.
Im ersten Teil dieser Arbeit wurden *P. tricornutum* Mutanten erstellt, die einen heterologen Glukosetransporter aus der Grünalge *Chlorella kessleri* exprimieren. Dabei handelt es sich um den Glukosetransporter HUP1 (Englisch: Hexose uptake protein, abgekürzt HUP), einen gut erforschten Hexose/H^+ Symporter (Tanner 2000). In Rahmen dieser Arbeit konnte gezeigt werden, das HUP1 heterolog in *P. tricornutum* exprimiert wird sowie, dass für eine signifikante Expression eine Modifizierung der Gensequenz nicht notwendig ist.
Neben zusätzlichen Genomeditierungstools wie beispielsweise Codon Harmonisierung oder endogenen Verstärkern, spielt die Wahl des Promoters bei der Expression von Proteinen eine große Rolle. In dieser Arbeit wurde der durch Licht induzierbare Fucoxanthin-Chlorophyll a/c-Bindeprotein A (fcpA) Promoter und der Nitratreduktase (NR) Promoter verwendet. Übereinstimmend mit Beispielen aus der Literatur (Pudney et al. 2019) zeigen die Daten der Gen- und Proteinexpression, dass eine Gen-Promoter Kombination ebenfalls einen Einfluss auf das Expressionslevel hat. Die höchste Expression konnte für das *hup1* Gen unter der Kontrolle des fcpA Promoters (T-HUP* Mutanten) detektiert werden. Im Gegensatz dazu zeigen Mutanten (N-HUP*/N-HUP Mutanten), die das HUP1 Protein unter der Kontrolle des NR Promoters exprimierten nur eine geringe Gen- und Proteinexpression.

Im Anschluss wurde mit Hilfe einer *in situ* Lokalisationstudie die Zielsteuerung des heterologen Proteins untersucht. Dazu wurden Transformanten generiert, die ein HUP1-eGFP Fusionsprotein (N-HUP*/T-HUP*) exprimieren. Die Ergebnisse einer *in silco* Analyse der N-terminalen Präsequenz des HUP1 Proteins sagten eine Zielsteuerungssequenz mit der Länge von 42 Aminosäuren voraus. Infolgedessen wurde ebenfalls eine N-terminale Sequenz des

HUP1 Proteins mit eGFP fusioniert und Mutanten (N-spHUP*/T-spHUP*), die dieses Protein exprimieren, untersucht.
Die Ergebnisse der Konfokalmikroskopie und eines superauflösenden Mikroskops bestätigten die korrekte Lokalisation des HUP1-eGFP Fusionsproteins an der Plasmamembran für T-HUP* Mutanten. Die Aufnahme der T-spHUP* Mutanten, welche die Präsequenz des HUP1-eGFP Proteins exprimierten, zeigten stattdessen ein Signal an der äußersten Membran der sekundären Chloroplasten. Diese wird als CERM (Englisch: chloroplast/endoplasmic reticlum compartement abgekürzt CERM) bezeichnet und umschließt sowohl den Nucleus als auch das ER und den Chloroplasten (Flori et al. 2016). Die Ergebnisse verdeutlichen einerseits, dass die N-terminale Zielsteuerungssequenz des HUP1 Proteins notwendig ist, damit das Protein das Kompartiment des ERs erreicht. Andererseits sind vermutlich weitere Motive im C-terminalen Bereich des Volllängenproteins für eine korrekte Adressierung an die Plasmamembran erforderlich. In T-HUP* Mutanten konnte zudem eine Ansammlung von GFP an der Plasmamembran gezeigt werden. Übereinstimmend mit vorherigen Untersuchungen (Matsui et al. 2018; Nakajima et al. 2013), legen diese Ansammlungen von GFP den Schluss nah, dass HUP1-eGFP Proteine vom ER mithilfe von Vesikeln über den Golgi-Apparat an die Plasmamembran transportiert werden. Sehr wahrscheinlich befindet sich in der HUP1 Proteinsequenz ein Signal Anchor, der in der verkürzten N-terminalen Präsequenz fehlt.
Zusätzlich wurden in einer umfassenden *in silco* Analyse sowohl Plasmamembran Transporter aus *P. tricornutum* als auch Glukosetransporter aus verschiedenen anderen Organismen untersucht. Eine eindeutige Vorhersage einer Zielsteuerungssequenz konnte nicht getroffen werden. Stattdessen konnte in der Analyse der Glukosetransporter ein C-terminales tri-aromatisches Motiv gefunden werden. Dieses wurde, wie bereits für andere Zuckertransporter, als ER-Exportsignal identifiziert (Yamada et al. 2017), und in einer Vielzahl der untersuchten Sequenzen gefunden. Weitere Untersuchungen in dem Bereich müssen die Rolle dieses Motivs in *P. tricornutum* aufklären.

Im weiteren Verlauf wurden die T-HUP* Mutanten charakterisiert, welche sich in den Untersuchungen durch hohe Gen- und Proteinexpression auszeichneten.
Obwohl die Aufnahme der radioaktiv gelabelten Glukose in den Mutanten vergleichbar mit Werten aus der Literatur war, konnten die Zellen nicht trophisch konvertiert und kein heterotrophes Wachstum der Zellen ermöglicht werden. Ein Grund hierfür könnte ein lichtabhängiger Glukosemetabolismus in dem *P. tricornutum* Stamm Pt4 UTEX 646 sein. Hierbei ist nicht auszuschließen, dass es innerhalb der *P. tricornutum* Spezies sowohl Unterschiede im Glukosemetabolismus als auch der Funktionalität der putativen, homologen Glukosetransportern gibt (Huang et al. 2015).

In dieser Arbeit durchgeführte Wachstumsexperimente haben gezeigt, dass das Wachstum von T-HUP* Mutanten bei sehr niedrigen Lichtintensitäten stimuliert wird. Weitere Untersuchungen des HUP1 Proteinlevels über einen Kultivierungszeitraum von zwei Wochen und unterschiedlichen Lichtintensitäten in diesen Mutanten zeigten die höchste Expression unter sehr schwachen Lichtintensitäten und geringen Glucosekonzentrationen. Unter den zuvor genannten Bedingungen wurde eine verbesserte Biomassenproduktion, und ein um 20% höheres Trockengewicht im Vergleich zu dem Wildtyp gemessen.
Die Proteinabnahme mit zunehmendem Alter der Kultur und die verminderte Glukoseaufnahmerate unter hohen pH-Werten weisen auf ungünstige Bedingungen zum Ende der Kultivierungsperiode hin. Wie die Ergebnisse der Aufnahmetests von radioaktiver Glukose gezeigt haben, sollte die Glukoseaufnahmerate bei neutralen pH Werten während der Wachstumsexperimente hoch sein. Die Konzentratiosmessungen der Glukosekonzentration im Medium mittels HPLC zeigten jedoch eine 16-fach geringere Glukoseaufnahme für das Wachstumsexperiment bei hoher Lichtintensität (120 µmol $m^{-1}s^{-2}$). Daher zeigen die in dieser Arbeit untersuchten T-HUP* Mutanten ein großes Potential unter angepassten, verbesserten Kultivierungsbedingungen erhöhte Zelltrockengewichte zu erzielen.

Im zweiten Teil dieser Arbeit wurde der Effekt von verschiedenen Kulturmedien auf das Wachstum und den Lipidgehalt von *P. tricornutum* Zellen untersucht. Hierzu wurde ein Photobioreaktor (PBR) mit einem Fassungsvermögen von einem Liter zur permanenten Überwachung des zellulären Wachstums, einschließlich der Aufzeichnung der pH-Werte und der maximalen Quantenausbeute des PSII, verwendet. Darüber hinaus wurde in regelmäßigen Zeitabschnitten Zellproben für die Analyse des Lipidgehaltes und der Biomassenproduktion entnommen.
In dieser Arbeit wurde ein kommerzielles Medium, F/2[2] mit unserem Labormedium ASP und entsprechenden modifizierten Versionen verglichen. Bei den modifizierten Versionen wurde sowohl der Nitrat und Phosphat Gehalt im Medium, als auch der generelle Salzgehalt bzw. der Gehalt von Spurenelementen verändert und der Einfluss dieser Änderungen auf die Zellen untersucht.

P. tricornutum Zellen zeigten eine hohe Biomassenproduktion und eine gesteigerte Lipidanreicherung bei Wachstum in dem kommerziellen F/2 Medium. Nach 7 Tagen Kultivierung wurde ein maximaler EPA Gehalt von 60 µg mg^{-1} Zelltrockengewicht erreicht

[2]Cell-Hi F2P; Varicon Aqua

einhergehend mit einer hohen Biomassenproduktion von ungefähr 60 mg l^{-1} d^{-1}. Für Zellen im $F/2_{SW}$ Medium lag die Biomassenproduktion an Tag 7, ca. 30% niedriger, die beiden anderen Messpunkte am Anfang und am Ende der Kultierungsperiode waren hingegen nur leicht verringert. Der Salzgehalt in diesem Medium liegt bei 3.54%, 7-mal höher als der des F/2 Mediums. Daher wurde kein positiver Effekt von erhöhten Salzkonzentrationen auf die Akkumulation von Lipiden beobachtet, wie zum Teil in der Literatur beschrieben wird (Wang et al. 2018).

In modifiziertem ASP_{VLNP} Medium mit sehr niedrigen Nitrat- und Phosphatkonzentrationen wurde für *P. tricornutum* Zellen ein geringes Wachstum, aber ein erhöhter Lipidgehalt verzeichnet. Durch die Untersuchung der Verteilung der Lipidklassen, als auch den Ergebnissen der *in vivo* Lipid Färbung kann bereits ab Tag 4 das Eintreten in die stationäre Wachstumsphase beobachtet werden. Im Gegenteil zu den Ergebnissen der Zellproben aus Wachstumsexperimenten mit höheren Nitrat- und Phosphatkonzentrationen (F/2; $F/2_{SW}$, ASP, ASP_{LNP}), wurde hier keine signifikante Umverteilung der Lipidklassen gemessen.

Des Weiteren konnte durch die, zu dem F/2 Medium vergleichbare Zugabe von Mikroelementen, in das ASP_{VLNP} Medium kein signifikant positiver Effekt auf das Wachstum oder den Lipidgehalt der Zellen beobachtet werden.
Im Vergleich zu den anderen in dieser Arbeit verwendeten Medien, hat F/2 einen mittleren Phosphat- und Nitratgehalt. Zellen, die in ASP_{LNP} Medium, mit angepassten Nitrat- und Phosphatkonzentrationen, wuchsen, zeigten konstant höhere Biomassenproduktionswerte. Für diese Zellen wurden zu Beginn der Wachstumsphase der höchste Wert von 82 mg l^{-1} d^{-1} gemessen Dieser Wert ist, obwohl die Lichtintensität um 40% reduziert wurde, doppelt so hoch wie bei Zellen, die in F/2 Medium kultiviert wurden. Die in dem ASP_{LNP} Medium gewachsenen Zellen zeigten ein verbessertes Wachstum über die gesamte Wachstumsperiode und produzierten vergleichbare Zelltrockengewichte trotz einer um 2 Tage verkürzten Kultivierungsperiode.
Die Lipidextraktion und die GC-MS Methode sind beides sensitive Methoden, die Kontrollexperimente benötigen. Beide Ergebnisse der Kontrollexperimente mit unterschiedlich eingesetzten Trockengewichten für die Lipidextraktion, und die daraufhin durchgeführten GC-MS Analysen deuten daraufhin, dass durch die unterschiedlich eingesetzen Trockengewichte ein Fehler verursacht wurde. Darüber hinaus zeigen die Daten der GC-MS Analyse mit verschiedenen internen Standards, dass der Fettsäuregehalt der Zellen in diesem Medium überprüft werden muss, um den geringeren ω-3 Fettsäuregehalt zu hinterfragen.

Die Ergebnisse beider Teile heben *P. tricornutum* als geeigneten Kandidaten für die heterologe Proteinexpression und als Biofabrik für ω-3 Fettsäuren, vor allem EPA hervor. Der Stamm Pt4 UTEX 646 sollte dabei im Fokus der Betrachtung stehen, da er robust und einfach zu handhaben ist und damit ein hohes Potential für industrielle Anwendungen hat. Für weitere Untersuchungen der T-HUP* Mutanten sollte das angepasste ASP_{LNP} Medium getestet werden. Die hier vorgestellten Untersuchungen zeigen, dass das Potential dieser optimierten Zellen noch nicht vollständig ausgeschöpft wurde. Unter überwachtem, konstanten und neutralem pH Wert, geringen Glukosekonzentrationen und einer auf den Lipidgehalt abgestimmten Kultivierungsperiode ist eine weiter verbesserte Ausbeute von der Biomasse und dem EPA Gehalt anzunehmen. Auch weiterführende Untersuchungen der Lipidkomposition aber auch der Lipidproduktion sollten im Fokus stehen, um mit Hilfe der Ergebnisse das Potential von *P. tricornutum* als Biofabrik zu erweitern.

13. Contributions

I am very thankful that I had the opportunity to supervise master and practical students and to build cooperation networks during my PhD thesis. Both have contributed to my work at some points.

Most data of the Chapter I is submitted to the Journal ‘Algal Research’ and is currently under revision. Thus, these figures are partly identical to the manuscript, as well as its captions.
In this project my master student Daniel Wasser (2019) and the short time internship students Björn Sabel, Fabian Haitz and Marcel Meyer worked with me on the topic ‘Improving the growth of *Phaeodactylum tricornutum* using genetic engineering - screening and characterization of mutants expressing a heterologous HUP1 glucose transporter’. The data that had been collected by them is displayed in:
Fig. 6; Fig. 14 ; Tab. S 4; Fig. S 2; Fig. S 3; Fig. S 4; Fig. S 6

In the Chapter II “Optimization of the culture medium yielding high lipid profile in wildtype *Phaeodactylum tricornutum* cells” my master student Kruijff (2021) worked with me on this topic. Furthermore, the GC-Ms data was analysed by my collaboration partner Peng Li from the working group of Prof. Lämmerhofer in Tübingen at the Institute of Molecular Biosciences. Also, here the information is written in the caption of the figures or mentioned in the text. The data that had been collected by them is displayed in:
Fig. 19; Fig. 20; Fig. 21; Fig. 22; Fig. 26; Fig. 27; Fig. 28; Fig. 29; Fig. S 9; Fig. S 10; Fig. S 11

List of figures

List of tables

References

Abida, H., Dolch, L.-J., Meï, C., Villanova, V., Conte, M., Block, M. A., et al. (2015). Membrane Glycerolipid Remodeling Triggered by Nitrogen and Phosphorus Starvation in *Phaeodactylum tricornutum*. *Plant Physiology, 167,* (*1*, 118–136). doi:10.1104/pp.114.252395

Adl, S. M., Simpson, A. G. B., Lane, C. E., Lukeš, J., Bass, D., Bowser, S. S., et al. (2012). The revised classification of eukaryotes. *The Journal of eukaryotic microbiology, 59,* (*5*, 429–493). doi:10.1111/j.1550-7408.2012.00644.x

Alegria-Schaffer, A., Lodge, A., & Vattem, K. (2009). Performing and Optimizing Western Blots with an Emphasis on Chemiluminescent Detection. *Methods in enzymology, 463,* (573–599). doi:10.1016/S0076-6879(09)63033-0

Alipanah, L., Winge, P., Rohloff, J., Najafi, J., Brembu, T., & Bones, A. M. (2018). Molecular adaptations to phosphorus deprivation and comparison with nitrogen deprivation responses in the diatom *Phaeodactylum tricornutum*. *PloS one, 13,* (*2*, e0193335). doi:10.1371/journal.pone.0193335

Angstenberger, M., Krischer, J., Aktaş, O., & Büchel, C. (2019). Knock-Down of a ligIV Homologue Enables DNA Integration via Homologous Recombination in the Marine Diatom *Phaeodactylum tricornutum*. *ACS synthetic biology, 8,* (*1*, 57–69). doi:10.1021/acssynbio.8b00234

Apt, K. E., Kroth-Pancic, P. G., & Grossman, A. R. (1996). Stable nuclear transformation of the diatom *Phaeodactylum tricornutum*. *Molecular & general genetics : MGG, 252,* (*5*, 572–579). doi:10.1007/BF02172403

Apt, K. E., & Behrens, P. W. (1999). Commercial developments in microalgal biotechnology. *Journal of Phycology, 35,* (*2*, 215–226). doi:10.1046/j.1529-8817.1999.3520215.x

Arao, T., & Yamada, M. (1994). Biosynthesis of polyunsaturated fatty acids in the marine diatom , *Phaeodactylum tricornutum*, *35,* (*5*, 4–8).

Archibald, J. M., & Keeling, P. J. (2002). Recycled plastids: a ‘green movement’ in eukaryotic evolution. *Trends in Genetics, 18,* (*11*, 577–584). doi:10.1016/S0168-9525(02)02777-4

Bailleul, B., Berne, N., Murik, O., Petroutsos, D., Prihoda, J., Tanaka, A., et al. (2015). Energetic coupling between plastids and mitochondria drives CO_2 assimilation in diatoms. *Nature, 524,* (*7565*, 366–369). doi:10.1038/nature14599

Bauer, C. M., Schmitz, C., Corrêa, R. G., Herrera, C. M., Ramlov, F., Oliveira, E. R., et al. (2019). In vitro fucoxanthin production by the *Phaeodactylum tricornutum* diatom. In *Bioactive Natural Products* (Studies in Natural Products Chemistry, vol. 63, pp. 211–242). Elsevier.

Berges, J. A., Franklin, D. J., & Harrison, P. J. (2001). Evolution of an artificial seawater medium: improvements in enriched seawater, artificial water over the last two decades. *Journal of Phycology, 37,* (*6*, 1138–1145). doi:10.1046/j.1529-8817.2001.01052.x

Berndt, U., Oellerer, S., Zhang, Y., Johnson, A. E., & Rospert, S. (2009). A signal-anchor sequence stimulates signal recognition particle binding to ribosomes from inside the exit tunnel. *PNAS, 106,* (*5*, 1398–1403). doi:10.1073/pnas.0808584106

Bisson, L. F., Coons, D. M., Kruckeberg, A. L., & Lewis, D. A. (1993). Yeast sugar transporters. *Critical reviews in biochemistry and molecular biology, 28,* (*4*, 259–308). doi:10.3109/10409239309078437

Bitaubé Pérez, E., Caro Pina, I., & Pérez Rodríguez, L. (2008). Kinetic model for growth of *Phaeodactylum tricornutum* in intensive culture photobioreactor. *Biochemical Engineering Journal, 40,* (*3*, 520–525). doi:10.1016/j.bej.2008.02.007

BLIGH, E. G., & DYER, W. J. (1959). A rapid method of total lipid extraction and purification. *Canadian journal of biochemistry and physiology, 37,* (*8*, 911–917). doi:10.1139/o59-099

Boles, E., & Oreb, M. (2018). A Growth-Based Screening System for Hexose Transporters in Yeast. *Methods in molecular biology (Clifton, N.J.), 1713,* (123–135). doi:10.1007/978-1-4939-7507-5_10

Bolte, K., Bullmann, L., Hempel, F., Bozarth, A., Zauner, S., & Maier, U.-G. (2009). Protein targeting into secondary plastids. *The Journal of eukaryotic microbiology, 56,* (*1*, 9–15). doi:10.1111/j.1550-7408.2008.00370.x

Bowler, C., Allen, A. E., Badger, J. H., Grimwood, J., Jabbari, K., Kuo, A., et al. (2008). The *Phaeodactylum* genome reveals the evolutionary history of diatom genomes. *Nature, 456,* (*7219*, 239–244). doi:10.1038/nature07410

Boyle, N. R., & Morgan, J. A. (2009). Flux balance analysis of primary metabolism in *Chlamydomonas reinhardtii*. *BMC systems biology, 3,* (4). doi:10.1186/1752-0509-3-4

Bumbak, F., Cook, S., Zachleder, V., Hauser, S., & Kovar, K. (2011). Best practices in heterotrophic high-cell-density microalgal processes: achievements, potential and possible limitations. *Applied Microbiology and Biotechnology, 91,* (*1*, 31–46). doi:10.1007/s00253-011-3311-6

Butler, T., Kapoore, R. V., & Vaidyanathan, S. (2020). *Phaeodactylum tricornutum*: A Diatom Cell Factory. *Trends in biotechnology, 38,* (*6*, 606–622). doi:10.1016/j.tibtech.2019.12.023

Caspari, T., Stadler, R., Sauer, N., & Tanner, W. (1994). Structure/function relationship of the Chlorella glucose/H+ symporter. *The Journal of biological chemistry, 269,* (*5*, 3498–3502).

Castell, C., Bernal-Bayard, P., Ortega, J. M., Roncel, M., Hervás, M., & Navarro, J. A. (2021). The heterologous expression of a plastocyanin in the diatom *Phaeodactylum tricornutum* improves cell growth under iron-deficient conditions. *Physiologia plantarum, 171,* (*2*, 277–290). doi:10.1111/ppl.13290

Cavalier-Smith, T. (1982). The origins of plastids. *Biological Journal of the Linnean Society, 17,* (*3*, 289–306). doi:10.1111/j.1095-8312.1982.tb02023.x

Cavalier-Smith, T. (1999). Principles of protein and lipid targeting in secondary symbiogenesis: euglenoid, dinoflagellate, and sporozoan plastid origins and the eukaryote family tree. *The Journal of eukaryotic microbiology, 46,* (*4*, 347–366). doi:10.1111/j.1550-7408.1999.tb04614.x

Cerón García, M. C., Fernández Sevilla, J. M., Acién Fernández, F. G., Molina Grima, E., & García Camacho, F. (2000). Mixotrophic growth of *Phaeodactylum tricornutum* on glycerol: growth rate and fatty acid profile. *Journal of Applied Phycology, 12,* (*3/5*, 239–248). doi:10.1023/A:1008123000002

Cerón García, M. C., Sánchez Mirón, A., Fernández Sevilla, J. M., Molina Grima, E., & García Camacho, F. (2005). Mixotrophic growth of the microalga *Phaeodactylum tricornutum*. *Process Biochemistry, 40,* (*1*, 297–305). doi:10.1016/j.procbio.2004.01.016

Cerón García, M. C., Miron, A., Sevilla, J. F., Christi, Y., & Grima, E. (2006). Mixotrophic production of marine microalga *Phaeodactylum tricornutum* on various carbon sources. *Journal of Microbiology and Biotechnology, 16,* (*5*, 689–694).

Chauton, M. S., Winge, P., Brembu, T., Vadstein, O., & Bones, A. M. (2013). Gene regulation of carbon fixation, storage, and utilization in the diatom *Phaeodactylum tricornutum* acclimated to light/dark cycles. *Plant Physiology, 161,* (*2*, 1034–1048). doi:10.1104/pp.112.206177

Chen, G.-Q., & Chen, F. (2006). Growing phototrophic cells without light. *Biotechnology letters, 28,* (*9*, 607–616). doi:10.1007/s10529-006-0025-4

Chen, H., & Wang, Q. (2021). Regulatory mechanisms of lipid biosynthesis in microalgae. *Biological reviews of the Cambridge Philosophical Society, 96,* (*5*, 2373–2391). doi:10.1111/brv.12759

Chevalier, A. S., Bienert, G. P., & Chaumont, F. (2014). A new LxxxA motif in the transmembrane Helix3 of maize aquaporins belonging to the plasma membrane intrinsic protein PIP2 group is required for their trafficking to the plasma membrane. *Plant Physiology, 166,* (*1*, 125–138). doi:10.1104/pp.114.240945

Chrachri, A., Hopkinson, B. M., Flynn, K., Brownlee, C., & Wheeler, G. L. (2018). Dynamic changes in carbonate chemistry in the microenvironment around single marine phytoplankton cells. *Nature communications, 9,* (*1*, 74). doi:10.1038/s41467-017-02426-y

Chu, L., Ewe, D., Río Bártulos, C., Kroth, P. G., & Gruber, A. (2016). Rapid induction of GFP expression by the nitrate reductase promoter in the diatom *Phaeodactylum tricornutum*. *PeerJ, 4,* (e2344). doi:10.7717/peerj.2344

Cosson, P., Perrin, J., & Bonifacino, J. S. (2013). Anchors aweigh: protein localization and transport mediated by transmembrane domains. *Trends in cell biology, 23,* (*10*, 511–517). doi:10.1016/j.tcb.2013.05.005

Crooks, G. E., Hon, G., Chandonia, J.-M., & Brenner, S. E. (2004). WebLogo: a sequence logo generator. *Genome research, 14,* (*6*, 1188–1190). doi:10.1101/gr.849004

Cui, Y., Thomas-Hall, S. R., & Schenk, P. M. (2019). *Phaeodactylum tricornutum* microalgae as a rich source of omega-3 oil: Progress in lipid induction techniques towards industry adoption. *Food chemistry, 297,* (124937). doi:10.1016/j.foodchem.2019.06.004

D'Adamo, S., Di Schiano Visconte, G., Lowe, G., Szaub-Newton, J., Beacham, T., Landels, A., et al. (2019). Engineering the unicellular alga *Phaeodactylum tricornutum* for high-value plant triterpenoid production. *Plant biotechnology journal, 17,* (*1*, 75–87). doi:10.1111/pbi.12948

Dell'Aquila, G., Zauner, S., Heimerl, T., Kahnt, J., Samel-Gondesen, V., Runge, S., et al. (2020). Mobilization and Cellular Distribution of Phosphate in the Diatom *Phaeodactylum tricornutum*. *Frontiers in plant science, 11,* (579). doi:10.3389/fpls.2020.00579

Derwenskus, F., Schäfer, B., Müller, J., Frick, K., Gille, A., Briviba, K., et al. (2020). Coproduction of EPA and Fucoxanthin with *P. tricornutum* – A Promising Approach for Up- and Downstream Processing. *Chemie Ingenieur Technik, 92,* (*11*, 1780–1789). doi:10.1002/cite.202000046

Derwenskus, F., Weickert, S., Lewandowski, I., Schmid-Staiger, U., & Hirth, T. (2020). Economic evaluation of up- and downstream scenarios for the co-production of fucoxanthin and eicosapentaenoic acid with *P. tricornutum* using flat-panel airlift photobioreactors with artificial light. *Algal Research, 51,* (102078). doi:10.1016/j.algal.2020.102078

Desbois, A. P., Lebl, T., Yan, L., & Smith, V. J. (2008). Isolation and structural characterisation of two antibacterial free fatty acids from the marine diatom, *Phaeodactylum tricornutum*. *Applied Microbiology and Biotechnology, 81,* (*4*, 755–764). doi:10.1007/s00253-008-1714-9

Dodson, V. J., Mouget, J.-L., Dahmen, J. L., & Leblond, J. D. (2014). The long and short of it: temperature-dependent modifications of fatty acid chain length and unsaturation in the galactolipid profiles of the diatoms *Haslea ostrearia* and *Phaeodactylum tricornutum*. *Hydrobiologia, 727,* (*1*, 95–107). doi:10.1007/s10750-013-1790-4

Doebbe, A., Rupprecht, J., Beckmann, J., Mussgnug, J. H., Hallmann, A., Hankamer, B., et al. (2007). Functional integration of the *HUP1* hexose symporter gene into the genome of *C. reinhardtii*: Impacts on biological H_2 production. *Journal of Biotechnology, 131,* (*1*, 27–33). doi:10.1016/j.jbiotec.2007.05.017

Dolch, L. J., & Maréchal, E. (2015). Inventory of fatty acid desaturases in the pennate diatom

Phaeodactylum tricornutum. *Marine drugs, 13,* (*3*, 1317–1339). doi:10.3390/md13031317

Domergue, F., Zank, T. K., Abbadi, A., Sperling, P., Meyer, A., Lerchl, J., et al. (2003). Fatty Acid Desaturases from the Diatom Phaeodactylum Tricornutum. In N. Murata, M. Yamada, I. Nishida, H. Okuyama, J. Sekiya, & W. Hajime (Eds.), *Advanced Research on Plant Lipids* (vol. 30, pp. 121–124). Dordrecht: Springer Netherlands.

Domergue, F., Spiekermann, P., Lerchl, J., Beckmann, C., Kilian, O., Kroth, P. G., et al. (2003). New insight into Phaeodactylum tricornutum fatty acid metabolism. Cloning and functional characterization of plastidial and microsomalv Δ-12 fatty acid desaturases. *Plant Physiology, 131,* (*April*, 1648–1660). doi:10.1104/pp.102.018317.color

Draaisma, R. B., Wijffels, R. H., Slegers, P. M. E., Brentner, L. B., Roy, A., & Barbosa, M. J. (2013). Food commodities from microalgae. *Current opinion in biotechnology, 24,* (*2*, 169–177). doi:10.1016/j.copbio.2012.09.012

Duarte, B., Feijão, E., Goessling, J. W., Caçador, I., & Matos, A. R. (2021). Pigment and Fatty Acid Production under Different Light Qualities in the Diatom *Phaeodactylum tricornutum*. *Applied Sciences, 11,* (*6*, 2550). doi:10.3390/app11062550

Elbourne, L. D. H., Tetu, S. G., Hassan, K. A., & Paulsen, I. T. (2017). TransportDB 2.0: a database for exploring membrane transporters in sequenced genomes from all domains of life. *Nucleic acids research, 45,* (*D1*, D320-D324). doi:10.1093/nar/gkw1068

Erdene-Ochir, E., Shin, B.-K., Huda, M. N., Kim, D. H., Lee, E. H., Song, D.-G., et al. (2016). Cloning of a novel endogenous promoter for foreign gene expression in *Phaeodactylum tricornutum*. *Applied Biological Chemistry, 59,* (*6*, 861–867). doi:10.1007/s13765-016-0235-y

Erdene-Ochir, E., Shin, B.-K., Kwon, B., Jung, C., & Pan, C.-H. (2019). Identification and characterisation of the novel endogenous promoter HASP1 and its signal peptide from *Phaeodactylum tricornutum*. *Scientific reports, 9,* (*1*, 9941). doi:10.1038/s41598-019-45786-9

Erdene-Ochir, E., Shin, B.-K., Huda, M. N., Lee, E. H., Song, D.-G., Jung, C., et al. (2021). Characterization of endogenous promoters of GapC1 and GS for recombinant protein expression in *Phaeodactylum tricornutum*. *MicrobiologyOpen, 10,* (*5*, e1239). doi:10.1002/mbo3.1239

Ewe, D., Tachibana, M., Kikutani, S., Gruber, A., Río Bártulos, C., Konert, G., et al. (2018). The intracellular distribution of inorganic carbon fixing enzymes does not support the presence of a C4 pathway in the diatom *Phaeodactylum tricornutum*. *Photosynthesis Research, 137,* (*2*, 263–280). doi:10.1007/s11120-018-0500-5

Fabris, M., George, J., Kuzhiumparambil, U., Lawson, C. A., Jaramillo-Madrid, A. C., Abbriano, R. M., et al. (2020). Extrachromosomal Genetic Engineering of the Marine Diatom *Phaeodactylum tricornutum* Enables the Heterologous Production of Monoterpenoids. *ACS synthetic biology, 9,* (*3*, 598–612). doi:10.1021/acssynbio.9b00455

Falciatore, A., & Bowler, C. (2002). Revealing the molecular secrets of marine diatoms. *Annual review of plant biology, 53,* (109–130). doi:10.1146/annurev.arplant.53.091701.153921

Falciatore, A., Jaubert, M., Bouly, J.-P., Bailleul, B., & Mock, T. (2020). Diatom Molecular Research Comes of Age: Model Species for Studying Phytoplankton Biology and Diversity. *The Plant cell, 32,* (*3*, 547–572). doi:10.1105/tpc.19.00158

Falkowski, Barber, & Smetacek. (1998). Biogeochemical Controls and Feedbacks on Ocean Primary Production. *Science (New York, N.Y.), 281,* (*5374*, 200–207). doi:10.1126/science.281.5374.200

Falkowski, P., & Knoll, A. H. (Eds.). (2007). *Evolution of Primary Producers in the Sea:* Elsevier.

Fernández Sevilla, J. M., Cerón García, M. C., Sánchez Mirón, A., Belarbi, E. H., García Camacho, F., & Molina Grima, E. (2004). Pilot-plant-scale outdoor mixotrophic cultures of *Phaeodactylum tricornutum* using glycerol in vertical bubble column and airlift photobioreactors: studies in fed-batch mode. *Biotechnology progress, 20,* (*3*, 728–736). doi:10.1021/bp034344f

Fischer, H., Robl, I., Sumper, M., & Kroger, N. (1999). Targeting and covalent modification of cell wall and membrane proteins heterologously expressed in the diatom *Cylindrotheca fusiformis* (Bacillariophyceae). *Journal of Phycology, 35,* (*1*, 113–120). doi:10.1046/j.1529-8817.1999.3510113.x

Flori, S., Jouneau, P.-H., Finazzi, G., Maréchal, E., & Falconet, D. (2016). Ultrastructure of the Periplastidial Compartment of the Diatom *Phaeodactylum tricornutum*. *Protist, 167,* (*3*, 254–267). doi:10.1016/j.protis.2016.04.001

Folch, J., Lees, M., & Stanley, G. S. (1957). A simple method for the isolation and purification of total lipides from animal tissues. *Journal of Biological Chemistry, 226,* (*1*, 497–509). doi:10.1016/S0021-9258(18)64849-5

Fu, C., Donovan, W. P., Shikapwashya-Hasser, O., Ye, X., & Cole, R. H. (2014). Hot Fusion: an efficient method to clone multiple DNA fragments as well as inverted repeats without ligase. *PloS one, 9,* (*12*, e115318). doi:10.1371/journal.pone.0115318

Fuhrmann, M., Hausherr, A., Ferbitz, L., Schödl, T., Heitzer, M., & Hegemann, P. (2004). Monitoring dynamic expression of nuclear genes in *Chlamydomonas reinhardtii* by using a synthetic luciferase reporter gene. *Plant molecular biology, 55,* (*6*, 869–881). doi:10.1007/s11103-005-2150-1

Gao, B., Chen, A., Zhang, W., Li, A., & Zhang, C. (2017). Co-production of lipids, eicosapentaenoic acid, fucoxanthin, and chrysolaminarin by *Phaeodactylum tricornutum* cultured in a flat-plate photobioreactor under varying nitrogen conditions. *Journal of Ocean University of China, 16,* (*5*, 916–924). doi:10.1007/s11802-017-3174-2

Geider, R. J., Osborne, B. A., & Raven, J. A. (1985). Light dependence of growth and photosynthesis in *Phaeodactylum tricornutum* (Bacillariophyceae). *Journal of Phycology, 21,* (*4*, 609–619). doi:10.1111/j.0022-3646.1985.00609.x

Genty, B., Briantais, J.-M., & Baker, N. R. (1989). The relationship between the quantum yield of photosynthetic electron transport and quenching of chlorophyll fluorescence. *Biochimica et Biophysica Acta (BBA) - General Subjects, 990,* (*1*, 87–92). doi:10.1016/S0304-4165(89)80016-9

Gillard, J. T. F., Hernandez, A. L., Contreras, J. A., Francis, I. M., & Cabrales, L. (2021). Potential for Biomass Production and Remediation by Cultivation of the Marine Model Diatom *Phaeodactylum tricornutum* in Oil Field Produced Wastewater Media. *Water, 13,* (*19*, 2700). doi:10.3390/w13192700

Giordano, M., Beardall, J., & Raven, J. A. (2005). CO_2 concentrating mechanisms in algae: mechanisms, environmental modulation, and evolution. *Annual review of plant biology, 56,* (99–131). doi:10.1146/annurev.arplant.56.032604.144052

Goldman, J. A. L., Bender, M. L., & Morel, F. M. M. (2017). The effects of pH and pCO_2 on photosynthesis and respiration in the diatom *Thalassiosira weissflogii*. *Photosynthesis research, 132,* (*1*, 83–93). doi:10.1007/s11120-016-0330-2

Goncalves, E. C., Wilkie, A. C., Kirst, M., & Rathinasabapathi, B. (2016). Metabolic regulation of triacylglycerol accumulation in the green algae: identification of potential targets for engineering to improve oil yield. *Plant biotechnology journal, 14,* (*8*, 1649–1660). doi:10.1111/pbi.12523

Goss, R., & Lepetit, B. (2015). Biodiversity of NPQ. *Journal of Plant Physiology, 172,* (13–32). doi:10.1016/j.jplph.2014.03.004

Gould, S. B., Waller, R. F., & McFadden, G. I. (2008). Plastid evolution. *Annual review of plant biology, 59,* (491–517). doi:10.1146/annurev.arplant.59.032607.092915

Graßl, R., Robl, I., Opekarovà, M., & Tanner, W. (2000). The C-terminal tetrapeptide HWFW of the *Chlorella* HUP1 hexose/H^+-symporter is essential for full activity and an α-helical structure of the C-terminus. *FEBS Letters, 468,* (*2-3*, 225–230). doi:10.1016/S0014-5793(00)01230-8

Green, B. R. (2011). After the primary endosymbiosis: an update on the chromalveolate hypothesis and the origins of algae with Chl c. *Photosynthesis Research, 107,* (*1*, 103–115). doi:10.1007/s11120-010-9584-2

Griffiths, D. J., Thresher, C. L., & Street, H. E. (1960). The Heterotrophic Nutrition of Chlorella vulgaris (Brannon No. 1 Strain). *Annals of Botany, 24,* (*1*, 1–11). doi:10.1093/oxfordjournals.aob.a083682

Gschloessl, B., Guermeur, Y., & Cock, J. M. (2008). HECTAR: a method to predict subcellular targeting in heterokonts. *BMC bioinformatics, 9,* (393). doi:10.1186/1471-2105-9-393

Guéguen, N., Le Moigne, D., Amato, A., Salvaing, J., & Maréchal, E. (2021). Lipid Droplets in Unicellular Photosynthetic Stramenopiles. *Frontiers in plant science, 12,* (639276). doi:10.3389/fpls.2021.639276

Guillard, R. R. L. (1975). Culture of Phytoplankton for Feeding Marine Invertebrates. In W. L. Smith, & M. H. Chanley (Eds.), *Culture of Marine Invertebrate Animals* (pp. 29–60). Boston, MA: Springer US.

Guillard, R. R. L., & Rhyter, J. H. (1962). Studies of marine planktonic diatoms. I. *Cyclotella nana* Hustedt, and *Detonula confervacea* (cleve) Gran. *Canadian Journal of Microbiology, 8,* (*2*, 229–239). doi:10.1139/m62-029

Guschina, I. A., & Harwood, J. L. (2006). Lipids and lipid metabolism in eukaryotic algae. *Progress in Lipid Research, 45,* (*2*, 160–186). doi:10.1016/j.plipres.2006.01.001

Hallmann, A., & Sumper, M. (1996). The Chlorella hexose/H^+ symporter is a useful selectable marker and biochemical reagent when expressed in *Volvox*. *PNAS, 93,* (*2*, 669–673). doi:10.1073/pnas.93.2.669

Hamilton, M. L., Haslam, R. P., Napier, J. A., & Sayanova, O. (2014). Metabolic engineering of Phaeodactylum tricornutum for the enhanced accumulation of omega-3 long chain polyunsaturated fatty acids. *Metabolic Engineering, 22,* (3–9). doi:10.1016/j.ymben.2013.12.003

Hamilton, M. L., Warwick, J., Terry, A., Allen, M. J., Napier, J. A., & Sayanova, O. (2015). Towards the industrial production of omega-3 long chain polyunsaturated fatty acids from a genetically modified diatom phaeodactylum tricornutum. *PloS one, 10,* (*12*, 1–15). doi:10.1371/journal.pone.0144054

Hamilton, M. L., Powers, S., Napier, J. A., & Sayanova, O. (2016). Heterotrophic production of omega-3 long-chain polyunsaturated fatty acids by trophically converted marine diatom *Phaeodactylum tricornutum*. *Marine drugs, 14,* (*3*). doi:10.3390/md14030053

Harrison, P. J., Waters, R. E., & Taylor, F. J. R. (1980). A broad spectrum artificial sea water medium for coastal and open ocean phytoplankton. *Journal of Phycology, 16,* (*1*, 28–35). doi:10.1111/j.0022-3646.1980.00028.x

Harwood, J. L. (1996). Recent advances in the biosynthesis of plant fatty acids. *Biochimica et Biophysica Acta (BBA) - Lipids and Lipid Metabolism, 1301,* (*1-2*, 7–56). doi:10.1016/0005-2760(95)00242-1

Heldt, H. W., Werdan, K., Milovancev, M., & Geller, G. (1973). Alkalization of the chloroplast stroma caused by light-dependent proton flux into the thylakoid space. *Biochimica et*

Biophysica Acta (BBA) - Bioenergetics, 314, (*2*, 224–241). doi:10.1016/0005-2728(73)90137-0

Hempel, F., & Maier, U. G. (2012). An engineered diatom acting like a plasma cell secreting human IgG antibodies with high efficiency. *Microbial Cell Factories, 11,* (126). doi:10.1186/1475-2859-11-126

Hempel, F., Lau, J., Klingl, A., & Maier, U. G. (2011). Algae as protein factories: expression of a human antibody and the respective antigen in the diatom *Phaeodactylum tricornutum*. *PloS one, 6,* (*12*, e28424). doi:10.1371/journal.pone.0028424

Hempel, F., Bozarth, A. S., Lindenkamp, N., Klingl, A., Zauner, S., Linne, U., et al. (2011). Microalgae as bioreactors for bioplastic production. *Microbial Cell Factories, 10,* (*1*, 81). doi:10.1186/1475-2859-10-81

Hempel, F., Maurer, M., Brockmann, B., Mayer, C., Biedenkopf, N., Kelterbaum, A., et al. (2017). From hybridomas to a robust microalgal-based production platform: molecular design of a diatom secreting monoclonal antibodies directed against the Marburg virus nucleoprotein. *Microbial Cell Factories, 16,* (*1*, 131). doi:10.1186/s12934-017-0745-2

Hess, S. K., Lepetit, B., Kroth, P. G., & Mecking, S. (2018). Production of chemicals from microalgae lipids - status and perspectives. *European Journal of Lipid Science and Technology, 120,* (*1*, 1700152). doi:10.1002/ejlt.201700152

Heydarizadeh, P., Boureba, W., Zahedi, M., Huang, B., Moreau, B., Lukomska, E., et al. (2017). Response of CO2-starved diatom *Phaeodactylum tricornutum* to light intensity transition. *Philosophical transactions of the Royal Society of London. Series B, Biological sciences, 372,* (*1728*, 20160396). doi:10.1098/rstb.2016.0396

Heydarizadeh, P., Veidl, B., Huang, B., Lukomska, E., Wielgosz-Collin, G., Couzinet-Mossion, A., et al. (2019). Carbon Orientation in the Diatom *Phaeodactylum tricornutum*: The Effects of Carbon Limitation and Photon Flux Density. *Frontiers in plant science,* (471). doi:10.3389/fpls.2019.00471

Higuchi, R., Fockler, C., Dollinger, G., & Watson, R. (1993). Kinetic PCR analysis: real-time monitoring of DNA amplification reactions. *Bio/technology (Nature Publishing Company), 11,* (*9*, 1026–1030). doi:10.1038/nbt0993-1026

Hildebrand, M., & Dahlin, K. (2000). Nitrate transporter genes from the diatom *Cylindrotheca fusiformis* (Bacillariophyceae): mrna levels controlled by nitrogen source and by the cell cycle. *Journal of phycology, 36,* (*4*, 702–713). doi:10.1046/j.1529-8817.2000.99153.x

Hiller, K., Grote, A., Scheer, M., Münch, R., & Jahn, D. (2004). PrediSi: prediction of signal peptides and their cleavage positions. *Nucleic acids research, 32,* (*Web Server issue*, W375-9). doi:10.1093/nar/gkh378

Hitschler, J., & Boles, E. (2020). Improving 3-methylphenol (m-cresol) production in yeast via in vivo glycosylation or methylation. *FEMS yeast research, 20,* (*8*). doi:10.1093/femsyr/foaa063

Holman, G. D. (2020). Structure, function and regulation of mammalian glucose transporters of the SLC2 family. *Pflugers Archiv : European journal of physiology, 472,* (*9*, 1155–1175). doi:10.1007/s00424-020-02411-3

Hopkinson, B. M., Dupont, C. L., Allen, A. E., & Morel, F. M. M. (2011). Efficiency of the CO_2-concentrating mechanism of diatoms. *Proceedings of the National Academy of Sciences, 108,* (*10*, 3830–3837). doi:10.1073/pnas.1018062108

Hu, Q., Sommerfeld, M., Jarvis, E., Ghirardi, M., Posewitz, M., Seibert, M., et al. (2008). Microalgal triacylglycerols as feedstocks for biofuel production: perspectives and advances. *The Plant journal : for cell and molecular biology, 54,* (*4*, 621–639). doi:10.1111/j.1365-313X.2008.03492.x

Huang, A., Liu, L., Yang, C., & Wang, G. (2015). *Phaeodactylum tricornutum* photorespiration takes part in glycerol metabolism and is important for nitrogen-limited response. *Biotechnology for Biofuels, 8,* (73). doi:10.1186/s13068-015-0256-5

Huang, B., Marchand, J., Blanckaert, V., Lukomska, E., Ulmann, L., Wielgosz-Collin, G., et al. (2019). Nitrogen and phosphorus limitations induce carbon partitioning and membrane lipid remodelling in the marine diatom *Phaeodactylum tricornutum*. *European Journal of Phycology, 54,* (*3*, 342–358). doi:10.1080/09670262.2019.1567823

Huang, R., Ding, J., Sun, J., Tian, Y., Bowler, C., Lin, X., et al. (2020). Physiological and molecular responses to ocean acidification among strains of a model diatom. *Limnology and Oceanography, 65,* (*12*, 2926–2936). doi:10.1002/lno.11565

Iancu, C. V., Zamoon, J., Woo, S. B., Aleshin, A., & Choe, J. (2013). Crystal structure of a glucose/H^+ symporter and its mechanism of action. *PNAS, 110,* (*44*, 17862–17867). doi:10.1073/pnas.1311485110

Ismail, A., Bannenberg, G., Rice, H. B., Schutt, E., & MacKay, D. (2016). Oxidation in EPA- and DHA-rich oils: an overview. *Lipid Technology, 28,* (*3-4*, 55–59). doi:10.1002/lite.201600013

Jallet, D., Caballero, M. A., Gallina, A. A., Youngblood, M., & Peers, G. (2016). Photosynthetic physiology and biomass partitioning in the model diatom *Phaeodactylum tricornutum* grown in a sinusoidal light regime. *Algal Research, 18,* (51–60). doi:10.1016/j.algal.2016.05.014

Jaussaud, A., Lupette, J., Salvaing, J., Jouhet, J., Bastien, O., Gromova, M., et al. (2020). Stepwise Biogenesis of Subpopulations of Lipid Droplets in Nitrogen Starved *Phaeodactylum tricornutum* Cells. *Frontiers in plant science, 11,* (48). doi:10.3389/fpls.2020.00048

Jeffrey, S. W., & Humphrey, G. F. (1975). New spectrophotometric equations for determining chlorophylls *a, b,* c_1 and c_2 in higher plants, algae and natural phytoplankton. *Biochemie und Physiologie der Pflanzen, 167,* (*2*, 191–194). doi:10.1016/S0015-3796(17)30778-3

Jiang, H., & Gao, K. (2004). Effects of lowering temperature during culture on the production of polyunsaturated fatty acids in the marine diatom *Phaeodactylum tricornutum* (Bacillariophyceae). *Journal of phycology, 40,* (*4*, 651–654). doi:10.1111/j.1529-8817.2004.03112.x

Juhas, M., & Büchel, C. (2012). Properties of photosystem I antenna protein complexes of the diatom *Cyclotella meneghiniana*. *Journal of Experimental Botany, 63,* (*10*, 3673–3681). doi:10.1093/jxb/ers049

Kadono, T., Miyagawa-Yamaguchi, A., Kira, N., Tomaru, Y., Okami, T., Yoshimatsu, T., et al. (2015). Characterization of marine diatom-infecting virus promoters in the model diatom *Phaeodactylum tricornutum*. *Scientific reports, 5,* (18708). doi:10.1038/srep18708

Katoh, K., & Standley, D. M. (2013). MAFFT multiple sequence alignment software version 7: improvements in performance and usability. *Molecular biology and evolution, 30,* (*4*, 772–780). doi:10.1093/molbev/mst010

Ke, J., Behal, R. H., Back, S. L., Nikolau, B. J., Wurtele, E. S., & Oliver, D. J. (2000). The role of pyruvate dehydrogenase and acetyl-coenzyme A synthetase in fatty acid synthesis in developing Arabidopsis seeds. *Plant Physiology, 123,* (*2*, 497–508). doi:10.1104/pp.123.2.497

Kennedy, E. P. (1961). Biosynthesis of complex lipids. *Federation proceedings, 20,* (934–940).

Kitessa, S. M., Abeywardena, M., Wijesundera, C., & Nichols, P. D. (2014). DHA-containing oilseed: a timely solution for the sustainability issues surrounding fish oil sources of the health-benefitting long-chain omega-3 oils. *Nutrients, 6,* (*5*, 2035–2058). doi:10.3390/nu6052035

Komor, E., & Tanner, W. (1971). Characterization of the active hexose transport system of *Chlorella vulgaris*. *Biochimica et biophysica acta, 241,* (*1*, 170–179). doi:10.1016/0005-2736(71)90314-2

Komor, E., & Tanner, W. (1974). The Hexose-Proton Cotransport System of *Chlorella*:. pH-Dependent Change in Km Values and Translocation Constants of the Uptake System. *The Journal of general physiology, 64,* (*5*, 568–581). doi:10.1085/jgp.64.5.568

Komor, E., Cho, B. H., Schricker, S., & Schobert, C. (1989). Charge and acidity compensation during proton-sugar symport in *Chlorella*: The H^+-ATPase does not fully compensate for the sugar-coupled proton influx. *Planta, 177,* (*1*, 9–17). doi:10.1007/BF00392149

Kräbs, G., & Büchel, C. (2011). Temperature and salinity tolerances of geographically separated *Phaeodactylum tricornutum* Böhlin strains: maximum quantum yield of primary photochemistry, pigmentation, proline content and growth. *Botanica Marina, 54,* (*3*). doi:10.1515/bot.2011.037

Kris-Etherton, P. M., Grieger, J. A., & Etherton, T. D. (2009). Dietary reference intakes for DHA and EPA. *Prostaglandins, leukotrienes, and essential fatty acids, 81,* (*2-3*, 99–104). doi:10.1016/j.plefa.2009.05.011

Krishnan, A., Likhogrud, M., Cano, M., Edmundson, S., Melanson, J. B., Huesemann, M., et al. (2021). Picochlorum celeri as a model system for robust outdoor algal growth in seawater. *Scientific reports, 11,* (*1*, 11649). doi:10.1038/s41598-021-91106-5

Krogh, A., Larsson, B., Heijne, G. von, & Sonnhammer, E. L. (2001). Predicting transmembrane protein topology with a hidden Markov model: application to complete genomes. *Journal of molecular biology, 305,* (*3*, 567–580). doi:10.1006/jmbi.2000.4315

Kroth, P. G., Chiovitti, A., Gruber, A., Martin-Jezequel, V., Mock, T., Parker, M. S., et al. (2008). A model for carbohydrate metabolism in the diatom *Phaeodactylum tricornutum* deduced from comparative whole genome analysis. *PloS one, 3,* (*1*, e1426). doi:10.1371/journal.pone.0001426

Kruijff, M. de. (2021). *Improvement of neutral lipid and polyunsaturated fatty acid biosynthesis in Phaeodactylum tricornutum. Master thesis,* Goethe University Frankfurt.

Kuzminov, F. I., & Gorbunov, M. Y. (2016). Energy dissipation pathways in Photosystem 2 of the diatom, *Phaeodactylum tricornutum*, under high-light conditions. *Photosynthesis Research, 127,* (*2*, 219–235). doi:10.1007/s11120-015-0180-3

Laemmli, U. K. (1970). Cleavage of structural proteins during the assembly of the head of bacteriophage T4. *Nature, 227,* (*5259*, 680–685). doi:10.1038/227680a0

Lee, Y.-K. (2001). Microalgal mass culture systems and methods: Their limitation and potential. *Journal of Applied Phycology, 13,* (*4*, 307–315). doi:10.1023/A:1017560006941

Lemoine, F., Correia, D., Lefort, V., Doppelt-Azeroual, O., Mareuil, F., Cohen-Boulakia, S., et al. (2019). NGPhylogeny.fr: new generation phylogenetic services for non-specialists. *Nucleic acids research, 47,* (*W1*, W260-W265). doi:10.1093/nar/gkz303

Leonardi, R., Zhang, Y.-M., Rock, C. O., & Jackowski, S. (2005). Coenzyme A: back in action. *Progress in Lipid Research, 44,* (*2-3*, 125–153). doi:10.1016/j.plipres.2005.04.001

Lewin, J. C. (1953). Heterotrophy in diatoms. *Journal of general microbiology, 9,* (*2*, 305–313). doi:10.1099/00221287-9-2-305

Leyland, B., Boussiba, S., & Khozin-Goldberg, I. (2020). A Review of Diatom Lipid Droplets. *Biology, 9,* (*2*). doi:10.3390/biology9020038

Leyland, B., Zarka, A., Didi-Cohen, S., Boussiba, S., & Khozin-Goldberg, I. (2020). High Resolution Proteome of Lipid Droplets Isolated from the Pennate Diatom *Phaeodactylum tricornutum* (Bacillariophyceae) Strain pt4 provides mechanistic insights into complex intracellular coordination during nitrogen deprivation. *Journal of Phycology, 56,* (*6*, 1642–

1663). doi:10.1111/jpy.13063

Li, X., Slavens, S., Crunkleton, D. W., & Johannes, T. W. (2021). Interactive effect of light quality and temperature on *Chlamydomonas reinhardtii* growth kinetics and lipid synthesis. *Algal Research, 53,* (102127). doi:10.1016/j.algal.2020.102127

Li-Beisson, Y., Shorrosh, B., Beisson, F., Andersson, M. X., Arondel, V., Bates, P. D., et al. (2010). Acyl-lipid metabolism. *The Arabidopsis Book, 8,* (e0133). doi:10.1199/tab.0133

Li-Beisson, Y., Thelen, J. J., Fedosejevs, E., & Harwood, J. L. (2019). The lipid biochemistry of eukaryotic algae. *Progress in Lipid Research, 74,* (31–68). doi:10.1016/j.plipres.2019.01.003

Liu, X., Duan, S., Li, A., Xu, N., Cai, Z., & Hu, Z. (2009). Effects of organic carbon sources on growth, photosynthesis, and respiration of *Phaeodactylum tricornutum*. *Journal of Applied Phycology, 21,* (*2*, 239–246). doi:10.1007/s10811-008-9355-z

Liu, J., & Hu, Q. (2013). *Chlorella* : Industrial Production of Cell Mass and Chemicals. In A. Richmond, & Q. Hu (Eds.), *Handbook of microalgal culture. Applied phycology and biotechnology* (pp. 327–338). Chicester, West Sussex: Wiley Blackwell.

Liu, X., Hempel, F., Stork, S., Bolte, K., Moog, D., Heimerl, T., et al. (2016). Addressing various compartments of the diatom model organism *Phaeodactylum tricornutum* via sub-cellular marker proteins. *Algal Research, 20,* (249–257). doi:10.1016/j.algal.2016.10.018

Livak, K. J., & Schmittgen, T. D. (2001). Analysis of relative gene expression data using real-time quantitative PCR and the $2^{-\Delta\Delta C_T}$ Method. *Methods (San Diego, Calif.), 25,* (*4*, 402–408). doi:10.1006/meth.2001.1262

Luschnig, C., & Vert, G. (2014). The dynamics of plant plasma membrane proteins: PINs and beyond. *Development, 141,* (*15*, 2924–2938). doi:10.1242/dev.103424

Mann, J. E., & Myers, J. (1968). ON PIGMENTS, GROWTH, AND PHOTOSYNTHESIS OF PHAEODACTYLUM TRICORNUTUM(1) (2). *Journal of Phycology, 4,* (*4*, 349–355). doi:10.1111/j.1529-8817.1968.tb04707.x

Mao, X., Ge, M., Wang, X., Yu, J., Li, X., Liu, B., et al. (2021). Transcriptomics and Metabolomics Analyses Provide Novel Insights into Glucose-Induced Trophic Transition of the Marine Diatom *Nitzschia laevis*. *Marine drugs, 19,* (*8*). doi:10.3390/md19080426

Martino, A. D., Meichenin, A., Shi, J., Pan, K., & Bowler, C. (2007). Genetic and phenotypic characterization of *Phaeodactylum tricornutum* (Bacillariophyceae) accessions. *Journal of phycology, 43,* (*5*, 992–1009). doi:10.1111/j.1529-8817.2007.00384.x

Martino, A. D., Bartual, A., Willis, A., Meichenin, A., Villazán, B., Maheswari, U., et al. (2011). Physiological and molecular evidence that environmental changes elicit morphological interconversion in the model diatom *Phaeodactylum tricornutum*. *Protist, 162,* (*3*, 462–481). doi:10.1016/j.protis.2011.02.002

Martins, D. A., Custódio, L., Barreira, L., Pereira, H., Ben-Hamadou, R., Varela, J., et al. (2013). Alternative sources of n-3 long-chain polyunsaturated fatty acids in marine microalgae. *Marine drugs, 11,* (*7*, 2259–2281). doi:10.3390/md11072259

Matsuda, Y., Hopkinson, B. M., Nakajima, K., Dupont, C. L., & Tsuji, Y. (2017). Mechanisms of carbon dioxide acquisition and CO2 sensing in marine diatoms: a gateway to carbon metabolism. *Philosophical transactions of the Royal Society of London. Series B, Biological sciences, 372,* (*1728*). doi:10.1098/rstb.2016.0403

Matsui, H., Hopkinson, B. M., Nakajima, K., & Matsuda, Y. (2018). Plasma Membrane-Type Aquaporins from Marine Diatoms Function as CO_2/NH_3 Channels and Provide Photoprotection. *Plant Physiology, 178,* (*1*, 345–357). doi:10.1104/pp.18.00453

Maxwell, K., & Johnson, G. N. (2000). Chlorophyll fluorescence—a practical guide. *Journal of*

Experimental Botany, 51, (*345*, 659–668). doi:10.1093/jexbot/51.345.659

McCarthy, J. K., Smith, S. R., McCrow, J. P., Tan, M., Zheng, H., Beeri, K., et al. (2017). Nitrate Reductase Knockout Uncouples Nitrate Transport from Nitrate Assimilation and Drives Repartitioning of Carbon Flux in a Model Pennate Diatom. *The Plant cell, 29,* (*8*, 2047–2070). doi:10.1105/tpc.16.00910

Megía-Hervás, I., Sánchez-Bayo, A., Bautista, L. F., Morales, V., Witt-Sousa, F. G., Segura-Fornieles, M., et al. (2020). Scale-Up Cultivation of *Phaeodactylum tricornutum* to Produce Biocrude by Hydrothermal Liquefaction. *Processes, 8,* (*9*, 1072). doi:10.3390/pr8091072

Millero, F. J., Feistel, R., Wright, D. G., & McDougall, T. J. (2008). The composition of Standard Seawater and the definition of the Reference-Composition Salinity Scale. *Deep Sea Research Part I: Oceanographic Research Papers, 55,* (*1*, 50–72). doi:10.1016/j.dsr.2007.10.001

Miyahara, M., Aoi, M., Inoue-Kashino, N., Kashino, Y., & Ifuku, K. (2013). Highly efficient transformation of the diatom *Phaeodactylum tricornutum* by multi-pulse electroporation. *Bioscience, biotechnology, and biochemistry, 77,* (*4*, 874–876). doi:10.1271/bbb.120936

Moog, D., Schmitt, J., Senger, J., Zarzycki, J., Rexer, K.-H., Linne, U., et al. (2019). Using a marine microalga as a chassis for polyethylene terephthalate (PET) degradation. *Microbial Cell Factories, 18,* (*1*, 171). doi:10.1186/s12934-019-1220-z

Morales-Sánchez, D., Martinez-Rodriguez, O. A., Kyndt, J., & Martinez, A. (2015). Heterotrophic growth of microalgae: metabolic aspects. *World journal of microbiology & biotechnology, 31,* (*1*, 1–9). doi:10.1007/s11274-014-1773-2

Morrissey, J., Sutak, R., Paz-Yepes, J., Tanaka, A., Moustafa, A., Veluchamy, A., et al. (2015). A novel protein, ubiquitous in marine phytoplankton, concentrates iron at the cell surface and facilitates uptake. *Current biology : CB, 25,* (*3*, 364–371). doi:10.1016/j.cub.2014.12.004

Mueckler, M., Hresko, R. C., & Sato, M. (1997). Structure, function and biosynthesis of GLUT1. *Biochemical Society Transactions, 25,* (*3*, 951–954). doi:10.1042/bst0250951

Mueckler, M., & Thorens, B. (2013). The SLC2 (GLUT) family of membrane transporters. *Molecular aspects of medicine, 34,* (*2-3*, 121–138). doi:10.1016/j.mam.2012.07.001

Mühlroth, A., Li, K., Røkke, G., Winge, P., Olsen, Y., Hohmann-Marriott, M. F., et al. (2013). Pathways of lipid metabolism in marine algae, co-expression network, bottlenecks and candidate genes for enhanced production of EPA and DHA in species of Chromista. *Marine drugs, 11,* (*11*, 4662–4697). doi:10.3390/md11114662

Müller, P., Li, X. P., & Niyogi, K. K. (2001). Non-photochemical quenching. A response to excess light energy. *Plant Physiology, 125,* (*4*, 1558–1566). doi:10.1104/pp.125.4.1558

Murchie, E. H., & Lawson, T. (2013). Chlorophyll fluorescence analysis: a guide to good practice and understanding some new applications. *Journal of Experimental Botany, 64,* (*13*, 3983–3998). doi:10.1093/jxb/ert208

Mus, F., Toussaint, J.-P., Cooksey, K. E., Fields, M. W., Gerlach, R., Peyton, B. M., et al. (2013). Physiological and molecular analysis of carbon source supplementation and pH stress-induced lipid accumulation in the marine diatom *Phaeodactylum tricornutum*. *Applied Microbiology and Biotechnology, 97,* (*8*, 3625–3642). doi:10.1007/s00253-013-4747-7

Nakajima, K., Tanaka, A., & Matsuda, Y. (2013). SLC4 family transporters in a marine diatom directly pump bicarbonate from seawater. *PNAS, 110,* (*5*, 1767–1772). doi:10.1073/pnas.1216234110

Neilson, A. H., & Lewin, R. A. (1974). The uptake and utilization of organic carbon by algae: an essay in comparative biochemistry. *Phycologia, 13,* (*3*, 227–264). doi:10.2216/i0031-8884-13-3-227.1

Nymark, M., Valle, K. C., Brembu, T., Hancke, K., Winge, P., Andresen, K., et al. (2009). An integrated analysis of molecular acclimation to high light in the marine diatom *Phaeodactylum tricornutum*. *PloS one, 4,* (*11*, e7743). doi:10.1371/journal.pone.0007743

Oakley, K. E. (2010). *Molecular mechanisms of urea uptake in marine diatoms,* UC San Diego. ProQuest ID: Oakley_ucsd_0033M_10937. Merritt ID: ark:/20775/bb53255161. Retrieved from https://escholarship.org/uc/item/9mr9p5gv.

Oliver, L., Dietrich, T., Marañón, I., Villarán, M. C., & Barrio, R. J. (2020). Producing Omega-3 Polyunsaturated Fatty Acids: A Review of Sustainable Sources and Future Trends for the EPA and DHA Market. *Resources, 9,* (*12*, 148). doi:10.3390/resources9120148

Pao, S. S., Paulsen, I. T., & Saier, M. H. (1998). Major facilitator superfamily. *Microbiology and Molecular Biology Reviews, 62,* (*1*, 1–34). doi:10.1128/MMBR.62.1.1-34.1998

Patel, A., Matsakas, L., Hrůzová, K., Rova, U., & Christakopoulos, P. (2019). Biosynthesis of Nutraceutical Fatty Acids by the Oleaginous Marine Microalgae *Phaeodactylum tricornutum* Utilizing Hydrolysates from Organosolv-Pretreated Birch and Spruce Biomass. *Marine drugs, 17,* (*2*, 119). doi:10.3390/md17020119

Perez-Garcia, O., Escalante, F. M. E., de-Bashan, L. E., & Bashan, Y. (2011). Heterotrophic cultures of microalgae: metabolism and potential products. *Water research, 45,* (*1*, 11–36). doi:10.1016/j.watres.2010.08.037

Pérez-López, P., González-García, S., Allewaert, C., Verween, A., Murray, P., Feijoo, G., et al. (2014). Environmental evaluation of eicosapentaenoic acid production by *Phaeodactylum tricornutum*. *The Science of the total environment, 466-467,* (991–1002). doi:10.1016/j.scitotenv.2013.07.105

Petroutsos, D., Amiar, S., Abida, H., Dolch, L. J., Bastien, O., Rébeillé, F., et al. (2014). Evolution of galactoglycerolipid biosynthetic pathways - From cyanobacteria to primary plastids and from primary to secondary plastids. *Progress in Lipid Research, 54,* (*1*, 68–85). doi:10.1016/j.plipres.2014.02.001

Popko, J., Herrfurth, C., Feussner, K., Ischebeck, T., Iven, T., Haslam, R., et al. (2016). Metabolome Analysis Reveals Betaine Lipids as Major Source for Triglyceride Formation, and the Accumulation of Sedoheptulose during Nitrogen-Starvation of *Phaeodactylum tricornutum*. *PloS one, 11,* (*10*, e0164673). doi:10.1371/journal.pone.0164673

Potvin, G., & Zhang, Z. (2010). Strategies for high-level recombinant protein expression in transgenic microalgae: a review. *Biotechnology advances, 28,* (*6*, 910–918). doi:10.1016/j.biotechadv.2010.08.006

Provasoli, L., McLaughlin, J. J., & Droop, M. R. (1957). The development of artificial media for marine algae. *Archiv fur Mikrobiologie, 25,* (*4*, 392–428). doi:10.1007/BF00446694

Pudney, A., Gandini, C., Economou, C. K., Smith, R., Goddard, P., Napier, J. A., et al. (2019). Multifunctionalizing the marine diatom *Phaeodactylum tricornutum* for sustainable co-production of omega-3 long chain polyunsaturated fatty acids and recombinant phytase. *Scientific reports, 9,* (*1*, 11444). doi:10.1038/s41598-019-47875-1

Qiao, H., Cong, C., Sun, C., Li, B., Wang, J., & Zhang, L. (2016). Effect of culture conditions on growth, fatty acid composition and DHA/EPA ratio of *Phaeodactylum tricornutum*. *Aquaculture, 452,* (311–317). doi:10.1016/j.aquaculture.2015.11.011

Ranjith Kumar, R., Hanumantha Rao, P., & Arumugam, M. (2015). Lipid Extraction Methods from Microalgae: A Comprehensive Review. *Frontiers in Energy Research, 2. doi:*10.3389/fenrg.2014.00061

Rastogi, A., Vieira, F. R. J., Deton-Cabanillas, A.-F., Veluchamy, A., Cantrel, C., Wang, G., et al. (2020). A genomics approach reveals the global genetic polymorphism, structure, and functional diversity of ten accessions of the marine model diatom *Phaeodactylum*

tricornutum. *The ISME journal, 14,* (*2*, 347–363). doi:10.1038/s41396-019-0528-3

Remmers, I. M., Martens, D. E., Wijffels, R. H., & Lamers, P. P. (2017). Dynamics of triacylglycerol and EPA production in *Phaeodactylum tricornutum* under nitrogen starvation at different light intensities. *PloS one, 12,* (*4*, e0175630). doi:10.1371/journal.pone.0175630

Remmers, I. M., D'Adamo, S., Martens, D. E., Vos, R. C. de, Mumm, R., America, A. H., et al. (2018). Orchestration of transcriptome, proteome and metabolome in the diatom *Phaeodactylum tricornutum* during nitrogen limitation. *Algal Research, 35,* (33–49). doi:10.1016/j.algal.2018.08.012

Rodolfi, L., Biondi, N., Guccione, A., Bassi, N., D'Ottavio, M., Arganaraz, G., et al. (2017). Oil and eicosapentaenoic acid production by the diatom *Phaeodactylum tricornutum* cultivated outdoors in Green Wall Panel (GWP®) reactors. *Biotechnology and Bioengineering, 114,* (*10*, 2204–2210). doi:10.1002/bit.26353

Roesle, P., Stempfle, F., Hess, S. K., Zimmerer, J., Río Bártulos, C., Lepetit, B., et al. (2014). Synthetic polyester from algae oil. *Angewandte Chemie (International ed. in English), 53,* (*26*, 6800–6804). doi:10.1002/anie.201403991

Rumin, J., Bonnefond, H., Saint-Jean, B., Rouxel, C., Sciandra, A., Bernard, O., et al. (2015). The use of fluorescent Nile red and BODIPY for lipid measurement in microalgae. *Biotechnology for Biofuels, 8,* (*1*, 1–16). doi:10.1186/s13068-015-0220-4

Rumin, J., Nicolau, E., Junior, R. G. d. O., Fuentes-Grünewald, C., Flynn, K. J., & Picot, L. (2020). A Bibliometric Analysis of Microalgae Research in the World, Europe, and the European Atlantic Area. *Marine drugs, 18,* (*2*, 79). doi:10.3390/md18020079

Ryall, K., Harper, J. T., & Keeling, P. J. (2003). Plastid-derived Type II fatty acid biosynthetic enzymes in chromists. *Gene, 313,* (139–148). doi:10.1016/S0378-1119(03)00671-1

Sachse, M., Sturm, S., Gruber, A., & Kroth, P. G. (2013). Identification and evaluation of endogenous reference genes for steady state transcript quantification by qPCR in the diatom *Phaeodactylum tricornutum* with constitutive expression independent from time and light. *Journal of Endocytobiosis and Cell Research,* (*24*, 1–7).

Santin, A., Caputi, L., Longo, A., Chiurazzi, M., Ribera d'Alcalà, M., Russo, M. T., et al. (2021). Integrative omics identification, evolutionary and structural analysis of low affinity nitrate transporters in diatoms, diNPFs. *Open biology, 11,* (*4*, 200395). doi:10.1098/rsob.200395

Sato, N., & Awai, K. (2017). "Prokaryotic Pathway" Is Not Prokaryotic: Noncyanobacterial Origin of the Chloroplast Lipid Biosynthetic Pathway Revealed by Comprehensive Phylogenomic Analysis. *Genome biology and evolution, 9,* (*11*, 3162–3178). doi:10.1093/gbe/evx238

Sauer, N., Caspari, T., Klebl, F., & Tanner, W. (1990). Functional expression of the *Chlorella* hexose transporter in *Schizosaccharomyces pombe*. *PNAS, 87,* (*20*, 7949–7952).

Sayanova, O., Mimouni, V., Ulmann, L., Morant-Manceau, A., Pasquet, V., Schoefs, B., et al. (2017). Modulation of lipid biosynthesis by stress in diatoms. *Philosophical Transactions of the Royal Society B: Biological Sciences, 372,* (*1728*, 20160407). doi:10.1098/rstb.2016.0407

Schmidl, S., Tamayo Rojas, S. A., Iancu, C. V., Choe, J., & Oreb, M. (2020). Functional Expression of the Human Glucose Transporters GLUT2 and GLUT3 in Yeast Offers Novel Screening Systems for GLUT-Targeting Drugs. *Frontiers in molecular biosciences, 7,* (598419). doi:10.3389/fmolb.2020.598419

Schnitzler, L., Zarzycki, J., Gerhard, M., Konde, S., Rexer, K.-H., Erb, T. J., et al. (2021). Lensless digital holographic microscopy as an efficient method to monitor enzymatic plastic degradation. *Marine pollution bulletin, 163,* (111950). doi:10.1016/j.marpolbul.2020.111950

Seo, S., Jeon, H., Hwang, S., Jin, E., & Chang, K. S. (2015). Development of a new constitutive

expression system for the transformation of the diatom *Phaeodactylum tricornutum*. *Algal Research, 11,* (50–54). doi:10.1016/j.algal.2015.05.012

Shao, S., & Hegde, R. S. (2011). Membrane protein insertion at the endoplasmic reticulum. *Annual review of cell and developmental biology, 27,* (25–56). doi:10.1146/annurev-cellbio-092910-154125

Sharma, N., Fleurent, G., Awwad, F., Cheng, M., Meddeb-Mouelhi, F., Budge, S. M., et al. (2020). Red Light Variation an Effective Alternative to Regulate Biomass and Lipid Profiles in *Phaeodactylum tricornutum*. *Applied Sciences, 10,* (*7*, 2531). doi:10.3390/app10072531

Shemesh, Z., Leu, S., Khozin-Goldberg, I., Didi-Cohen, S., Zarka, A., & Boussiba, S. (2016). Inducible expression of Haematococcus oil globule protein in the diatom *Phaeodactylum tricornutum* : Association with lipid droplets and enhancement of TAG accumulation under nitrogen starvation. *Algal Research, 18,* (321–331). doi:10.1016/j.algal.2016.07.002

Siaut, M., Cuiné, S., Cagnon, C., Fessler, B., Nguyen, M., Carrier, P., et al. (2011). Oil accumulation in the model green alga *Chlamydomonas reinhardtii*: characterization, variability between common laboratory strains and relationship with starch reserves. *BMC biotechnology, 11,* (7). doi:10.1186/1472-6750-11-7

Sicko-Good, L., Simmons, M. S., Lazinsky, D., & Hall, J. (1988). Effect of light cycle on diatom fatty acid composition and quantitative morphology. *Journal of Phycology, 24,* (*1*, 1–7). doi:10.1111/j.1529-8817.1988.tb04448.x

Song, Z., Lye, G. J., & Parker, B. M. (2020). Morphological and biochemical changes in *Phaeodactylum tricornutum* triggered by culture media: Implications for industrial exploitation. *Algal Research, 47,* (101822). doi:10.1016/j.algal.2020.101822

Sörensen, S. (1968). Enzyme Studies II. The Measurement and Meaning of Hydrogen Ion Concentration in Enzymatic Processes. In H. M. Leicester (Ed.), *Source Book in Chemistry, 1900–1950* (Source Books in the History of the Sciences, vol. 10, pp. 16–19). s.l.: Harvard University Press.

Sorokin, C. (1969). Growth Rate Measurements on Phytoplanktonic Organisms. *Chesapeake Science, 10,* (*3/4*, 313). doi:10.2307/1350476

Spiess, M., Junne, T., & Janoschke, M. (2019). Membrane Protein Integration and Topogenesis at the ER. *The protein journal, 38,* (*3*, 306–316). doi:10.1007/s10930-019-09827-6

Stork, S., Moog, D., Przyborski, J. M., Wilhelmi, I., Zauner, S., & Maier, U. G. (2012). Distribution of the SELMA translocon in secondary plastids of red algal origin and predicted uncoupling of ubiquitin-dependent translocation from degradation. *Eukaryotic cell, 11,* (*12*, 1472–1481). doi:10.1128/EC.00183-12

Strassert, J. F. H., Irisarri, I., Williams, T. A., & Burki, F. (2021). A molecular timescale for eukaryote evolution with implications for the origin of red algal-derived plastids. *Nature Communications, 12,* (*1*, 1879). doi:10.1038/s41467-021-22044-z

Takata, K., Kasahara, T., Kasahara, M., Ezaki, O., & Hirano, H. (1992). Ultracytochemical localization of the erythrocyte/HepG2-type glucose transporter (GLUT1) in cells of the blood-retinal barrier in the rat. *Investigative ophthalmology & visual science, 33,* (*2*, 377–383).

Tan, C. K., & Johns, M. R. (1996). Screening of diatoms for heterotrophic eicosapentaenoic acid production. *Journal of Applied Phycology, 8,* (*1*, 59–64). doi:10.1007/BF02186223

Tanner, W. (1969). Light-driven active uptake of 3-O-methylglucose via an inducible hexose uptake system of Chlorella. *Biochemical and Biophysical Research Communications, 36,* (*2*, 278–283). doi:10.1016/0006-291X(69)90326-X

Tanner, W. (2000). The *chlorella* hexose/H^+-symporters. In K. W. Jeon (Ed.), *International Review of Cytology* (International Review of Cell and Molecular Biology, v.200, 1st ed., vol. 200, pp. 101–141). s.l.: Elsevier textbooks.

The UniProt Consortium. (2021). UniProt: the universal protein knowledgebase in 2021. *Nucleic acids research, 49,* (*D1*, D480-D489). doi:10.1093/nar/gkaa1100

Tripp, J., Essl, C., Iancu, C. V., Boles, E., Choe, J., & Oreb, M. (2017). Establishing a yeast-based screening system for discovery of human GLUT5 inhibitors and activators. *Scientific reports, 7,* (*1*, 6197). doi:10.1038/s41598-017-06262-4

Villanova, V., & Spetea, C. (2021). Mixotrophy in diatoms: Molecular mechanism and industrial potential. *Physiologia plantarum, 173,* (*2*, 603–611). doi:10.1111/ppl.13471

Villanova, V., Fortunato, A. E., Singh, D., Bo, D. D., Conte, M., Obata, T., et al. (2017). Investigating mixotrophic metabolism in the model diatom *Phaeodactylum tricornutum*. *Philosophical Transactions of the Royal Society B: Biological Sciences, 372,* (*1728*). doi:10.1098/rstb.2016.0404

Villanova, V., Singh, D., Pagliardini, J., Fell, D., Le Monnier, A., Finazzi, G., et al. (2021). Boosting Biomass Quantity and Quality by Improved Mixotrophic Culture of the Diatom *Phaeodactylum tricornutum*. *Frontiers in plant science, 12. doi:*10.3389/fpls.2021.642199

Waissman-Levy, N., Leu, S., Khozin-Goldberg, I., & Boussiba, S. (2019). Manipulation of trophic capacities in *Haematococcus pluvialis* enables low-light mediated growth on glucose and astaxanthin formation in the dark. *Algal Research, 40,* (101497). doi:10.1016/j.algal.2019.101497

Wang, X., Liu, Y.-H., Wei, W., Zhou, X., Yuan, W., Balamurugan, S., et al. (2017). Enrichment of Long-Chain Polyunsaturated Fatty Acids by Coordinated Expression of Multiple Metabolic Nodes in the Oleaginous Microalga Phaeodactylum tricornutum. *Journal of agricultural and food chemistry, 65,* (*35*, 7713–7720). doi:10.1021/acs.jafc.7b02397

Wang, H., Zhang, Y., Chen, L., Cheng, W., & Liu, T. (2018). Combined production of fucoxanthin and EPA from two diatom strains *Phaeodactylum tricornutum* and Cylindrotheca fusiformis cultures. *Bioprocess and Biosystems Engineering, 41,* (*7*, 1061–1071). doi:10.1007/s00449-018-1935-y

Ward, O. P., & Singh, A. (2005). Omega-3/6 fatty acids: Alternative sources of production. *Process Biochemistry, 40,* (*12*, 3627–3652). doi:10.1016/j.procbio.2005.02.020

Wasser, D. (2019). *Trophische Konversion der obligat photoautotrophen Diatomee Phaeodactylum tricornutum*. *master thesis,* Goethe University Frankfurt.

Watanabe, Y., Kadono, T., Kira, N., Suzuki, K., Iwata, O., Ohnishi, K., et al. (2018). Development of endogenous promoters that drive high-level expression of introduced genes in the model diatom *Phaeodactylum tricornutum*. *Marine Genomics, 42,* (41–48). doi:10.1016/j.margen.2018.06.003

Wen, Z.-Y., & Chen, F. (2000). Production potential of eicosapentaenoic acid by the diatom *Nitzschia laevis*. *Biotechnology letters, 22,* (*9*, 727–733). doi:10.1023/A:1005666219163

Wen, Z. Y., & Chen, F. (2001). A perfusion-cell bleeding culture strategy for enhancing the productivity of eicosapentaenoic acid by Nitzschia laevis. *Applied Microbiology and Biotechnology, 57,* (*3*, 316–322). doi:10.1007/s002530100786

Weylandt, K. H., Serini, S., Chen, Y. Q., Su, H.-M., Lim, K., Cittadini, A., et al. (2015). Omega-3 Polyunsaturated Fatty Acids: The Way Forward in Times of Mixed Evidence. *BioMed research international, 2015,* (143109). doi:10.1155/2015/143109

Wieczorke, R., Dlugai, S., Krampe, S., & Boles, E. (2003). Characterisation of mammalian GLUT glucose transporters in a heterologous yeast expression system. *Cellular physiology and biochemistry : international journal of experimental cellular physiology, biochemistry,*

and pharmacology, 13, (*3*, 123–134). doi:10.1159/000071863

Wittwer, C. T., Herrmann, M. G., Moss, A. A., & Rasmussen, R. P. (1997). Continuous fluorescence monitoring of rapid cycle DNA amplification. *BioTechniques, 22,* (*1*, 130-1, 134-8). doi:10.2144/97221bi01

Wong, D. M., & Franz, A. K. (2013). A comparison of lipid storage in *Phaeodactylum tricornutum* and *Tetraselmis suecica* using laser scanning confocal microscopy. *Journal of microbiological methods, 95,* (*2*, 122–128). doi:10.1016/j.mimet.2013.07.026

Wu, S., Huang, A., Zhang, B., Huan, L., Zhao, P., Lin, A., et al. (2015). Enzyme activity highlights the importance of the oxidative pentose phosphate pathway in lipid accumulation and growth of *Phaeodactylum tricornutum* under CO_2 concentration. *Biotechnology for Biofuels, 8,* (78). doi:10.1186/s13068-015-0262-7

Yamada, K., Osakabe, Y., & Yamaguchi-Shinozaki, K. (2017). A C-terminal motif contributes to the plasma membrane localization of *Arabidopsis* STP transporters. *PloS one, 12,* (*10*, e0186326). doi:10.1371/journal.pone.0186326

Yang, Z.-K., Zheng, J.-W., Niu, Y.-F., Yang, W.-D., Liu, J.-S., & Li, H.-Y. (2014). Systems-level analysis of the metabolic responses of the diatom *Phaeodactylum tricornutum* to phosphorus stress. *Environmental Microbiology, 16,* (*6*, 1793–1807). doi:10.1111/1462-2920.12411

Yang, R., & Wei, D. (2020). Improving Fucoxanthin Production in Mixotrophic Culture of Marine Diatom *Phaeodactylum tricornutum* by LED Light Shift and Nitrogen Supplementation. *Frontiers in bioengineering and biotechnology, 8,* (820). doi:10.3389/fbioe.2020.00820

Yoneda, K., Yoshida, M., Suzuki, I., & Watanabe, M. M. (2016). Identification of a Major Lipid Droplet Protein in a Marine Diatom *Phaeodactylum tricornutum*. *Plant & cell physiology, 57,* (*2*, 397–406). doi:10.1093/pcp/pcv204

Yoon, H. S., Hackett, J. D., Ciniglia, C., Pinto, G., & Bhattacharya, D. (2004). A molecular timeline for the origin of photosynthetic eukaryotes. *Molecular biology and evolution, 21,* (*5*, 809–818). doi:10.1093/molbev/msh075

Yu Guilan, Kroth, P. G., & Gruber, A. (2017). Controlled supply of CO_2 to batch cultures of the diatom *Phaeodactylum tricornutum*. *Endocytobiosis and cell Research,* (*28*, 62–66).

Zaslavskaia, L. A., Lippmeier, J. C., Kroth, P. G., Grossman, A. R., & Apt, K. E. (2000). Transformation of the diatom *Phaeodactylum tricornutum* (Bacillariophyceae) with a variety of selectable marker and reporter genes. *Journal of phycology, 36,* (*2*, 379–386). doi:10.1046/j.1529-8817.2000.99164.x

Zaslavskaia, L. A., Lippmeier, J. C., Shih, C., Ehrhardt, D., Grossman, A. R., & Apt, K. E. (2001). Trophic conversion of an obligate photoautotrophic organism through metabolic engineering. *Science (New York, N.Y.), 292,* (*5524*, 2073–2075). doi:10.1126/science.160015

Zhang, H., Zeng, R., Chen, D., & Liu, J. (2016). A pivotal role of vacuolar H^+-ATPase in regulation of lipid production in *Phaeodactylum tricornutum*. *Scientific reports, 6,* (31319). doi:10.1038/srep31319

Zheng, Y., Quinn, A. H., & Sriram, G. (2013). Experimental evidence and isotopomer analysis of mixotrophic glucose metabolism in the marine diatom *Phaeodactylum tricornutum*. *Microbial cell factories, 12. doi:*10.1186/1475-2859-12-109

Zulu, N. N., Zienkiewicz, K., Vollheyde, K., & Feussner, I. (2018). Current trends to comprehend lipid metabolism in diatoms. *Progress in Lipid Research, 70,* (1–16). doi:10.1016/j.plipres.2018.03.001

Supporting Information

1. SI: General introduction

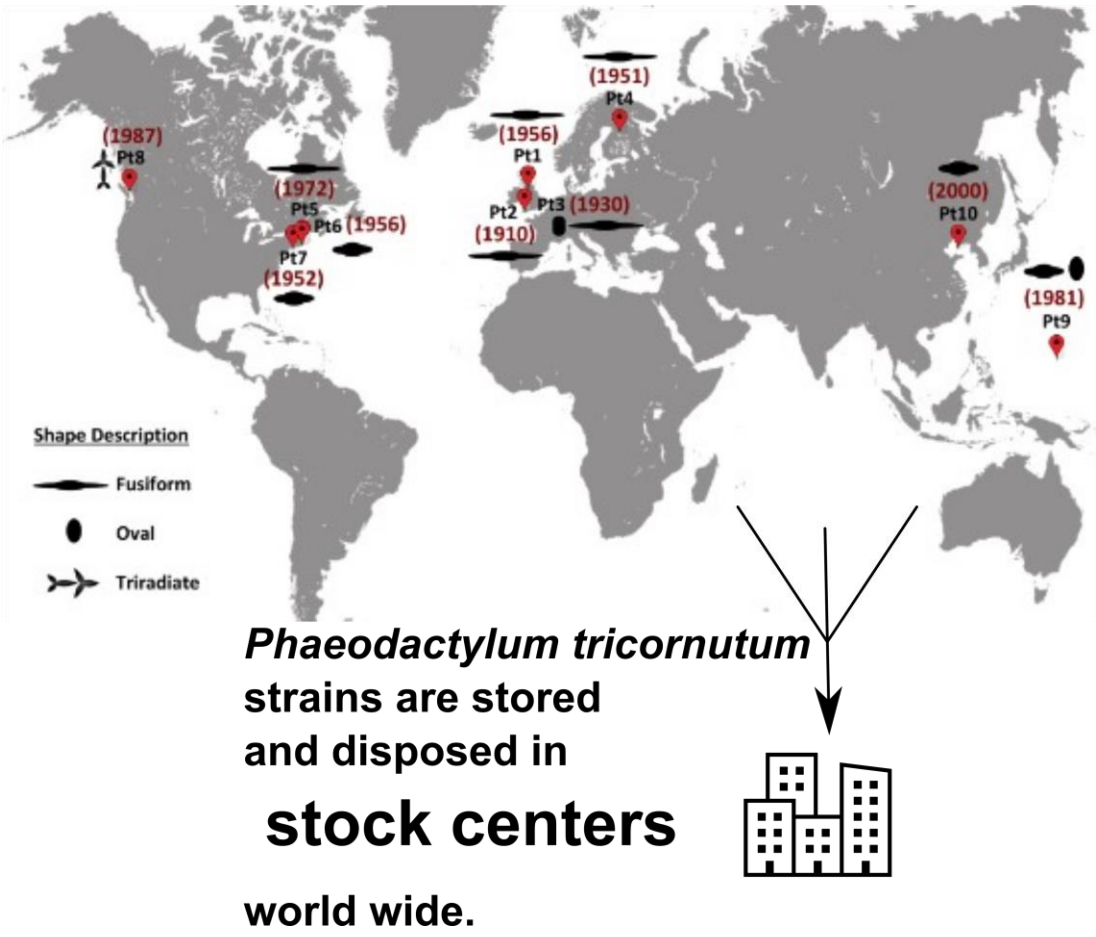

Fig. S 1 Morphotypes of *Phaeodactylum tricornutum* sampled worldwide and corresponding library names (Pt1-Pt10). P. tricornutum has been sampled and morphologically and genetically categorized. The shape description is displayed in the legend and varies within the species. The *P. tricornutum* strains are stored in stock centers around the world and receive a specific accession number. Image modified from Rastogi et al. 2020.

Tab. S 1: Listed litertaure worked with *Phaeodactylum tricornutum* strain Pt4 (UTEX 646). If title is marked with asterix (*) they used inly the libary name Pt4, or id its marked with (**) it is a review. One study is not published yet and marked with red.

First author	Year	Title	Main topic
Alberte	1986	Antheraxanthin, a light harvesting carotenoid found in a chromophyte alga	photosynthesis
Friedman	1986	Biogenesis and light regulation of the major light harvesting chlorophyll-protein of diatoms	photosynthesis
Mayasich	1986	Growth responses of Nannochloris oculata droop and Phaeodactylum tricornutum bohlin to the herbicide atrazine as influenced by light intensity and temperature	growth
Friedman	1987	Phylogenetic distribution of the major diatom light-harvesting pigment-protein determined by immunological methods	photosynthesis
Schoch	1987	The Action of Chlorophyllase on Chlorophyll-Protein Complexes	photosynthesis
Manodori	1990	Sequence Homology Between Light Harvesting Polypeptides of Plants and the Diatom Phaeodactylum tricornutum	photosynthesis
Shreve	1990	Two-photon excitation spectroscopy of thylakoid membranes from Phaeodactylum tricornutum: Evidence for an in vivo two-photon-allowed	methods
Trautmann	1990	Femtosecond dynamics of carotenoid-to-chlorophyll energy transfer in thylakoid membrane preparations from Phaeodactylum tricornutum and Nannochloropsis sp	photosynthesis
Yongmanitchai	1991	Screening of algae for potential alternative sources of eicosapentaenoic acid	lipids
Jarvis	1992	DNA nucleoside composition and methylation in several species of microalgae	genome engineering
Pyszniak	1992	Immunocytochemical localization of photosystem I and the fucoxanthin-chlorophylla/c light-harvesting complex in the diatom Phaeodactylum tricornutum	photosynthesis
Bahaya	1993	Characterization of gene clusters encoding the fucoxanthin chlorophyll proteins of the diatom Phaeodactylum tricornutum	photosynthesis
Bhaya	1993	Characterization of gene clusters encoding the fucoxanthin chlorophyll proteins of the diatom Phaeodactylum tricornutum	photosynthesis
Ting	1994	The Effects of Excess Irradiance on Photosynthesis in the Marine Diatom Phaeodactylum tricornutum	photosynthesis
Jenks	2001	Immunolocalization and distribution of form ii rubisco in the pyrenoid and chloroplast stroma of amphidinium carterae and form i rubisco in the symbiont-derived plastids of peridinium foliaceum (dinophyceae)	photosynthesis
Domergue	2002	Cloning and functional characterization of Phaeodactylum tricornutum front-end desaturases involved in eicosapentaenoic acid biosynthesis.	lipids
Domergue	2003	New insight into Phaeodactylum tricornutum fatty acid metabolism. Cloning and functional characterization of plastidial and microsomalv Δ-12 fatty acid desaturases.	lipids
Domergue	2003	Fatty Acid Desaturases from the Diatom Phaeodactylum Tricornutum.	lipids
Rousch	2004	Protein expression during heat stress in thermo-intolerant and thermo-tolerant diatoms	growth
Gruber	2007	Protein targeting into complex diatom plastids: functional characterisation of a specific targeting motif	photosynthesis

First author	Year	Title	Main topic
Martino	2007	Genetic and phenotypic characterization of Phaeodactylum tricornutum (Bacillariophyceae) accessions.	genome engineering
Stanley	2007	Whole cell adhesion strength of morphotypes and isolates of Phaeodactylum tricornutum (Bacillariophyceae)	other
Desbois	2008	Isolation and structural characterisation of two antibacterial free fatty acids from the marine diatom, Phaeodactylum tricornutum	lipids
Akazaki	2009	Crystallization and structural analysis of cytochrome c(6) from the diatom Phaeodactylum tricornutum at 1.5 A resolution	genome engineering
Bailleul*	2010	An atypical member of the light-harvesting complex stress-related protein family modulates diatom responses to light	photosynthesis
Bonsang	2010	Isoprene emission from phytoplankton monocultures: the relationship with chlorophyll-a, cell volume and carbon content	photosynthesis
Joshi-Deo	2010	Characterization of a trimeric light-harvesting complex in the diatom Phaeodactylum tricornutum built of FcpA and FcpE proteins	photosynthesis
Bruckner	2011	Growth and release of extracellular organic compounds by benthic diatoms depend on interactions with bacteria	growth
Carsten	2011	Interactions of the algicidal bacterium Kordia algicida with diatoms: regulated protease excretion for specific algal lysis	growth
Hempel	2011	Algae as protein factories: expression of a human antibody and the respective antigen in the diatom Phaeodactylum tricornutum.	biofactory
Lang	2011	Fatty acid profiles and their distribution patterns in microalgae: a comprehensive analysis of more than 2000 strains from the SAG culture collection	lipids
Dambek	2012	Biosynthesis of fucoxanthin and diadinoxanthin and function of initial pathway genes in Phaeodactylum tricornutum	photosynthesis
Hempel	2012	An engineered diatom acting like a plasma cell secreting human IgG antibodies with high efficiency	biofactory
Juhas	2012	Properties of photosystem I antenna protein complexes of the diatom Cyclotella meneghiniana.	photosynthesis
Nishikawa	2012	Isolation of mitochondrial and plastid ftsZ genes and analysis of the organelle targeting sequence in the diatom Chaetoceros neogracile (Diatoms, Bacillariophyceae)	genome engineering
Erickson	2013	Microfluidic cytometer for high-throughput measurement of photosynthetic characteristics and lipid accumulation in individual algal cells	methods
Gundermann	2013	Identification of several sub-populations in the pool of light harvesting proteins in the pennate diatom Phaeodactylum tricornutum	photosynthesis
Lavaud*	2013	An explanation for the inter-species variability of the photoprotective non-photochemical chlorophyll fluorescence quenching in diatoms	photosynthesis
Lepetit	2013	High light acclimation in the secondary plastids containing diatom Phaeodactylum tricornutum is triggered by the redox state of the plastoquinone pool	photosynthesis
Rottberger	2013	Influence of nutrients and light on autotrophic, mixotrophic and heterotrophic freshwater chrysophytes	growth
Sachse	2013	Identification and evaluation of endogenous reference genes for steady state transcript quantification by qPCR in the diatom Phaeodactylum tricornutum with constitutive expression independent from time and light	methods
Schellenberger	2013	Blue light is essential for high light acclimation and photoprotection in the diatom Phaeodactylum tricornutum	photosynthesis
Schellenberger	2013	Aureochrome 1a is involved in the photoacclimation of the diatom Phaeodactylum tricornutum	photosynthesis
Şeyma	2013	Sediment toxicity for evaluation of sediment quality guidelines and bioavailability of copper and zinc	other

First author	Year	Title	Main topic
Sturm	2013	A novel type of light-harvesting antenna protein of red algal origin in algae with secondary plastids	photosynthesis
Chuang	2014	Important role of biomolecules from diatoms in the scavenging of particle-reactive radionuclides of thorium, protactinium, lead, polonium, and beryllium in the ocean: A case study with Phaeodactylum tricornutum	growth
Dambeck	2014	Antioxidative activities of algal keto carotenoids acting as antioxidative protectants in the chloroplast	photosynthesis
Hamilton	2014	Metabolic engineering of Phaeodactylum tricornutum for the enhanced accumulation of omega-3 long chain polyunsaturated fatty acids.	lipids
Juhas	2014	A novel cryptochrome in the diatom Phaeodactylum tricornutum influences the regulation of light-harvesting protein levels	photosynthesis
Jungandreas	2014	The acclimation of Phaeodactylum tricornutum to blue and red light does not influence the photosynthetic light reaction but strongly disturbs the carbon allocation pattern	photosynthesis
Roesle	2014	Synthetic polyester from algae oil	biofactory
Roháček	2014	Relaxation of the non-photochemical chlorophyll fluorescence quenching in diatoms: kinetics, components and mechanisms	photosynthesis
Chuang	2015	Molecular level characterization of diatom-associated biopolymers that bind 234Th, 233Pa, 210 Pb, and 7Be in seawater: A case study with Phaeodactylum tricornutum	growth
Egue	2015	Expression of the retrotransposons Surcouf and Blackbeard in the marine diatom Phaeodactylum tricornutum under thermal stress	genome engineering
Hamilton.	2015	Towards the industrial production of omega-3 long chain polyunsaturated fatty acids from a genetically modified diatom phaeodactylum tricornutum	biofactory
Kadono	2015	Characterization of marine diatom-infecting virus promoters in the model diatom Phaeodactylum tricornutum	genome engineering
Nunez	2015	Changes in growth and composition of the marine microalgae Phaeodactylum tricornutum and Nannochloropsis salina in response to changing sodium bicarbonate concentrations	growth
Wolfram	2015	A Metabolic Probe-Enabled Strategy Reveals Uptake and Protein Targets of Polyunsaturated Aldehydes in the Diatom Phaeodactylum tricornutum	growth
Zecher	2015	An efficient screening method for the isolation of heterotrophic bacteria influencing growth of diatoms under photoautotrophic conditions	growth
Barka	2016	Identification of a triacylglycerol lipase in the diatom Phaeodactylum tricornutum.	lipids
Buhmann	2016	Bacteria may induce the secretion of mucin-like proteins by the diatom Phaeodactylum tricornutum	growth
Chu	2016	Rapid induction of GFP expression by the nitrate reductase promoter in the diatom Phaeodactylum tricornutum	genome engineering
Eilers	2016	Identification of genes coding for functional zeaxanthin epoxidases in the diatom Phaeodactylum tricornutum	photosynthesis
Eilers	2016	Limitations in the biosynthesis of fucoxanthin as targets for genetic engineering in Phaeodactylum tricornutum	photosynthesis
Erdene-Ochir	2016	Cloning of a novel endogenous promoter for foreign gene expression in Phaeodactylum tricornutum	genome engineering
Hamilton	2016	Heterotrophic production of omega-3 long-chain polyunsaturated fatty acids by trophically converted marine diatom Phaeodactylum tricornutum	lipids
Kira	2016	Nuclear transformation of the diatom Phaeodactylum tricornutum using PCR-amplified DNA fragments by microparticle bombardment	genome engineering

First author	Year	Title	Main topic
Kuzminov	2016	Energy dissipation pathways in Photosystem 2 of the diatom, Phaeodactylum tricornutum, under high-light conditions	photosynthesis
Popko	2016	Metabolome Analysis Reveals Betaine Lipids as Major Source for Triglyceride Formation, and the Accumulation of Sedoheptulose during Nitrogen-Starvation of Phaeodactylum tricornutum	lipids
Shemesh	2016	Inducible expression of Haematococcus oil globule protein in the diatom Phaeodactylum tricornutum: Association with lipid droplets and enhancement of TAG accumulation under nitrogen starvation.	biofactory
Suleiman	2016	Interkingdom Cross-Feeding of Ammonium from Marine Methylamine-Degrading Bacteria to the Diatom Phaeodactylum tricornutum	growth
taddei	2016	Multisignal control of expression of the LHCX protein family in the marine diatom Phaeodactylum tricornutum	photosynthesis
Chu	2017	Shuttling of (deoxy-) purine nucleotides between compartments of the diatom Phaeodactylum tricornutum.	genome engineering
Hempel	2017	From hybridomas to a robust microalgal-based production platform: molecular design of a diatom secreting monoclonal antibodies directed against the Marburg virus nucleoprotein	biofactory
Heydarizadeh	2017	Response of CO2-starved diatom Phaeodactylum tricornutum to light intensity transition	growth
König	2017	The Influence of a Cryptochrome on the Gene Expression Profile in the Diatom Phaeodactylum tricornutum under Blue Light and in Darkness	growth
Lepetit	2017	The diatom Phaeodactylum tricornutum adjusts nonphotochemical fluorescence quenching capacity in response to dynamic light via fine-tuned Lhcx and xanthophyll cycle pigment synthesis	photosynthesis
Rodolfi	2017	Oil and eicosapentaenoic acid production by the diatom Phaeodactylum tricornutum cultivated outdoors in Green Wall Panel (GWP®) reactors.	biofactory
Schreiber	2017	The Central Vacuole of the Diatom Phaeodactylum tricornutum: Identification of New Vacuolar Membrane Proteins and of a Functional Di-leucine-based Targeting Motif.	genome engineering
Yu	2017	Controlled supply of CO2 to batch cultures of the diatom Phaeodactylum tricornutum.	growth
Zecher	2017	Draft Genome Sequence of Donghicola sp. Strain KarMa, a Model Organism for Monomethylamine-Degrading Nonmethylotrophic Bacteria	growth
Zulu*	2017	Heterologous co-expression of a yeast diacylglycerol acyltransferase (ScDGA1) and a plant oleosin (AtOLEO3) as an efficient tool for enhancing triacylglycerol accumulation in the marine diatom Phaeodactylum tricornutum	biofactory
Adler-Agnon	2018	Novel promoters for constitutive and inducible expression of transgenes in the diatom Phaeodactylum tricornutum under varied nitrate availability	genome engineering
Buck	2018	Blasticidin-S deaminase, a new selection marker for genetic transformation of the diatom Phaeodactylum tricornutum	genome engineering
Río Bártulos	2018	Mitochondrial Glycolysis in a Major Lineage of Eukaryotes	genome engineering
Sabir	2018	Phylogenetic analysis and a review of the history of the accidental phytoplankter, Phaeodactylum tricornutum Bohlin (Bacillariophyta)	genome engineering
Schober	2018	Isolation of Plastid Fractions from the Diatoms Thalassiosira pseudonana and Phaeodactylum tricornutum	methods
Sitnik	2018	DGAT1 from the arachidonic-acid-producing microalga Lobosphaera incisa shows late gene expression under nitrogen starvation and substrate promiscuity in a heterologous system	lipids

First author	Year	Title	Main topic
Wang	2018	Combined production of fucoxanthin and EPA from two diatom strains Phaeodactylum tricornutum and Cylindrotheca fusiformis cultures	lipids
Zecher**	2018	A multi-step approach for testing non-toxic amphiphilic antifouling coatings against marine microfouling at different levels of biological complexity	other
Ziegler	2018	Long-term algal toxicity of oxidant treated ballast water	growth
Angstenberger	2019	Knock-Down of a ligIV Homologue Enables DNA Integration via Homologous Recombination in the Marine Diatom Phaeodactylum tricornutum	genome engineering
Bauer	2019	In vitro fucoxanthin production by the Phaeodactylum tricornutum diatom	biofactory
Buck	2019	Lhcx proteins provide photoprotection via thermal dissipation of absorbed light in the diatom Phaeodactylum tricornutum	photosynthesis
Erdene-Ochir	2019	Identification and characterisation of the novel endogenous promoter HASP1 and its signal peptide from Phaeodactylum tricornutum	genome engineering
He	2019	Comparison of fatty acid composition and positional distribution of microalgae triacylglycerols for human milk fat substitutes	lipid
Heydarizadeh	2019	Carbon Orientation in the Diatom Phaeodactylum tricornutum: The Effects of Carbon Limitation and Photon Flux Density.	methods
Huang	2019	Nitrogen and phosphorus limitations induce carbon partitioning and membrane lipid remodelling in the marine diatom Phaeodactylum tricornutum	lipids
Liu	2019	Addressing various compartments of the diatom model organism Phaeodactylum tricornutum via sub-cellular marker proteins.	genome engineering
Madhuri	2019	A strategy to complement PtAUREO1a in TALEN knockout strains of Phaeodactylum tricornutum.	genome engineering
Moog	2019	Using a marine microalga as a chassis for polyethylene terephthalate (PET) degradation	biofactory
Patel	2019	Biosynthesis of Nutraceutical Fatty Acids by the Oleaginous Marine Microalgae Phaeodactylum tricornutum Utilizing Hydrolysates from Organosolv-Pretreated Birch and Spruce Biomass	lipids
Pudney	2019	Multifunctionalizing the marine diatom Phaeodactylum tricornutum for sustainable co-production of omega-3 long chain polyunsaturated fatty acids and recombinant phytase.	biofactory
Taparia	2019	A novel endogenous selection marker for the diatom Phaeodactylum tricornutum based on a unique mutation in phytoene desaturase 1.	genome engineering
Dautermann	2020	An algal enzyme required for biosynthesis of the most abundant marine carotenoids	photosynthesis
Dell'Aquila	2020	Mobilization and Cellular Distribution of Phosphate in the Diatom Phaeodactylum tricornutum.	transporter
Derwenskus	2020	Coproduction of EPA and Fucoxanthin with P. tricornutum – A Promising Approach for Up- and Downstream Processing	biofactory
Haslam*	2020	Overexpression of an endogenous type 2 diacylglycerol acyltransferase in the marine diatom Phaeodactylum tricornutum enhances lipid production and omega-3 long-chain polyunsaturated fatty acid content	lipids
Huang*	2020	Physiological and molecular responses to ocean acidification among strains of a model diatom	genome engineering
Leyland	2020	High Resolution Proteome of Lipid Droplets Isolated from the Pennate Diatom Phaeodactylum tricornutum (Bacillariophyceae) Strain pt4 provides mechanistic insights into complex intracellular coordination during nitrogen deprivation	lipids
Mann	2020	The Aureochrome Photoreceptor PtAUREO1a Is a Highly Effective Blue Light Switch in Diatoms	photosynthesis

First author	Year	Title	Main topic
Rastogi	2020	A genomics approach reveals the global genetic polymorphism, structure, and functional diversity of ten accessions of the marine model diatom Phaeodactylum tricornutum.	genome engineering
Sethi	2020	Diatoms for Carbon Sequestration and Bio-Based Manufacturing	biofactory
Song	2020	Morphological and biochemical changes in Phaeodactylum tricornutum triggered by culture media: Implications for industrial exploitation	growth
Von der Au	2020	Single cell-inductively coupled plasma-time of flight-mass spectrometry approach for ecotoxicological testing	other
Buck	2021	Identification of sequence motifs in Lhcx proteins that confer qE-based photoprotection in the diatom Phaeodactylum tricornutum	photosynthesis
Erdene-Ochir	2021	Characterization of endogenous promoters of GapC1 and GS for recombinant protein expression in Phaeodactylum tricornutum	genome engineering
Gillard	2021	Potential for Biomass Production and Remediation by Cultivation of the Marine Model Diatom Phaeodactylum tricornutum in Oil Field Produced Wastewater Media	lipids
Kwon**	2021	Fucoxanthin biosynthesis has a positive correlation with the specific growth rate in the culture of microalga Phaeodactylum tricornutum	photosynthesis
Santin*	2021	Integrative omics identification, evolutionary and structural analysis of low affinity nitrate transporters	transporter
Schnitzler	2021	Lensless digital holographic microscopy as an efficient method	biofactory
Seydoux*	2021	Impaired photoprotection in Phaeodactylum tricornutum KEA3 mutants reveals the proton regulatory circuit of diatoms light acclimation	photosynthesis
Smith	2021	Plastidial acyl carrier protein Δ9-desaturase modulates eicosapentaenoic acid biosynthesis and triacylglycerol accumulation in Phaeodactylum tricornutum	lipids

Tab. S 2 Products produced by *Phaeodactylum tricornutum* strains for industrial usage. Abbrevation used in this tabe: DW: Dry weight; PBR: Photobioreactor

Product class	Product	Strain		Product yield/ productivity reporteda	Operational conditions	Refs
		Library name	Accession no.			
Lipids	EPA	Pt3	UTEX 640	3% DW; 56 mg/l/d	Outdoor chemostat split-cylinder airlift PBR (50–60 l), Almeria, Spain; photoautotrophic/mixotrophic with glycerol	(Fernández Sevilla et al. 2004)
		Pt3	UTEX 640	40.2 mg/g DW 54.2 mg/l/day	Indoor flat-panel airlift photobioreactors (30 l); photoautotrophic	(Derwenskus, Schäfer et al. 2020)
		Pt3	UTEX 640	40.5 mg/g DW 31.0 mg/g (recovered)	Indoor flat-panel airlift photobioreactors (180 l); photoautotrophic	(Derwenskus, Weickert et al. 2020)
		Pt4	UTEX 646	62.55 mg/l	Indoor hanging bag photobioreactor (20 l); photoautotrophic	(Wang et al. 2018)
	DHA	Pt4	UTEX 646 (R) Pt_El05	0.64% DW	Indoor horizontal fence PBR (550 l); photoautotrophic	(Hamilton et al. 2015)
		Pt4	UTEX 646 (R) Pt_El05	0.26% DW	Indoor raceway (1250 l); photoautotrophic	
		Pt1	CCAP 1055/1 (R) Pt_MCAT_PtD5b	0.92% DW	Indoor flasks; photoautotrophic	(Wang et al. 2017)
	ARA	Pt1	CCAP 1055/1 (R) Pt_MCAT_PtD5b	1.89% DW	Indoor flasks; photoautotrophic	(Wang et al. 2017)
	TAG	Pt3	UTEX 640	58.5 mg/l/day, 45% DW	Green wall panel III (≤40 l); outdoor; photoautotrophic	(Rodolfi et al. 2017)
	Brassicosterol	Pt1	CCAP 1055/1 (R) LjLUS-25	~1µg/l	Lab PBR (≤1 l); photoautotrophic	(D'Adamo et al. 2019)
Carbohydrates	Chrysolaminarin		CAS	14% DW; 94 mg/l/day	Indoor flat-plate PBR (50 l); photoautotrophic	(Gao et al. 2017)
Terpenoids	Fucoxanthin		CAS	0.7% DW; 4.7 mg/l/day	Indoor flat-plate PBR (50 l); photoautotrophic	(Gao et al. 2017)
		Pt4	UTEX 646	8.32 mg/l	Indoor hanging bag photobioreactor (20 l); photoautotrophic	(Wang et al. 2018)
		Pt3	UTEX 640	20.1 mg/g DW		

				22.4 mg/l/day	Indoor flat-panel airlift photobioreactors (30 l); photoautotrophic	(Derwenskus, Schäfer et al. 2020)
		Pt3	UTEX 640	16.3 mg/g DW 7.1 mg/g (recovered)	Indoor flat-panel airlift photobioreactors (180 l); photoautotrophic	(Derwenskus, Weickert et al. 2020)
	Lupeol	Pt1	CCAP 1055/1 (R) LjLUS-25	0.01% DW	Lab Algem PBR (≤1 l); photoautotrophic	(D'Adamo et al. 2019)
		Pt1	CCAP 1055/1 (R) AtLUS-6	0.0013% DW	Indoor horizontal fence PBR (550 l); photoautotrophic	(D'Adamo et al. 2019)
	Betulin	Pt1	CCAP 1055/1 (R) LjLUS-25	Detectable levels	Lab Algem PBR (≤1 l); photoautotrophic	(D'Adamo et al. 2019)
Heterologous compounds and proteins	Polyhydroxybutyrate (PHB)			10.6% DW	Indoor flasks (≤1 l); photoautotrophic	(Hempel, Bozarth et al. 2011)
	Human IgGαHBsAg: antibody against hepatitis B virus surface protein	Pt4	UTEX 646 (R)	0.0021% DW; 8.7% TSP	Indoor flasks (≤1 l); photoautotrophic	(Hempel, Lau et al. 2011)
	IgG1/kappa Ab CL4mAb antibody against hepatitis B virus	Pt4	UTEX 646 (R)	2.5 mg/l (secreted)	Indoor flasks (≤1L); photoautotrophic	(Hempel and Maier 2012)
	Monoclonal IgG antibodies against the nucleoprotein of Marburg virus	Pt4	UTEX 646 (R)	2 mg/l (secreted)	Indoor flasks (≤1L); photoautotrophic	(Hempel et al. 2017)
	Polyethylene terephthalate	Pt4	UTEX 646 (R)	n/a	Indoor flasks (≤1L); photoautotrophic	(Moog et al. 2019)
		Pt4	UTEX 646 (R)	n/a	Indoor flasks (≤1L); photoautotrophic	(Schnitzler et al. 2021)
Other Compounds	Polyester-17/19.17/19	Pt4	UTEX 646	n/a	Indoor flasks (≤1L); photoautotrophic	(Roesle et al. 2014)
Whole cell	Wet biomass is used to produce biocrude by hydrothermal liquefaction (HTL)	Pt1	CCAP 1055/1	56.01 mg/L/d HHV 39.71 MJ/kg	Indoor bubble column PBR (90 l)	(Megía-Hervás et al. 2020)
	Biomass	Pt1	CCAP 1055/3	11.55 g/l	Indoor PBR (2 l); mixotrophic (4.6 g/l glycerol)	(Villanova et al. 2021)
		Pt3	UTEX 640	25.4 g/l, 1.7 g/l/day	Outdoor split-cylinder airlift PBR (60 l); mixotrophic (0.1 M glycerol)	(Fernández Sevilla et al. 2004)

2. SI: Chapter I

Tab. S 3 *In situ* analysis of proteins putatively targeted to the plasma membrane in *Phaeodactylum tricornutum*. The protein marked with an asterix (*) is from *Cylindrotheca fusiformis*; proteins marked grey are localized at the plasma membrane (see reference for more detail). Abbreviations: plas: plasma membrane; E.R.: endoplasmatic reticulum; extr: extracellular; chlo: chloroplast; Y: yes; (-): no

			TMHMM	WoLFSPORT	HECTAR	PREDISI		
Function	**Multispanning IMP**	**Protein ID (NCBI)**	**TMD**	**Localization**	**Predicted targeting category**	**Cleavage side**	**Signal peptide**	**References**
Aquaporin	PtAQP1	BBB86745.1	6	plas	-	45	Y	(Matsui et al. 2018)
	PtAQP2	LC341923.1	6	plas	-	50	-	
Urea transporter	JGI_Pt_20424	XP_002180571.1	15	plas	signal anchor	53	-	(Oakley 2010)
HCO_3^- transporter	ptSCL4_2	BAM75352.1	9	plas	signal peptide	33	Y	(Nakajima et al. 2013)
Glycerol transporter	Gly-3-P	EEC50542.1	12	plas	-	42	-	(Villanova et al. 2017)
Nitrate transporter	NRT2	XP_002178487.1	11	plas	signal anchor	63	-	(McCarthy et al. 2017)
	NAT(*)	AAD49570.1	11	plas	signal anchor	63	-	(Hildebrand and Dahlin 2000)
	NPF1	XP_002181410.1	12	plas	-	34	-	(Santin et al. 2021)
	NPF2	XP_002181273.1	10	plas	-	58	-	
Phosphate transporter	PtNapi2	XP_002184358.1	10	plas	-	60	-	(Dell'Aquila et al. 2020)
	PtNapi3	XP_002181465.1	10	plas	signal anchor	49	-	
	PtNapi4	XP_002181914.1	10	plas	-	16	-	
	PtNapi5	XP_002184725.1	10	plas	signal anchor	61	-	
	Small IMP							
Phosphatase	PtPhos3	XP_002180117.1	1 (N-term.)	E.R.	-	28	-	(Dell'Aquila et al. 2020)
	PtPhos8	XP_002182197.1	1 (C-term.)	plas	signal peptide	17	Y	
	ISIPa2	EEC48748.1	1 (C-term.)	extr	signal peptide	22	Y	(Morrissey et al. 2015)
	PDZ1	EEC46446.1	1 (C-term.)	chlo	signal peptide	23	Y	(Liu et al. 2016)
	PDZ2	EEC46542.1	1 (C-term.)	plas	signal peptide	34	Y	

Tab. S 4 List of vectors used in this study.

Name	Promoter	Resistence	Purpose	Origin
pPhat-eGFP	fcpA	zeocin	Localisation study; expression of eGFP	S. Jäger, Uni Frankfurt
pPHAT-eGFP-HUP	fcpA	zeocin	Localisation study; expression of eGFP-HUP fusion protein	D. Wasser, Uni Frankfurt
pPHAT-eGFP-SP	fcpA	zeocin	Localisation study	D. Wasser, Uni Frankfurt
pPHAN-HUP	NR	nourseothricin	Expression of eGFP-HUP fusion protein	This study
pPHAN-eGFP	NR	zeocin	Localisation study; expression of eGFP	D. Wasser, Uni Frankfurt
pPHAN-eGFP-HUP	NR	zeocin	Localisation study; expression of eGFP-HUP fusion protein	D. Wasser, Uni Frankfurt
pPHAN-eGFP-SP	NR	zeocin	Localisation study	D. Wasser, Uni Frankfurt
pGREEN35s2x-eGFP	CaMV 35S	bialaphos	Cloning eGFP	This study
Empty vectors				
pPha-NR	NR	nourseothricin	Standard expression vector	(Stork et al. 2012)
pPha-NR	NR	zeocin	Standard expression vector	

Tab. S 5 List of primers used in the characterization of HUP1 glucose transporter in *Phaeodactylum tricornutum*.

Name	Sequence (5'-3')	Purpose
pPhat_seq_fw	TTGCTTCGTCGGGAATCCCTACG	Sequencing
pPhat_seq_rv	GAGCAAGGATGCCCATTTGTGC	-Sequencing -Control genomic insertion
pPhaNR_fwd	CGGATCCTTCCAGCAACCATTC	-Sequencing -Control genomic insertion
pPhaNR_rev	CCTAACAGTGATCCTCATCGTCG	-Sequencing -Control genomic insertion
GFP_rev	AGCAGGACCATGTGATCG	-Sequencing -Control genomic insertion
Ck_s01p	TGGCTGTGATCTGCATCTTCATC	-Sequencing -Control genomic insertion
Ck_s02p	GCGAGGTTGACGCTGAGTTT	Sequencing
Ck_s02m	GATGACAAAGCTGGTCAGTAGCT	-Sequencing -RT-qPCR
CkHup_r01p	GTCCCCCAACTTCCTTGTAGA	RT-qPCR
q-TBP-F	ATCGATTTGTCAATCCACGAG	RT-qPCR
q-TBP-R	ATACAGATTCTGTGTCCACGG	RT-qPCR
H4fw3	GGTCCTTCGCGACAATATCC	RT-qPCR
H4pt-qrt-rv	TTAACCTCCGAATCCGTAGAG	RT-qPCR

Tab. S 6 Overview of the *in situ* analysis by different web-based programs for sugar transporters from different species. Subkingdom clarified with NCBI. Abbreviations: plas: plasma membrane; chlo: chloroplast; vacu: vacuole; E.R.: endoplasmatic reticulum; Y: yes; (-): no; x: motif found; v: variation of motif and (-): no motif found.

					WoLFSPORT	TMHMM	HECTAR	PREDISI			
Subkingdom	**Species**	**Sugar transporter**	**Protein ID/Uniprot**	**Length [aa]**	**Localization**	**TMD**	**Predicted targeting category**	**Cleavage side**	**Signal peptide**	**tri aromatic motif**	
Metazoa	*Homo sapiens*	Glut1	P11166	492	plas	12	signal peptide	27	-		-
	Homo sapiens	Glut2	P11168	524	vacu	12	-	20	-		-
	Homo sapiens	Glut 3	P11169	496	plas	10	signal peptide	21	-		-
Chromista	*Phaeodactylum tricornutum*	VCT3	B7GBW9	515	plas	12	-	63	-		-
	Phaeodactylum tricornutum	SLC	B7FZR4	434	plas	11	signal peptide	18	Y		-
Fungi	*Saccharomyces cerevisiae*	Hxt1	P32465	570	plas	11	-	58	-	YxxxxxxW	v
	Saccharomyces cerevisiae	Hxt2	H9U0Q4	541	plas	12	-	64	-	YxxxxxxW	v
	Saccharomyces cerevisiae	Hxt4	P32467	576	plas	11	-	26	-	WxxxxxxW	v
	Scheffersomyces stipitis	Sut1	O94155	553	plas	11	-	64	Y	YxxxxxxW	-
Viridiplantae	*Amborella trichopoda*	-	W1PQN3	524	plas	12	signal anchor	38	Y	WxxHxxW	x
	Amborella trichopoda	-	W1NZP8	522	vacu	12	-	37	-	WxxHxxW	x
	Apostasia shenzhenica	STP7	A0A2I0BCL1	523	plas	12	signal peptide	40	Y	WxxHxxW	x
	Arabidopsis thaliana	STP1	P23586	522	plas	12	-	38	Y	WxxHxxW	x
	Arabis alpina	-	A0A087GLM6	516	plas	12	signal anchor	42	Y	WxxHxxW	x
	Auxenochlorella protothecoides	HUP2	A0A087SMA1	509	vacu	11	signal anchor	42	Y	FxxHxxW	v
	Auxenochlorella protothecoides	-	A0A1D2AEF1	547	plas	11	-	18	-	FxxHxxW	v
	Auxenochlorella protothecoides		A0A1D2A3V5	495	plas	11	signal peptide	57	Y	FxxHxxW	v
	Auxenochlorella protothecoides	HUP2	A0A087SIW5	542	vacu	11	signal anchor	37	Y	FxxHxxW	v
	Auxenochlorella protothecoides	-	A0A1D1ZNA8	514	plas		-	20	-	FxxHxxW	v
	Auxenochlorella protothecoides	HUP3	A0A087SI97	533	plas	11	-	35	Y	FxxHxxW	v
	Brachypodium distachyon	Sugar/inositol transporter	I1H4E9	412	plas	9	signal peptide	24	-	FxxHxxW	v
	Brassica napus	-	A0A078JNZ4	503	vacu	12	-	36	-	WxxHxxW	x
	Brassica napus-	-	A0A0Q3NUR6	518	vacu	11	signal peptide	33	Y	WxxHxxW	x
	Brassica oleracea var, oleracea	HUP	A0A0D3DCM9	507	plas	12	-	38	-	WxxHxxW	x
	Capsella rubella	-	R0FKW4	504	plas	12	-	37	-	WxxHxxW	x
	Chlorella kessleri	HUP1	P15686	534	plas	12	signal anchor	42	Y	WxxHxxW	x

	Chlorella kessleri	TP-HUP1		48	cyto	1	signal anchor	42	Y		
	Chlorella kessleri	HUP2	Q39524	540	plas	11	-	44	-	FxxHxxW	v
	Chlorella kessleri	HUP3	Q39525	534	plas	12	signal peptide	41	Y	YxxHxxW	v
	Chlorella sorokiniana	-	A0A2P6TVY2	559	plas	11	signal anchor	56	Y	FxxHxxW	v
	Chlorella sp,/Coccomyxa sp, C-169	-	I0YV94	547	plas	11	signal peptide	41	Y	WxxHxxW	x
	Chlorella variabilis	-	E1ZKB2	550	plas	12	signal anchor	38	Y	FxxHxxW	v
	Chlorella variabilis	STP13	E1ZKC0	568	plas	11	-	42	Y	YxxHxxW	v
	Coccomyxa subellipsoidea	HUP	0YTU0	526	plas	11	signal anchor	35	Y	WxxHxxW	x
	Coffea canephora	-	A0A068UQ08	510	plas	11	signal anchor	38	Y	WxxHxxW	x
	Corchorus olitorius	-	A0A1R3KKS1	488	vacu	9	signal anchor	38	Y	WxxHxxW	x
	Corchorus olitorius	Sugar/inositol transporter	A0A1R3K9K8	505	plas	11	signal anchor	38	Y	WxxHxxW	x
	Corchorus olitorius	Sugar/inositol transporter	A0A1R3KSY8	506	vacu	11	signal anchor	38	Y	WxxHxxW	x
	Corchorus olitorius	Sugar/inositol transporter	A0A1R3G353	505	vacu	12	signal anchor	38	Y	WxxHxxW	x
	Corchorus olitorius	Sugar/inositol transporter	A0A1R3KT26	506	plas	11	signal anchor	38	Y	WxxHxxW	x
	Corchorus olitorius	Sugar/inositol transporter	A0A1R3KNN9	491	plas	11	signal anchor	38	Y	WxxHxxW	x
	Corchorus olitorius	Sugar/inositol transporter	A0A1R3H323	505	vacu	11	signal anchor	38	Y	WxxHxxW	x
	Corchorus olitorius	Sugar/inositol transporter	A0A1R3K9H0	505	vacu	11	signal anchor	38	Y	WxxHxxW	x
	Erythranthe guttata	-	A0A022QFI0	500	plas	12	signal anchor	43	Y	WxxHxxW	x
	Genlisea aurea	-	S8CGH0	497	vacu	11	-	37	Y	WxxHxxW	x
	Helicosporidium sp, ATCC 50920	-	A0A059LM10	504	vacu	12	signal anchor	41	Y	FxxHxxW	v
	Hordeum vulgare subsp, vulgare	HUP	F2D3M3	517	plas	11	signal peptide	34	Y	WxxHxxW	x
	Klebsormidium nitens	HUP	A0A0U9HKX6	544	plas	11	signal anchor	38	Y	FxxHxxW	v
	Micractinium conductrix	HUP2	A0A2P6VQ10	549	plas	11	-	51	Y	FxxHxxW	v
	Morus notabilis	-	W9RYH3	507	vacu	11	-	38	-	WxxHxxW	x
	Morus notabilis	-	W9RYC6	530	vacu	12	-	17	-	WxxHxxW	x
	Parasponia andersonii	HUP	A0A2P5E3K4	502	vacu	12	-	37	-	WxxHxxW	x
	Physcomitrella patens subsp, patens	-	A9RGL8	513	vacu	12	signal anchor	35	Y	WxxHxxW	x
	Physcomitrium patens	MST4-like	A9RGL7	514	plas	12	-	36	Y	WxxHxxW	x
	Punica granatum	STP	A0A218WCM5	511	vacu	12	signal anchor	38	-	WxxHxxW	x
	Ricinus communis	Sugar/inositol transporter	B9RTZ7	530	vacu	12	-	37	-	WxxHxxW	x
	Selaginella moellendorffii	-	D8SL40	522	plas	12	-	37	Y	WxxHxxW	x
	Selaginella moellendorffii	-	D8QR37	517	plas	12	-	33	Y	WxxHxxW	x

	Selaginella moellendorffii	Sugar/inositol transporter	D8R7U7	517	plas	12	-	33	Y	WxxHxxW	x
	Selaginella moellendorffii	Sugar/inositol transporter	D8QPD6	526	plas	12	-	37	Y	WxxHxxW	x
	Trema orientalis	-	A0A2P5FWR7	502	vacu	12	-	37	-	WxxHxxW	x
	Triticum aestivum	-	A0A3B6C605	517	plas	11	signal peptide	34	Y	WxxHxxW	x
	Triticum aestivum	STP	A0A1D5T8Y9	517	plas	11	signal peptide	34	Y	WxxHxxW	x
	Vitis vinifera	HUP	A5BTU8	506	plas	11	signal anchor	34	Y	WxxHxxW	x
	Vitis vinifera	Sugar/inositol transporter	D7T6V3	475	plas	12	-	61	Y	WxxHxxW	x
Viridiplantae	*Wollemia nobilis*	HUP	A0A0C9S5U6	518	nucl	11	-	42	-	WxxHxxW	x
Viridiplantae	*Zostera marina*	STP13	A0A0K9PQH5	509	plas	12	signal anchor	33	Y	WxxHxxW	x

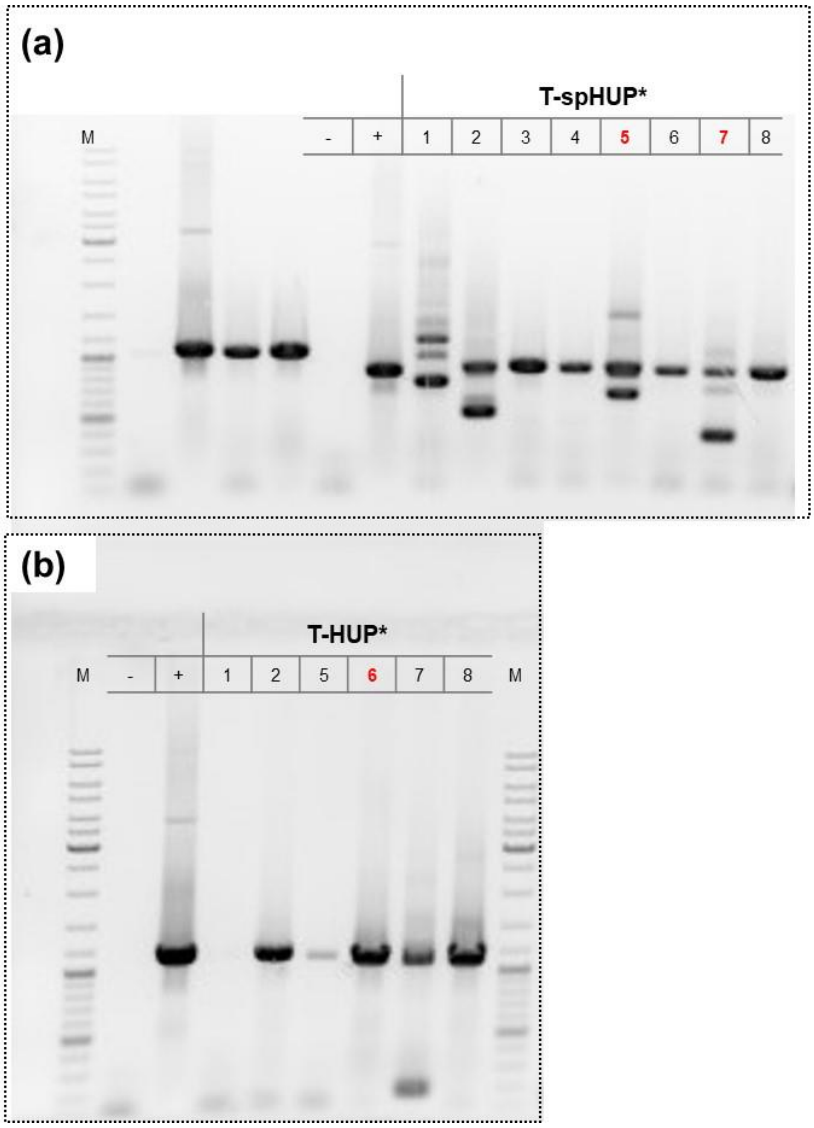

Fig. S 2 Transformed strains *of P. tricornutum* screened for insertion of the *hup1* gene under the control of the fcpA promoter. Non template control (-) and vector DNA (+) were used as controls. Cells were heterologously expressing the eGFP-tagged N-terminal sequence of the HUP1 (T-spHUP*) or the full length HUP1 transporter under the fcpA promoter (T-HUP*) (a). Primer combinations are GFP_rev and Ck_a02p_pPHAN in (a) and GFP_rev and CK_s01p in (b). M= GeneRuler^{TM} DNA Ladder Mix. Transformants used in this study are marked red. Data was collected by Wasser (2019).

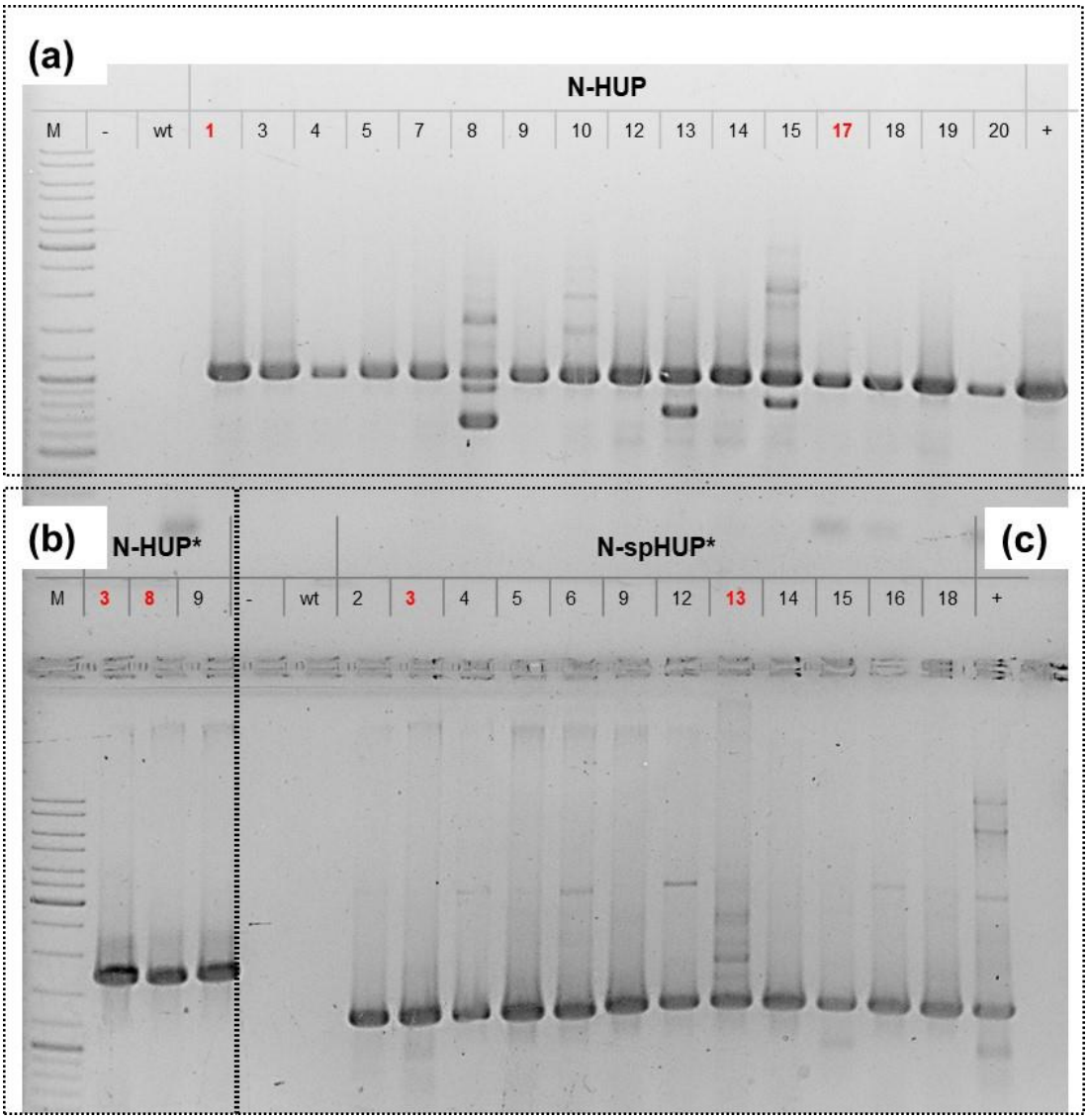

Fig. S 3 Transformed strains of *P. tricornutum* screened for insertion of the *hup1* gene under the control of the Nitrate Reductase promoter. Wildtype (wt), non template control (-), and vector DNA (+) were used as control. Cells heterologously expressing the HUP1 transporter under the nitrate promoter (N-HUP) (a), eGFP-tagged HUP1 transporter under the NR promoter (N-HUP*) (b) or only the N-terminal sequence (N-spHUP*) (c). Primer combinations were pPhaNR_rev and CK_s02p (a) and (b); pPhaNR_rev and pPhaNR_fwd (c). Transformants shown in this study are marked red. Data was collected by Wasser (2019).

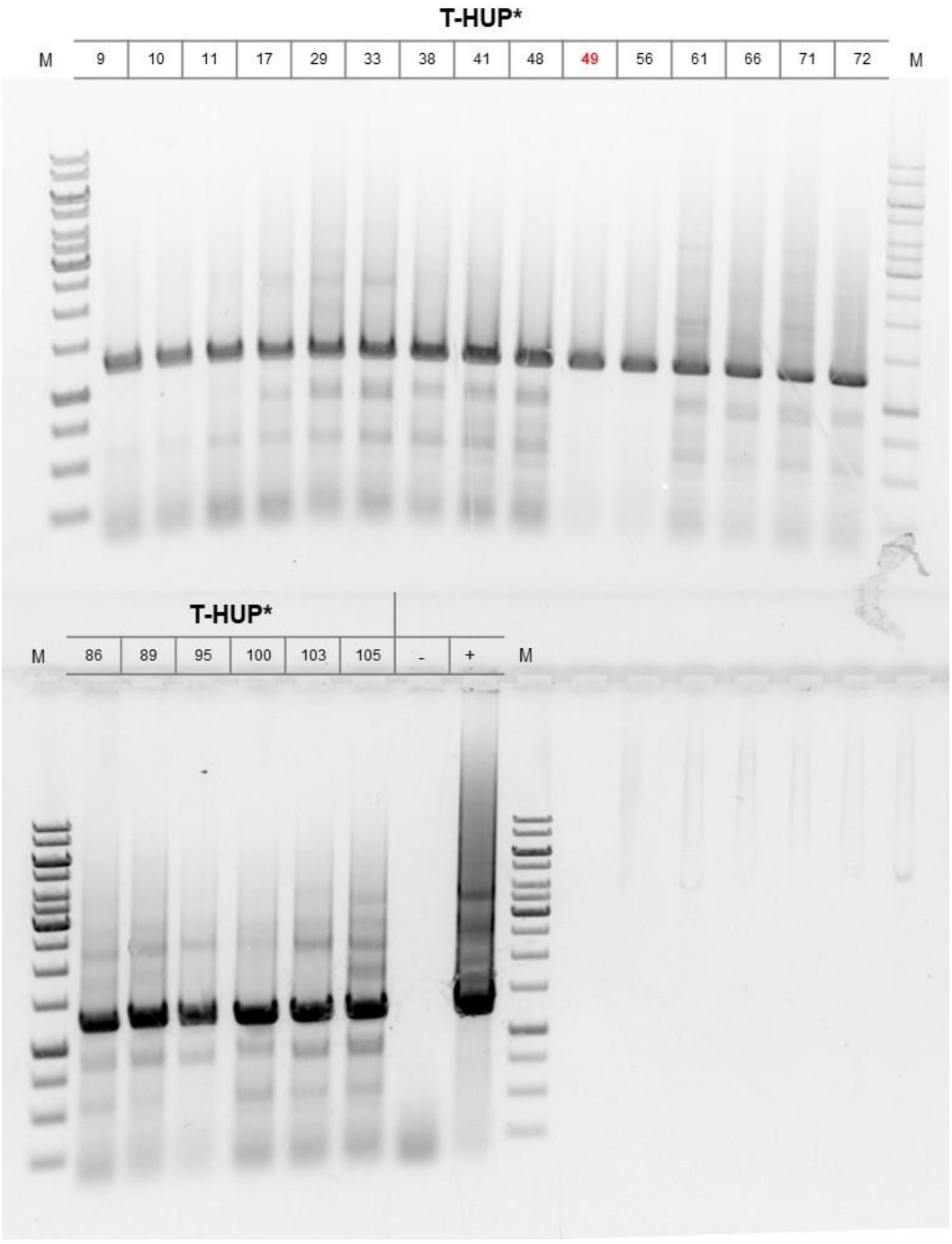

Fig. S 4 Transformed strains of *P. tricornutum* screened for insertion of *hup1* gene under the control of the fcpA promoter. Wildtype (wt) and vector DNA (+) were used as controls. Cells heterologously expressing eGFP-tagged HUP1 transporter under the fcpA promoter (T-HUP*) were tested using pPHAT_seq_rv and CK_s01p; M= GeneRuler™ DNA Ladder Mix. Transformants shown in this study is marked red.

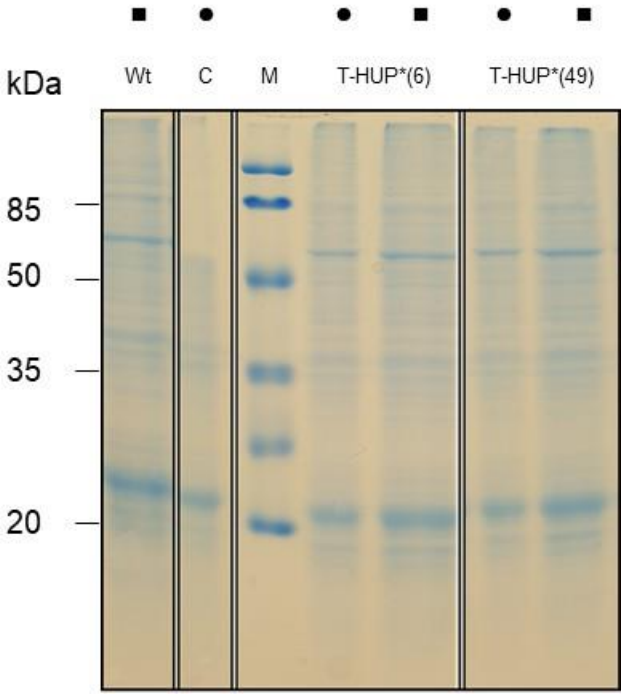

Fig. S 5 Loading control for the comparison of protein expression of HUP transformants (seeFig. 7). Samples of wild type (Wt), a positive control (C) expressing a cytoplasmic eGFP and two Hup mutants were loaded on the SDS-Gel that was stained using Coomassie. The expected molecular weight of the control is 26.9 kDa and that of the Hup1-GFP full-length protein is 84.6 kDa. 5 µl of the Prestained Protein Molecular Weight Marker (Thermo Scientific) was loaded as protein size reference. Samples corresponding to10 µg Chl_a (■) or 5 µg Chl_a (●) were loaded.

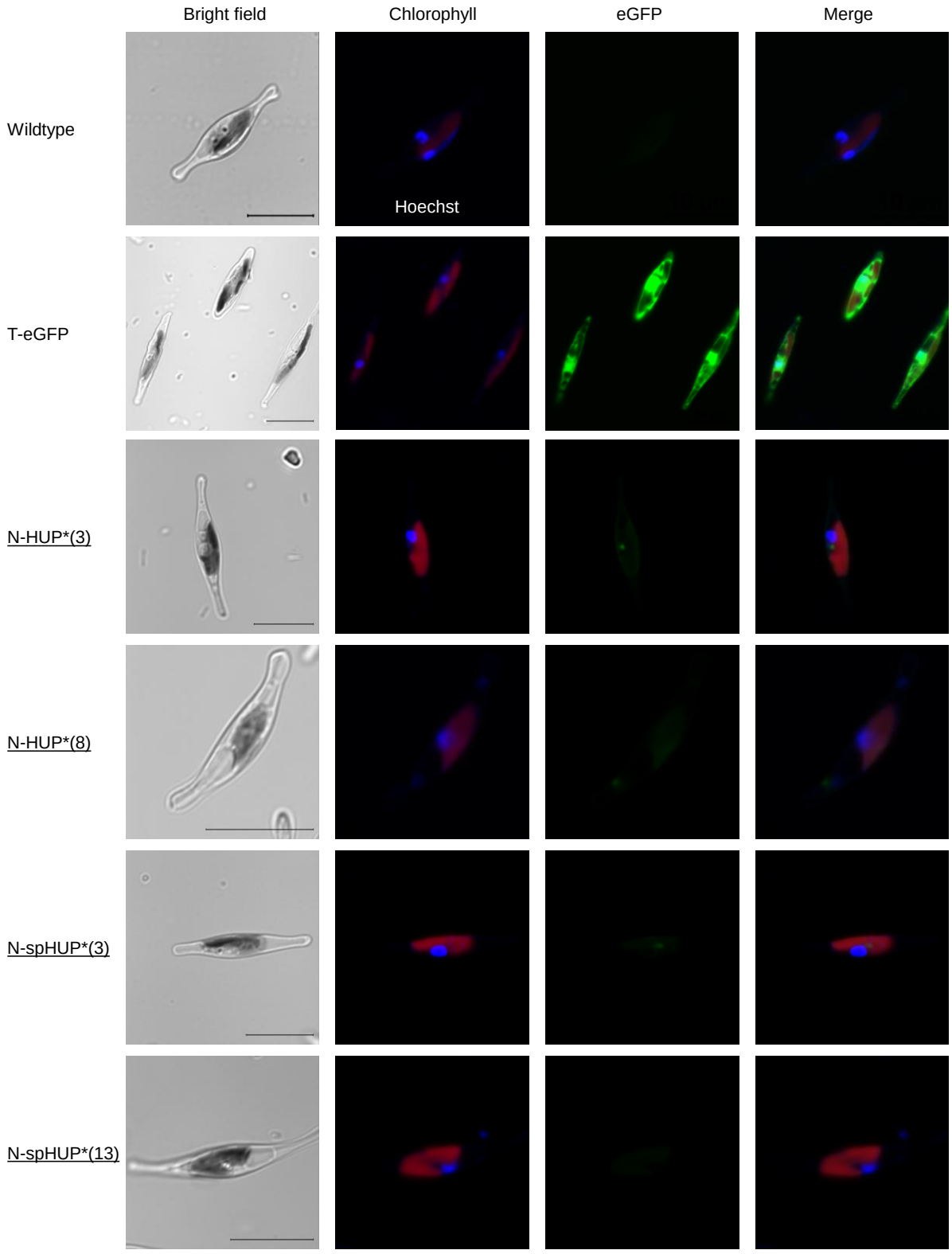

Fig. S 6 *In situ* localization study of mutants heterologously expressing the glucose transporter HUP1 and control cells in *Phaeodactylum tricornutum*. From left to right: Bright field, Hoechst stained nucleus (blue) and autofluorescence of chlorophyll (red), eGFP signal (green) and merged image. Shown are images of *P. tricornutum* wildtype, a mutant expressing cytosolic eGFP (T-eGFP, positive control) and cells heterologously expressing eGFP-tagged HUP1 transporter under a NR promoter (N-HUP*) or a fcpA promoter (T-HUP*), or only the N-terminal sequence (N-spHUP*) under the two promoters, respectively. Scale bars correspond to 10 µm. Images with underlined caption are collected by Wasser (2019).

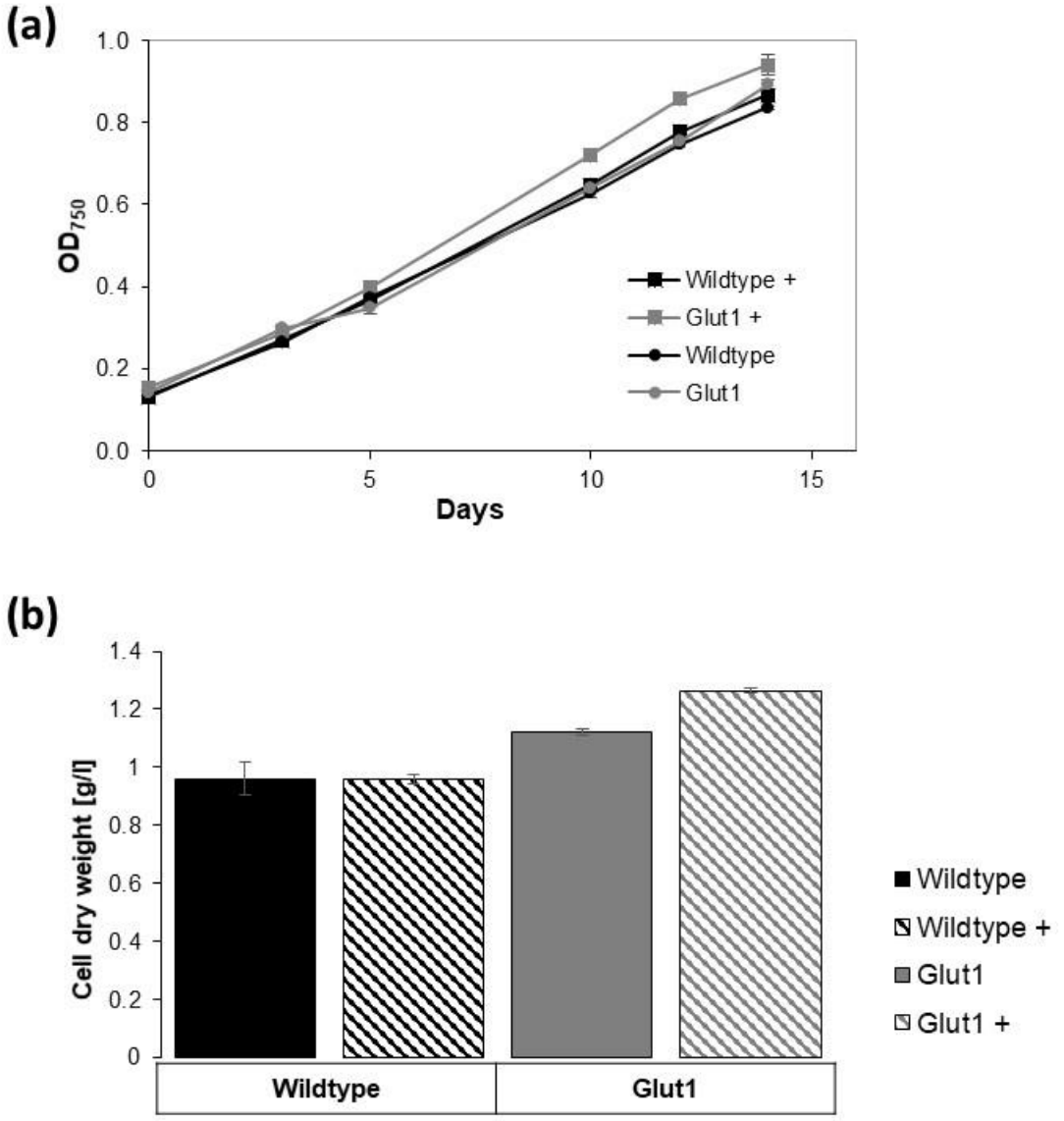

Fig. S 7 Growth of wildtype and Glut1 cells for 14 days. Wildtype and the positive control Glut1 were grown in biological duplicates under a light field of 120 µmol·m^{-2}·s^{-1} with a 16-hour light/8-hour dark cycle at 18°C and a controlled CO_2 value of 480 ppm with (+) or without the addition of 5 mM glucose. Growth was measured using a microplate reader by monitoring the OD at 750 nm (a). Values are mean ± SD (n=6). A comparison of the CDW at the end of the growth experiment for cells with (striped bars) or without (solid bars) 5 mM glucose (b). Values are mean ± SD (n=4).

3. SI: Chapter II

Tab. S 7 Chemical composition of media used in this study. Differences to the common ASP medium are displayed with bold letters. A more detailed overview of the medium composition of the commercial F/2 medium is given in Fig. S 8.

		ASP	**ASP_{LNP}**	**ASP_{VLNP}**	**$ASP^{+}{}_{VLNP}$**	**F/2**	**$F/2_{SW}$**
	Component	**Conc. [mM]**	**Conc. [mM]**	**Conc. [mM]**	**Conc.**	**Conc.**	**Conc.**
Salinity	NaCl	86			86 mM	86 mM	
	$MgSO_4 \cdot 7H_2O$	8.1			**39 mM**		
	KCl	21			21 mM	K= 0.8 mM	
	$CaCl_2$	2.72			2.72 mM		
Nitrate	$NaNO_3$	11.8	**1.8**	**0.9**	**0.9 mM**	**1.7 mM**	**1.7 mM**
Phosphate	K_2HPO_4	0.58	**0.07**	**0.04**	**0.04 mM**	**0.1 mM**	**0.1 mM**
							~1l Seawater[a]
Total salt concentration		0.99%	0.90%	0.89%	1.75%	0.54%	3.54%
Tris	Tris	4			4 mM		
Trace element	EDTA	0.924			0.924 mM		
	$FeCl_3$	0.820			0.820 mM	Fe= 0.1 mM	
	$MnCl_2 \cdot 4H_2O$	0.488			0.488 mM	trace	
	$ZnCl_2$	1.205			1.205 mM	trace	
	$CoCl_2 \cdot 6H_2O$	0.020			0.020 mM	trace	
	$NaMoO_4 \cdot 2H_2O$	0.010			**0.52 µM**	trace	
	$CuCl_2 \cdot 2H_2O$	0.007			0.072 mM	trace	
	KBr	-			**0.725 mM**		
	NaF	-			**6.57 µM**	Na= 10.3 mM	
	$Fe(NH_4)_2(SO_4) \cdot 6H_2O$	-			**5.362 µM**	trace	
	Na_2SeO_3	-			**10 nM**		
Vitamin	Vitamin B12	-			**2.94 nM**	trace	
	Vitamin B1	-			**0.594 µM**	trace	
	Vitamin B7	-			**0.818 mM**	trace	
						Cell-Hi F2P powder [1g/l]	**Cell-Hi F2P powder [1g/l]**

[a]collected from the Helgoland trench, filtered through 0.45 µm and 0.1µm filter; autoclaved, Alfred-Wegener-Institute, Bremerhaven, Bremen, Germany

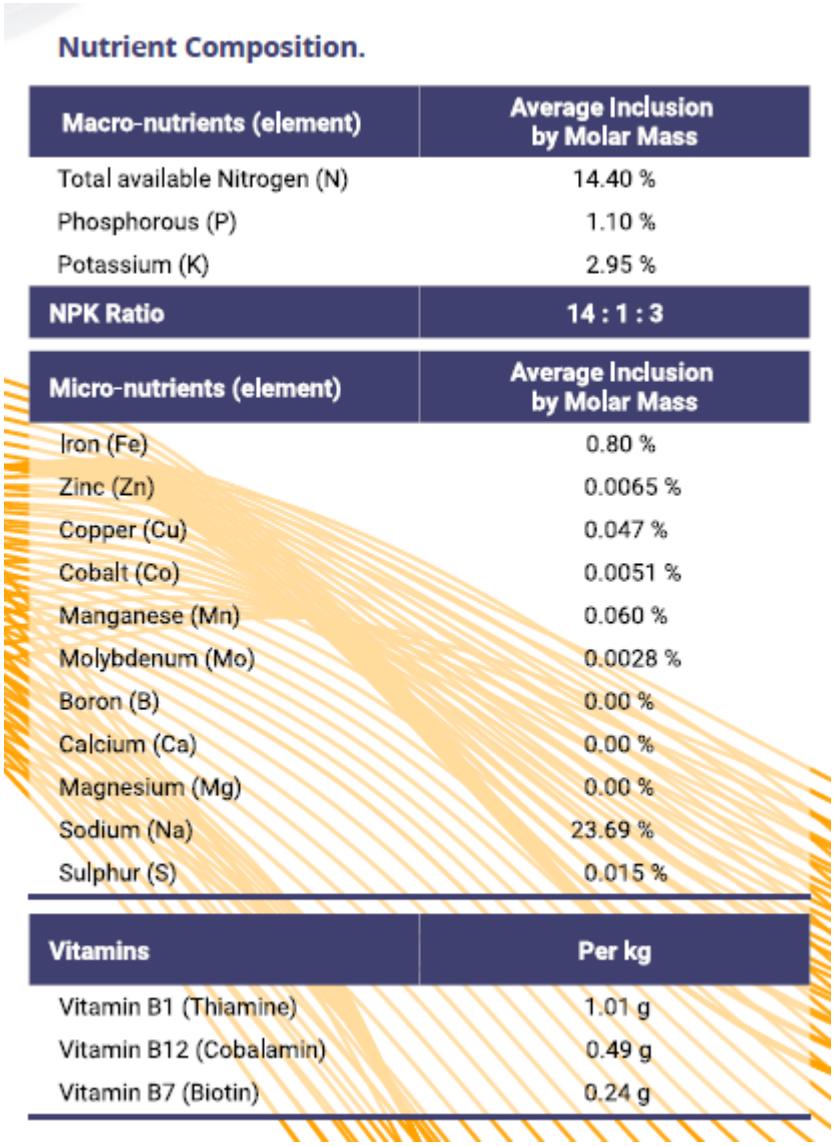

Nutrient Composition.

Macro-nutrients (element)	Average Inclusion by Molar Mass
Total available Nitrogen (N)	14.40 %
Phosphorous (P)	1.10 %
Potassium (K)	2.95 %
NPK Ratio	**14 : 1 : 3**

Micro-nutrients (element)	Average Inclusion by Molar Mass
Iron (Fe)	0.80 %
Zinc (Zn)	0.0065 %
Copper (Cu)	0.047 %
Cobalt (Co)	0.0051 %
Manganese (Mn)	0.060 %
Molybdenum (Mo)	0.0028 %
Boron (B)	0.00 %
Calcium (Ca)	0.00 %
Magnesium (Mg)	0.00 %
Sodium (Na)	23.69 %
Sulphur (S)	0.015 %

Vitamins	Per kg
Vitamin B1 (Thiamine)	1.01 g
Vitamin B12 (Cobalamin)	0.49 g
Vitamin B7 (Biotin)	0.24 g

Fig. S 8 Medium composition of the commercial Cell-Hi F2P. The medium is from varicon aqua and here called F/2. This is a copy of the original flyer from the company Varicon aqua.

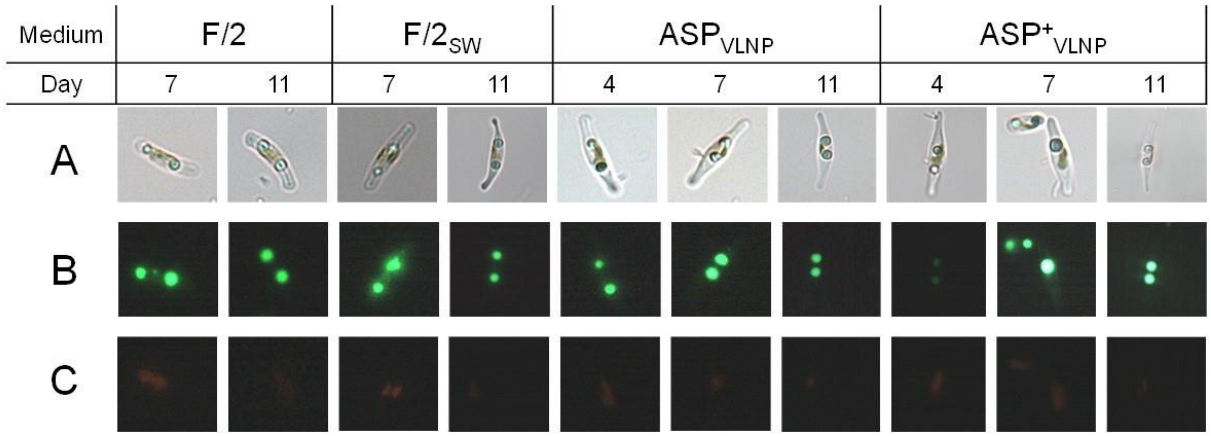

Fig. S 9 Visualizing lipids of stained cells grown for 11 days in photobioreactor. Wildtype cells grew in 1L photobioreactor FMT150 have been sampled after 4, 7 and 11 days and stained with BODIPY 505/515. As a control, cells have been recorded using bright field (A). BODIPY 505/515 was excited by 425 - 445 nm and fluorescence detected at 460 - 500 nm (B). Chlorophyll was excited with 570 - 645 nm autofluorescence was detected at 675 nm (C). Data was collected by deKruiff (2021).

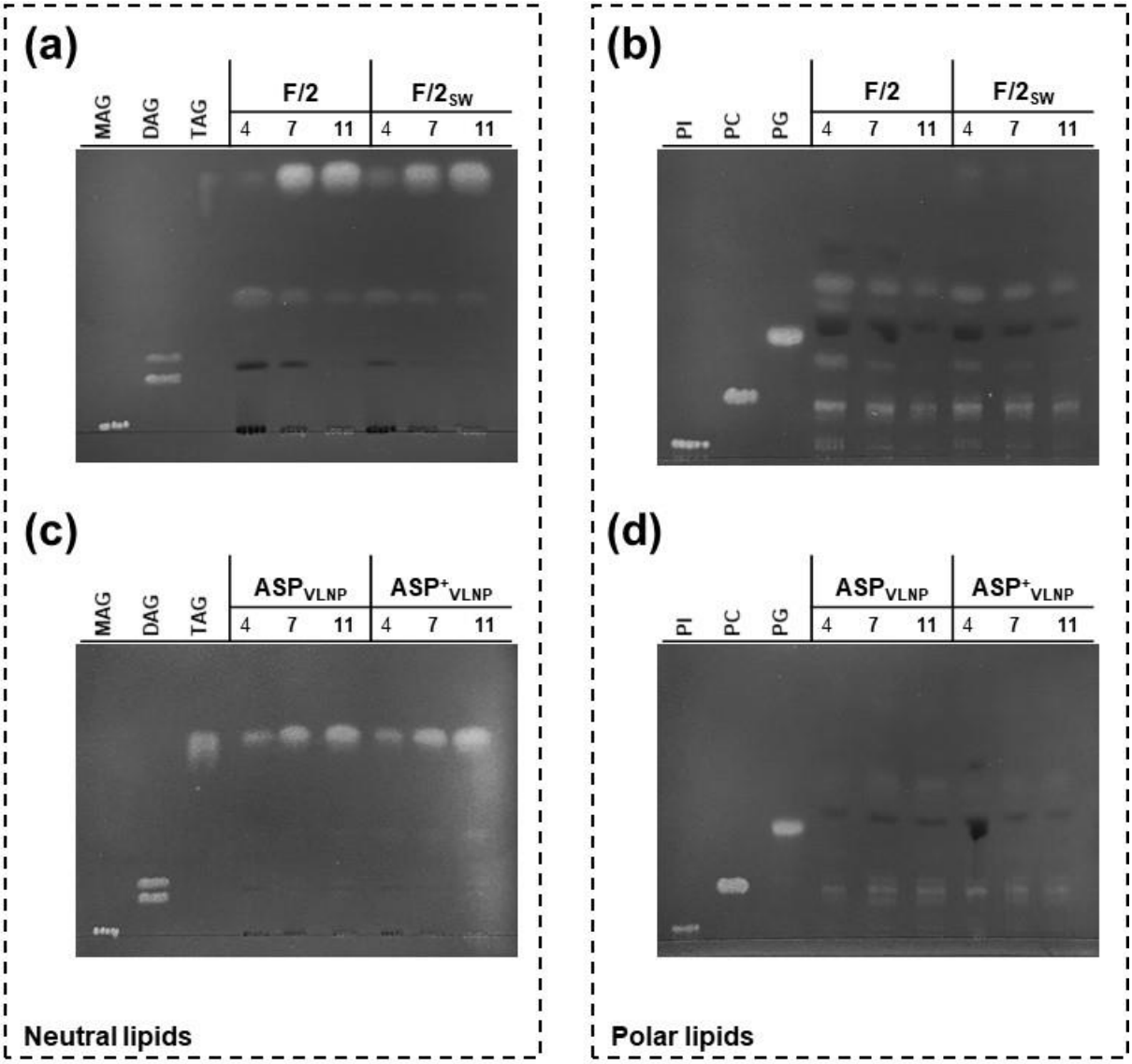

Fig. S 10 Lipid composition analysis using thin layer chromatography of wildtype cells grew in 1l photobioreactor FMT150. Wildtype cells were sampled after 4, 7 and 11 days and lipids were extracted as described (see 8.4). Equal amounts of total lipids were loaded per lane on the stationary phase, here TLC Silica Gel 60 plates (Merck). For mobile phase following solution were used: [NL: hexane–diethylether–acetic acid (70:30:1) (v/v)] and [PL: chloroform–methane–ammonia solution (65:25:5) (v/v)]. Primuline stained TLC plates were illuminated with UV light. White fluorescence signal corresponds to lipids whereas black spots are pigments. Lipid standards: tripalmitate (TAG); glyceryl-1,3- and 1-2-dipalmitate (DAG), DL-α-palmitate (MAG), phosphatidylinositol (PI), phosphatidylcholine (PC) and phosphatidylglycerol (PG). Data was collected by deKruiff (2021).

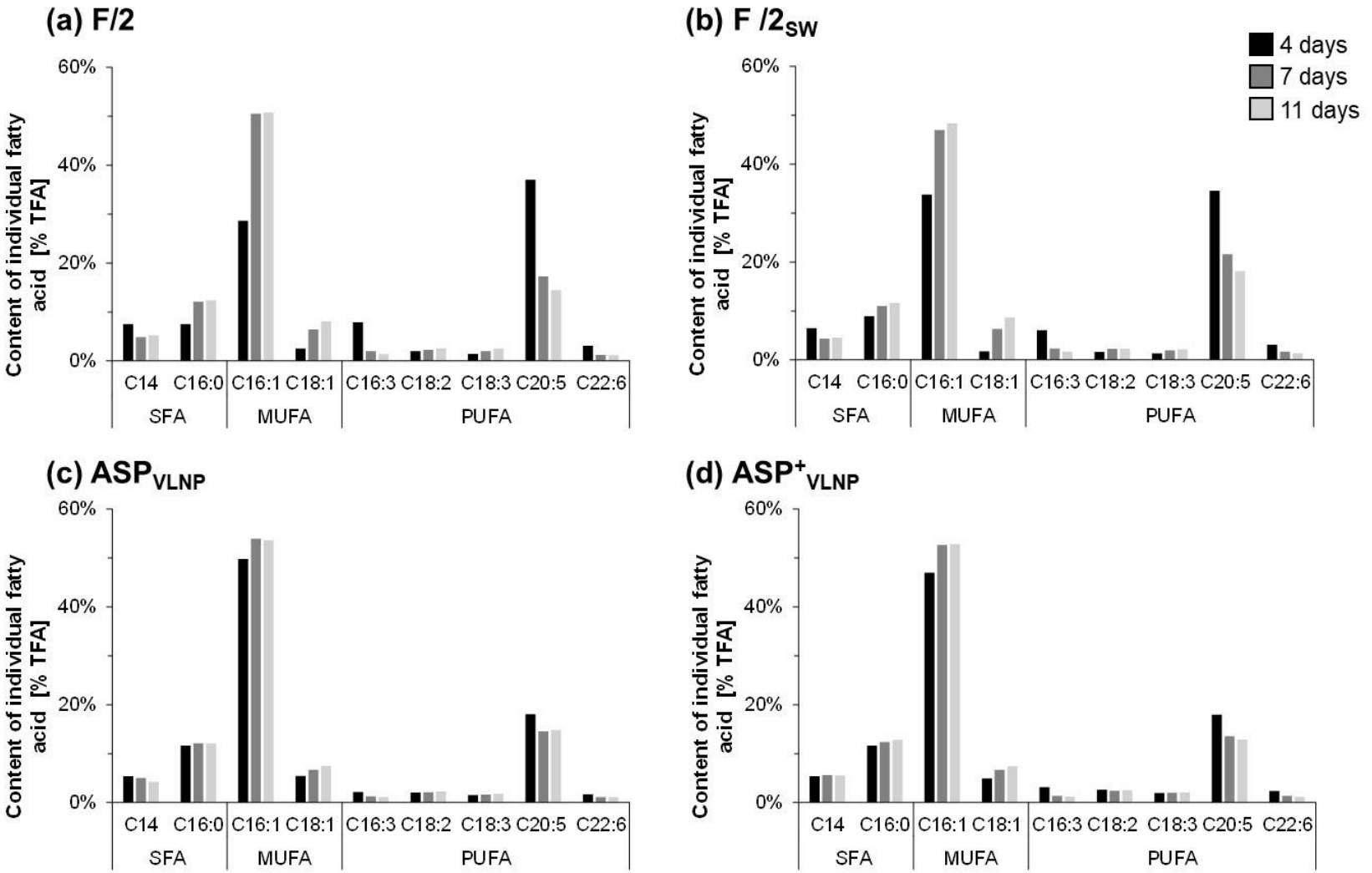

Fig. S 11 Fatty acid content analyzed from cells grown in different media. *P. tricornutum* was cultured in 1l FMT150 over a period of 11 days and samples were taken after 4 (black), 7 (dark grey) and 11 days (light grey). Lipid extracts of cells have been analyzed using GC-MS. Abbreviations used in this figure: SFA: saturated fatty acids; MUFA: monounsaturated fatty acids; PUFA: polyunsaturated fatty acids; TFA: total fatty acids. Raw data of fatty acid analysis were aquired by Peng Li (Uni Tübingen).

Tab. S 8 Fatty acid content [µg] per mg dry biomass analyzed from cells grown in different media. Cells were grown either in medium F/2, F/2SW, ASPVLNP or ASP+VLNP as it is described in or in ASPLNP as it is described in **Fig. 19** and **Fig. 23**. Abbreviations used in this table: rec.: recovery; SFA: saturated fatty acids; MUFA: monounsaturated fatty acids; PUFA: polyunsaturated fatty acids; TFA: total fatty acids; TC: total content. Raw data of fatty acid analysis were aquired by Peng Li (Uni Tübingen).

Medium and culture period [d]		IS1 rec. [%]	Biomass [mg]	SFA				MUFA				PUFA							TC			
				C14:0	C16:0	C18:0	C24:0	C14:1	C15:1	C16:1	C18:1	C16:3	C18:2	C18:3	C20:4	C20:5	C20:3	C22:6	SFA	MUFA	PUFA	TFA
		IS1a																				
F/2	4	0.6	6.9	11.1	11.1	0.7	0.7			42.1	3.7	11.6	3	2.1	1.0	54.4	0.8	4.6	23.6	45.8	77.5	146.9
	7	0.4	13.2	17.2	42.7	1.6	0.7			177.8	22.7	7.1	8	7.2	1.0	60.8	0.8	4.4	62.2	200.5	89.3	352.0
	11	0.6	17.9	14.7	34.8	1.4	0.6			142.3	22.7	4.0	7.3	7.1	0.9	40.6	0.5	3.3	51.5	165.0	63.7	280.2
$F/2_{SW}$	4	0.7	6.8	9.2	12.7	0.9	0.8			48.0	2.5	8.7	2.3	1.9	0.8	49.1	0.8	4.4	23.6	50.5	68.0	142.1
	7	0.6	10.8	12.3	31.0	1.5	1.0			132.1	17.9	6.5	6.3	5.5	0.7	60.7	0.8	4.8	45.8	150.0	85.3	281.1
	11	0.7	15.8	12.9	33.0	1.4	0.8			136.9	24.6	4.8	6.5	6.1	0.6	51.4	0.4	3.9	48.1	161.5	73.7	283.3
ASP_{VLNP}	4	0.6	5.3	13.3	28.8	1.8	1.1			123.0	13.4	5.4	5.1	3.8	1.3	44.6	1.1	4.2	45.0	136.4	65.5	246.9
	7	0.5	6.9	18.0	43.5	1.8	1.1			193.2	24	4.5	7.6	5.8	1.1	52.3	1.1	4.1	64.4	217.2	76.5	358.1
	11	0.4	7.2	21.4	60.7	2.5	1.3			268.4	37.5	5.8	11.3	9.2	1.4	74.2	1.2	5.6	85.9	305.9	108.7	500.5
ASP^{+}_{VLNP}	4	0.6	3.4	13.5	29.3	2.4	1.5			118.0	12.4	7.9	6.6	4.9	1.9	45.1	1.5	6.0	46.7	130.4	73.9	251.0
	7	0.6	5.7	18.8	41.4	2.3	1.1			175.7	22.4	4.7	8.1	6.7	1.3	45.3	1.1	4.7	63.6	198.1	71.9	333.6
	11	0.6	6.6	18.4	42.8	2.0	0.9			176.2	24.7	4.1	8.5	6.9	1.2	43.0	0.9	4.0	64.1	200.9	68.6	333.6
		IS1b																				
ASP_{LNP}	3	0.5	7.4	5.1	2.8	0.3	0.6	4.9	0.8	21.4	1.9	11.0	3.6	1.8	4.2	13.4		3.2	8.9	29.0	37.1	75.0
	5	0.9	9.9	5.9	3.4	0.3	0.5	5.4	0.6	22.3	1.8	13.0	3.7	2.2	2.9	22.1		3.4	10.0	30.1	47.3	87.4
	7	0.8	14.8	6.1	5.8	0.2	0.4	6.1	0.4	30.7	3.5	8.3	2.4	2.2	2.0	21.3		2.8	12.5	40.7	39.1	92.3
	9	0.5	17.6	6.3	6.7	0.2	0.3	7.8	0.3	44.4	3.7	7.1	1.7	2.2	1.8	19.5		2.3	13.6	56.2	34.6	104.4

Tab. S 9 Fatty acid content [µg] per mg dry biomass analyzed from cells grown in ASP media. As control cells were grown as it is described in Fig. **28**. Abbreviations used in this table: rec.: recovery; SFA: saturated fatty acids; MUFA: monounsaturated fatty acids; PUFA: polyunsaturated fatty acids; TFA: total fatty acids; TC: total content. Raw data of fatty acid analysis were aquired by Peng Li (Uni Tübingen).

			SFA				MUFA				PUFA							TC			
Extraction time	**IS1 rec. [%]**	**Biomass [mg]**	C14:0	C16:0	C18:0	C24:0	C14:1	C15:1	C16:1	C18:1	C16:3	C18:2	C18:3	C20:4	C20:5	C20:3	C22:6	SFA	MUFA	PUFA	TFA
	IS1a																				
01/2021	1.3	3.3	6.8	7.9	1.6	1			45	2.5	19.2	4.3	0.7		45	0.8	3	17.3	47.5	73	138
	1.8	3.5	6.6	7.3	1.5	0.8			43.2	3.3	18.2	3.8	0.4		43.4	0.6	2.8	16.2	46.5	69	132
	0.1	3.4	156.6	184.6	40.8	18.2			1067	54.7	454.9	89.1	12.5		840.3	17.5	61.1	400.2	1121	1475	2997
	1.7	6.9	6.8	6.5	0.8	0.6			38.3	3.0	19.3	3.5	0.4	0.4	47	0.4	2.8	14.7	41.3	74	130
	1.5	7.4	6.8	6.3	0.8	0.7			39.5	3.0	17.7	3.3	0.4	0.4	46	0.4	3.2	14.6	42.5	71	128
	1.7	6.9	5.8	5.6	0.7	0.6			35.6	2.7	16.5	2.8	0.3	0.4	40.2	0.4	2.6	12.7	38.3	63	114
	1.6	9.6	6.1	5.5	0.6	0.7			33.4	3.3	18.3	3.3	0.3	0.4	45.7	0.5	3.3	12.9	36.7	72	121
	0.6	9.8	6.5	5.4	0.5	1.1			31.8	3.0	18.4	3.5	1.0	0.8	45.3	0.8	4.2	13.5	34.8	74	122
	0.5	8.9	6.7	5.9	0.5	1.3			35.9	3.2	19.3	3.8	1.4	1	50.2	1	4.1	14.4	39.1	81	134
	0.5	14.7	6.6	5.2	0.4	1.2			32.3	3.3	19.5	3.7	1.2	0.7	47.9	0.7	4.6	13.4	35.6	78	127
	0.0	14.9	291.5	230.3		131			1799	120.9	0.0	276.2			1514		267.2	652.8	1920	2057	4629
	0.0	13.6	293.1	213.3		114.9			1657	172.9	0.0	238.0			1739		222.9	621.3	1830	2200	4650
	IS1b																				
11/2021	0.3	7.2	5.4	4.3	0.8	0.9	0.6	1.1	34.9	1.9	16.0	3.4	1.1	6.0	21.8		5.0	11.4	38.5	56.0	105.9
	0.5	6.9	3.1	3.3	0.6	0.7	0.5	0.9	27.0	0.3	11.8	2.2	1.8	4.5	20.9		3.7	7.74	29.83	46.0	83.6
	0.3	6.6	4.0	4.2	0.7	1.0	0.7	1.2	35.5	0.4	15.4	2.7	1.1	6.9	14.2		5.3	10.03	38.46	49.2	97.6
	0.3	17.4	4.7	3.0	0.3	0.7	6.7	0.7	32.3	1.8	18.5	4.4	2.9	2.7	36.5		4.6	8.68	41.54	66.9	117.1
	0.3	17.3	4.6	2.1	0.3	0.5	5.0	0.6	27.0	1.4	13.0	2.9	2.1	2.2	23.4		3.3	7.41	32.81	45.9	86.1
	0.3	15.9	5.4	3.0	0.4	0.6	5.8	0.7	32.0	1.1	18.5	4.1	3.2	2.8	30.8		4.3	9.452	38.95	60.2	108.6

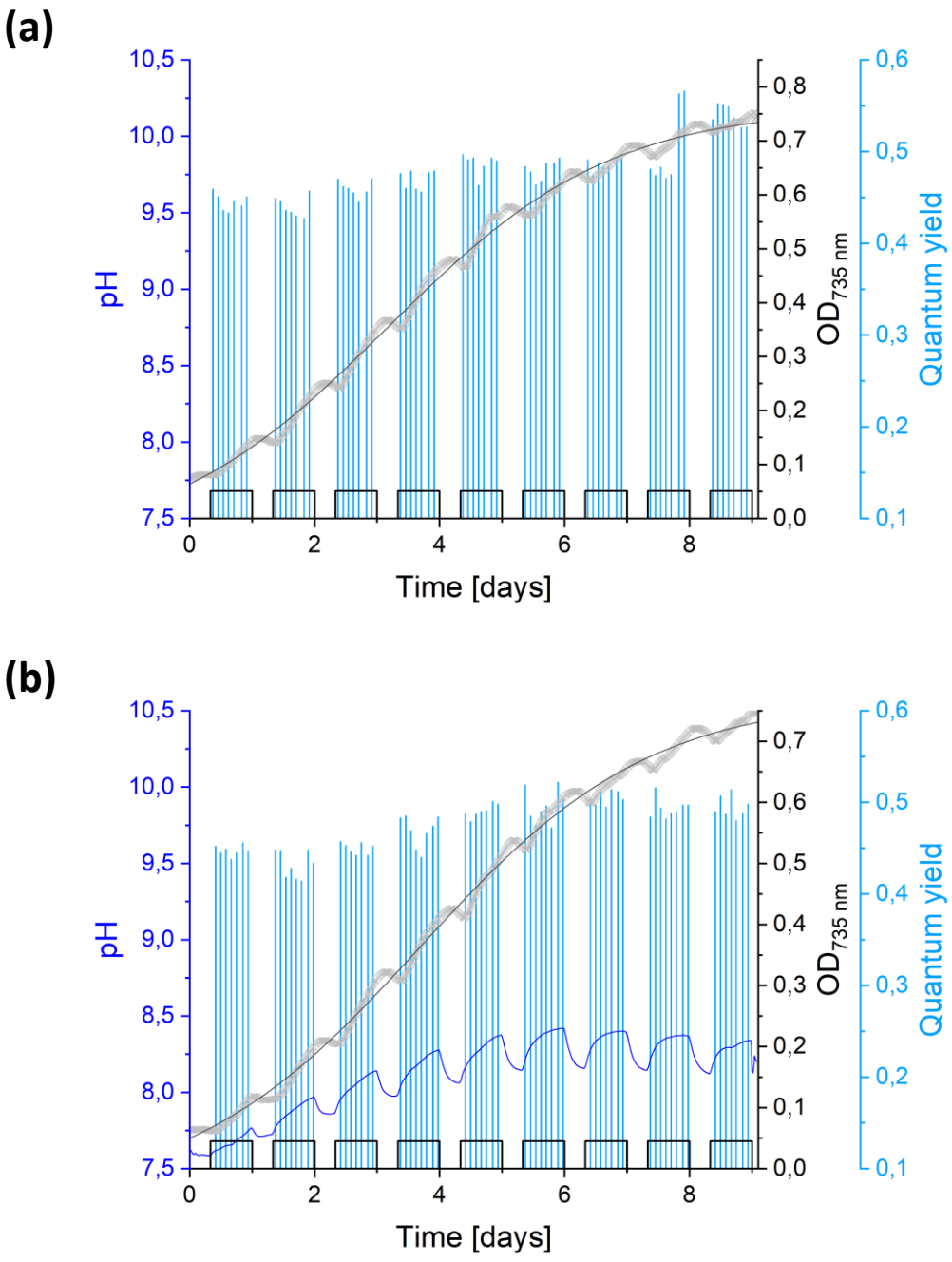

Fig. S 12 Growth curve of cells with adapted nitrogen and phosphat concentration. Here, as biological replicate, wildytpe cells grew in 1L photobioreactor FMT150 in (a) ASP_{LNP} medium supplemented with an antibiotic cocktail to gurantee axenic growth of the cells. (b) As control cells were grown without antibiotic cocktail, but under the same condition as described before. Both cultivations were measured over 9 days with a light intensity of 60 µmol·photons $m^{-2}·s^{-1}$ with a 16-hour light/8-hour dark cycle (indicated with white bars) at 18°C. The pH (dark blue) and the optical density, OD_{735} (grey) was monitored constantly, whereas maximum quantum yield of photosystem II (F_V/F_M) was measured only in light period and is displayed in light blue. Boltzmann regression line is calculated and shown in black with R^2 for the Boltzmannn fit with (a) 99.66% and (b) 99.7%.